Development of Accurate Physically Grounded Force Fields for Intermolecular Cation-π Interactions based on SAPT Energy Decomposition Analysis and Computational Investigation of Covalent Irreversible Vinyl Sulfone-based Protease Inhibitors

Dissertation zur Erlangung des
naturwissenschaftlichen Doktorgrades
der
Julius-Maximilians-Universität Würzburg

vorgelegt von
Kay Ansorg

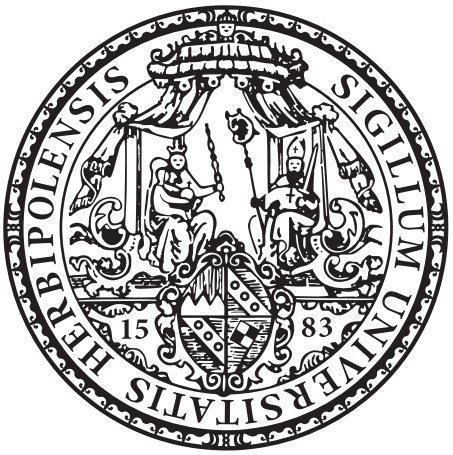

Würzburg 2015

Eingereicht bei der Fakultät für Chemie und Pharmazie am

_____

Gutachter der schriftlichen Arbeit

1. Gutachter: _____
2. Gutachter: _____

Prüfer des öffentlichen Promotionskolloquiums

1. Prüfer: _____
2. Prüfer: _____
3. Prüfer: _____

Datum des öffentlichen Promotionskolloquiums

_____

Doktorurkunde ausgehändigt am

_____

Contents

Part I.

Development of Accurate Physically Grounded Force Fields for Intermolecular Cation-π Interactions based on SAPT Energy Decomposition Analysis

1. Introduction and Motivation

1.1. Non-covalent Interactions

The interactions between atoms or molecules can be separated into covalent and non-covalent interactions (NCI). The nature of a covalent bond is well understood, it is formed when two systems with unfilled electronic shells start to overlap. Then the electron density between them increases and a covalent bond is created. The bond length depends on the overlap, so the range of chemical bonds is approximately between 1-4 Å. The origin of non-covalent interactions lies in the electric, and to a lesser extent, magnetic properties of the systems. These forces, resulting from permanent, induced, and time-dependent electric multipoles, have a range of sometimes more than 10 Å.[1] In general, the notation of a covalent single bond is a short full line (e.g. H-H or H_2), while there is no defined notation of non-covalent bonds. As suggested in the literature[1,2] three dots (e.g. He...He or $(He)_2$) represent the non-covalent interaction between two monomers. This notation will also be used in this thesis for labeling non-covalent interactions.

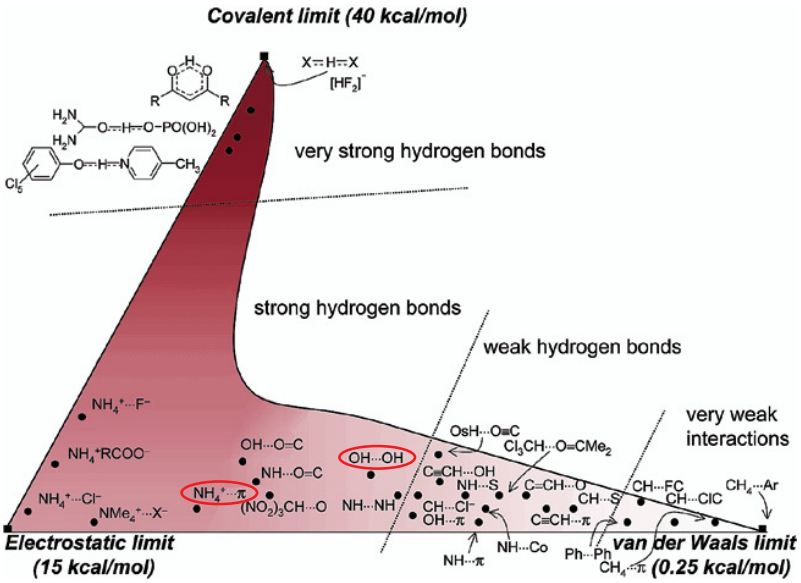

Figure 1.1.: This figure serves as a rough guide categorizing non-covalent interactions into the three extreme situations of widely differing energies. The coloring attempts to provide a visual scale of energies. The red marked interaction ($OH \cdots OH$ and $NH_4^+ \cdots \pi$) are highlighted since they are a central part of this work. Reprinted with permission from Acc. Chem. Res., 2002, 35 (7), 565-573. Copyright 2002 American Chemical Society.

Fig. 1.1 gives an approximate overview of the bond strength of NCI compared to covalent bonds. NCI are easily formed and can be easily broken. This property represents its advantages, since a supermolecule formed with NCI is allowed to repeat the bond forming and breaking process without changing any important structural and electronic features. The importance of these properties for biological processes will be described in chapter 1.1.1. The interaction energy can be split into several long- and short-range contributions.[3] The major contributions to NCI are the following.

Electrostatic energy can be separated into a long- and short-range part. The long-range part, where overlap between the electron densities nearly vanishes, includes interactions with permanent multipole moments, namely charges (= monopoles), dipoles, quadrupoles, and higher multipoles. The energy between two subsystems is

proportional to the product of multipoles and the first or higher power of reciprocal distance. The short-range electrostatics include the charge penetration effects, since the electrons of subsystem A respond to the nuclei of subsystem B and vice versa. The separation in long- and short-range electrostatics is important for the development of physically grounded force fields (see section 2.2).

Induction or polarization energy is the interaction between statically polarized charge densities of subsystems and is always attractive.

Dispersion energy is due to dynamically polarized charge distributions and is always attractive. The long-range part is proportional to the product of the polarizabilities of the subsystems and a sixth (or higher) power of reciprocal distance.

Exchange-repulsion term describes two effects: an attractive part which arises since the electrons can move over both monomers and a (more dominant) repulsive part which is caused by the Pauli antisymmetry requirement. The exchange-dispersion, exchange-induction and charge transfer effects also arise when wave functions begin to overlap. The charge transfer is often considered separately but should better be viewed within the induction interaction.

Resonance and magnetic contributions are also feasible. Resonance effects require a degenerate (e.g. excited) state, hence they do not occur between closed-shell molecules in ground states. Magnetic contributions are very small and require unpaired spins in each molecule.
Usually the electrostatic energy dominates the NCI energy compared to other energy terms. Its decay is inversely proportional to the distance R of the monomers ($\sim 1/R$), while the decay of the induction and dispersion behaves like $\sim 1/R^6$ and the exchange-repulsion $\sim e^{-R}$. To form a stable NCI complex the sum of all mentioned types of non-covalent interactions must be lower than the sum of the energies of its

separated subsystems.

$$\Delta E(A...B) < \Delta E(A) + \Delta E(B)$$

The focus in this thesis is on a special NCI type, namely the cation-π interaction including organic cations. Metal cation-π [4,5] interactions e.g. selectivity in potassium channels [6] or cation-sigma interactions [7] are not considered.

1.1.1. Cation-π Interactions in Biological Systems

The wide occurrence of such interactions, e.g. its relevance in host-guest complexes, material science, catalysis, and biological systems is a topic of Mahadevi and Sastry's review. [8] As can be seen from Fig. 1.1 the strength of cation-π interactions is comparable to the strength of hydrogen bonds. Its importance in biological structures and processes [9–14], namely side chain interactions in proteins, protein ligand recognition processes and catalysis [15], was systematically analyzed by the group of Dougherty. [13] To get a picture of these interactions the following example of Gallivan and Dougherty [16] is shown using the CAPTURE (cation-π trends using realistic electrostatics) program. The program searches interactions between Lys or Arg and aromatic amino acids (Phe, Tyr, and Trp). The amino acids Lys and Arg are assumed to be protonated due to their pKs values of 10.67 (Lys) and 12.10 (Arg). [17] Fig. 1.2 shows the cation-π interactions found in 323 proteins. The authors found a cation-π interaction for every 77th residues of protein length and concluded that the cation-π interaction must also be taken into account as hydrogen bonds, salt bridges, and hydrophobic effects in the analysis of protein structures.

Factor Xa One of the most impressive examples of cation-π interactions in molecular recognition processes is found in the S4 pocket of factor Xa. [18–21] The serine endopeptidase Factor Xa plays a critical role in the blood coagulation pathway. The

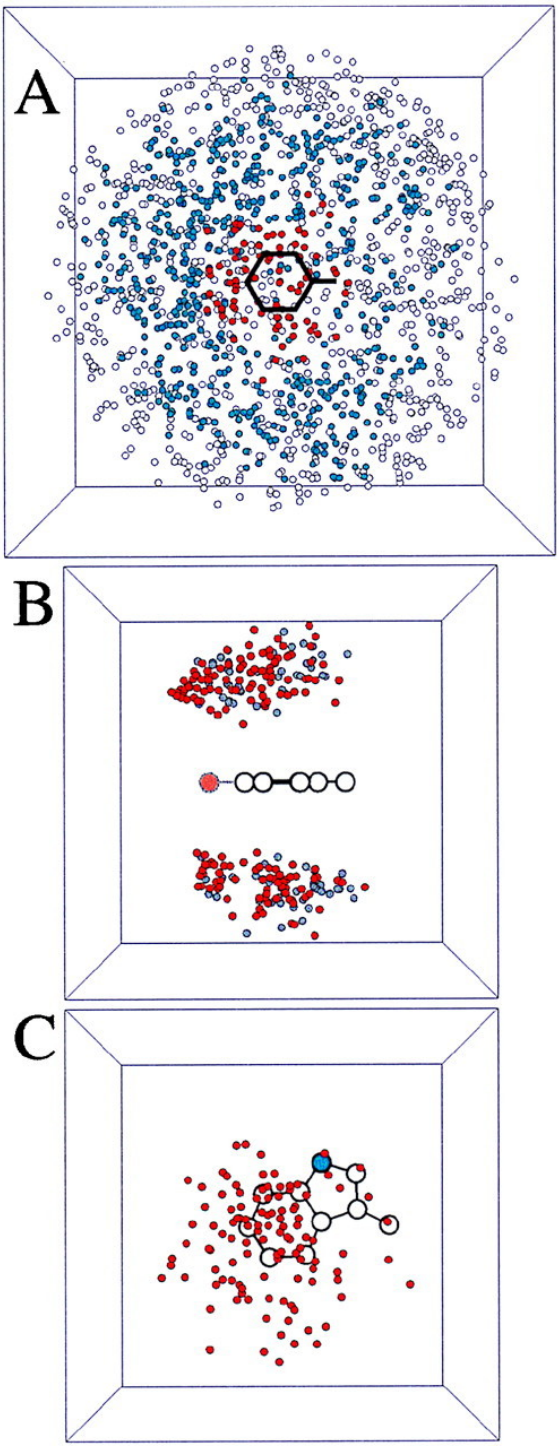

Figure 1.2.: Cation-π interactions in biological systems. Reprinted with permission from PNAS, 1999, 96 (17), 9459-9464.[16] Copyright by the National Academy of Sciences. A dot represents the location of the Lys sidechain nitrogen atom. The box size of A is 10x10x10 Å and the size of box B and C 7x7x7 Å. In (A) the red dots show an accepted cation-π interaction of a Lys/Phe pair. The blue and gray interactions do not fulfill the criteria of cation-π interactions. In (B) the interaction of Lys/Phe (blue) and Lys/Tyr (red), in (C) the Lys/Trp interactions are shown.

S4 pocket of factor Xa and the inhibitor (±)-1[‡] is shown in Fig. 1.3. The amino acid residues Tyr99, Phe174 and Trp215 form a pi-cage wherein the quarternary ammonium ion part of (±)-1 is located. The authors could show that the substitution of the quarternary ammonium ion with a *tert*-butyl residue leads to poorer inhibition [19] (the free enthalpy for the cation-π interaction decreases approximately 0.9 kcal/mol per aromatic ring), while the substitution to a trimethylphosphonium yields a similar binding affinity to factor Xa as (±)-1 [20]. Thus, the binding affinity of the cation-π interaction is not influenced by the size and nature of the cation.

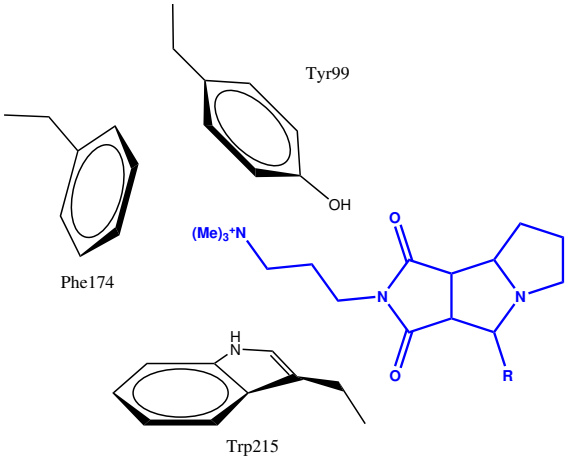

Figure 1.3.: Schematic representation of cation-π interaction in the S4 pocket of factor Xa (black) complexed with inhibitor (±)-1 (blue) (2BOK.pdb) [18]. The DFT-SAPT energies are shown in Tab 7.1 (p. 143).

1.2. Theoretical determination of non-covalent Interactions (NCI)

The exact theoretical description of NCI is still a hot topic in recent scientific research. One main problem is how to include long-range dispersion effects. This, however, can only be calculated using high level *ab initio* methods combined with

‡ [amino(4-(3aS,4R,8aS,8bR)-1,3-dioxo-2-[3-(trimethylammino)propyl]decahydropyrrolo[3,4-a]pyrro-lizin-4-ylphenyl)methylene]ammonium [18,19]

large basis sets. Hence, to compute the interaction energy of large molecules within the accuracy of high level methods, appropriate post Hartree-Fock, DFT (dispersion-corrected variants) or force field methods are needed. In the following chapter (1.2.1) the post HF and DFT methods will be compared and discussed. For the calculation of NCI in biomolecules (DNA, proteins) the use of force field methods is essential, and will be discussed in chapter 1.2.2.

To obtain the interaction energy (E_{int}) of a non-covalent bonded dimer the so-called supramolecular approach is commonly used. Regarding this approach the two monomers A and B form a molecular complex $A...B$ which is held together only by NCI (denoted by the expression ...). The resulting interacting energy is given by:

$$E_{int} = E_{product} - E_{reactants} = E(A...B) - (E(A) + E(B)) \,. \qquad 1.2.1$$

The interaction energy is negative for attractive forces between the monomers and positive in case of a repulsive interaction between A and B. Due to shortcomings in the used atomic orbital basis sets this procedure leads to a basis set superposition error (BSSE). During the calculation of the dimer energy the orbitals of A and B are present, whereas for the calculation of the monomers A and B only the orbitals of the respective monomer are available. That implies that the monomers contained in the dimer are better described by more basis functions than in the respective monomers alone, which results in a overestimation of the interacting energy. To avoid this overestimation Boys and Bernardi in 1970 suggested the counterpoise (CP) method.[22,23] Here the monomer energies are calculated within the full basis set of the dimer. The difference between the CP corrected energy and the uncorrected energy is the BSSE. The use of the CP method for the calculation of NCI is still a basis for discussions in recent literature.[24,25] The correction becomes less important by using large basis sets, but it always has to be taken into account since it depends on the system and the used method. It has to be pointed out that

some dispersion corrected DFT functionals (e.g. DFT-D3[26] and DFT-D3(BJ)[27]) include corrections to avoid the BSSE, in this case no CP correction should be used.

1.2.1. *Ab initio* Methods

In theoretical chemistry only the Full CI method can deliver the right results for the right reason. Due to the large computational afford other methods have to be used to approximate the exact values. Therefore, in the last years several benchmark studies[28] were performed using diverse data sets of non-covalent interacting dimer systems.[29–31] A selection of NCI based benchmark databases is listed below:

- IDISP (intramolecular dispersion interaction)[26,32–34]
- WATER27 (water clusters)[35]
- S22/S66 (non-covalent bond dimers)[1,36–39]
- ADIM6 (n-alkane dimers)[26]
- HEAVY28 (NCI between heavy element hydrides)[26]
- PCONF (relative energies of phenylalanyl-glycyl-glycine tripeptide conformers)[40]
- ACONF (relative energies of alkane conformers)[41]
- SCONF (relative energies of sugar conformers)[42,43]
- CYCONF (relative energies of cysteine conformers)[44]

The benchmark studies are used to select the right computational methods for the calculation of the respective NCI. Below the results for the most important methods are listed.

Full Configuration Interaction calculations (FCI) are exact but only feasible for small NCI complexes (e.g. $Li_2...H_2$, $LiH...H_2$, $BeH_2...H_2$, $LiH...Li_2$) and were performed by Hobza *et al.*[45] using the 6-31G* basis set to enable the possibility of such calculations. The results were used as reference values for the Coupled Cluster methods (CCSDTQP, CCSDTQ(P), and CCSDTQ).

Coupled Cluster Methods The CCSDTQP, CCSDTQ(P), and CCSDTQ methods are in accordance with the FCI results within an accuracy of 0.01 kcal/mol which was designated a NCI accuracy and corresponds to the spectroscopic accuracy of 1 cm^{-1}.

The CCSD(T)/CBS method (close to a complete basis set (CBS) limit) is usually taken as reference value in benchmark studies.[1,37] This method is the "Golden Standard in Calculation of Noncovalent Interactions"[25]. The CCSD(T) energies are exact within the "subchemical accuracy" of 0.1 kcal/mol according to Hobza *et al.*[45] The CCSD(T) procedure is the only genuine *ab initio* technique for computing NCI, since all quantities are calculated and no empirical parameter is adopted. The price for the high accuracy of the computational results is the enormous computational cost since the CCSD(T) method scales about N^7 with N = number of basis functions.

Møller-Plesset Perturbation Theory The MP2 method was commonly used in the past to calculate NCI since the moderate scaling (N^5) of this method allows the calculation of larger molecules using basis sets of moderate size. A drawback of this method is the underestimation of the uncoupled Hartree-Fock (UCHF) dispersion energy which results in an overestimation of NCI binding energies by as much as 20%. As a consequence, Hesselmann developed the MP2C (MP2 'coupled')[46] method where the intermolecular interaction energy derived by MP2 is corrected using TDDFT. Therein the UCHF dispersion contribution is replaced with the cou-

pled dispersion energy obtained from the time-dependent density functional theory (TDDFT) method. A further possibility to improve the MP2 method was developed by Hobza *et al* who establish the MP2.5 (scaling: N^6) method which combines the MP2 and MP3 (scaling: N^6) methods. This mixed method gives similar good energy values as the reference CCSD(T)/CBS method.[1,37]

Symmetry-Adapted Perturbation Theory Using the SAPT[47] method (for details see chapter 2.1) the NCI are calculated using a perturbation approach. To improve this method static and time-dependent DFT theory is used to calculate the intramolecular correlation effects of the individual SAPT terms. The resulting method is called SAPT(DFT)[48] or DFT-SAPT[49–52] (scaling N^6). (In this work the SAPT method as implemented in the Molpro program package[53] is used, hence it is called DFT-SAPT.) The pure SAPT method provides as accurate results as the high-level wave function based methods like CCSD(T). The DFT-SAPT method produces also very accurate values which are comparable to the SAPT method results if the exact density exchange-correlation (XC) functional and frequency-dependent XC kernel are known. The amount of works in the literature where the SAPT methods are used to get a deeper insight in the nature of NCI problems is very large and growing and prove the usefulness of this method.[54–77] The implementation of density fitting to approximate integrals in SAPT (DF-DFT-SAPT scales N^5) allows the computation of larger molecules. Hence, a better understanding of biological processes is provided by the SAPT method, since insight in the energy contributions between the biomolecules is possible.[78–80]

Density Functional Theory The scaling of density functional theory (DFT) methods - N^4 - allows the computation of rather large molecules in a reasonable time. The limitation of DFT is the poor description of dispersion interaction. In order to calculate the exact dispersion energy a nonlocal description of the total XC energy

is required. Since the XC energy in DFT is calculated using the electron density and the reduced electron density gradient the total XC is also local. Grimme *et al.* improved the DFT methods by adding an empirical dispersion function which also includes a correction term for the BSSE.[27,81,82] A benchmark of the resulting DFT-D methods[28,83] using NCI dimers yield highly accurate values. Unfortunately using the DFT-D method for the calculation of NCI is not a black box method. So it is still necessary to compare the DFT-D results with highly accurate methods. In addition, the nonlocal correlation functionals have been developed and tested.[84]

Semiempirical methods were primary developed for covalent bonding, so their use for non-covalent complexes was limited.[25] Recent implementations of the PM6 method add correction functions for dispersion interactions (empirical dispersion term) and hydrogen-bonding (additional electrostatic term) called DH correction to reach a chemical accuracy of $\sim$ 1 kcal/mol for non-bonded complexes.[85] The electrostatic term is directional and provide a better description of H-bonds compared to standard semiempirical QM methods. The second-generation of the DH correction developed by Korth *et al.*[86] improves the performance of PM6, AM1, OM3 and SCC-DFTB methods, since additional parameters describing H-bonds are included.

In conclusion, NCI calculations using CCSD(T) methods are very expensive. DFT methods on the other hand are less expensive, but need dispersion correction. For larger (e.g. biological) systems DFT proves to be too expensive. To tackle such problems accurate force fields are needed. To develop physically more grounded force fields (see chapter 2.2 we must calculate NCI with SAPT methods to understand the right physics of the interactions.

1.2.2. Force Field Methods

Non-covalent interactions play a major role in determining the structure of biomolecules. Since their functions are dependent on the structure the need of accurate force fields that can describe this non-covalent interactions is essential. The biggest problem is to describe all attractive (electrostatic, dispersion, and induction energy) and repulsive (exchange repulsion) energy contributions within a force field. The development of polarizable force fields certainly improved the contributions of the induction energy part[87], but unfortunately failed to address the other energy parts. In literature several force fields (MM2[88,89], MM3[90–93], AMBER[94–96], OPLS-AA[97–100], MMFF94[101–106]) were tested to see if they can reproduce the non-covalent interaction energies compared with high level quantum mechanical methods.[75,107] The authors, using the S22 and JCSH-2005 training data sets, conclude that the force field values agree quite well with the QM reference values, but they underestimate the strength of the H-bonded complexes. Furthermore, the force fields are less good in repulsive regions. As a reason for this they suggest that it is due to the bad description of the short-range repulsion. This issue was tackled by Tafipolsky and Engels[108] by adding a charge penetration energy term directly to the AMOEBA[109] force field. The so generated intermolecular potentials is believed to capture the right physics of intermolecular interactions and can reproduce high level QM results. In this thesis the work of Tafipolsky and Engels will be extended to describe cation-π interactions in gas phase and liquid environment with a physically grounded force field.

Experimental determination of non-covalent Interactions The experimental determination of NCI is a difficult task since there are only a few properties observable. A direct measurement of the structure of NCI complexes is not possible. An indirect alternative is to determine the structure from rotational constants measured from microwave spectroscopy. This method is used to study various molecular proper-

ties, i.a. non-covalent interactions of molecular clusters and biomolecules in the gas phase.[110–113] To measure the stabilization energy a mass-resolved version of the zero-electron kinetic energy spectroscopy (ZEKE)[114], namely mass analysed threshold ionization (MATI)[115], can be used as the only choice out of various experimental methods. The work of Müller-Dethlefs *et al.* studing the stabilization energy of phenol...N_2 and phenol...CO complexes demonstrates the success of this experimental method.[116–119] For further details concerning experimental methods of detection and characterization of non-covalent interactions including cation-π interactions the reviews in the literature should be used.[1,8,120]

1.3. Aim of this Work

This thesis seeks to obtain a more detailed insight into the cation-π interactions in biological systems by using an energy decomposition scheme, namely the DFT-SAPT method. Due to the lack of experimental data about cation-π interactions reliable theoretical description is necessary to predict the right behavior of the biological systems. Furthermore, these interactions should be expressed using a force field method. Therefore, the physically grounded force field introduced by Tafipolsky and Engels[108] will be tested and if necessary, modified to reproduce high level QM results using the force field avoiding error cancellation as much as possible. An important part is also the right description of the influence of environmental effects on cation-π interactions, e.g. the influence of explicit water molecules.

2. Methods and Computational Details

2.1. Symmetry-Adapted Perturbation Theory

The use of symmetry-adapted perturbation theory (SAPT) for calculating energies of intermolecular interactions brings several benefits. The SAPT method delivers results within the accuracy of CCSD(T) values, while the scaling of SAPT (N^7) is comparable with the scaling of CCSD(T) methods (N^7). Since intramonomer correlation effects are well described by DFT methods the combination from DFT and SAPT methods to SAPT(DFT) yields also highly accurate results and scales with N^5 using hybrid DFT and N^4 for non-hybrid DFT methods, which is comparable to the scaling of the Hartree-Fock (HF) method (N^4).[121] The second benefit is the decomposing of the interaction energy into electrostatic ($E_{el}^{(1)}$), exchange ($E_{exch}^{(1)}$), induction ($E_{ind}^{(2)}$), and dispersion energy ($E_{disp}^{(2)}$) as well as the exchange counterparts of the induction ($E_{ind-exch}^{(2)}$), and dispersion energy ($E_{disp-exch}^{(2)}$)

$$E_{int}^{SAPT} = E_{el}^{(1)} + E_{exch}^{(1)} + E_{disp}^{(2)} + E_{disp-exch}^{(2)} + E_{ind}^{(2)} + E_{ind-exch}^{(2)} + \delta(HF) \qquad 2.1.1$$

where

$$\delta(HF) = E_{int}^{SAPT}(HF) - E_{el}^{(1)}(HF) - E_{exch}^{(1)}(HF) - E_{ind}^{(2)}(HF) - E_{ind-exch}^{(2)}(HF). \qquad 2.1.2$$

The $\delta(HF)$ term is calculated as the difference between the counterpoise corrected HF total dimer interaction energy and the sum of uncorrelated SAPT contributions through second order in the intermolecular interaction operator.

The basic Ideas behind SAPT[121]

Within SAPT weak intermolecular interactions such as dispersion, induction and electrostatics only have a small influence on the distortion of molecules. Hence SAPT starts from unperturbed molecular systems (isolated monomers). As a first step the Schrödinger equations for isolated monomers A and B are solved:

$$\hat{H}_X \phi_X = E_X \phi_X \qquad X = A \text{ or } B \tag{2.1.3}$$

with the Hamiltonian operator ($\hat{H}_X$), the wave function (ϕ_X),and the energy (E_X) of monomer X. In the second step the monomers are considered (together) as one dimer system. SAPT calculates the interaction between the monomers by treating the interaction energy and wave function as small quantities resulting from the mutual perturbation of monomers by the Coulombic intermonomer interactions. In this configuration all electrons and nuclei of one monomer interact with all electrons and nuclei of the other monomer according to Coulomb's law. The total Hamiltonian ($\hat{H}$) of the dimer includes these Coulomb interactions which are summed up in the intermolecular interaction operator $\hat{V}$

$$\hat{H} = \hat{H}_A + \hat{H}_B + \hat{V} = \hat{H}_0 + \hat{V}. \tag{2.1.4}$$

The wave function of the unperturbed system ($\Psi^{(0)}$) can be treated as a product of the separated monomers wave functions ϕ_A and ϕ_B

$$\Psi^{(0)} = \phi_A \phi_B \qquad E^{(0)} = E_A + E_B. \tag{2.1.5}$$

The effects caused by the interaction operator can be calculated using the Rayleigh-Schrödinger (RS) perturbation theory.[47] In this case the interaction energy E_{int} is defined as the sum of perturbation corrections of the nth order $E_{RS}^{(n)}$

$$E_{int} = E_{RS}^{(1)} + E_{RS}^{(2)} + ... \ . \tag{2.1.6}$$

The drawback of this approach is the disability to predict the existence of van der Waals minima on potential energy surfaces.[122] This is caused by the fact that the unperturbed wave function $\Psi^{(0)}$ and the RS wave-function corrections do not fulfills the Pauli principle, namely the permutation (exchange) of electron between monomers does not give the same wave function relating to the sign. The so-called antisymmetrizer $\hat{A}$ is used to correct the wave function so that the resulting wave function $\hat{A}\Psi^{(0)}$ fulfill the Pauli principle. The operator $\hat{A}$ includes the sum of all intermonomer permutation operators with appropriate signs. In the case of two interacting hydrogen atoms containing the unperturbed orbitals a and b, with $\hat{A} = 1 - \hat{P}_{12}$ ($\hat{P}_{12}$ permutes electrons 1 and 2), so that

$$\hat{A}[a(1)b(2)] = a(1)b(2) - a(2)b(1). \tag{2.1.7}$$

From here on the RS theory can not be used anymore, since $\hat{A}\Psi^{(0)}$ is not an eigenfunction of $\hat{H}_0$. To solve this problem the so-called symmetry-adapted perturbation theories were developed which are able to use such an unperturbed function. A detailed description of the SAPT method is given in a review from Jeziorski et al.[47], a derivation of the method will go beyond the scope of this thesis, so I will focus on the fundamental ideas and limitations of SAPT. The symmetrized Rayleigh-Schrödinger (SRS) theory[123] provides the basic principles for the simplest possible SAPT expansion.

Rayleigh-Schrödinger (RS) Perturbation Method

In the polarization theory (an application of the RS perturbation method) the Hamiltonian ($\hat{H}$) for the dimer AB is extended by the parameter ξ, which defines the order of perturbation expansion.

$$(\hat{H}_0 + \xi\hat{V})\Phi_{AB} = E_{AB}\Phi_{AB} \tag{2.1.8}$$

The parameter ξ could be seen as a switch, since for $\xi = 0$ the intermolecular interaction operator $\hat{V}$ vanishes and the dimer energy becomes equal to the sum of the unperturbed monomers. For $\xi = 1$ all interactions included in $\hat{V}$ are also included in the Hamiltonian and the corresponding wave function $\Phi_{AB}(1)$ and energy $E_{AB}(1)$ become the exact, physical wave function and energy of the dimer.

The expression of the interaction energy ($E_{int} = E_{AB} - E_0$) is

$$E_{int}(\xi) = \langle\Phi_0|\xi\hat{V}\Phi_{AB}(\xi)\rangle \tag{2.1.9}$$

where the polarization series of the wave function and the interaction energy are defined as power series in ξ:

$$\Phi_{AB}(\xi) = \sum_{n=0}^{\infty} \xi^{(n)}\Phi_{pol}^{(n)} \tag{2.1.10}$$

$$E_{int}(\xi) = \sum_{n=1}^{\infty} \xi^{(n)}E_{pol}^{(n)} \tag{2.1.11}$$

The individual corrections $\Phi_{pol}^{(n)}$ and $E_{pol}^{(n)}$ are referred to as the nth-order polarization wave functions and polarization energies. The polarization energy of the nth-order is given by

$$E_{pol}^{(n)} = \langle\Phi_0|\hat{V}\Phi_{pol}^{(n-1)}\rangle \tag{2.1.12}$$

The polarization function is given by

$$\Phi_{pol}^{(n)} = -\hat{R}_0 \ \hat{V} \ \Phi_{pol}^{(n-1)} + \sum_{k=1}^{n-1} E_{pol}^{(k)} \ \hat{R}_0 \ \Phi_{pol}^{(n-k)}. \tag{2.1.13}$$

To solve this recursion equation the polarization function of zeroth order ($\Phi_{pol}^{(0)}$) is needed which is equal to the wave function of the unperturbed wave function $\Phi_0 = \Phi_A \ \Phi_B$. $\hat{R}_0$ (the reduced resolvent of $\hat{H}_0$) is defined as:

$$\hat{R}_0 = (\hat{H}_0 - E_0 + P_0)^{-1} Q_0 \tag{2.1.14}$$

$$= \sum_{m \neq 0} \frac{\mid \Phi_m \rangle \langle \Phi_m \mid}{E_m - E_0} \tag{2.1.15}$$

where $P_0 = \mid \Phi_0 \rangle \langle \Phi_0 \mid$ and $Q_0 = 1 - P_0$. $\hat{R}_0$ is the "inverse" of the singular operator $\hat{H}_0 - E_0$ which is in the space orthogonal to Φ_0. Φ_m are excited eigenfunctions and E_m, E_0 the representative eigenvalues.

Using the SAPT method the polarization energies through third order have an appealing, partly classical, physical interpretation. In the following the first-(electrostatic) and second-order (induction, dispersion) energies will be discussed shortly.

Electrostatic Interaction

The first-order polarization energy is defined as

$$E_{pol}^{(1)} = \langle \Phi_A \ \Phi_B \mid \hat{V} \ \Phi_A \ \Phi_B \rangle. \tag{2.1.16}$$

Using the operator $\hat{V}$ and integrateing over all coordinates of the electrons (except for one electron on the monomer A or monomer B), $E_{pol}^{(1)}$ could be represented in terms of the total charge distribution $\rho_A^{tot}(\mathbf{r})$ and $\rho_B^{tot}(\mathbf{r})$ of the monomers:

$$E_{pol}^{(1)} = \iint \rho_A^{tot}(\mathbf{r}_1)\frac{1}{r_{12}}\rho_B^{tot}(\mathbf{r}_2)\ d^3\mathbf{r}_1\ d^3\mathbf{r}_2 \qquad 2.1.17$$

with $r_{12} = \mid \mathbf{r}_1 - \mathbf{r}_2 \mid$. The total charge distribution of monomer A (in atomic units) is:

$$\rho_A^{tot}(\mathbf{r}) = \sum_\alpha Z_\alpha \delta(\mathbf{r} - \mathbf{R}_\alpha) - \rho_A(\mathbf{r}) \qquad 2.1.18$$

$Z_\alpha\delta(\mathbf{r}-\mathbf{R}_\alpha)$ represents the distribution of the positive point charges (Z_α) at the position of the nuclei (α). The electronic charge distribution ($-\rho_A(\mathbf{r})$) corresponds to the diagonal element of the first-order density matrix. The equations show the electrostatic (Coulomb) interaction of the monomers charge distributions. This energy could be written as sum of the classical electrostatic interactions between permanent multipoles of the unperturbed monomers at large intermonomer distances (R). The electrostatic energy also includes important short-range contributions due to the mutual overlap of the monomer electron clouds. This short-range terms are important for the exact description of van der Waals complexes.

Induction Interaction

The second-order polarization energy is given by:

$$E_{pol}^{(2)} = -\langle \Phi_0 \mid \hat{V}\ \hat{R}_0\ \hat{V} \mid \Phi_0 \rangle \qquad 2.1.19$$

$$= -\sum_{m\neq 0} \frac{\mid \langle \Phi_0 \mid \hat{V} \mid \Phi_m \rangle \mid^2}{E_m - E_0}. \qquad 2.1.20$$

The induction energy results if the sum of all states includes just the single excited eigenfunctions of $\hat{H}$, i.e. only functions of the form $\Phi_m = \Phi_A\Phi_B^*$ and $\Phi_m = \Phi_A^*\Phi_B$.

are considered. The energy resulting from $E^{(2)}_{pol}$ is denoted as $E^{(2)}_{ind}$ with:

$$E^{(2)}_{ind} = E^{(2)}_{ind}(A) + E^{(2)}_{ind}(B) \tag{2.1.21}$$

$$E^{(2)}_{ind}(A) = -\langle \Phi_A \mid \Omega_B \ \hat{R}^A_0 \ \Omega_B \mid \Phi_A \rangle. \tag{2.1.22}$$

Ω_B is the operator of the electrostatic potential which is generated from the unperturbed monomer B.

$$\Omega_B = \sum_{i \epsilon A} \omega_B(\mathbf{r}_i) \tag{2.1.23}$$

$$\omega_B(\mathbf{r}_i) = \int \frac{1}{r_{12}} \rho^{tot}_B(\mathbf{r}_j) \ d^3\mathbf{r}_j \tag{2.1.24}$$

$$\hat{R}^A_0 = (\hat{H}_A - E_A + P_A)^{-1} Q_A \tag{2.1.25}$$

$$P_A = \mid \Psi_A \rangle \langle \Psi_A \mid \tag{2.1.26}$$

$$Q_A = 1 - P_A \tag{2.1.27}$$

Dispersion Interaction

The second-order dispersion energy ($E^{(2)}_{disp}$) is defined as

$$E^{(2)}_{disp} = E^{(2)}_{pol} - E^{(2)}_{ind} \tag{2.1.28}$$

$$= -\langle \Phi_0 \mid \hat{V} \ \hat{R}^{AB}_0 \ \hat{V} \mid \Phi_0 \rangle \tag{2.1.29}$$

with $\hat{R}^{AB}_0 = \hat{R}_0 - \hat{R}^A_0 P_B - \hat{R}^B_0 P_A$ as the dispersion part of the resolvent $\hat{R}_0$. $\hat{R}_0$ includes only double excitation states $\Phi_m = \Phi^*_A \Phi^*_B$ in the sum-over-states formula eq. 2.1.19. An alternative possibility of writing this equation is:

$$E^{(2)}_{disp} = \langle \Phi_0 \mid \hat{V} \ \Phi^{(1)}_{disp} \rangle \text{ where} \tag{2.1.30}$$

$$\Phi^{(1)}_{disp} = -\hat{R}^{AB}_0 \ \hat{V} \Phi_0. \tag{2.1.31}$$

The Failure of Polarization Theory

The intermolecular interacting operator $\hat{V}$ causes a tunneling of the electron from the potential energy well at the nucleus A to that at nucleus B (and vice versa). A simultaneous tunneling of two electrons is called the electron exchange effect. In the case of two hydrogen atoms at large distances R the exact wave function becomes a linear combination of two equally weighted "resonance structures" $\Phi_0 = 1s_A(1)1s_B(2)$ and $P_{12}\Phi_0 = 1s_A(2)1s_B(1)$, the second of which cannot be recovered by a low-order polarization theory.

Expanding the system from a hydrogen atom dimer to a larger system with more electrons, more simultaneous electron tunneling processes are possible. For a system with N_A and N_B electrons there are $M = (N_A+N_B)!/(N_A!\,N_B!)$ possible "resonance structures". The zeroth-order polarization function represents only one of these M possible structures, since all except one of these M electron configurations violate the Pauli principle the wave function has to be approximated. This is done by antisymmetrization of any of the M possible wave functions (usually Φ_0).

SAPT - Weak Symmetry Forcing

As shown above the correct zeroth-order wave function is $\mathcal{A}\Phi_0$ ($\mathcal{A}$: antisymmetrizer) instead of Φ_0. The wave function $\mathcal{A}\Phi_0$ could not be used in RS perturbation theory since it is not an eigenfunction to $\hat{H}_0 = \hat{H}_A + \hat{H}_B$. A possibility to avoid this problem is to modify the perturbation method in that way that $\mathcal{A}\Phi_0$ could be used. This is usually done by the so called *weak symmetry adaption/forcing* using the symmetrized Rayligh-Schrödinger (SRS) theory. Here the antisymmetrizer $\mathcal{A}$ is only used in the energy expressions. The perturbation equations do not include $\mathcal{A}$. The antisymmetrizer is used in eq. 2.1.9 to project away all Pauli forbidden configurations of the wave function $\Phi_{AB}(\zeta)$. The resulting expression for the SRS

interacting energy is:

$$E_{SRS}(\zeta) = \frac{\langle \Phi_0 \mid \zeta \, \hat{V} \, \mathcal{A} \, \Phi_{AB}(\zeta) \rangle}{\langle \Phi_0 \mid \mathcal{A} \, \Phi_{AB}(\zeta) \rangle} \tag{2.1.32}$$

where the wave function $\Phi_{AB}(\zeta)$ is still the same as mentioned before in the polarization theory. The individual perturbation energies $E^{(n)}_{SRS}$ are defined by expanding $E_{SRS}(\zeta)$ in powers of ζ

$$E^{(n)}_{SRS} = N_0(\langle \Phi_0 \mid \hat{V} \, \mathcal{A} \, \Phi^{(n-1)}_{pol} \rangle - \sum_{k=1}^{n-1} E^{(k)}_{SRS} \langle \Phi_0 \mid \mathcal{A} \, \Phi^{(n-k)}_{pol} \rangle) \tag{2.1.33}$$

with $N_0 = \langle \Phi_0 \mid \mathcal{A} \, \Phi_0 \rangle^{-1}$ and $\Phi^{(k)}_{pol}$ are the polarization functions given by eq. 2.1.13. By decomposing the antisymmetrizer into contributions of inter- and intramonomer permutations of electrons one can show that the nth-order SRS correction is a sum of the nth-order polarization energy $E^{(n)}_{pol}$ and the short-range correction involving those parts of $\mathcal{A}$ which interchange electrons between monomers

$$E^{(n)}_{SRS} = E^{(n)}_{pol} + E^{(n)}_{exch}. \tag{2.1.34}$$

These short-range corrections represent an exchange effect and are denoted as $E^{(n)}_{exch}$. The low-order exchange corrections have also a simple physical interpretation due to their close relationship to the low-order polarization functions.

First-order Exchange

The first-order energy is:

$$E^{(1)} = \frac{\langle \Phi_0 \mid \hat{V} \, \mathcal{A} \, \Phi_0 \rangle}{\langle \Phi_0 \mid \mathcal{A} \, \Phi_0 \rangle} \tag{2.1.35}$$

This energy is identical with the so called Heitler-London energy (E_{HL}):

$$E_{HL} = \frac{\langle \mathcal{A}\ \Phi_0 \mid \hat{H} - E_A - E_B \mid \mathcal{A}\ \Phi_0 \rangle}{\langle \mathcal{A}\ \Phi_0 \mid \mathcal{A}\ \Phi_0 \rangle} \tag{2.1.36}$$

To separate the exchange and polarization part from $E^{(1)}$ the antisymmetrizer has to be split up:

$$\mathcal{A} = \frac{N_A! N_B!}{(N_A + N_B)!} \mathcal{A}_A \mathcal{A}_B (1 + \mathcal{P}) \tag{2.1.37}$$

where $\mathcal{A}_A$ and $\mathcal{A}_B$ are the antisymmetrizers of the monomers A and B. $\mathcal{P}$ includes all permutations which include at least one pair of electrons which permute between both monomers. Using eq. 2.1.37 one gets:

$$E^{(1)} = E^{(1)}_{pol} + E^{(1)}_{exch} \tag{2.1.38}$$

$$\tag{2.1.39}$$

where

$$E^{(1)}_{exch} = \frac{\langle \Phi_0 \mid (\hat{V} - \overline{\hat{V}}) \mathcal{P}\ \Phi_0 \rangle}{1 + \langle \Phi_0 \mid \mathcal{P}\ \Phi_0 \rangle} \tag{2.1.40}$$

and $\overline{\hat{V}} = \langle \Phi_0 \mid \hat{V}\ \Phi_0 \rangle$.

At the vdW distance $E^{(1)}_{exch}$ includes over 90% of the total exchange energy. In view of eq. 2.1.36 $E^{(1)}_{exch}$ gives the expectation value of the full Hamiltonian resulting from the easiest possible zeroth-order wave function $\mathcal{A}\Phi_0$, which represents all possible electron permutations. For monomer distances around the vdW minima eq. 2.1.40 could be simplified by considering only single electron exchanges and neglect all higher-order electron permutations. The resulting approximated value of $E^{(1)}_{exch}(S^2)$ depends quadratic on the intermolecular overlap integral $S_{\lambda\mu} = \langle \phi_\lambda \mid \phi_\mu \rangle$, or more

precisely from the intermolecular density overlap $\varrho_{\lambda\mu}(\mathbf{r}) = \phi_\lambda(\mathbf{r})\phi_\mu(\mathbf{r})$.

$$E^{(1)}_{exch}(S^2) = -\langle \Phi_0 \mid (\hat{V} - \overline{\hat{V}})\mathcal{P}_1 \ \Phi_0 \rangle \tag{2.1.41}$$

where $\mathcal{P}_1$ is the sum of all $N_A N_B$ permutations of electrons between the monomers.

Exchange-Induction Interaction

The second-order exchange energy is given in SRS theory as $E^{(2)}_{exch} = E^{(2)}_{SRS} - E^{(2)}_{pol}$ and could be separated in two components, exchange-induction and exchange-dispersion:

$$E^{(2)}_{exch} = E^{(2)}_{exch-ind} + E^{(2)}_{exch-disp} \tag{2.1.42}$$

For distances around the vdW minima it is sufficient to consider only the single exchange contribution from the exchange-induction interaction. Within this approximation $E^{(2)}_{exch-ind}$ is given with:

$$E^{(2)}_{exch-ind}(S^2) = -\langle \Phi_0 \mid (V - \overline{V})(\mathcal{P}_1 - \overline{\mathcal{P}_1})\Phi^{(1)}_{ind} \rangle \tag{2.1.43}$$

where $\overline{\mathcal{P}_1} = \langle \Phi_0 \mid \mathcal{P}_1 \Phi_0 \rangle$ and $\Phi^{(1)}_{ind} = \Phi^{(1)}_{ind}(A)\Phi_B + \Phi_A \Phi^{(1)}_{ind}(B)$. $\Phi^{(1)}_{ind}(A)$ and $\Phi^{(1)}_{ind}(B)$ are the induction functions of the deformation of the monomer wave function which is induced by the average electrostatic field from the interacting partner. As the repulsive part of the intermolecular potential the exchange-induction energy quenches an important part of the induction contribution and must not be neglected in quantitative calculations.

Exchange-Dispersion Interaction

The exchange-dispersion interaction $E^{(2)}_{exch-disp}$ is an energetic effect of the antisymmetrization of the dispersion function $\Phi^{(1)}_{disp}$, as already mentioned in chapter 2.1.

The assumption that the single exchange is sufficient is also done here:

$$E^{(2)}_{exch-disp}(S^2) = -\langle \Phi_0 \mid (\hat{V} - \overline{\hat{V}})(\mathcal{P}_1 - \overline{\mathcal{P}_1})\Phi^{(1)}_{disp}\rangle \qquad 2.1.44$$

The calculation of $E^{(2)}_{exch-disp}(S^2)$ for many electron systems is complicated, since this value could not be expressed in terms of monomer properties. The exchange-dispersion part is relatively small and quenches only a few percent of the dispersion energy.

DFT-SAPT[49–52]

The first- and second-order electrostatic properties for the intramolecular correlation effects resulting from SAPT, or better Hartree-Fock SAPT (HF-SAPT), are often inaccurate. In contrast to HF-SAPT static and time-dependent DFT theory is able to compute the polarization terms ($E^{(1)}_{pol}$, $E^{(2)}_{ind}$, $E^{(2)}_{disp}$) are potentially exact. Assuming that the exact exchange-correlation (xc) potential and the exact (frequency-dependent) xc response kernel of the monomers were known the polarization terms would be exact. Kohn-Sham (KS) theory can only provide a good approximation to the exact density matrix of a many-body system, so the resulting exchange terms are not exact. The solution to correct the wrong asymptotic behavior of the xc potential is the asymptotic correction approach of Grüning *et al.*[124] A shift parameter (Δ_{xc}) for the bulk potential is established as the difference between the HOMO energy (ε_{HOMO}) obtained from the respective standard KS calculation and the (negative) ionization potential (IP) of the respective monomers.

$$\Delta_{xc} = \varepsilon_{HOMO} - (-IP) \qquad 2.1.45$$

For the investigation of large molecules a density fitting approach can be used to approximate the integrals in DFT-SAPT.[125] In this thesis all SAPT calculations are performed using the DF-DFT-SAPT method, however, the name is simplified

to DFT-SAPT.

The resulting terms from DFT-SAPT method and the physical interpretation are: [3]

- Electrostatic energy ($E_{el}^{(1)}$): classically calculated interaction energy derived from unperturbed Kohn-Sham (KS) charge distribution
- Exchange repulsion ($E_{exch}^{(1)}$): the exchange of electrons between KS monomers results in a modification to the first-order energy - also called the closed-shell repulsion
- Induction energy ($E_{ind}^{(2)}$): the unperturbed KS charge distribution of one monomer causes a field which distorts the other monomer
- Exchange induction ($E_{ind-exch}^{(2)}$): arises when exchange effects are taken into account
- Dispersion energy ($E_{disp}^{(2)}$): the correlated fluctuations of KS electron distributions of each monomer produce the dispersion energy
- Exchange dispersion ($E_{disp-exch}^{(2)}$): arises when exchange effects are taken into account
- Induction correction ($\delta(HF)$): includes the estimate of higher-order terms

2.2. Force Field Methods - Why do we need another Force Field?

The SAPT method splits the total interaction energy into physically meaningful parts which can be directly compared with the counterparts derived from force field

methods:

$$E_{Int} = E_{el}^{(1)} + E_{exch}^{(1)} + E_{disp}^{(2)} + E_{disp-exch}^{(2)} + E_{ind}^{(2)} + E_{ind-exch}^{(2)} + \delta(HF) \quad 2.2.1$$

$$E_{El} = E_{el}^{(1)} \quad 2.2.2$$

$$E_{vdW} = E_{exch}^{(1)} + E_{disp}^{(2)} + E_{disp-exch}^{(2)} \quad 2.2.3$$

$$E_{Disp} = E_{disp}^{(2)} + E_{disp-exch}^{(2)} \quad 2.2.4$$

$$E_{Pol} = E_{ind}^{(2)} + E_{ind-exch}^{(2)} + \delta(HF) \quad 2.2.5$$

To distinguish energy terms derived from SAPT methods and energy terms derived from force field methods the following nomenclature is used: the energy terms derived from SAPT calculations are named with small letters, while the energy terms used in force fields begin with a capital letter. In this work the AMOEBA09 force field[?] is used as a concrete example to demonstrate the weak points of modern force fields. The electrostatic interaction is well defined for long and short distances, until the nuclei come into contact. That means the electrostatic interaction has a finite energy even if the molecules overlap strongly. Since the electrostatic energy is described as power series of $1/R$ the series diverges as $R \to 0$.[3] Consequently, the electrostatic energy derived from multipole expansion represents only the long-range (sufficiently large R) contribution to the exact electrostatic energy. The truncation of the power series results in a so called "truncation error". This means that charge penetration effects (see page 5) are not taken into account in common force fields. Since the power series treats molecules as points which do not extend into space, the resulting error is called "penetration error".

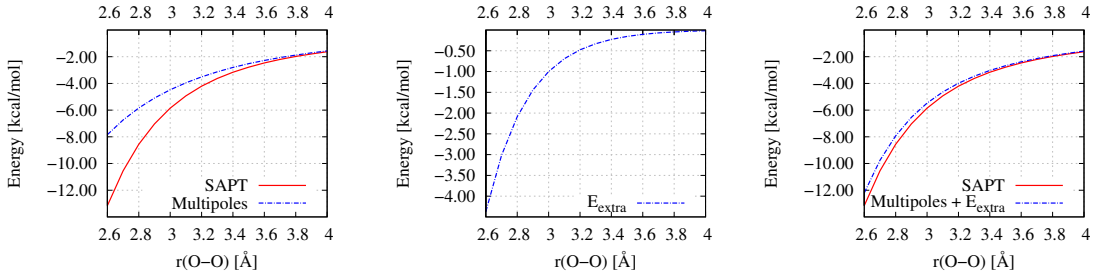

Figure 2.1.: Electrostatic energy of OH water dimer (see p. 62 for more detailed information) derived from multipole expansion as implemented in AMOEBA force field (left) and corrected electrostatic energy as implemented in the new modified force fields (right). The correction term E_{extra} is shown in the middle. The total electrostatic energy derived from the DFT-SAPT method is shown as a reference. The total energy minimum of the OH water dimer lies at r(O-O)=3.0 Å.

As an example, in Fig. 2.1 (left picture) the electrostatic energy of the water dimer, derived from SAPT and multipole expansion is shown. The force field energy is too repulsive compared with the exact electrostatic energy, since the short-range electrostatic effects are neglected. To include these effects, Spackman suggested to use the promolecule density to approximate the penetration contribution to the intermolecular electrostatic energy.[126] This short-range interaction involves a sum over Coulombic interactions between pairs of spherical atomic charge densities. The energy between atoms a and b separated by R is

$$E_{ab}(R) = \frac{2}{\pi}\int_0^\infty [Z_a - f_a(s)]\,[Z_b - f_b(s)]\,\frac{sin(sR)}{sR}ds \qquad 2.2.6$$

where Z_a is the nuclear charge, $f_a(s)$ the atomic scattering factor as a function of the scattering vector ($s = 4\pi sin\Theta/\lambda$)) defined in terms of the spherical atomic electron density, $\rho(r)$ (r is the electron radial coordinate), by the expression

$$f_a(s) = 4\pi\int_0^\infty \rho_a(r)\frac{sin(sr)}{sr}dr. \qquad 2.2.7$$

The electron densities are obtained analytically from atomic ground-state wave functions expanded in Slater-type functions developed by Su and Coppens.[127] Tafipolsky and Engels[108] modified Eq. 2.2.6 by including a parameter "kappa" to contract ($\kappa > 1$) or expand ($\kappa < 1$) the radial dependence of the spherical valence charge densities of the atoms. By including the expansion-contraction parameters ("kappa") in Eq. 2.2.6 one gets

$$E_{ab}(R) = \frac{2}{\pi} \int_0^\infty \left[Z_a - f_a(s/\kappa_a)\right] \left[Z_b - f_b(s/\kappa_b)\right] \frac{sin(sR)}{sR} ds = E_{extra}. \qquad 2.2.8$$

The resulting E_{extra} energy term is shown in Fig. 2.1 (middle). According to Spackman this energy term can be a large, and sometimes even the dominant, contribution to the total electrostatic energy. Tafipolsky[128] used a genetic algorithm (GA) PIKAIA[129] (which was introduced by Charbonneau to model the rotation curve of galaxies) to optimize the expansion-contraction parameters (Eq. 2.2.8). The root-mean-square deviation

$$rmsd = \sqrt{\frac{\sum_{i=1}^{N} (E_{ref}^i - E_{model}^i)^2}{N}} \qquad N = \text{number of dimers} \qquad 2.2.9$$

is used as a fitness function between the exact electrostatic energies (SAPT) and the sum of the long-range part (distributed multipoles) and the short-range part represented by a sum of Coulombic interactions between spherical atoms.

atom class	κ
C (benzene) [108]	1.0
H (benzene) [108]	1.4
N (ammonium ion) [130]	0.93
H (ammonium ion) [130]	3.5
O (water) [131]	0.86
H (water) [131]	3.7

Table 2.1.: Expansion-contraction parameters "kappa" used in FF-SAPT 1 and FF-SAPT 2.

Since the resulting electrostatic energy term is more attractive compared to the original term, the repulsive part of vdW term, has to be adjusted. Comparing the AMOEBA vdW energy term with the corresponding SAPT energy, the AMOEBA energy is too attractive. To adjust the vdW energy term, two parametrization strategies are used: (1) the standard vdW potential (buffered 14-7) was fitted against the energies obtained from SAPT computations, and (2) the dispersion and exchange-repulsion parts of the vdW energy are fitted separately. The force field resulting from (1) is named FF-SAPT 1 [130] and the one resulting from (2) is called FF-SAPT 2 [131]. In commonly used force fields the short-range electrostatic contribution due to charge penetration is considered in the "repulsion" part of the vdW term. Since the new force fields include explicitly the short-range contribution in the electrostatic energy term, the parameters of the vdW term have to be readjusted appropriately.

FF-SAPT 1: [108,130] In FF-SAPT 1 the functional form of the vdW energy term (Eq. 2.2.10) used in AMOEBA force field is adopted, since the buffered 14-7 form provides a better fit to *ab initio* gas phase results and liquid properties of noble gases. For heterogeneous atom pairs the cubic-mean combination rule for minimum-energy distances R^0 (Eq. 2.2.11) and the harmonic mean of the harmonic- and geometric-mean (HHG) values for the well depth ϵ (Eq. 2.2.12) are used. As fitness function for the GA the RMSD between the vdW energy derived from SAPT calculations

(Eq. 2.2.3) and the vdW part of the force field is used to re-optimize the parameters atom size (r in Å), homoatomic well depth (ϵ in kcal/mol), and reduction factor of the hydrogen atoms.

$$U_{vdW}^{Buf-14-7}(ij) = \epsilon_{ij} \left(\frac{1.07}{p_{ij} + 0.07} \right)^7 \left(\frac{1.12}{p_{ij}^7 + 0.12} - 2 \right) \quad 2.2.10$$

$$R_{ij}^0 = \frac{(R_{ii}^0)^3 + (R_{jj}^0)^3}{(R_{ii}^0)^2 + (R_{jj}^0)^2} \quad 2.2.11$$

$$\epsilon_{ij} = \frac{4\epsilon_{ii}\epsilon_{jj}}{(\sqrt{\epsilon_{ii}}\sqrt{\epsilon_{jj}})^2} \quad 2.2.12$$

ϵ_{ij} [kcal/mol]: potential well depth, $p_{ij} = R_{ij}/R_{ij}^0$, R_{ij} [Å]: actual distance between i and j, R_{ij}^0 [Å]: minimal distance

atom class	r [Å]	ϵ [kcal/mol]	reduction
C (benzene) [130]	4.23	0.0412	
H (benzene) [130]	3.18	0.0143	0.91
N (ammonium ion) [130]	3.41	0.0568	
H (ammonium ion) [130]	3.18	0.0143	0.78
O (water)	3.33	0.0847	
H (water)	3.66	0.0103	0.88

Table 2.2.: Refined parameters for vdW terms in FF-SAPT 1.

The advantage of the FF-SAPT 1 force field is that the best functional form (buffered 14-7) can be used without adding more parameters to that energy expression. The SAPT method provides a separation of the repulsive exchange and the attractive dispersion energy part. A significant drawback of the buffered 14-7 potential is that these two energy parts can not be fitted separately.

FF-SAPT 2: [131] The second force field based on SAPT results divides the vdW energy in an exchange-repulsion and dispersion part. The advantage of the Buck-

ingham potential approach (Eq. 2.2.13) is the ability to fit the repulsive and the attractive energy contributions separately. The repulsive part (Eq. 2.2.14) is represented by the Born-Mayer potential, while the dispersion (Eq. 2.2.15) energy is represented by the London formula which is damped at short distances using a universal damping function (Eq. 2.2.16). The damping factor of water was chosen twice as large(0.78) as usual one (0.39).

$$U_{vdW}^{Buckingham}(R) = U_{exch-rep}(R) - U_{disp}(R) \tag{2.2.13}$$

$$U_{exch-rep}(R) = 290000 A_{ab} e^{-B_{ab}R} \tag{2.2.14}$$

$$U_{disp}(R) = f_{damp}(\beta_{ab}R)\frac{C_{ab}}{R^6} \tag{2.2.15}$$

$$f_{damp}(\beta R) = 1 - e^{-\beta R}\sum_{n=0}^{6}\frac{(\beta R)^n}{n!} \tag{2.2.16}$$

R is the interatomic distance and $A_{ab}, B_{ab}, C_{ab}, \beta_{ab}$ are the fitted parameters between atoms a and b. The parameters B and β are combined for unlike atoms using a harmonic rule, and A and C are combined using a geometric combining rule (Eqs. 2.2.17-2.2.20).

$$A_{ab} = \sqrt{A_{aa}A_{bb}} \tag{2.2.17}$$

$$B_{ab} = \frac{2B_{aa}B_{bb}}{B_{aa} + B_{bb}} \tag{2.2.18}$$

$$C_{ab} = \sqrt{C_{aa}C_{bb}} \tag{2.2.19}$$

$$\beta_{ab} = \frac{2\beta_{aa}\beta_{bb}}{\beta_{aa} + \beta_{bb}} \tag{2.2.20}$$

atom class	A [kcal/mol]	B [1/Å]	C [kcal/mol Å^6]	β [1/Å]
C (benzene)[131]	0.1017	3.090	647	3.861
H (benzene)[131]	0.0035	3.458	29	4.441
N (ammonium ion)	0.4332	3.856	445	4.3596
H (ammonium ion)	0.0017	3.684	8	4.9800
O (water)[131]	0.2719	3.662	673	3.439
H (water)[131]	0.0011	3.240	13	4.113

Table 2.3.: Parameters for vdW terms in FF-SAPT 2.

The focus of developing new force fields should include the right reproduction of physically interpretable components even if more parameters are needed to derive this.

2.3. Geometries and Computational Details

Geometries The geometries of the ammonium cation and the benzene were optimized using the RI-MP2/TZVPP method as implemented in the Turbomole 6.5[132] program. The optimized monomer structures (ammonium cation: d(N-H)=1.0268 Å; benzene: d(C-C)=1.3934 Å, d(C-H)=1.0837 Å) are merged to dimer structures to get the respective systems studied in chapter 3. The vibrationally averaged[133] monomer structure of water (d(O-H)=0.9716 Å, ϕ(H-O-H)=104.690°) was used for the calculation of water dimers.[134]

To develop and test the new force field (see chapter 2.2) two separate data sets were used. A training data set, including homodimers only, was generated to fit the parameters for the FF-SAPT 1 and FF-SAPT 2, respectively. To verify the performance of the force fields a validation data set was established. The training data set for the parametrization of water contains 2510 water dimers including, among others, vicinities of minima and saddle points, and characteristic configurations for liquid water and ice.[135] The interaction energy of the water dimers is also taken

from Ref.[135].

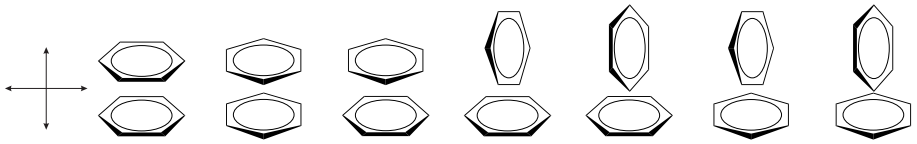

Figure 2.2.: Training data set of benzene dimers in sandwich (left) and t-shaped (right) arrangement. The dimers are shifted horizontal and vertical along the shown axis which results in 155 dimer conformations.[130]

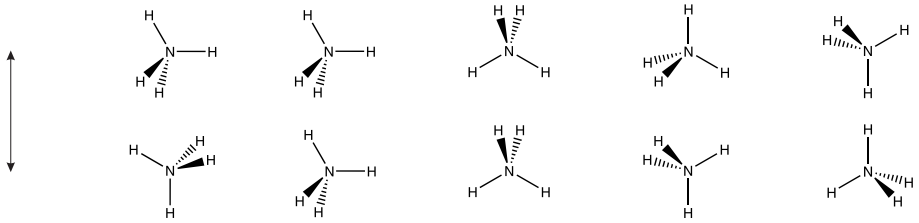

Figure 2.3.: Training data set of ammonium cation dimers. The dimers are shifted along the shown axis which yields 54 dimer conformations.[130]

Energies As reference values all stabilization energies were calculated using the CCSD(T) method combined with the aug-cc-pVXZ (X = D, T) basis set (abbreviated as avdz or avtz) as implemented in Gaussian09 program[136]. The resulting interaction energies were BSSE corrected using the counterpoise correction of Boys and Bernardi.[22,23].

DFT-SAPT calculations: Density functional theory(DFT)/symmetry-adapted perturbation theory[47] (SAPT) (DFT-SAPT[49–52,67]) as implemented in the MOLPRO 2010.1[53] program package was used to calculate the dimer interaction energy and to separate the interaction energy (E_{int}^{SAPT}) into a sum of physically meaningful terms, namely the electrostatic ($E_{el}^{(1)}$), exchange ($E_{exch}^{(1)}$), dispersion ($E_{disp}^{(2)}$), dispersion-exchange ($E_{disp-exch}^{(2)}$), induction ($E_{ind}^{(2)}$), and induction exchange ($E_{ind-exch}^{(2)}$) energies. The DFT-SAPT method would yield the exact polarization terms ($E_{el}^{(1)}$, $E_{disp}^{(2)}$, $E_{ind}^{(2)}$) if the exact exchange-correlation (xc) potential and the exact exchange-correlation

response kernel of the monomers were known. To correct the wrong asymptotic behavior of the exchange-correlation potential in DFT functionals the gradient-regulated asymptotic correction approach of Grüning et. al.[124] is used. Therefore, a shift parameter (Δ_{xc}) for the bulk potential, the difference between the HOMO energy (ϵ_{HOMO}) and the (negative) ionization potential (IP) from the respective monomer, is used (see Tab. 2.4).

	calc.		exp.
	ϵ_{HOMO}	IP	IP
C_6H_6	-0.2679	0.342339730	0.339702526[137]
NH_4^+	-0.8365	0.976410420	
H_2O	-0.3339	0.466015424	0.463813027[137]

Table 2.4.: Experimental and computed (PBE0/avdz) ionization potentials with the corresponding energies of the highest occupied molecular orbitals (HOMO). These energies are needed to calculate the asymptotic correction via $\Delta_{xc} = \epsilon_{HOMO} - (-IP)$. Energies are in atomic units (a.u.).

To obtain the ϵ_{HOMO} and IP values PBE0/avtz calculations were performed using MOLPRO 2010.1[53] program package. The exchange-correlation potential DFT calculation was performed using the PBE0AC[124,138–142] functional. To decrease the computational effort the density fitting DFT-SAPT[125] (DF-DFT-SAPT) was used to approximate the integrals in SAPT. It allows to calculate larger molecules with reasonable basis sets. Nevertheless, the size of the used basis set was not large enough to derive a converged dispersion part. This well known problem could be solved by an extrapolation of the dispersion energy to the complete basis set limit (CBS) using Eqs. 2.3.1 (DT extrapolation) and 2.3.2 (TQ extrapolation).[143–145]

$$E_{Disp}^{SAPT}(CBS) = \frac{3^3 E_{Disp}^{SAPT}(avtz) - 2^3 E_{Disp}^{SAPT}(avdz)}{3^3 - 2^3} \quad 2.3.1$$

$$E_{Disp}^{SAPT}(CBS) = \frac{4^3 E_{Disp}^{SAPT}(avqz) - 3^3 E_{Disp}^{SAPT}(avtz)}{4^3 - 3^3} \quad 2.3.2$$

3. Results

This chapter is constructed in the following way. After the short introduction of an example, the interactions of the respective model systems are analyzed using DFT-SAPT calculation results. In doing so the total interaction energies are compared to CCSD(T) energies. Further the absolute energies of the energy decomposition are compared as well as the energy contribution to the overall stabilization energy of the attractive energy parts. Finally, the performance of the newly developed force fields is tested by comparing with the DFT-SAPT results. The chapter is closed with a summary and conclusion.

3.1. Example: Factor Xa

To demonstrate the importance of cation-π interactions in biological systems the interaction of factor Xa with the ligand (±)-1 was selected (see section 1.1.1). The S4 pocket of this enzyme is formed by three aromatic residues, namely Tyr99, Phe174, and Trp215. The trimethylammonium residue of the inhibitor (±)-1 is located inside this aromatic pocket (Fig. 3.1). To calculate the individual interaction energies between the cation and the respective aromatic systems the model system shown in Fig. 3.1 on the right hand side was cut out of the X-ray crystal structure (2BOK.pdb[18]). For the computation the ligand is simplified to a tetramethylammonium cation (TMA), while the amino acid residues are simplified to benzene, phenol, and indole. Since we investigate biological systems, the calculated interactions are still named by its amino acid nomenclature. The added hydrogens were optimized using the SCS-MP2/TZVP method, while the positions of the heavy atoms were

kept fixed. The DFT-SAPT and CCSD(T) calculations are performed as described in the previous chapter.

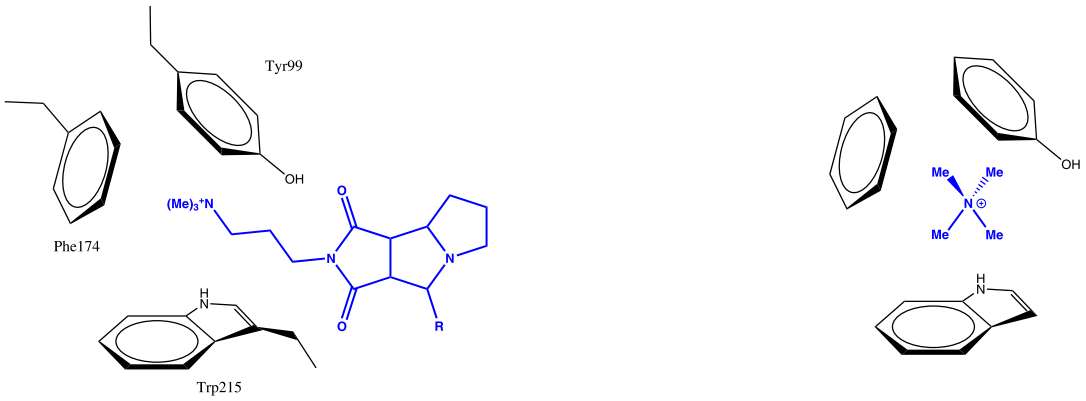

Figure 3.1.: Schematic representation of cation-π interactions in the S4 pocket of factor Xa (black) complexed with inhibitor (±)-1 (blue) (2BOK.pdb)[18]. The DFT-SAPT energies are shown in Tab. 7.1 (p. 143).

The separate interaction energies between TMA and Phe (-6.3), Tyr (-7.4), and Trp (-9.3 kcal/mol) indicate a strong NCI between the cation and the representative aromatic system. The calculated results indicate that due to a larger number of interacting atoms ($N_{atoms}(Phe) < N_{atoms}(Tyr) < N_{atoms}(Trp)$) the NCI energy increases. This is a first hint to the important influence of the electrostatic interaction to the total interaction energy. Considering the contribution of the attractive energy parts to the total stabilization energy, as shown in Fig. 3.2, the electrostatic energy part amounts two-thirds of the interaction energy. The induction and dispersion energies contribute almost equally and account for about one-sixth of the overall attractive energy, respectively. Compared with hydrogen bonding in a water dimer interaction (around -5 kcal/mol[146]), the studied cation-π interactions are up to two times stronger.

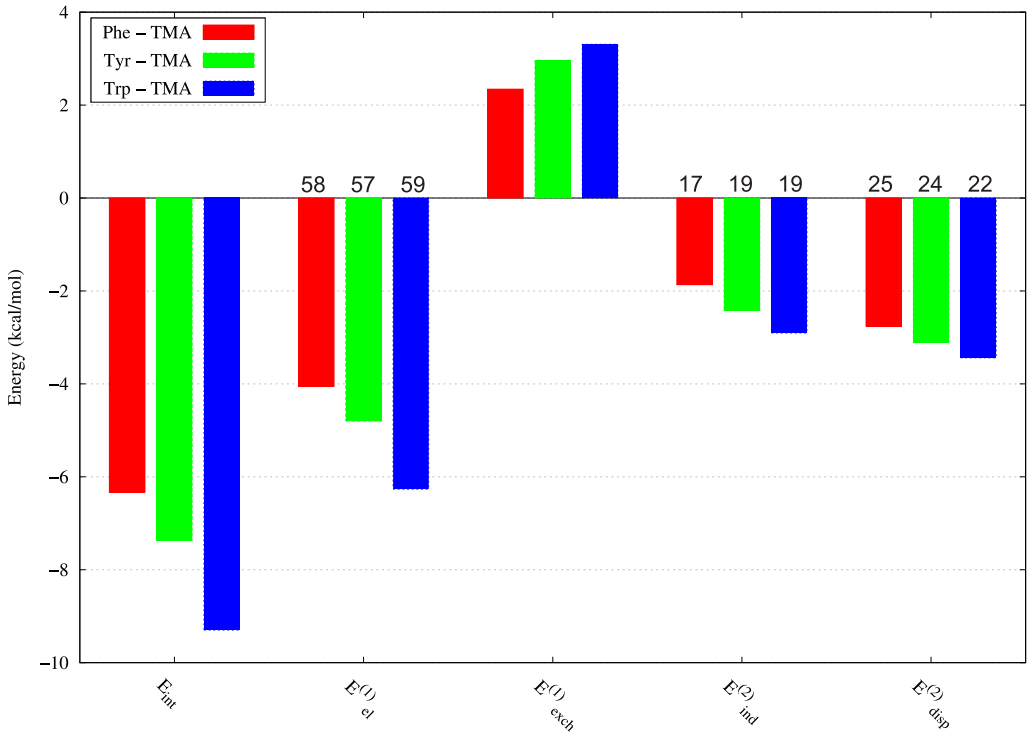

Figure 3.2.: DFT-SAPT/avtz energy decomposition of the separate interactions of tetramethylammonium with benzene, phenol, and indole representing the model system of the factor Xa S4 pocket. The contributions to the total attractive energy in % for the electrostatic, dispersion and induction energy are given within the separate numbers above bars.

3.2. $C_6H_6...NH_4^+$ Dimer

3.2.1. Validation of Methods using the optimized Dimer Geometry

As a model system for the investigation of the cation-π interaction the $C_6H_6...NH_4^+$ dimer was used. To obtain the minimum energy structure the dimer was pre-optimized using the B-LYP/TZVP method followed by an optimization using the MP2/avtz method. The optimized structure is illustrated in Fig. 3.3. The ammonium ion is located nearly perpendicular to the ring plane above the center of the benzene ring (COB) with an COB-N distance of 2.88 Å. One hydrogen atom of the ammonium ion points towards a carbon atom of the benzene ring (C5) with a

C-H distance of 2.17 Å. The distances between the nitrogen atom and the carbon atoms of the ring are (in Å) 3.18 (C5), 3.19 (C4, C6), 3.21 (C1, C3), and 3.22 (C2), respectively.

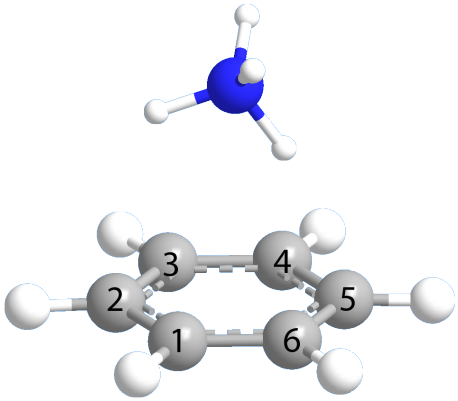

Figure 3.3.: Optimized minimum structure of $C_6H_6...NH_4^+$ dimer using the MP2/avtz method. The cartesian coordinates are listed in Tab. 7.2 on page 144.

The interaction energy of this structure was calculated using CCSD(T) and MP2 level of theory. The basis set dependency of the interaction energy and the basis set superposition error (BSSE) are given in Tab.3.1. The CCSD(T)/cc-pvqz method yields the best interaction energy of -18.96 kcal/mol, while the result for the aug-cc-pvtz basis set (-18.89 kcal/mol) is similar but nearly three times faster in computation time.

The MP2 based methods yield poor results. The MP2 values overestimate, and the SCS-MP2 and SOS-MP2 values underestimate the interaction energies. The method of choice for the model system is the CCSD(T)/aug-cc-pvtz method using the counterpoise correction from Boys and Bernardy.

The basis set dependence of the DFT-SAPT results was also investigated using various basis set combinations as shown in Tab. 3.2. An increase of the basis set leads to a better description of the calculated system on the one hand but it also increases the computational cost on the other hand. Using the avtz basis set

basis set	(CPU time)	CCSD(T)	BSSE	MP2	SCS-MP2	SOS-MP2
cc-pvdz	(2)	-14.89	2.06	-16.28	-14.88	-14.18
cc-pvtz	(97)	-18.12	0.96	-19.35	-17.71	-16.89
cc-pvqz	(1192)	-18.96	0.39	-20.12	-18.45	-17.61
aug-cc-pvdz	(32)	-17.48	3.55	-18.67	-17.07	-16.26
aug-cc-pvtz	(395)	-18.89	1.29	-19.98	-18.30	-17.46

Table 3.1.: Comparing the obtained energies from CCSD(T) and MP2 methods using different basis sets. The used geometry is shown in Fig. 3.3. Energies are given in kcal/mol, CPU time in h.

the electrostatic, exchange, induction, and induction-exchange energies are mostly converged. The dispersion energy terms did not converge since the applied basis sets are not large enough. The extrapolation of the total dispersion energy (Tab. 3.3) was done using Eqs. 2.3.1 and 2.3.2. The correction of the dispersion energy reduces the energy difference between DFT-SAPT and CCSD(T) from 1.12 kcal/mol to 0.90 kcal/mol comparing the DFT-SAPT/CBS interaction energy (-17.99 kcal/mol) with the CCSD(T)/avtz energy (-18.89 kcal/mol).

The biggest advantage of the DFT-SAPT method is the saving of computational time (DFT-SAPT is approx. 20 times faster than CCSD(T)). The DFT-SAPT method combined with the avtz basis set is a suitable choice to get high accurate values which are comparable with the CCSD(T)/avtz with a quite affordable computational cost.

Basis	(CPU time)	E_{int}	$E_{el}^{(1)}$	$E_{exch}^{(1)}$	$E_{ind}^{(2)}$
C,N = avdz; H = vdz	(1)	-16.9732	-13.8284	14.7578	-14.6675
C,N,H = avdz	(1)	-17.0729	-13.6886	14.7450	-14.7255
C,N = avtz; H = vtz	(10)	-17.6595	-13.7092	14.7168	-14.8413
C,N,H = avtz	(17)	-17.7729	-13.7084	14.7108	-14.8481
C,N = avqz; H = vtz	(21)	-17.7972	-13.6968	14.7075	-14.8456
C,N = avqz; H = vqz	(35)	-17.8432	-13.6816	14.7083	-14.8484
C,N,H = avqz	(82)	-17.8821	-13.6731	14.7072	-14.8519

Basis	$E_{ind-exch}^{(2)}$	$E_{disp}^{(2)}$	$E_{disp-exch}^{(2)}$	δ_{HF}
C,N = avdz; H = vdz	5.2099	-5.7490	0.7455	-3.4414
C,N,H = avdz	5.2183	-5.9340	0.7716	-3.4597
C,N = avtz; H = vtz	5.2787	-6.4660	0.8681	-3.5066
C,N,H = avtz	5.2752	-6.5783	0.8902	-3.5142
C,N = avqz; H = vtz	5.2762	-6.6261	0.9033	-3.5158
C,N = avqz; H = vqz	5.2763	-6.6978	0.9234	-3.5234
C,N,H = avqz	5.2768	-6.7532	0.9372	-3.5249

Table 3.2.: Comparing different basis sets for DFT-SAPT calculations using the MP2/avtz optimized geometry. The extrapolation of the dispersion energy ($E_{Disp}^{(2)}(avdz) = -5.1624$, $E_{Disp}^{(2)}(avtz) = -5.6881$, $E_{Disp}^{(2)}(avqz) = -5.8160$) yields $E_{Disp}^{(2)}(CBS/DT) = -5.9095$ and $E_{Disp}^{(2)}(CBS/DT) = -5.9093$. Energies are given kcal/mol.

Dimer Geometries

To investigate the cation-π interaction on the basis of the $C_6H_6...NH_4^+$ dimer all possible arrangements of the ammonium ion above the plane of the benzene ring have to be taken into account. To cover all possible cases three ideal arrangements of the ammonium ion above the benzene were taken. The geometries of the used monomers were optimized separately (SCS-MP2/avtz). The center of the ammonium ion was placed perpendicular above the center of the benzene (COB) ring with one (mono-), two (bi-), and three (tridentate) hydrogen atoms pointing towards the benzene ring

(Fig. 3.4). To generate the potential energy curves the ammonium is shifted in z- or x-direction, whereas the respective distances h or X in Å (see the coordinate system in Fig. 3.4) are the distances between the COB and the nitrogen atom of the ammonium ion. All energies are obtained from single point calculations.

It is important to keep in mind that the monomer geometries of thus generated systems differ from the monomer geometries mentioned in the previous section. Thus, the calculated results (see Tab. 7.3) are more comparable among themselves but without considering the deformation energy of the monomers.

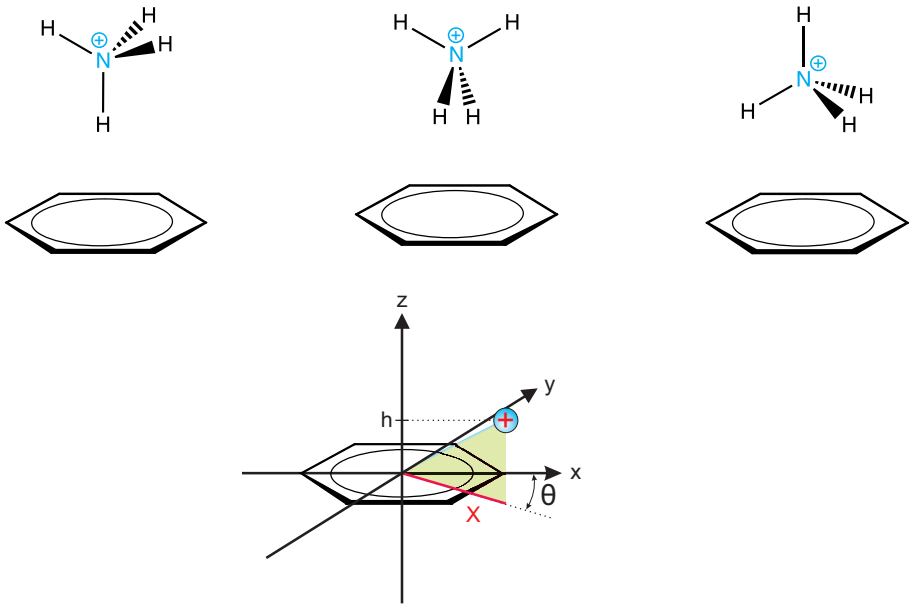

Figure 3.4.: Extended $C_6H_6...NH_4^+$ dimer model systems: (a) mono-, (b) bi-, and (c) tridentate arrangements of the ammonium ion above the benzene ring and the defined course within the coordinate system of the cation shifts above the benzene ring.

3.2.2. DFT-SAPT Results

$C_6H_6...NH_4^+$ h-shift CCSD(T) and DFT-SAPT Total Interaction Energies

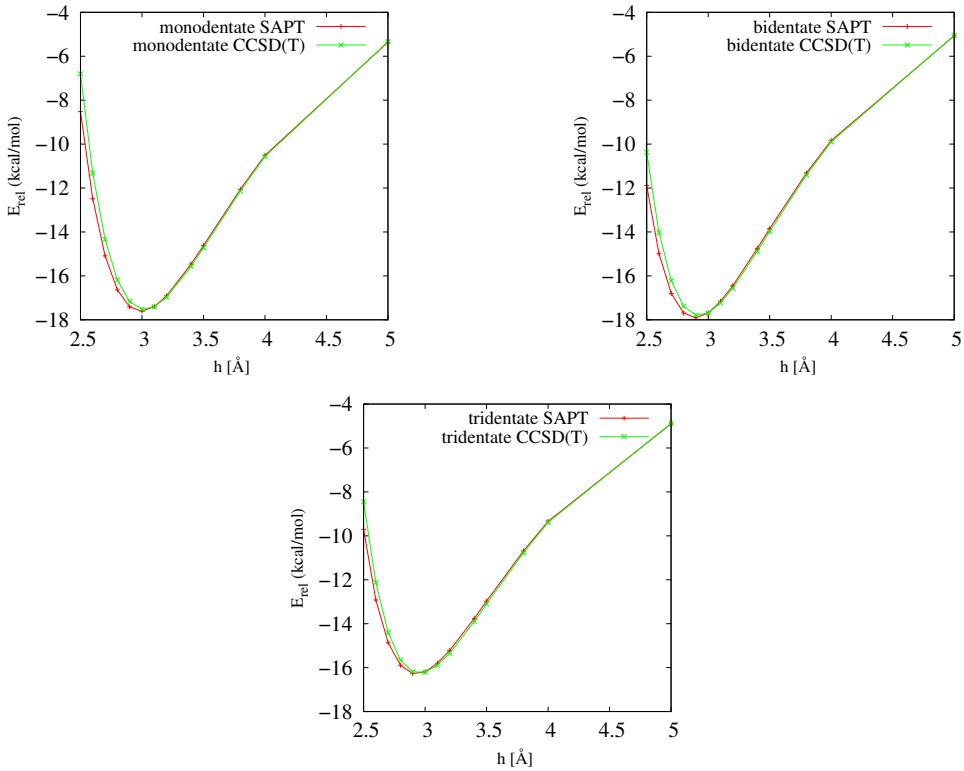

Figure 3.5.: Total CCSD(T)/avtz and DFT-SAPT/avtz interaction energies (in kcal/mol) of $C_6H_6...NH_4^+$ dimer in mono- (left), bi- (right), and tridentate (bottom) configurations as function of the nitrogen-COB distance (in Å).

Fig. 3.5 shows the potential energy curves of the three dimer configurations, calculated with the CCSD(T) and DFT-SAPT methods. The CCSD(T) and DFT-SAPT interaction energies and the DFT-SAPT decomposition energies are listed in detail in Tab. 7.4, and 7.5 on pages 145 - 146.

The calculated equilibrium distances of the dimers are identical for both methods, 3.0 Å in case of the monodentate configuration and 2.9 Å for the bi- and tridentate configuration. The DFT-SAPT method overestimates the interaction energies at

these points approximately by 0.1 kcal/mol. The DT extrapolation of the dispersion energy results in an approx. 0.2 kcal/mol more stable interaction which rises the energy difference between CCSD(T) and DFT-SAPT up to 0.3 kcal/mol. In the three mentioned cases the error cancellation of the standard DFT-SAPT method leads to an error which is in the range of the subchemical accuracy compared to the "gold standard".

A discrepancy between the used methods can be found comparing the minimum energies of the optimized dimer structure and the bidentate minimum energy structure. The CCSD(T) energy indicates that the interaction energy of the optimized structure is 1.1 kcal/mol more stable than the bidentate one. The DFT-SAPT method on the other hand prefers the bidentate structure with 0.1 kcal/mol lower energy (Tab. 7.3). Within the accuracy of the methods the DFT-SAPT method can not distinguish between the two geometries. This dissimilar trend found for the total energies can be explained by poor convergence of the dispersion energy part in the DFT-SAPT method. The extrapolation of the dispersion energy term gives identical energies for the optimized and bidentate dimer configurations (Tab. 3.3). Comparing the two methods the shape of the energy curves is almost identical.

DFT-SAPT energy decomposition of the minimum structures Considering the optimized minimum structure the total dispersion energy $E_{Disp}(avtz)$ is -5.69 kcal/mol in which the repulsive $E^{(2)}_{disp-exch}$ (0.89 kcal/mol) cancels 14% of $E^{(2)}_{disp}$ (-6.58 kcal/mol). The extrapolated dispersion energy is -0.22 kcal/mol lower and accounts only for 1% of the total interaction energy. The induction energy (-13.08 kcal/mol) together with the electrostatic energy (-13.71 kcal/mol) are the most important contributions to the attractive forces. Note that $E^{(2)}_{ind}$ (-14.85 kcal/mol) is the most attractive contribution whereas 36% of this is compensated by the repulsive $E^{(2)}_{ind-exch}$ (5.28 kcal/mol). The higher-order induction and exchange-induction estimate δ_{HF} adds -3.51 kcal/mol to the attractive interaction. In Fig. 3.6 the DFT-SAPT re-

sults of the optimized and minimum energy mono-, bi-, and tridentade $C_6H_6...NH_4^+$ dimers are compared. The total interaction energy of the tridentate dimer is about two kcal/mol lower than the other energies. The contribution of the electrostatic and induction energy to the total attractive energy is equal with about two-fifth, respectively, while the dispersion energy contributes one-fifth. The shown results indicate that the cation-π interaction is not dominated by one specific attractive energy term, but, precisely, the cation-π interaction is a subtle interplay of various physical forces.

structure	$E^{(2)}_{Disp}(avdz)$	$E^{(2)}_{Disp}(avtz)$	$E^{(2)}_{Disp}(CBS)$	$E^{SAPT}_{int}(CBS)$
optimized	-5.16	-5.69	-5.91	-17.99
monodentate	-4.63	-5.08	-5.27	-17.71
bidentate	-5.12	-5.63	-5.84	-18.00
tridentate	-4.74	-5.20	-5.40	-16.39

Table 3.3.: Extrapolation of the dispersion contribution using the DT (see Eq. 2.3.1) to obtain the cbs-extrapolated DFT-SAPT interaction energy in kcal/mol. The TZ $\rightarrow$ QZ extrapolation was done using the optimized dimer structure. The extrapolation gives the same $E^{(2)}_{Disp}(CBS)$ value which leads to a corrected interaction energy of -17.91 kcal/mol.

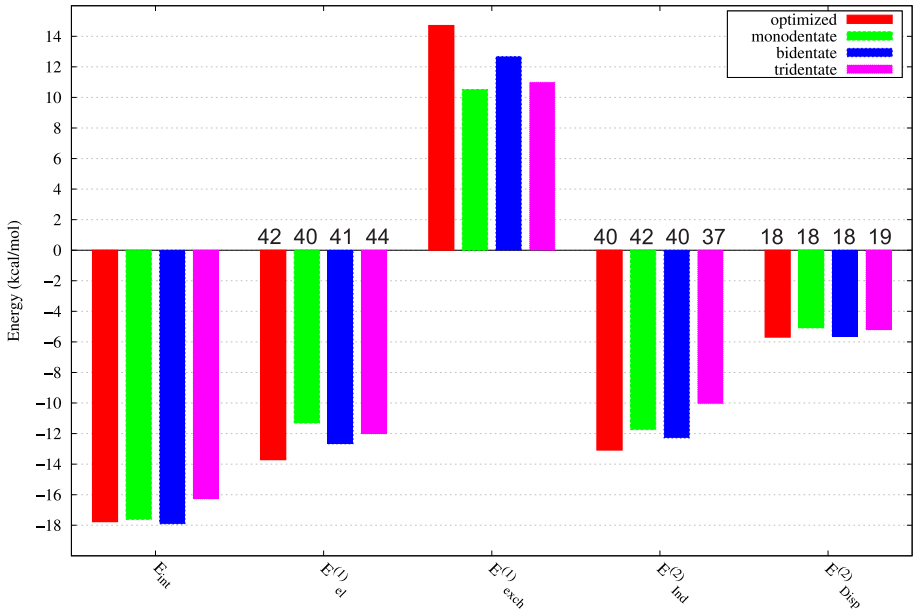

Figure 3.6.: DFT-SAPT/avtz interaction energies of the optimized and minimum energy mono-, bi-, and tridentade $C_6H_6...NH_4^+$ dimers in kcal/mol. The contribution of the electrostatic, dispersion, and induction energy to the total attractive energy in % is given within the numbers above the bars.

DFT-SAPT - h-shift - Energy Decomposition Analysis

The DFT-SAPT computation analysis of the cation shift along the z-axis (h-shift) is discussed using the three ideal dimer conformations. To get a deeper insight into the distance-dependence of the cation-π interaction the total DFT-SAPT interaction energy is separated into individual attractive (electrostatic, dispersion, and induction energy) and repulsive (exchange energy) components (Fig. 3.8). The individual SAPT terms $E^{(2)}_{disp}$ and $E^{(2)}_{disp-exch}$ are combined to give $E^{(2)}_{Disp}$ and $E^{(2)}_{ind}$, $E^{(2)}_{ind-exch}$ and δ_{HF} are combined to give $E^{(2)}_{Ind}$.

The total DFT-SAPT interaction energies (see also Fig. 3.5) are similar considering the three conformations. The major effect can be found in the exchange energy part since the repulsion is directly comparable with the distance between the monomers. As shown in Fig. 3.7 the distance between the hydrogen related to the ammonium cation and the benzene ring depends on the rotation of the cation. Hence

the "real" or "corrected" distance between the ammonium cation and the benzene is closer and the exchange energy higher e.g. considering the monodentate configuration compared with the bi-, and tridentate configuration for a given distance h. The electrostatic, dispersion, and induction energy run almost parallel and become less attractive upon decrease of the distance. The dispersion energy is less attractive compared to the electrostatic and induction energies. For closer distances the induction energy is slightly more attractive than the electrostatic energy for the monodentate configuration. Going to the bi-, and tridentate configuration the induction energy becomes less attractive. The extrapolation of the dispersion energy term (Tab. 7.5) results in 0.2 kcal/mol more attractive energy in the range of the equilibrium distance. Going to larger distances this difference vanishes. Since the energy correction is small it could be neglected.

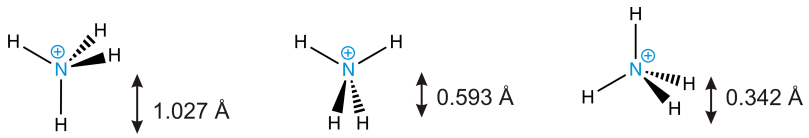

Figure 3.7.: Rotation dependent distance between the nitrogen center and the vertical frontier of the ammonium ion. The computed energies are plotted with respect to the nitrogen-COB distance. To obtain the hydrogen-COB distance the plotted values have to be corrected using the distances shown above.

The trend of the absolute energy curves shown in Fig. 3.8 (left side) is nearly identical. To distinguish between the energies, the percentage contribution of the electrostatic, dispersion and induction energy to the overall attractive energy is given on the right side of Fig. 3.8.

The induction and electrostatic energy alternate the maximum contribution, while the dispersion energy plays a minor role (not exceeding 20%). Going from shorter to larger intermolecular distances the attractive force becomes more dominated by the electrostatic part, while the contribution of induction and dispersion terms decrease.

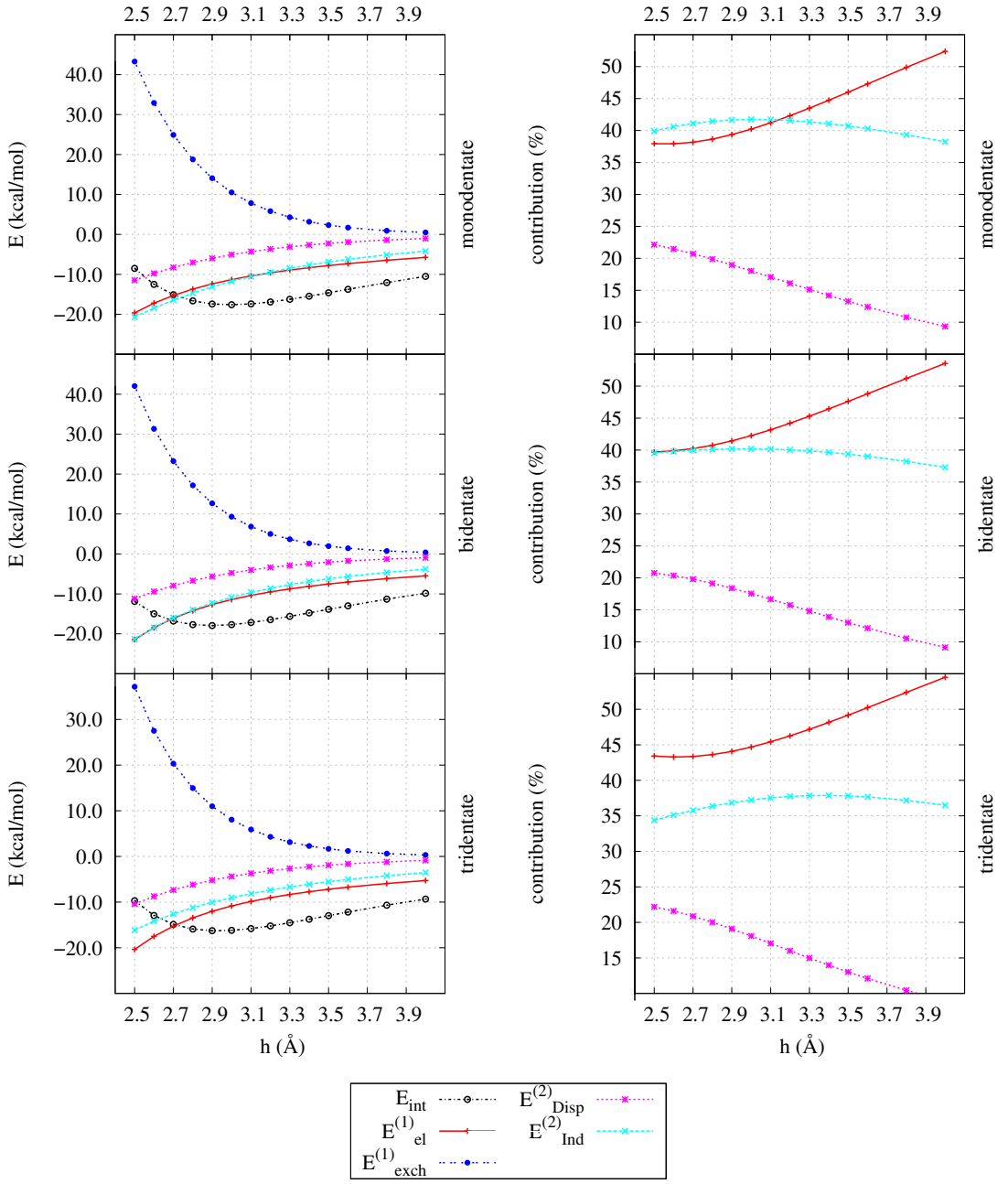

Figure 3.8.: DFT-SAPT energy contributions (in kcal/mol) with respect to the intermolecular distance h [Å] of the mono-, bi-, and tridentate h-shift. The minimum distances are 3.0 Å (monodentate) and 2.9 Å (bi- and tridentate). The energy values are listed in Tab. 7.5 on page 146.

DFT-SAPT - X-shift - Energy Decomposition Analysis

In this section the results of the cation shift along the x-axis (X-shift, see Fig. 3.4 right side) are shown. In doing so the ammonium ion is located above the COB (h=3.0 Å) and shifted along the x-axis in two possible ways. (1) $\theta = 0°$: The NH_4^+ moves over the atoms of the benzene ring, namely a carbon atom (X=1.4 Å) and hydrogen atom (X=2.5 Å). (2) $\theta = 30°$: The cation is shifted over a carbon-carbon bond (X=1.2 Å) of the benzene ring.

Again, the three possible dimer conformations are considered. The DFT-SAPT energies are illustrated in Fig. 3.10 (left side: $\theta = 0°$, right side $\theta = 30°$), the energy contributions to the attractive energies are shown in Fig. 3.11 and the energies are listed in detail in Tab. 7.6, 7.7, 7.8, on pages 147 - 149.

The total DFT-SAPT interaction energies of the various structures and X-shifts decrease while the cation is shifted away from the center of the benzene ring. The total interacting energy curves of the six possibilities shown are very similar, starting from the energetically favorable structures with approx. -17 kcal/mol and decrease more or less linearly up to around -5 kcal/mol at a distance of X=4.0 Å.

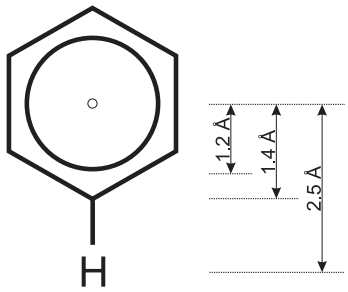

Figure 3.9.: X-shift distances from COB to carbon-carbon bond, benzene carbon atom and benzene hydrogen.

The already mentioned effect of the interaction of the ammonium ion with an atom of the benzene ring at $\theta = 0°$ can be best seen considering the exchange-repulsion energy of the monodentate conformation, since in this case the hydrogen-benzene distance is the shortest. Between 0 and 1.5 Å the exchange repulsion and the induction

attraction increase till the cation passed the carbon atoms of the ring. There is no significant difference between the energies for $\theta = 0°$ and $\theta = 30°$. This indicates that the behavior of the energies mainly depends on the interaction between the cation and the delocalized π-orbitals without influence of the position of the nuclei. The electrostatic and dispersion energy contributions do not change significantly while the cation is located somewhere above the ring (X=0-1.5 Å), for larger X-shifts these energies become smaller. For the bi- and tridentate conformations the shown trends are similar but less obvious. In Fig. 3.11 the energy contributions of the electrostatic, induction and dispersion energies are shown. The dispersion energy plays a minor role (not exceeding 20%) in the stabilization of the dimer. As long as the cation is located above the ring, the contributions of the electrostatic and induction energies are more or less equal. Upon moving the cation away from the center, the electrostatic energy decreases very fast (contribution is below 20% at X=4.0 Å), while the induction energy becomes the dominant part.

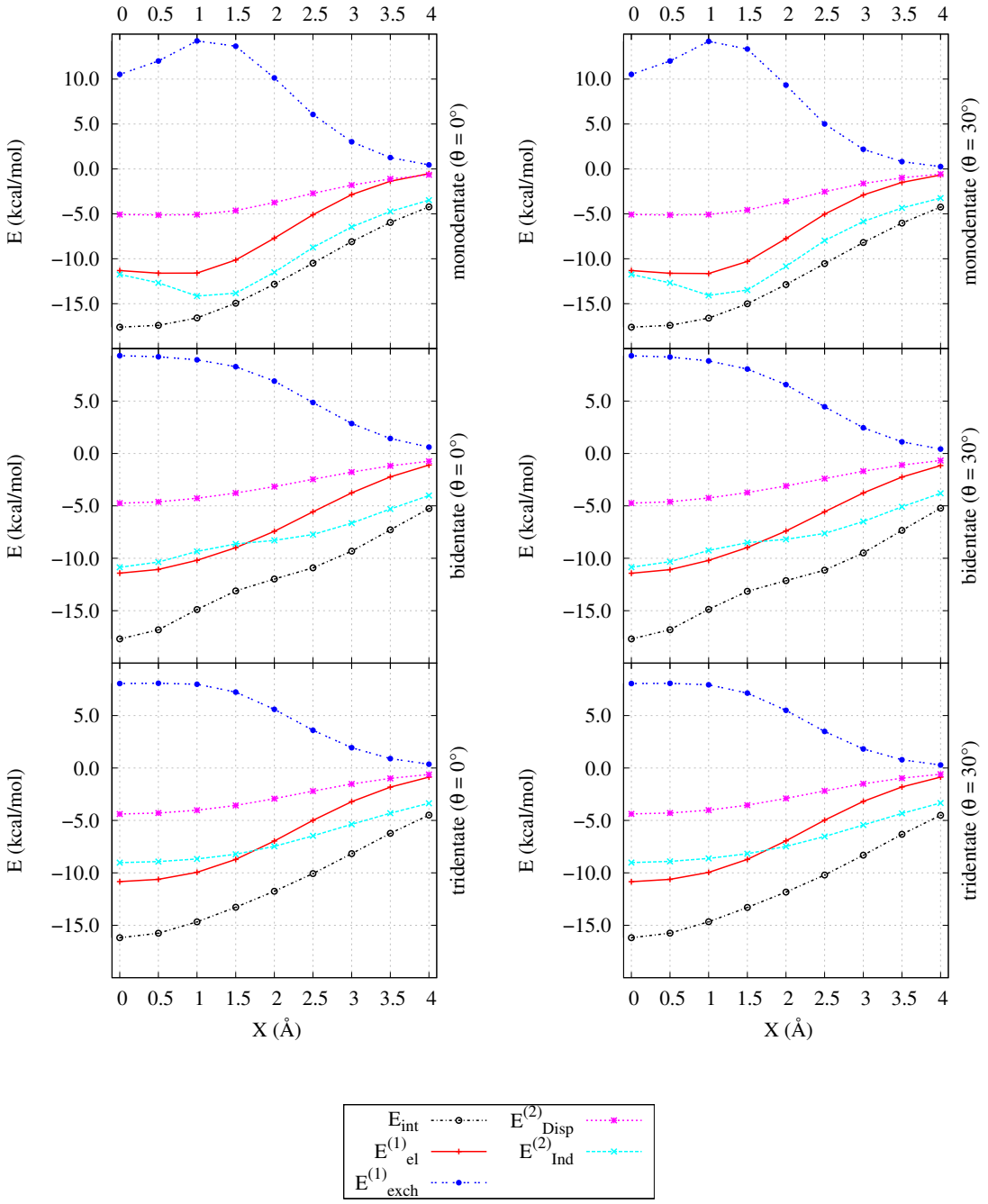

Figure 3.10.: X-shift DFT-SAPT energy contributions of mono-, bi- and tridentate conformation of the cation-π dimer at h=3.0 Å. The energy values are listed in Tab.7.6, 7.7, and 7.8, on page 147 - 149

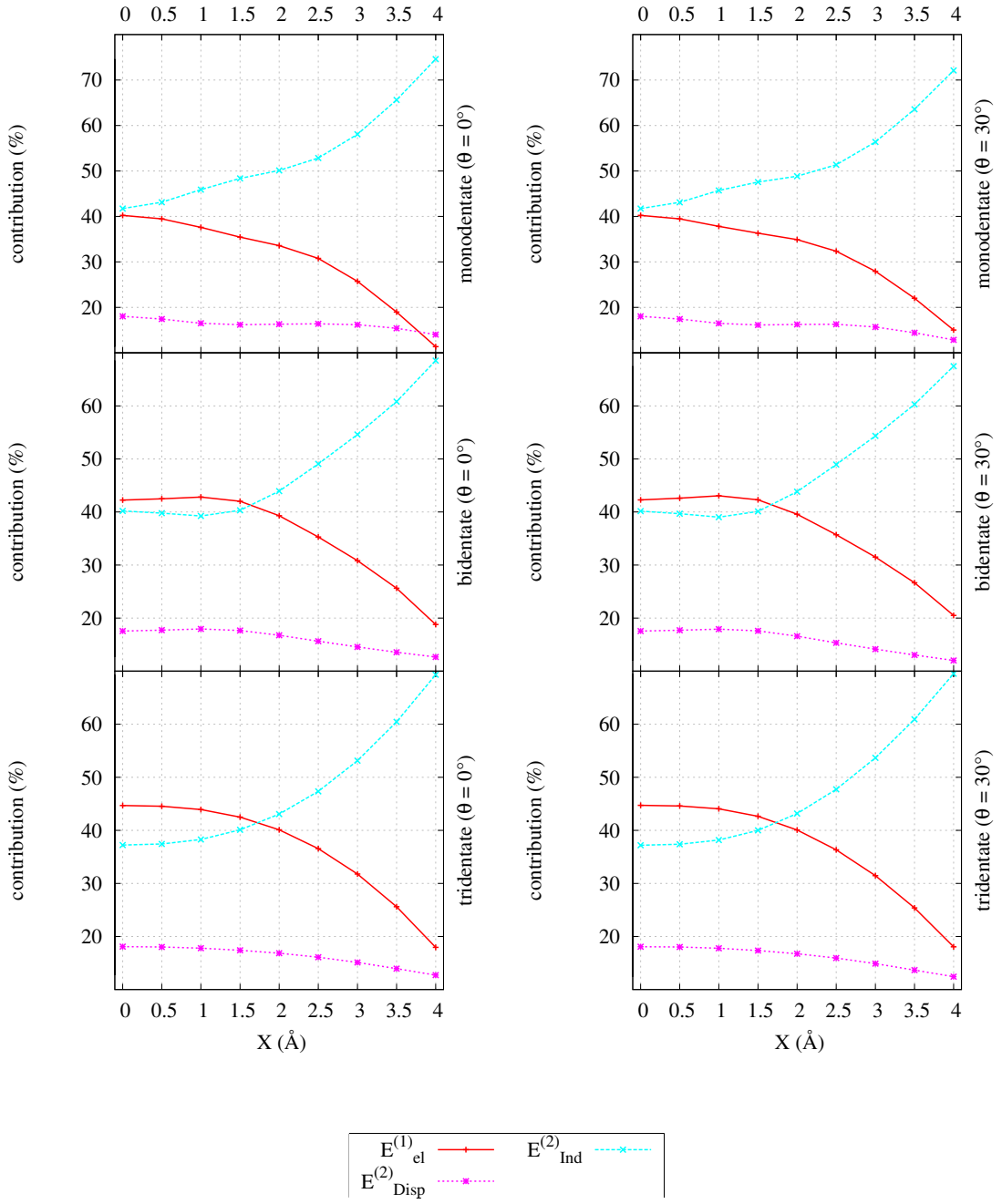

Figure 3.11.: X-shift DFT-SAPT energy contributions of mono-, bi- and tridentate conformation of the cation-π dimer at h=3.0 Å. Values are listed in Tab.7.6, 7.7, and 7.8, on page 147 - 149

3.2.3. Force Field Results

In Figs. 3.12-3.14 the total interaction energies computed using the DFT-SAPT, AMOEBA09, FF-SAPT 1, and FF-SAPT 2 methods are shown. Further, the energy contributions of the force field are compared with the representative contributions derived from the DFT-SAPT method.

The equilibrium distances of the DFT-SAPT method are 3.0 Å, 2.9 Å, and 2.9 Å (mono-, bi-, and triedentate, respectively). The AMOEBA force field (3.1 Å, 2.9 Å, 2.8 Å) yields distances which agree with the reference values within the deviation of 0.1 Å. The FF-SAPT 1 force field (3.2 Å, 2.9 Å, 2.9 Å) could reproduce the exact minimum distances except for the monodentate dimer. The FF-SAPT 2 force field (3.1 Å, 2.8 Å, 2.8 Å) also shows a small discrepancy with to the DFT-SAPT values not exceeding the value of 0.1 Å.

To compare the energy contributions of the respective force fields and conformations the energies of the minimum energy dimers derived from the DFT-SAPT method are used. The sign of the compared energies is negative if the energy derived from the respective force field is more attractive and positive if the energy is repulsive.

The AMOEBA force field underestimates the interaction energy of the monodentate conformation (+0.74 kcal/mol) and overestimates the bi- and tridentate conformations with -2.02 and -3.68 kcal/mol. The FF-SAPT 1 force field also underestimates the monodentate dimer (+2.79) and overestimates the bi- and tridentate dimers (-0.11 and -2.44 kcal/mol). This trend is also observed for the FF-SAPT 2 force field where the mono-, bi-, and tridentate values differ from the DFT-SAPT values by +1.93, -0.90, and -3.22 kcal/mol, respectively.

The long-range multipole electrostatics as implemented in the AMOEBA force field can reproduce the reference electrostatic contribution at distances larger than 3.4 Å (bi-, and tridentate) or 4.0 Å (monodentate). Going to closer distances the physically correct behavior of the electrostatic interaction as computed to the DFT-SAPT

method can not be obtained using the multipole approach, since the short-range electrostatic effects are not included. The multipole electrostatic energy is too repulsive and shows in the worst case (monodentate) a wrong behavior. The shown curve of the optimized electrostatic energy used in the FF-SAPT force fields is in good agreement with the DFT-SAPT results. At the equilibrium distance the new electrostatic energy is underestimated for the monodentate (0.37 kcal/mol) configuration and overestimated in the case of the bi- and tridentate (1.44 and 1.64 kcal/mol) conformation.

In the newly developed force fields FF-SAPT 1 and FF-SAPT 2, the vdW energy term is fitted to the DFT-SAPT vdW energy ($E^{(1)}_{exch} + E_{Disp}$). The vdW energy of the monodentate configuration derived from the FF-SAPT 1 force field is by 1.50 kcal/mol too repulsive, while the energy of the bidentate one is correct and the tridentate energy is by 0.62 kcal/mol too attractive. The FF-SAPT 2 force field produces a too repulsive vdW term for the monodentate dimer (0.85 kcal/mol), while it produces too attractive vdW values for the bi- and tridentate dimers (0.76 and 1.04 kcal/mol). Since a Buckingham potential is applied in the FF-SAPT 2 force field the vdW energy can be separated in a dispersion and exchange energy parts. Comparing the FF-SAPT 2 dispersion energy the deviation from the DFT-SAPT energies are -0.20, -0.01, and -0.06 kcal/mol, while the exchange energies deviate by +1.05, -0.75, and -0.98 kcal/mol, respectively.

The polarization energy used in all three force fields is the same. The mono- and bidentate polarization energies are underestimated (+0.73 and +0.87 kcal/mol) while the tridentate energy is overestimated by -0.54 kcal/mol.

As can be seen in Figs. 3.12-3.14 the good performance of the total interaction energy of the AMOEBA force field depends on a successful error compensation. The new FF-SAPT 1 and 2 force fields can reproduce the right behavior of the separate energy contributions. In case of the bidentate conformation the FF-SAPT 1 force field can reproduce the reference energy curve nearly exact. The reason for the less

satisfactory results of the other curves can be found in all energy contributions. The largest deviation of the vdW terms are of 1.5 or 1.0 kcal/mol (FF-SAPT 1/2), the electrostatic energy deviates by 1.6 kcal/mol and the polarization energy by 0.9 kcal/mol. The deviation of the dispersion energy is 0.2 kcal/mol and can be neglected compared with the exchange energy part (1.1 kcal/mol). To improve the performance of the new force fields the exchange energy term should be better reproduce the reference, since it gives the largest error of the total vdW energy deviation.

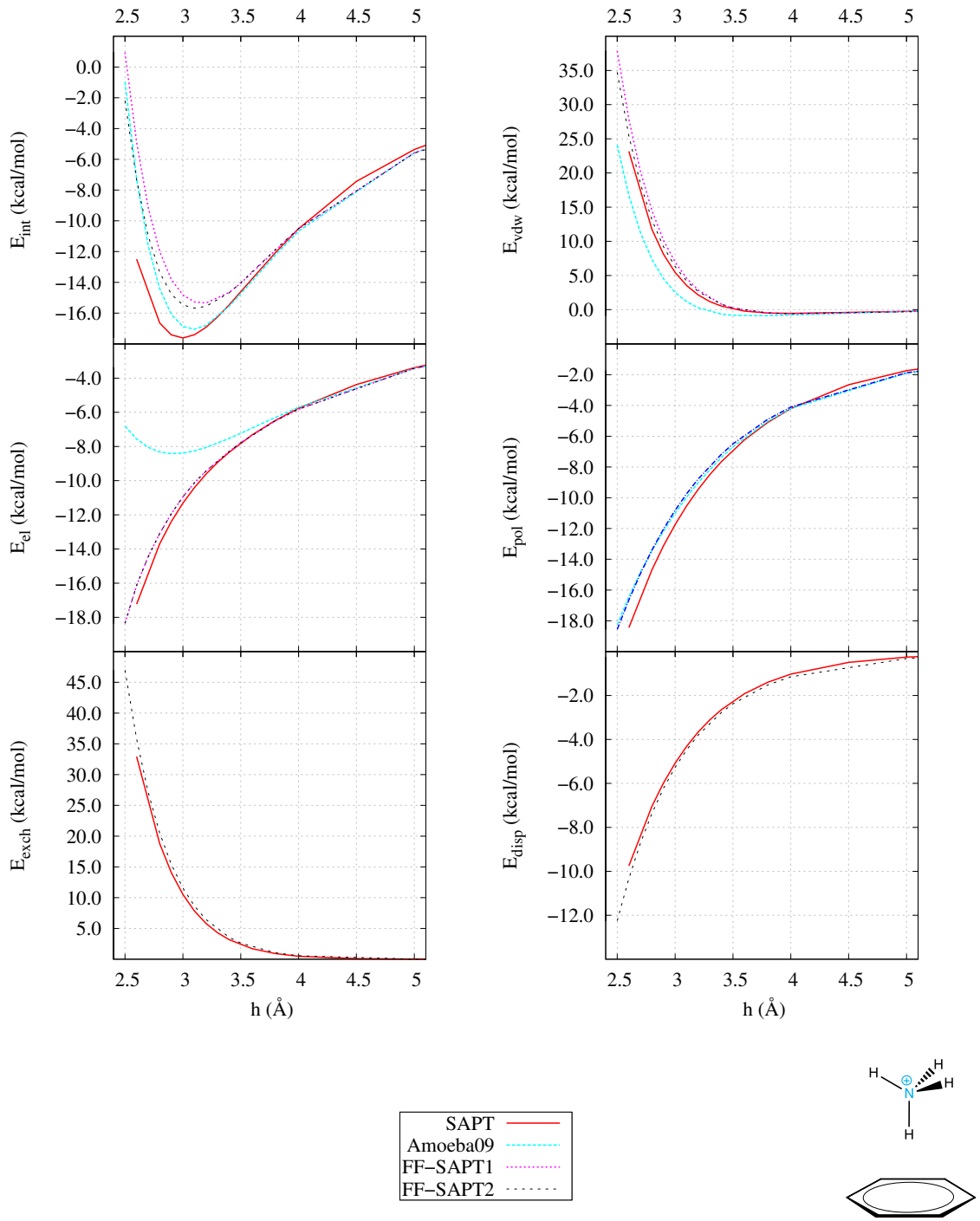

Figure 3.12.: Benchmark of newly developed FF-SAPT force fields against AMOEBA09 and DFT-SAPT methods. $C_6H_6...NH_4^+$ monodentate conformation. The force field energies are listed in Tabs. 7.15 and 7.16.

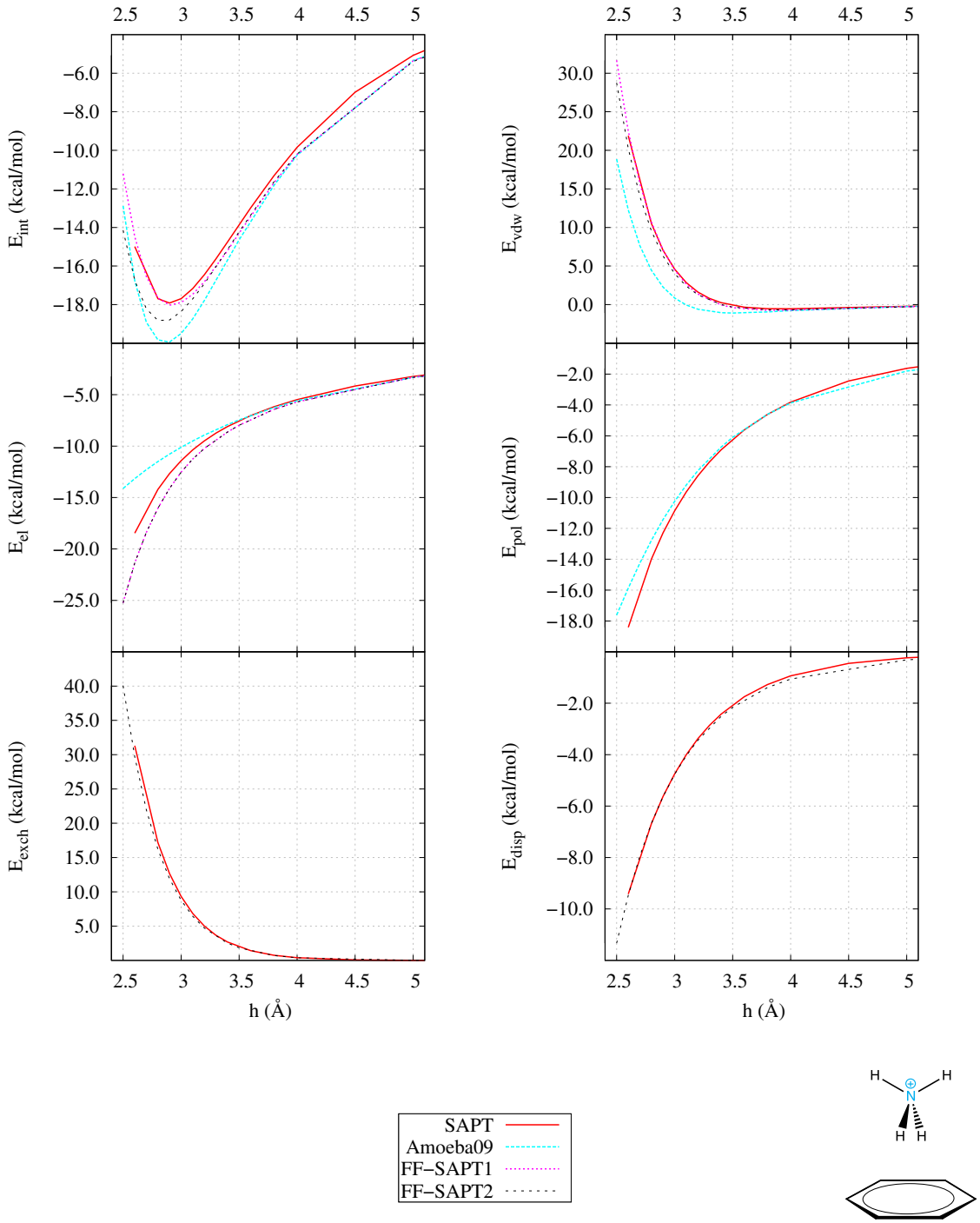

Figure 3.13.: Benchmark of newly developed FF-SAPT force fields against AMOEBA09 and DFT-SAPT methods. $C_6H_6...NH_4^+$ bidentate conformation. The force field energies are listed in Tabs. 7.15 and 7.16.

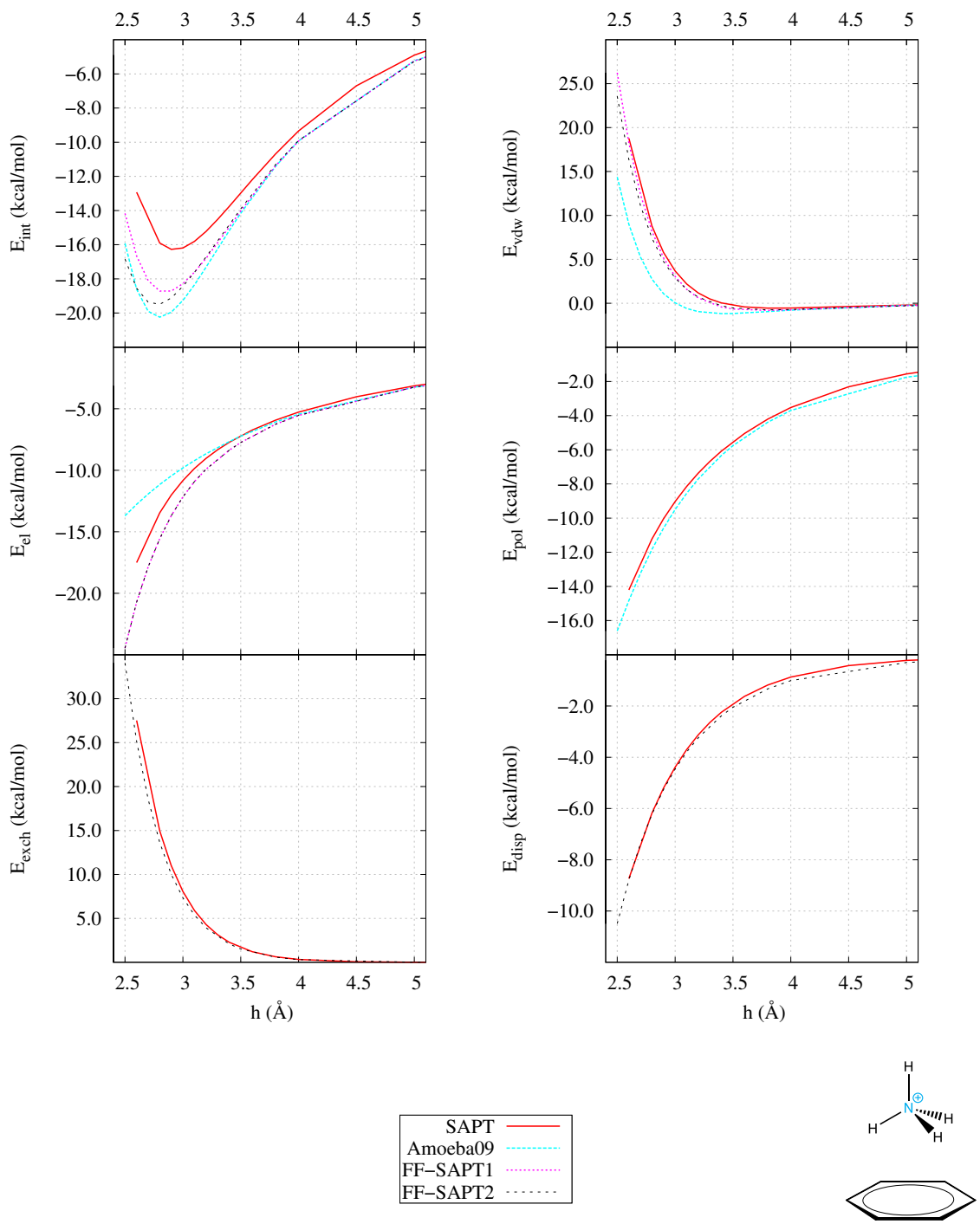

Figure 3.14.: Benchmark of newly developed FF-SAPT force fields against AMOEBA09 and DFT-SAPT methods. $C_6H_6...NH_4^+$ tridentate conformation. The force field energies are listed in Tabs. 7.15 and 7.16.

3.3. $H_2O...H_2O$ Results

3.3.1. SAPT Results

To investigate the interactions of the water dimers, three conformations, shown in Fig. 3.15, are used. The first (and most important) dimer configuration shows the O-H interaction, which forms a typical hydrogen bond. The O-O and H-H dimers represent the repulsive dimers which also have to be taken into account. In Fig. 3.16 the energy decomposition of the DFT-SAPT energy as a function of the intermolecular distance is shown for the three water dimers. The equilibrium distance of the O-H dimer is 3.0 Å with an energy of -4.24 kcal/mol. The main energy contribution comes from the electrostatic energy whereas the dispersion and induction energy account for less than 20%. The potential energy curves of the O-O and H-H dimers possess no energy minimum, since the dominant electrostatic energy term is repulsive. The dispersion energy becomes here the most important attractive energy contribution for small repulsive total interaction energies (3.0 Å O-O, 4.0 Å H-H). Going to smaller distances the induction energy dominates the attractive intermolecular interaction of the H-H dimer. The TQ extrapolation of the dispersion energy makes it more attractive by only 0.04 kcal/mol and can thus be neglected.

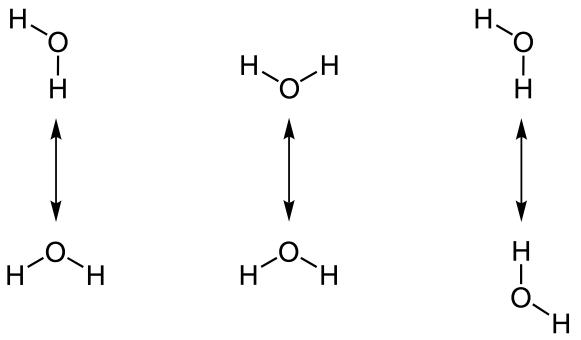

Figure 3.15.: Nomenclature of the water dimers. From left: O-H, O-O, and H-H.

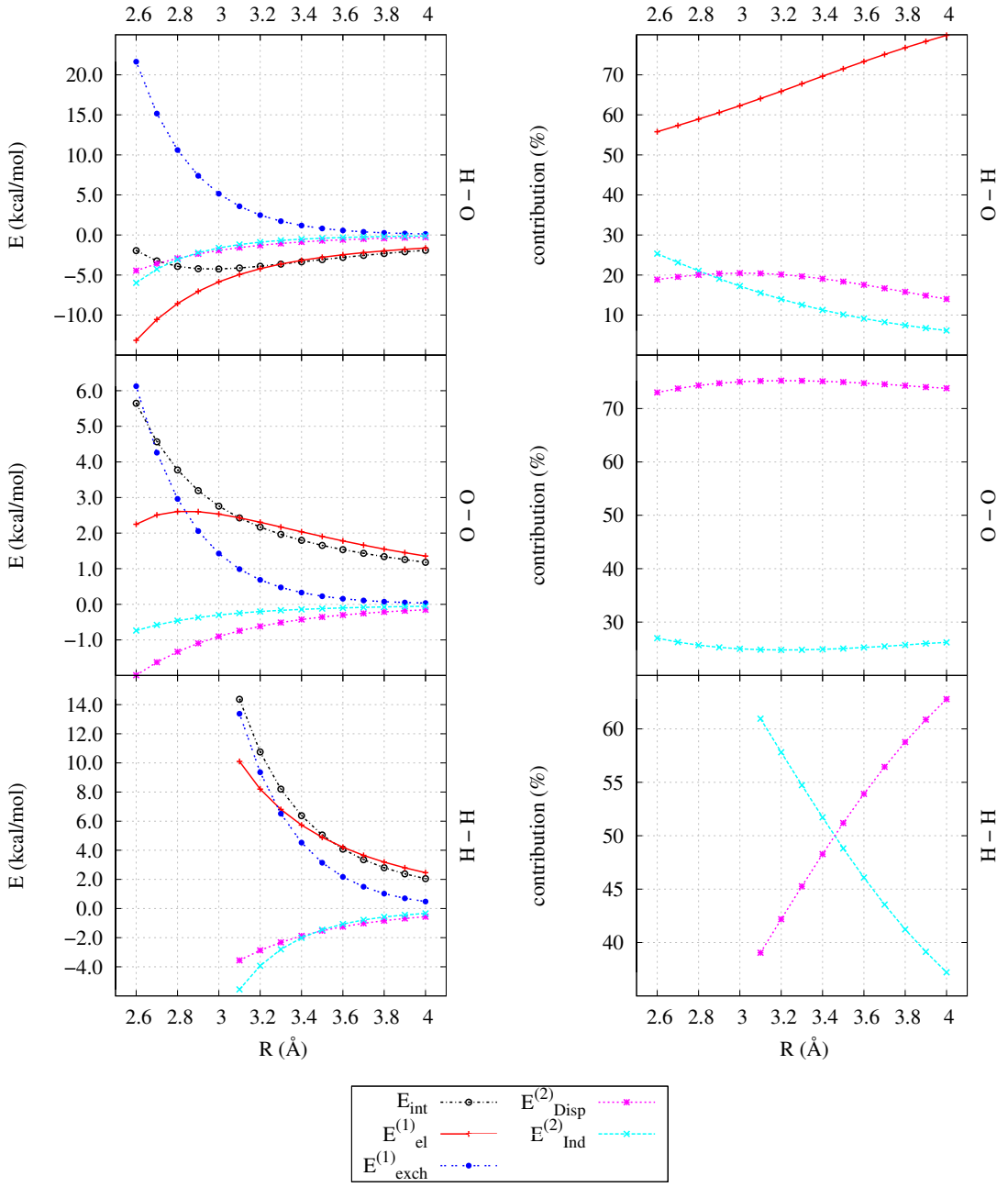

Figure 3.16.: DFT-SAPT energy contributions (in kcal/mol) as a function of the intermolecular distance R [Å] of the O-H, O-O, and H-H dimers. The energy values are listed in Tab.7.9 on page 150

3.3.2. Force Field Results

In Figs. 3.17-3.19 the potential energy curves calculated with the AMOEBA09 and FF-SAPT 1 and 2 force fields are compared with the DFT-SAPT energies. The O-H potential energy curve (Fig. 3.17) of the AMOEBA09 force field shows the best agreement with the DFT-SAPT values. The FF-SAPT 1 force field underestimates the interaction (+0.78 kcal/mol) and shows an equilibrium distance of 3.1 Å. The FF-SAPT 2 force field also underestimates the interaction (+1.59 kcal/mol) and predicts an equilibrium distance of 3.2 Å. The main error comes from in the exchange (+1.05 kcal/mol) and electrostatic (+0.31 kcal/mol) energies. The deviation of the polarization energy (+0.18 kcal/mol) is small and the dispersion energy difference (+0.05 kcal/mol) is negligible. The FF-SAPT 2 force field shows good performance for the O-O interaction since the exchange energy is reproduced quite well and so the vdW energy term is accurate. The deviation from the DFT-SAPT energy results mainly from the electrostatic energy. In contrast the H-H electrostatics of the new force fields agree very well with the reference values and the deviation of the total interaction energy can be attributed to in the vdW energy term, or more specific, to the exchange energy contribution.

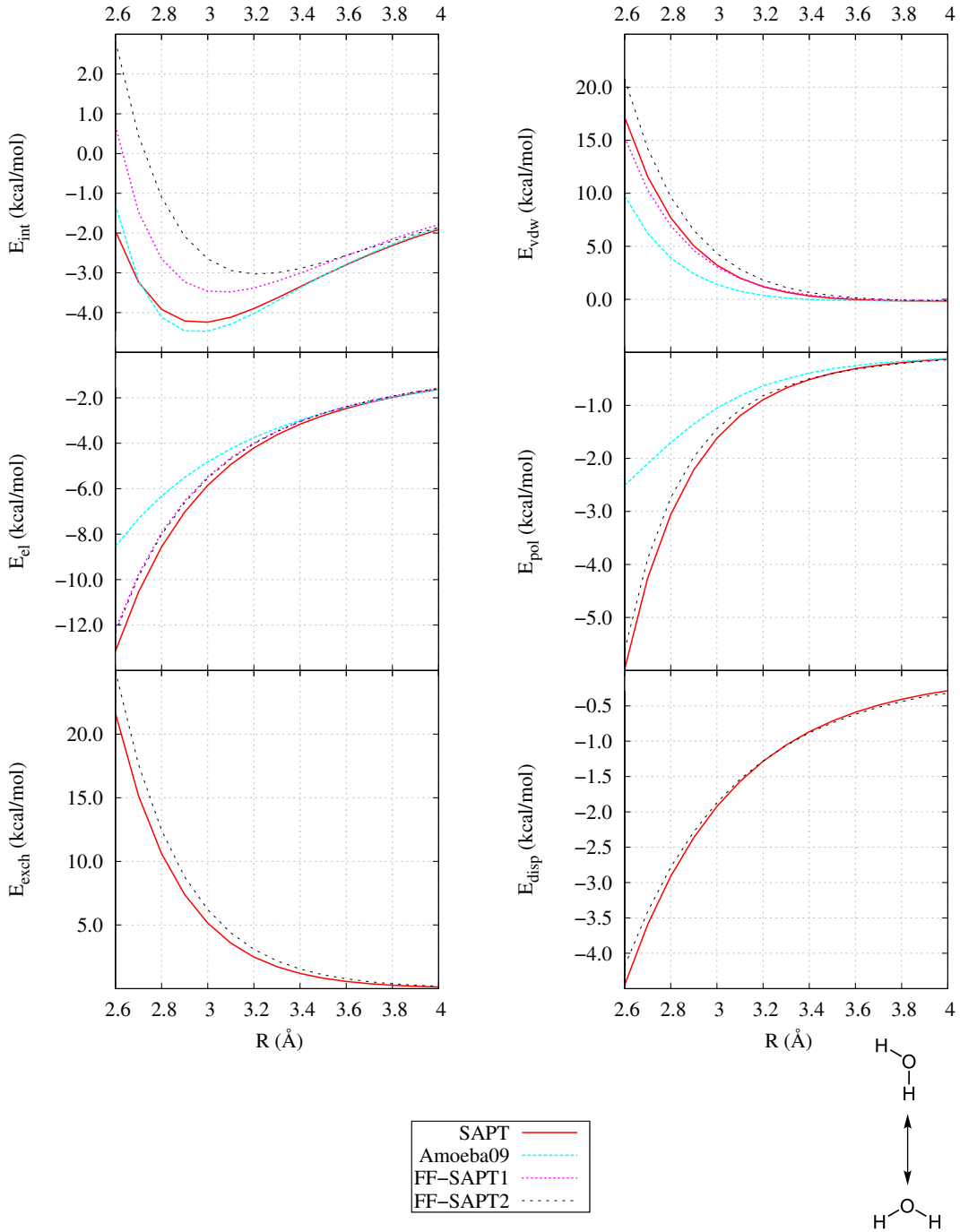

Figure 3.17.: Benchmark of newly developed FF-SAPT force fields against AMOEBA09 and DFT-SAPT methods. H_2O...H_2O O-H conformation. The force field energies are listed in Tabs. 7.17 and 7.18.

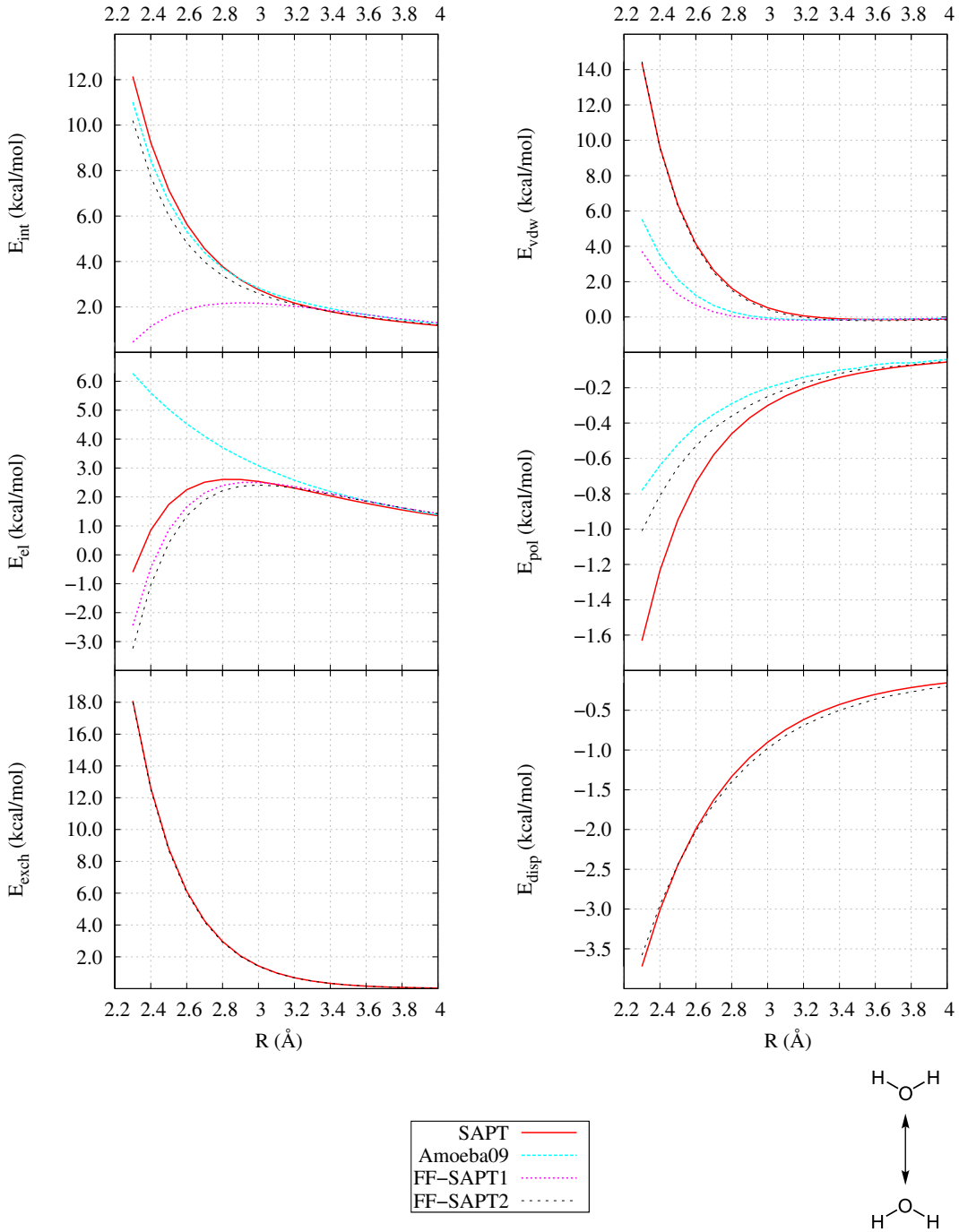

Figure 3.18.: Benchmark of newly developed FF-SAPT force fields against AMOEBA09 and DFT-SAPT methods. $H_2O...H_2O$ O-O conformation. The force field energies are listed in Tabs. 7.17 and 7.18.

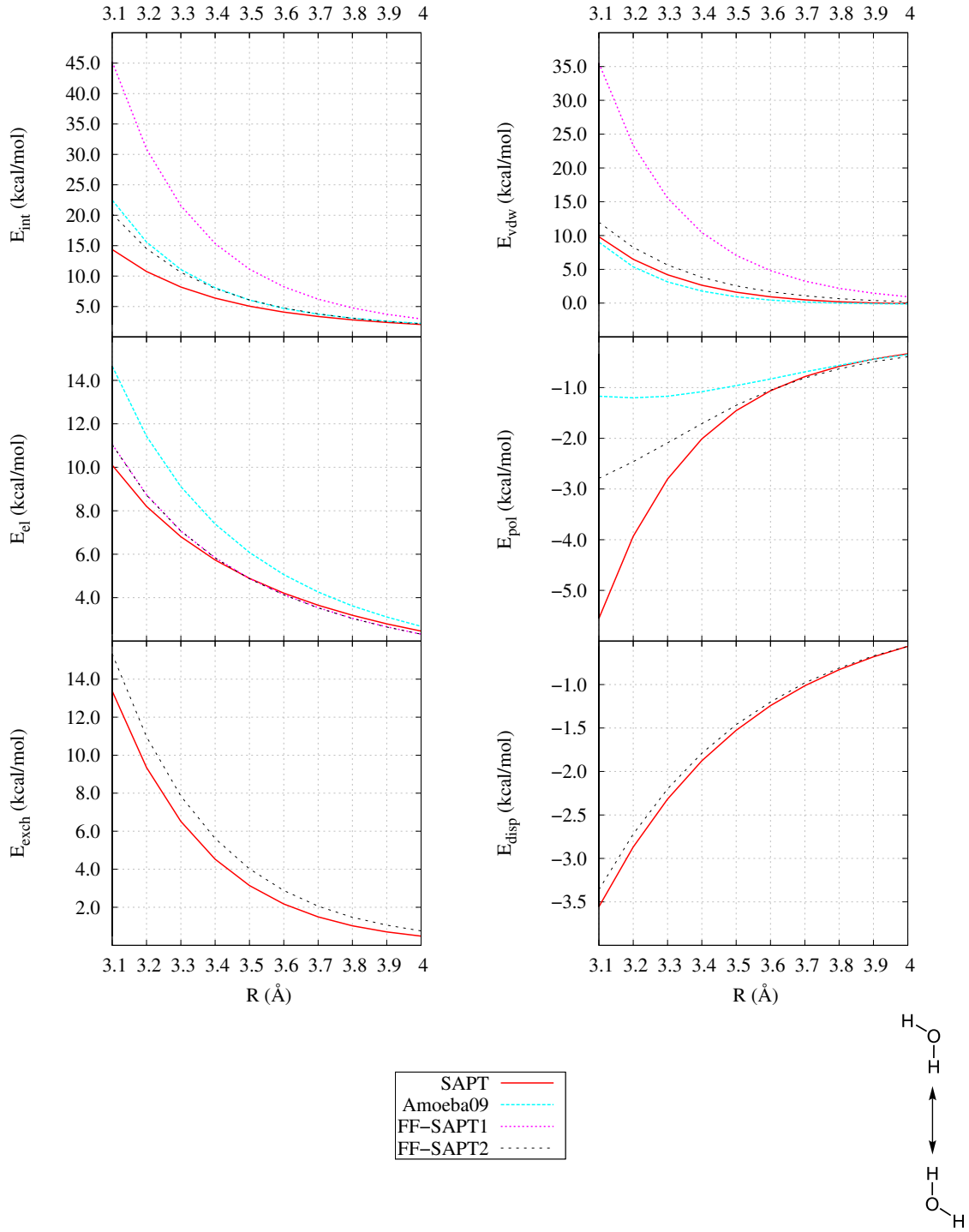

Figure 3.19.: Benchmark of newly developed FF-SAPT force fields against AMOEBA09 and DFT-SAPT methods. H_2O...H_2O H-H conformation. The force field energies are listed in Tabs. 7.17 and 7.18.

3.3.3. Influence of free electron pairs

The question arises, whether if it is possible to predict the orbital type, either rabbit ears or MO p-type orbitals, of the oxygen wherein the free electron pairs are located. To investigate this problem two dimers are arranged which should give insights into the orbital interaction. The fist dimer (left side of Fig. 3.20) shows the O-H interaction. The rotation of the left monomer includes all possible orbital-hydrogen interactions. The dimer on the right side of Fig. 3.20 is arranged in such a way that there is a maximal overlap of the orbitals if they exist in a rabbit ears style.

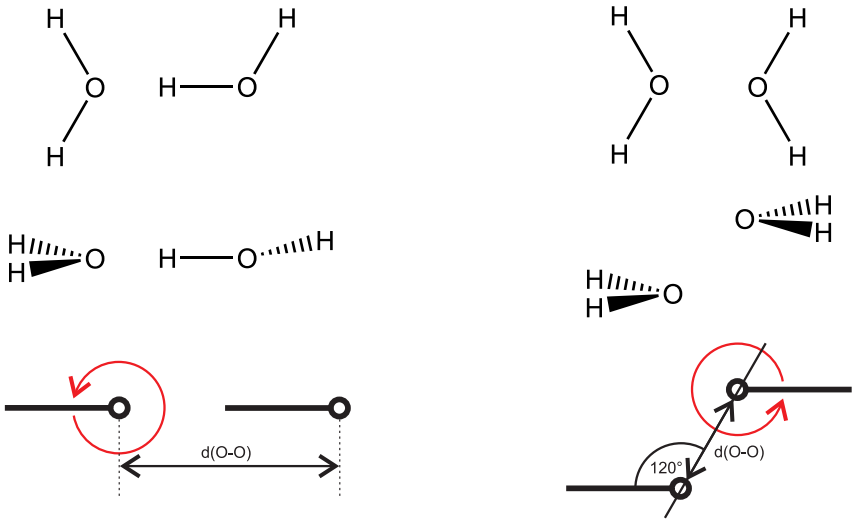

Figure 3.20.: Arrangement of water dimers to investigate the anisotropic orbitals of the oxygen. Left: O-H interaction. Right: O-O interaction. From top to bottom: top view, side view, and schematic side view for orbital representation used in Figs. 3.21 - 3.24. The circle represents the position of the oxygen atoms.

O-H rotation. The interacting energy curve in Fig. 3.21 and 3.22 shows two minima around $\phi = 120$ and 240°. This is a first hint for the existence of rabbit ear orbitals. Looking further the exchange energy is minimal at 180 degrees, there is no interaction between the hydrogen and any orbitals. This is a second hint for rabbit

ear type orbitals since in case of a p-type orbital there should be a higher exchange repulsion as it is in this case at 120 and 240 degrees. Finally, the electrostatic energy establishes the presence of rabbit ears, since the energy at 120 and 270 degrees is approx. 0.5 kcal/mol more attractive than at 90, 180 and 270 degrees. The induction energy also changes with respect to the rotation, but only about 0.3 kcal/mol between 60 and 300 degrees. The dispersion energy is most attractive at zero degree, from there the interaction energy parabolic becomes less attractive reaching its maximum at 180 degree and rises to 360.

O-O rotation. In Fig. 3.23 and 3.24 the energies of the O-O rotation are shown. The interaction energy shows a minimum at 90 degree (O-O dist. 2.5Å) and 75 degree (O-O dist. 3.0Å). The interaction energy has two repulsive maxima at 180 and 320 degree. The exchange energy term is maximal at 60 degree, at this point the hydrogen atom of one monomer points towards the oxygen center of the second monomer. Hence, the electrostatic energy is here most attractive. The induction and dispersion energies also follow this trend. A differentiation between the two orbital types is not possible.

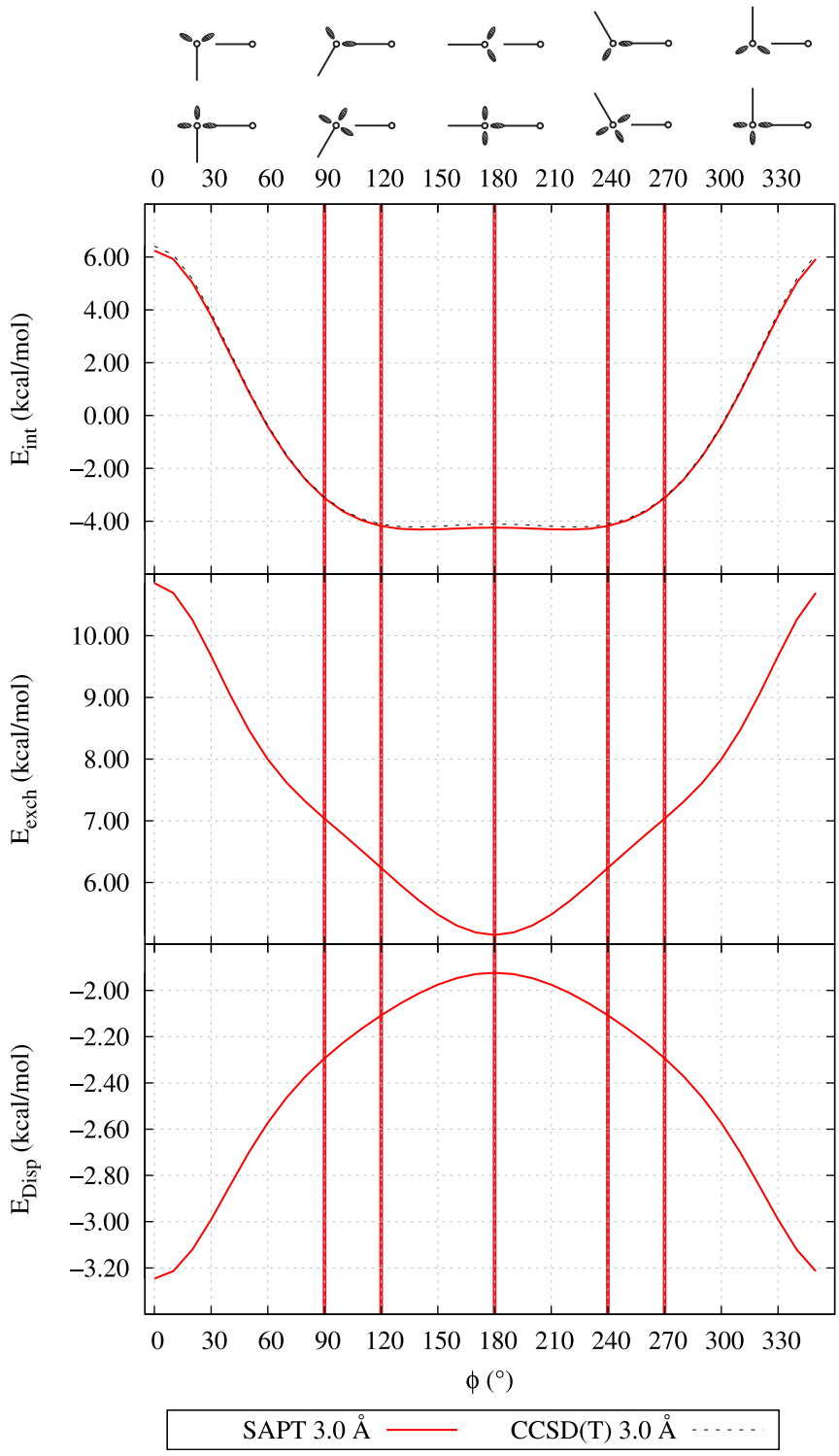

Figure 3.21.: Energy decomposition (DFT-SAPT/avqz) of water dimer rotation. The orientation of the rabbit ear (upper graphics) and MO (lower graphics) orbitals is given on top of the graphs. The vertical red lines show the corresponding position of the orbital representations in the illustration.

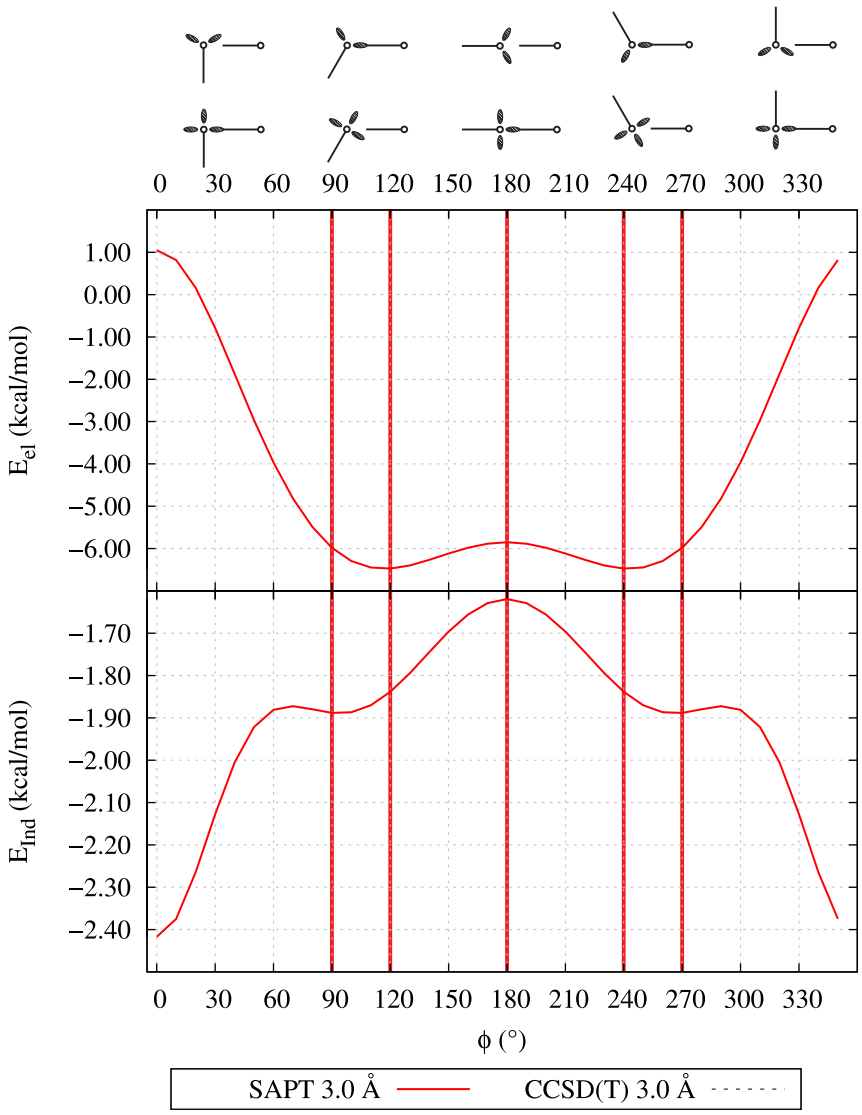

Figure 3.22.: Energy decomposition (DFT-SAPT/avqz) of water dimer rotation. The orientation of the rabbit ear (upper graphics) and MO (lower graphics) orbitals is given on top of the graphs. The vertical red lines show the corresponding position of the orbital representations in the illustration.

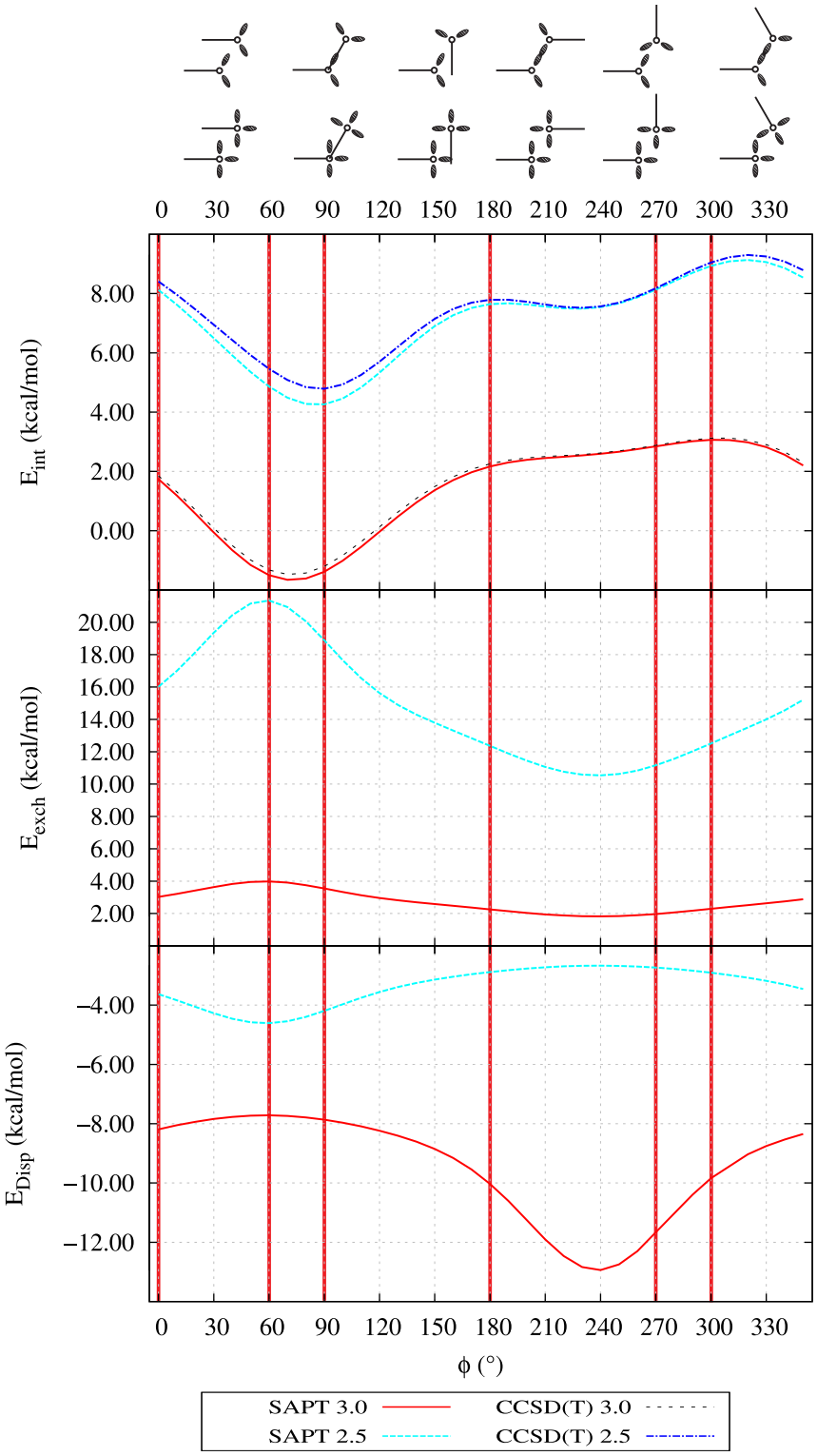

Figure 3.23.: Energy decomposition (DFT-SAPT/avqz) of water dimer rotation. The orientation of the rabbit ear (upper graphics) and MO (lower graphics) orbitals is given on top of the graphs. The vertical red lines show the corresponding position of the orbital representations in the illustration.

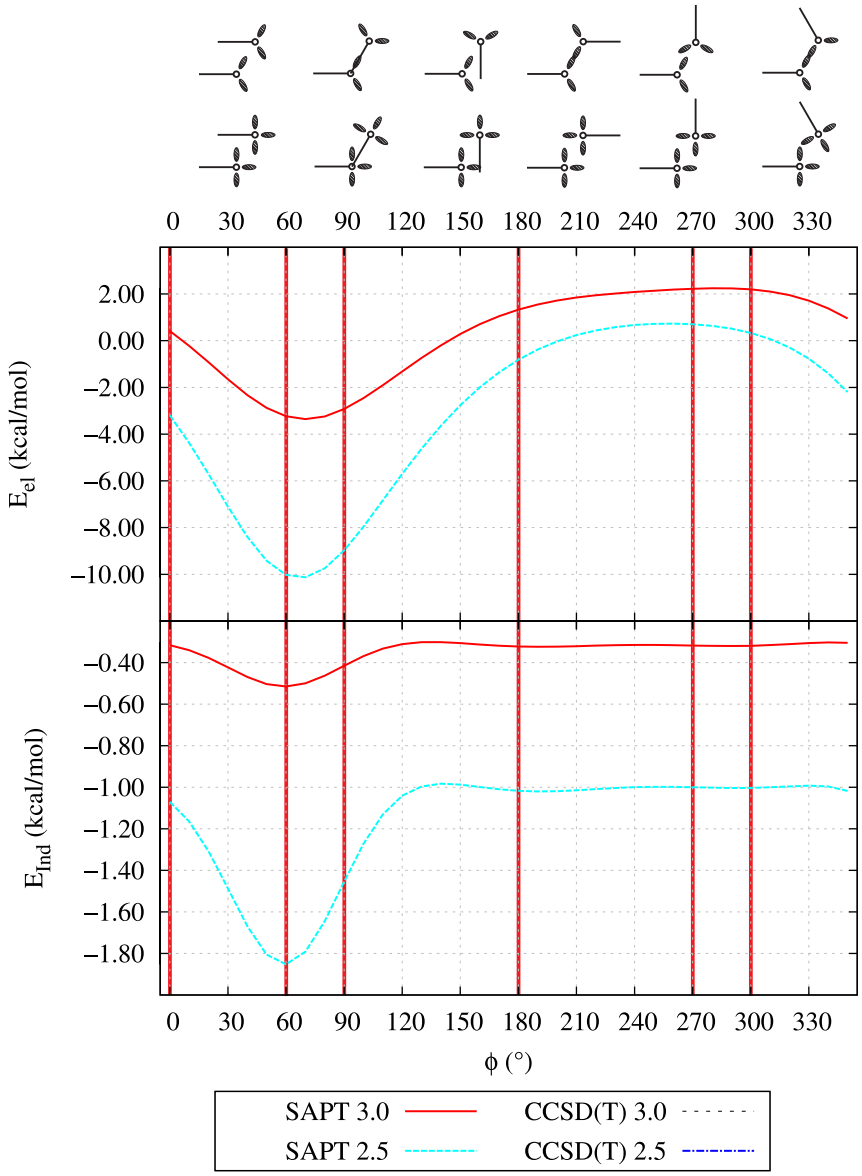

Figure 3.24.: Energy decomposition (DFT-SAPT/avqz) of water dimer rotation. The orientation of the rabbit ear (upper graphics) and MO (lower graphics) orbitals is given on top of the graphs. The vertical red lines show the corresponding position of the orbital representations in the illustration.

3.4. $H_2O...NH_4^+$ Results

The calculations of the $H_2O...NH_4^+$ dimers are done to check the performance of the newly developed force fields. Therefore the DFT-SAPT interaction energies are compared with the respective energy parts derived from the force fields. The investigated water...ammonium cation dimer conformations (Fig. 3.25) could be separated into attractive and repulsive interacting dimers, whereas the first ones are of major interest. The DFT-SAPT interaction energies and the energy decomposition are shown in Fig. 3.26.

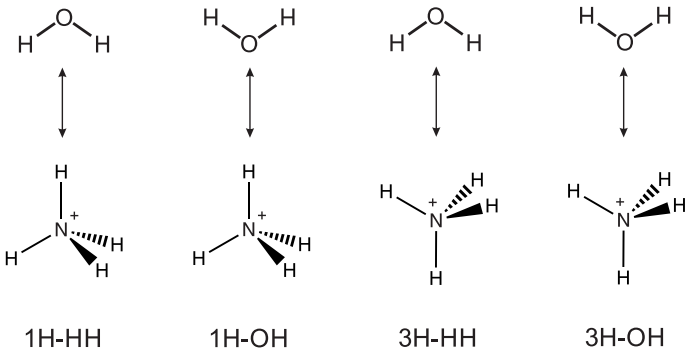

Figure 3.25.: Arrangement of the $H_2O...NH_4^+$ dimers. The distance (R) between the monomers is defined as the distance between the oxygen and nitrogen atom.

3.4.1. DFT-SAPT Results

The equilibrium distance of the 1H-OH dimer is 2.7 Å with the stabilization energy of -19.8 kcal/mol. The attractive forces are dominated by the electrostatic and induction terms. The dispersion energy plays only a minor role with a contribution below 10%. The 3H-OH dimer shows an equilibrium distance of 1.7 Å with the stabilization energy of -15.1 kcal/mol. The 1H-OH dimer exhibits a less attractive induction energy. So the dominating contribution to the total interaction energy is the electrostatic energy. The energies of the remaining dimer configurations show a similar behavior exhibiting of the repulsive electrostatic energy contribution. It

can be seen that in the case of a direct atom-atom contact (1H-OH, 1H-HH) the induction energy becomes more attractive compared with the remaining two dimers.

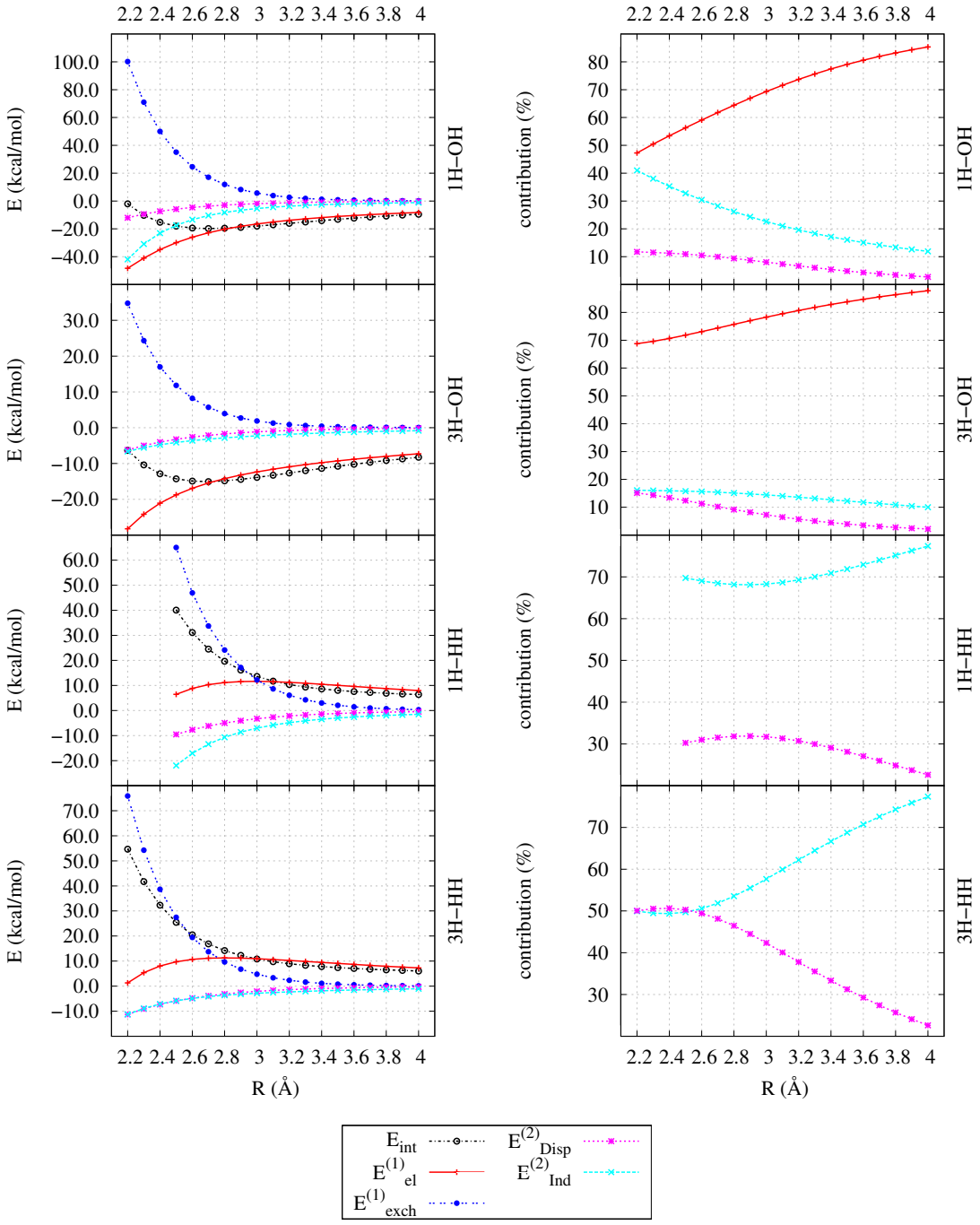

Figure 3.26.: DFT-SAPT energy contributions for the $H_2O...NH_4^+$ dimers. From top to bottom: 1H-OH, 3H-OH (equilibrium distances: 2.7 Å each), 1H-HH, and 3H-HH. Energies in kcal/mol as a function of the intermolecular O-N distance (in Å).

3.4.2. Force Field Results

The performance of the AMOEBA09 and FF-SAPT force fields is compared with the reference DFT-SAPT results in Figs. 3.27-3.30. The AMOEBA09 force field shows the best agreement considering the total interaction energy. The 1H-OH and 3H-OH dimers vdW energy calculated with the FF-SAPT 2 force field agrees well with the reference values, since the exchange and dispersion energy match also the reference energies. The reason for the deviation can be found in the polarization energy (1H-OH) and in the electrostatic energy (3H-OH). The total interaction energy in the 1H-HH dimer is underestimated (too repulsive) due to a wrong behavior of the calculated electrostatic energy using the force field methods. Considering the right behavior of the electrostatic energy contribution within the 3H-HH dimer, the total interaction energy agrees very well with the reference energy.

In all four cases the changed polarization parameter of the water oxygen and hydrogen atoms results in a slightly better values for this energy contribution.

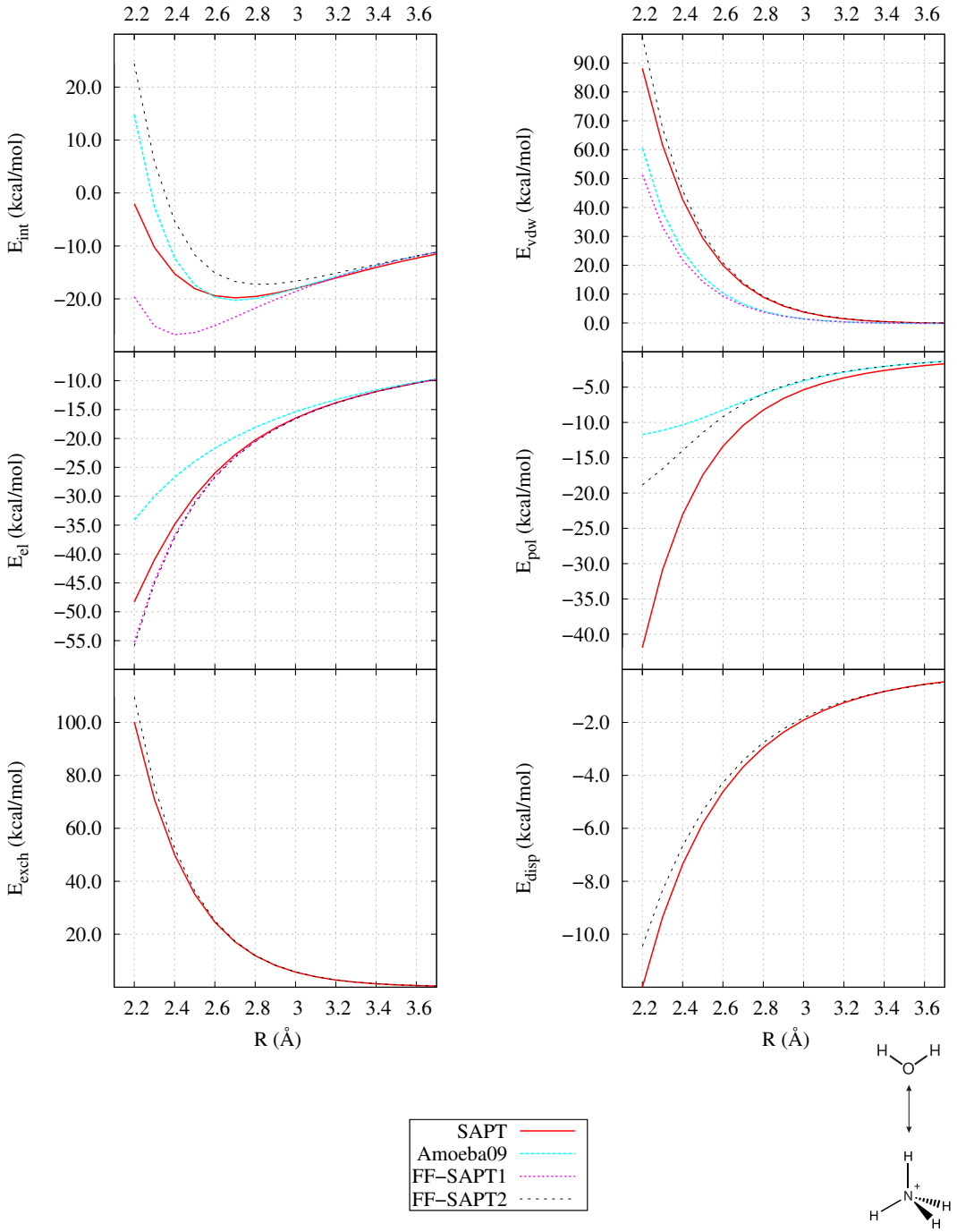

Figure 3.27.: Benchmark of newly developed FF-SAPT force fields against AMOEBA09 and DFT-SAPT methods. $H_2O...NH_4^+$ 1H-OH dimer conformation. The force field energies are listed in Tabs. 7.23 and 7.24.

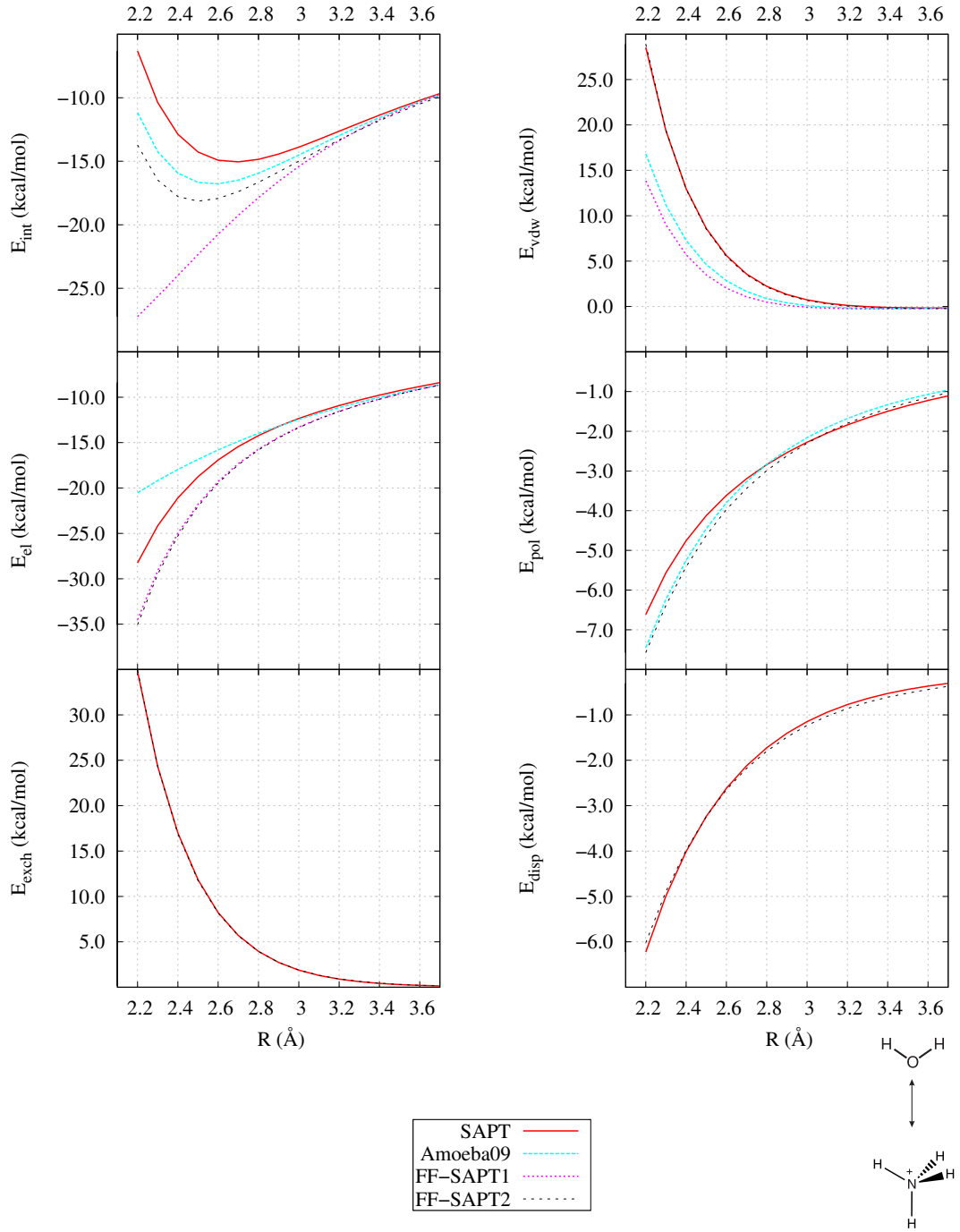

Figure 3.28.: Benchmark of newly developed FF-SAPT force fields against AMOEBA09 and DFT-SAPT methods. $H_2O...NH_4^+$ 3H-OH dimer conformation. The force field energies are listed in Tabs. 7.25 and 7.26.

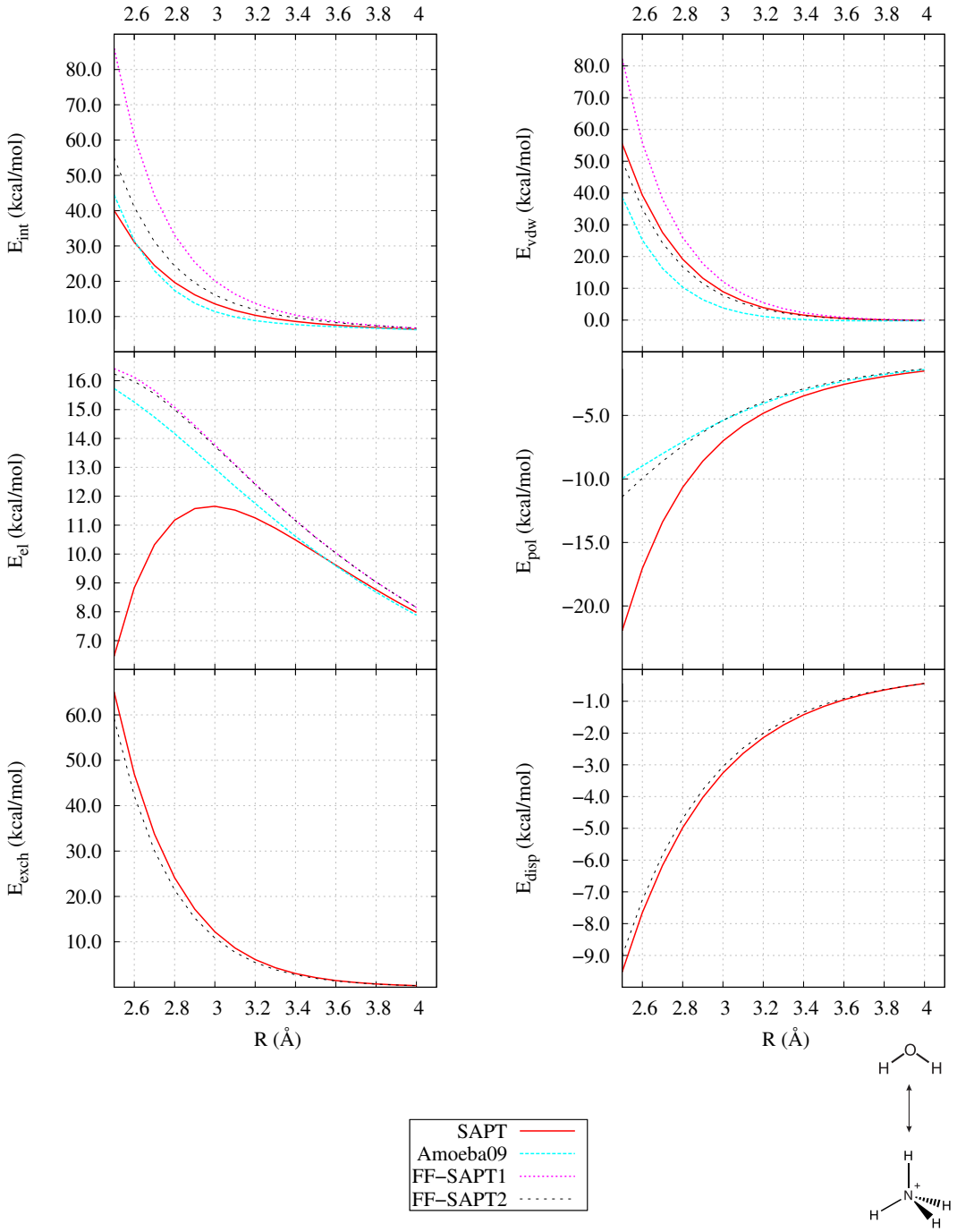

Figure 3.29.: Benchmark of newly developed FF-SAPT force fields against AMOEBA09 and DFT-SAPT methods. $H_2O...NH_4^+$ 1H-HH dimer conformation. The force field energies are listed in Tabs. 7.23 and 7.24.

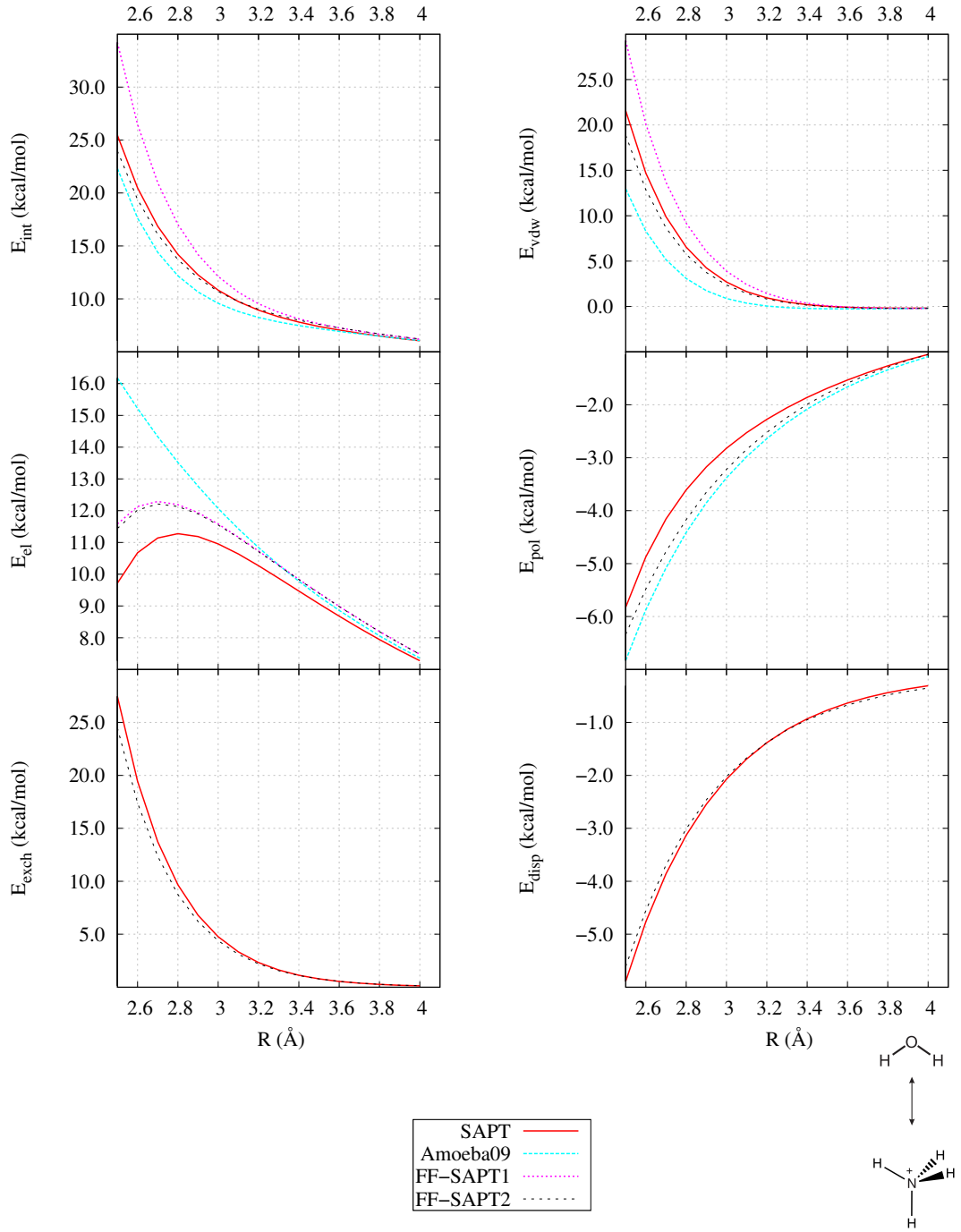

Figure 3.30.: Benchmark of newly developed FF-SAPT force fields against AMOEBA09 and DFT-SAPT methods. $H_2O...NH_4^+$ 3H-HH dimer conformation. The force field energies are listed in Tabs. 7.25 and 7.26.

3.5. $H_2O...C_6H_6$ Results

The interaction between a water and benzene molecule can be separated in water-π and water-H (side on) interactions. In case of the water-π interaction on the one side the attractive H-π interaction and the repulsive O-π interaction are considered. The side-on conformation dimers include the O-H interaction since the H-H repulsion is not of interest. The discussed dimer configurations are shown in Fig. 3.31.

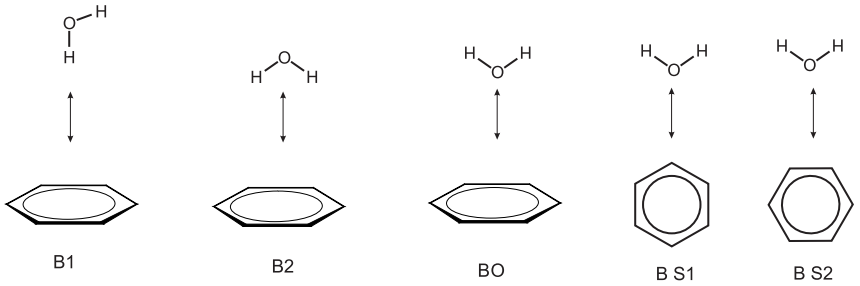

Figure 3.31.: Arrangement of the $H_2O...C_6H_6$ dimers. The distance (R) between the monomers is defined as the distance between the oxygen atom and COB.

3.5.1. DFT-SAPT Results

The DFT-SAPT energies for the water-π interaction are shown in Fig. 3.32 and for the side-on interactions in Fig. 3.33 as a function of the intermolecular distance. The equilibrium distances of the B1 and B2 dimers are 3.4 Å each. The behavior of the individual energy contributions is very similar. The attractive contributions are dominated by the electrostatic and dispersion energy, while the induction has only a minor influence (below 15%) on the dimer stabilization. The BO dimer has no energy minimum. The minimum energy distances of the side-on dimers are 5.0 Å (B S1) and 4.7 Å (B S1). Again, the contribution of the induction energy is below 15 %. The attractive forces in the B S2 dimer are dominated by the dispersion energy as seen before in the B1 and B2 dimers. The B S1 dimer energies show a reversed order. Here the electrostatic energy is more attractive than the dispersion energy.

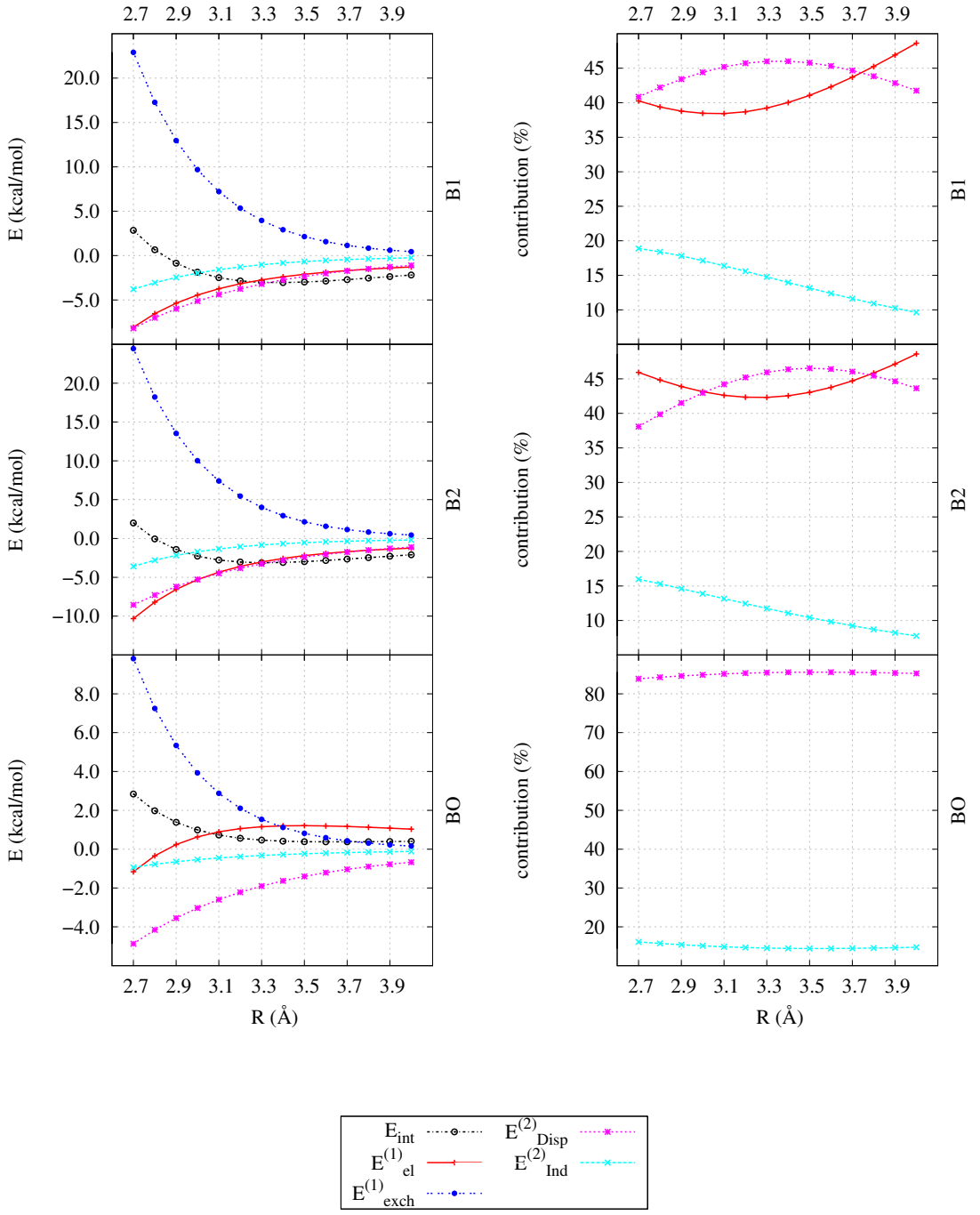

Figure 3.32.: DFT-SAPT energy contributions (in kcal/mol) as function of the intermolecular distance R [Å] of the $H_2O...C_6H_6$ dimers. The energy values are listed in Tabs. 7.10 and 7.11 on page 151.

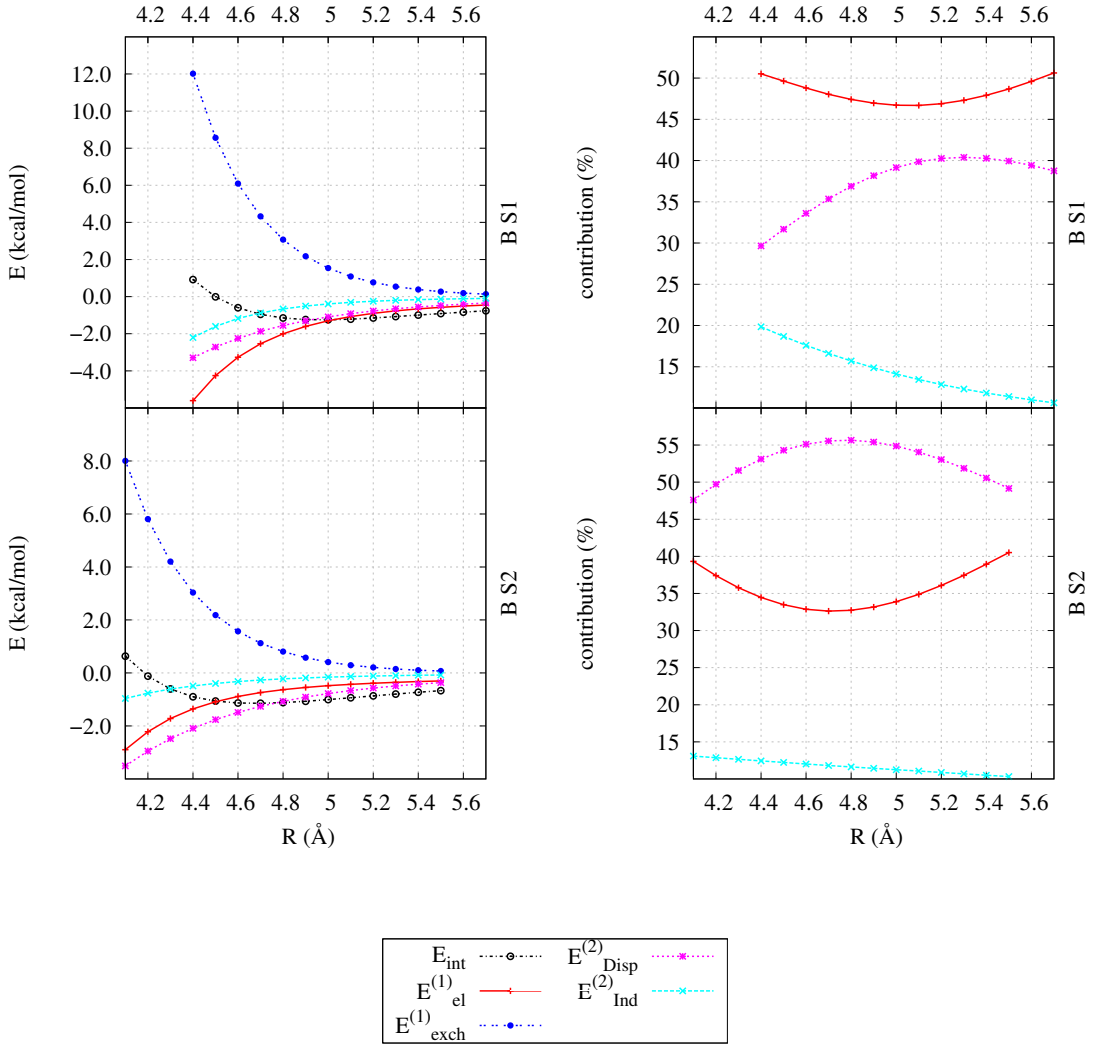

Figure 3.33.: DFT-SAPT energy contributions (in kcal/mol) as function of the intermolecular distance R [Å] of the $H_2O...C_6H_6$ dimers. The energy values are listed in Tabs. 7.10 and 7.11 on page 151.

3.5.2. Force Field Results

The total energy of the B1 dimer is underestimated from all force field methods. The predicted equilibrium distances are too large by +0.2 Å (AMOEBA09) up to 0.4 Å(FF-SAPT 2) and 0.5 Å (FF-SAPT 1). The reason for that failure can be

found in all energy contributions whereas the main error results from the vdW and electrostatic (+1.24 kcal/mol) energy contributions. The FF-SAPT 2 force field shows that the vdW error results from an overestimation of the exchange energy by +1.12 kcal/mol. The overestimation of the dispersion energy leads to only a small error compensation within the vdW energy term (-0.27 kcal/mol) and a small underestimation of the polarization energy (+0.16 kcal/mol) can be neglected.

The total interaction energy calculated with the AMOEBA09 force field for the B2 dimer shows the best agreement with the energies derived from the reference method. The predicted equilibrium distance is by 0.1 Å shorter, whereas the distances from the FF-SAPT 1 and FF-SAPT 2 force fields are by 0.2 and 0.1 Å longer, respectively. The new force fields underestimate the interaction by 0.95 (FF-SAPT 1) and 0.31 kcal/mol (FF-SAPT 2). Going to shorter distances the performance of the force fields degrades since the electrostatic energy becomes too repulsive (FF-SAPT 1 and 2) and the FF-SAPT 1 vdW energy increases too fast. The exchange and dispersion energy resulting from the FF-SAPT 2 force field are in good agreement with the DFT-SAPT energies.

The AMOEBA09 and FF-SAPT 2 force fields deliver a good agreement for the total interaction energy for the repulsive BO dimer. The FF-SAPT 1 force field failed completely since the vdW energy term is not repulsive enough. Both FF-SAPT force fields overestimate the electrostatic energy. Their good performance for the total energy is caused by an error cancellation resulting from a too repulsive exchange and hence vdW energy contribution. The deviation of the polarization energy can be neglected.

Considering the side-on dimer B S1 the AMOEBA09 and FF-SAPT 2 force fields show a much better agreement with the DFT-SAPT equilibrium distances and the total interaction energy. Whereas the AMOEBA09 force field benefits from the error cancellation, the FF-SAPT 2 force field is able to reproduce the reference exchange, dispersion and vdW energy contribution and has only small error in the electrostatic

and polarization energies. The FF-SAPT 1 force field again fails because the vdW energy term is not repulsive enough.

The total energies of the B S2 dimer from the AMOEBA09 and FF-SAPT 2 force fields are very similar and deviate only by -0.35 kcal/mol compared with the reference energies. The calculated equilibrium distance is by 0.1 Å too short. The FF-SAPT 2 force field overestimates the electrostatic energy (-0.5 kcal/mol) whereas the vdW energy is slightly too repulsive (+0.16 kcal/mol). The vdW energy term benefits from an error cancellation between the exchange (+0.30 kcal/mol) and dispersion (-0.14 kcal/mol) energy contributions. The FF-SAPT 1 results are poor.

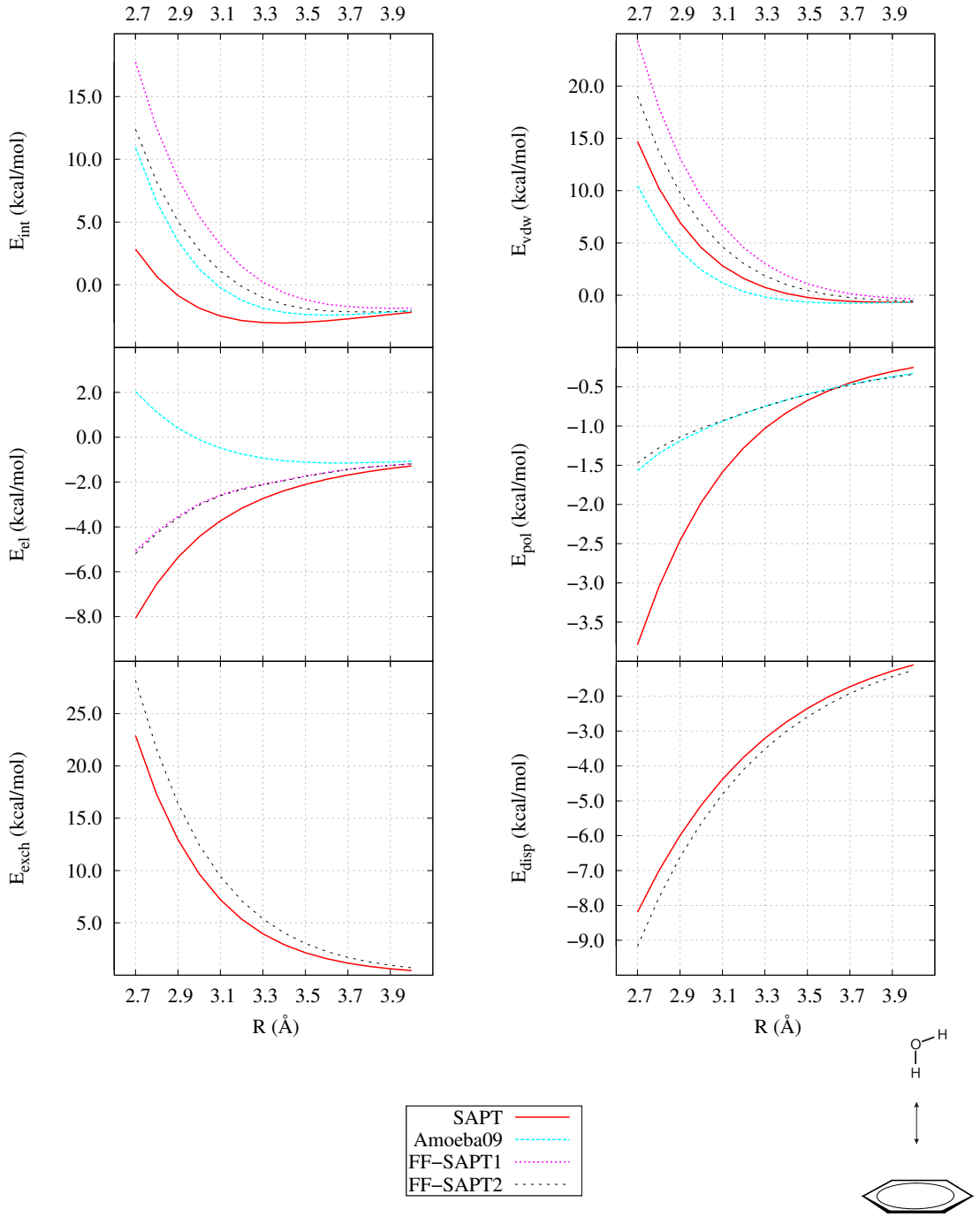

Figure 3.34.: AMOEBA09 and FF-SAPT force fields total energy and energy contributions against the DFT-SAPT reference energies (in kcal/mol) for the $H_2O...C_6H_6$ B1 dimer as a function of the intermolecular distance. The equilibrium distance is 3.4Å. The force field energies are listed in Tabs. 7.19 and 7.20.

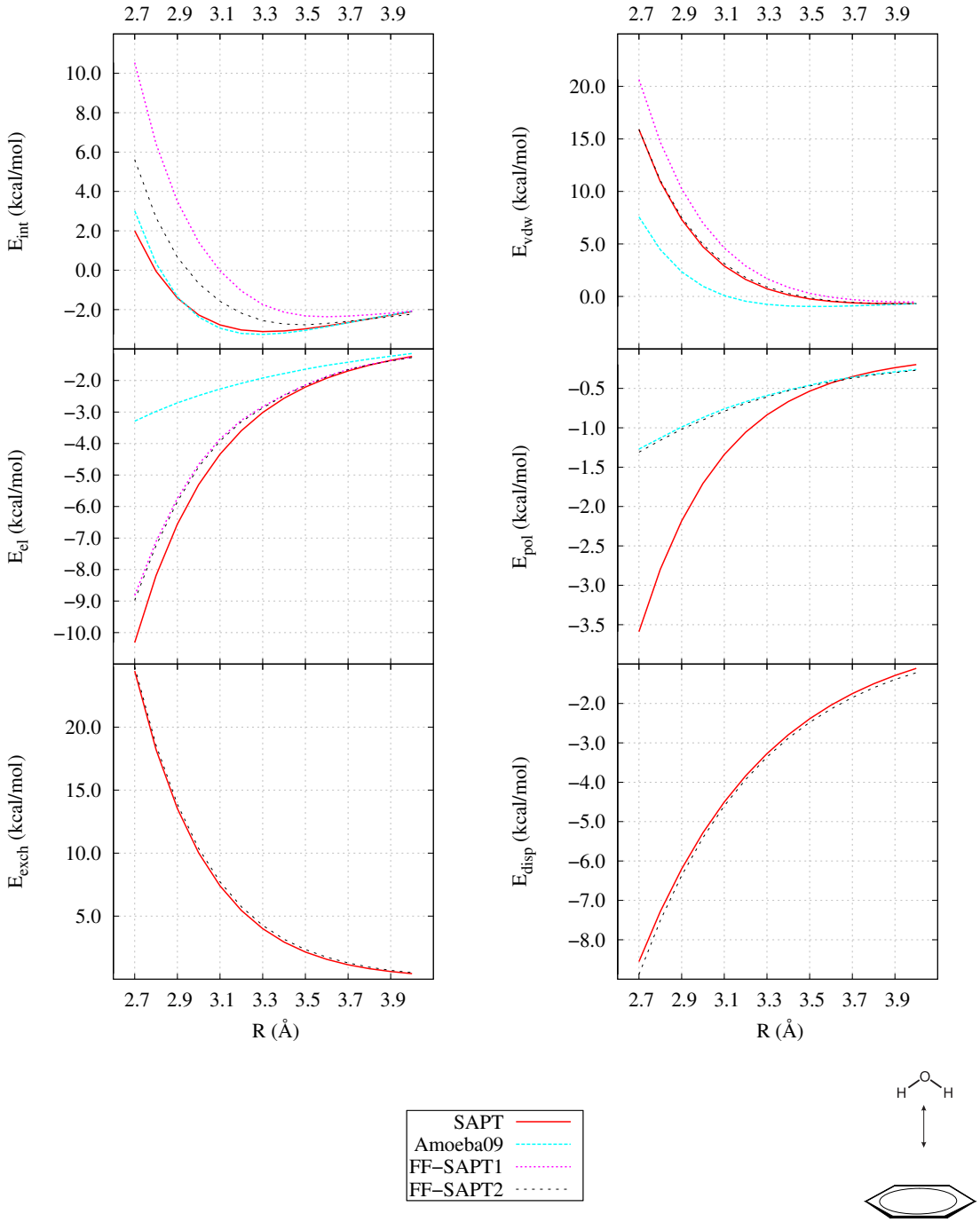

Figure 3.35.: AMOEBA09 and FF-SAPT force fields total energy and energy contributions against the DFT-SAPT reference energies (in kcal/mol) for the $H_2O...C_6H_6$ B2 dimer as a function of the intermolecular distance. The equilibrium distance is 3.4Å. The force field energies are listed in Tabs. 7.19 and 7.20.

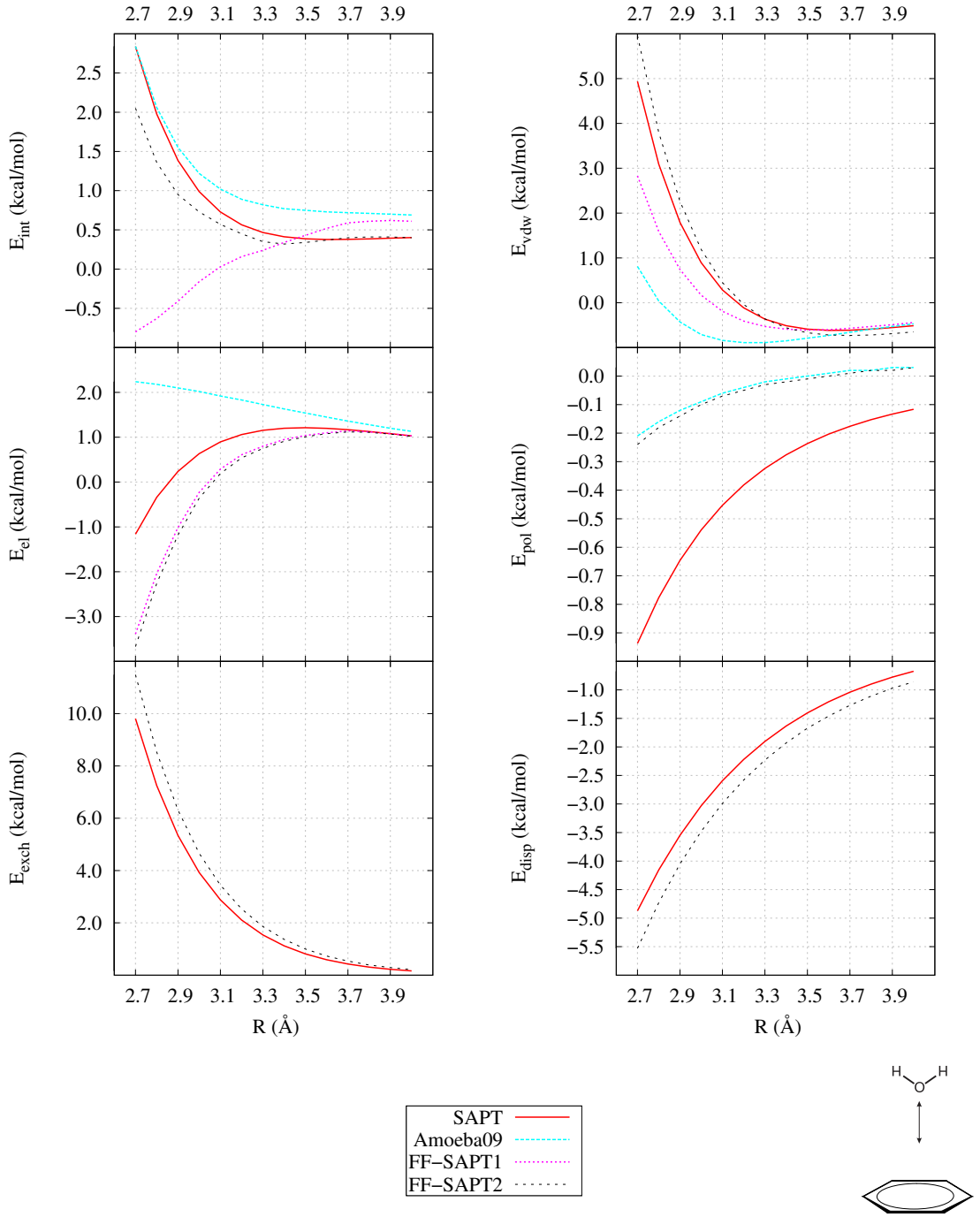

Figure 3.36.: AMOEBA09 and FF-SAPT force fields total energy and energy contributions against the DFT-SAPT reference energies (in kcal/mol) for the $H_2O...C_6H_6$ BO dimer as a function of the intermolecular distance. The force field energies are listed in Tabs. 7.19 and 7.20.

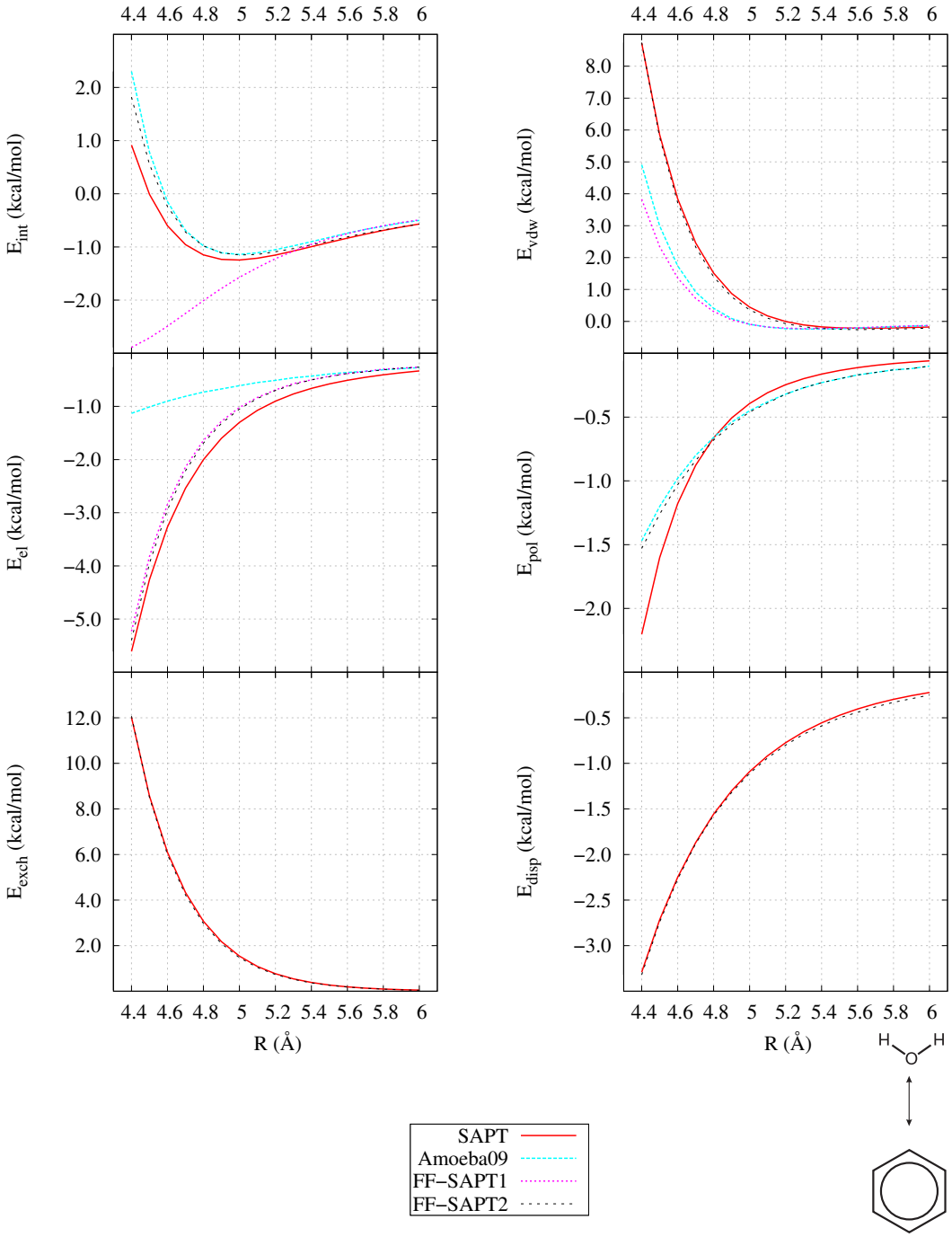

Figure 3.37.: AMOEBA09 and FF-SAPT force fields total energy and energy contributions against the DFT-SAPT reference energies (in kcal/mol) for the $H_2O...C_6H_6$ B S1 dimer as a function of the intermolecular distance. The equilibrium distance is 5.0Å. The force field energies are listed in Tabs. 7.21 and 7.22.

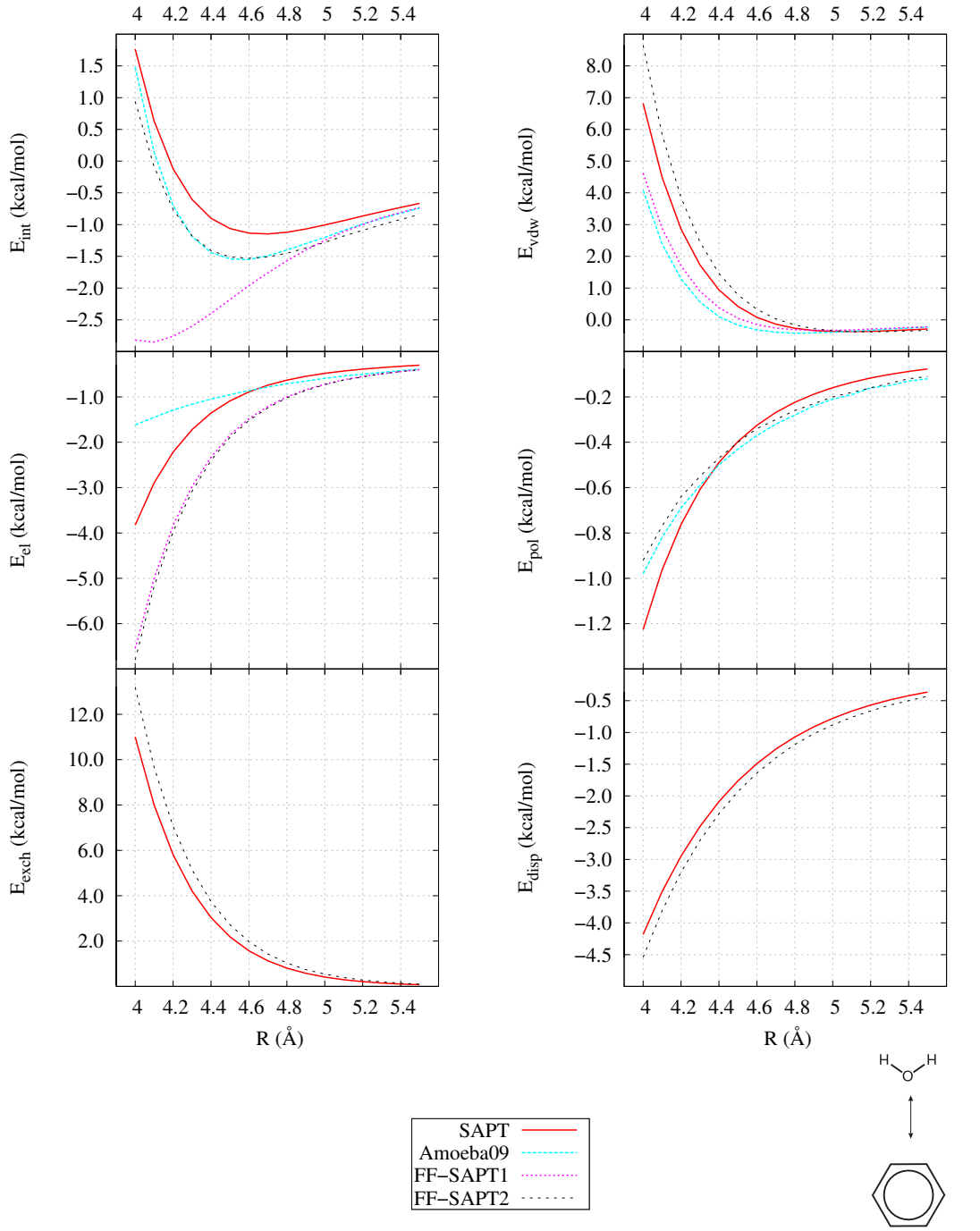

Figure 3.38.: AMOEBA09 and FF-SAPT force fields total energy and energy contributions against the DFT-SAPT reference energies (in kcal/mol) for the $H_2O...C_6H_6$ B S2 dimer as a function of the intermolecular distance. The equilibrium distance is 4.7Å. The force field energies are listed in Tabs. 7.21 and 7.22.

3.6. $H_2O...NH_4^+...C_6H_6$ Results

To check the reliability of the newly developed force fields, the $NH_4^+...C_6H_6$ complex was solvated using three (monodentate) or four (bi-, tridenate) explicit water molecules as can be seen in Fig. 3.40. The position of the water molecules were optimized while the positions of the NH_4^+ and C_6H_6 molecules were fixed. The reference energies were computed with the BLYP-D3/TZVP method since the system size is too large to use the CCSD(T)/avtz method. To evaluate the performance of the BLYP-D3/TZVP method, interaction energies of the monodentate h-shift (see fist graph in Fig. 3.5) are compared with the CCSD(T)/avtz energies. As recommended by the developer of the D3 correction, no counterpoise correction was used. The calculated energies are in good agreement. The DFT method overestimates the interaction by 0.5 kcal/mol and predicts a slightly larger (+0.1 Å) equilibrium distance of 3.1 Å.

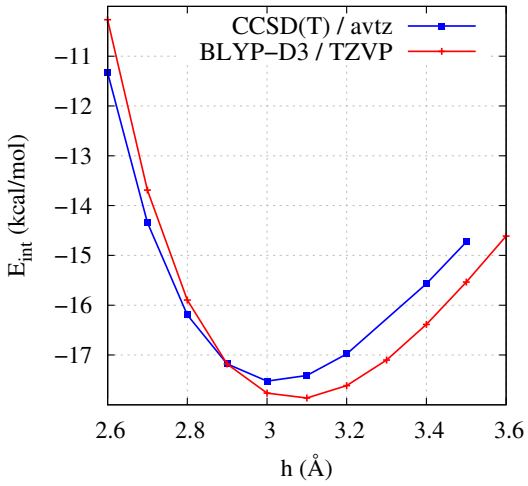

Figure 3.39.: Total interaction energies of the monodentate $NH_4^+...C_6H_6$ dimer using the CCSD(T) and dispersion corrected BLYP-D3 methods as function of the intermolecular distance. (in Å)

To calculate the interaction energy of the $NH_4^+...C_6H_6$ complex with the surrounding

water molecules, all possible types of interaction have been computed separately. The resulting complexes and the interactions included are summarized in Tab. 3.4.

	systems	interactions
	$C_6H_6 + NH_4^+ + H_2O$	$C_6H_6...NH_4^+$
		$C_6H_6...H_2O$
		$NH_4^+...H_2O$
		$H_2O...H_2O$
-	$C_6H_6 + H_2O$	$C_6H_6...H_2O$
		$H_2O...H_2O$
-	$NH_4^+ + H_2O$	$NH_4^+...H_2O$
		$H_2O...H_2O$
+	H_2O	$H_2O...H_2O$
$\sum =$	$C_6H_6...NH_4^+$	

Table 3.4.: Procedure to calculate the interaction between the $C_6H_6...NH_4^+$ dimer and the surrounding water molecules.

The computed potential energy surfaces of the solvated mono-, bi, and tridentate conformations are shown in Fig. 3.40. The force fields can reproduce the interaction energy of the monodentate conformation very accurately. The deviation produced by the force field methods in the vicinity of the equilibrium distance is below 1 kcal/mol. Compared to the DFT reference energies the force fields overestimate the bi- and tridentate interaction energies by about 1.0 and 1.5 kcal/mol, respectively. Upon the shift of the monodentate system the three water molecules are connected to the three hydrogen atom of the ammonium cation. The resulting energy curve is smooth since the position of these water molecules were frozen. Considering the region around the equilibrium distance of the bidentate system, the fluctuation of

the interaction energy is a result of the reorientation of the water molecules. At shorter distances a molecule chain $H_2O...H_2O...NH_4^+...H_2O...H_2O$ is present where two water molecules connecting the two available hydrogen atoms of the ammonium cation. Shifting the cation to larger distances, one $H_2O...H_2O$ chain is broken and now three water molecules are attached to the cation. The water molecules of the tridentate system are equally distributed around the cation at a large distance. Upon moving the cation closer to the benzene ring, the water is pushed away by the cation. This effect can be seen at a distance of h=4.0 Å.

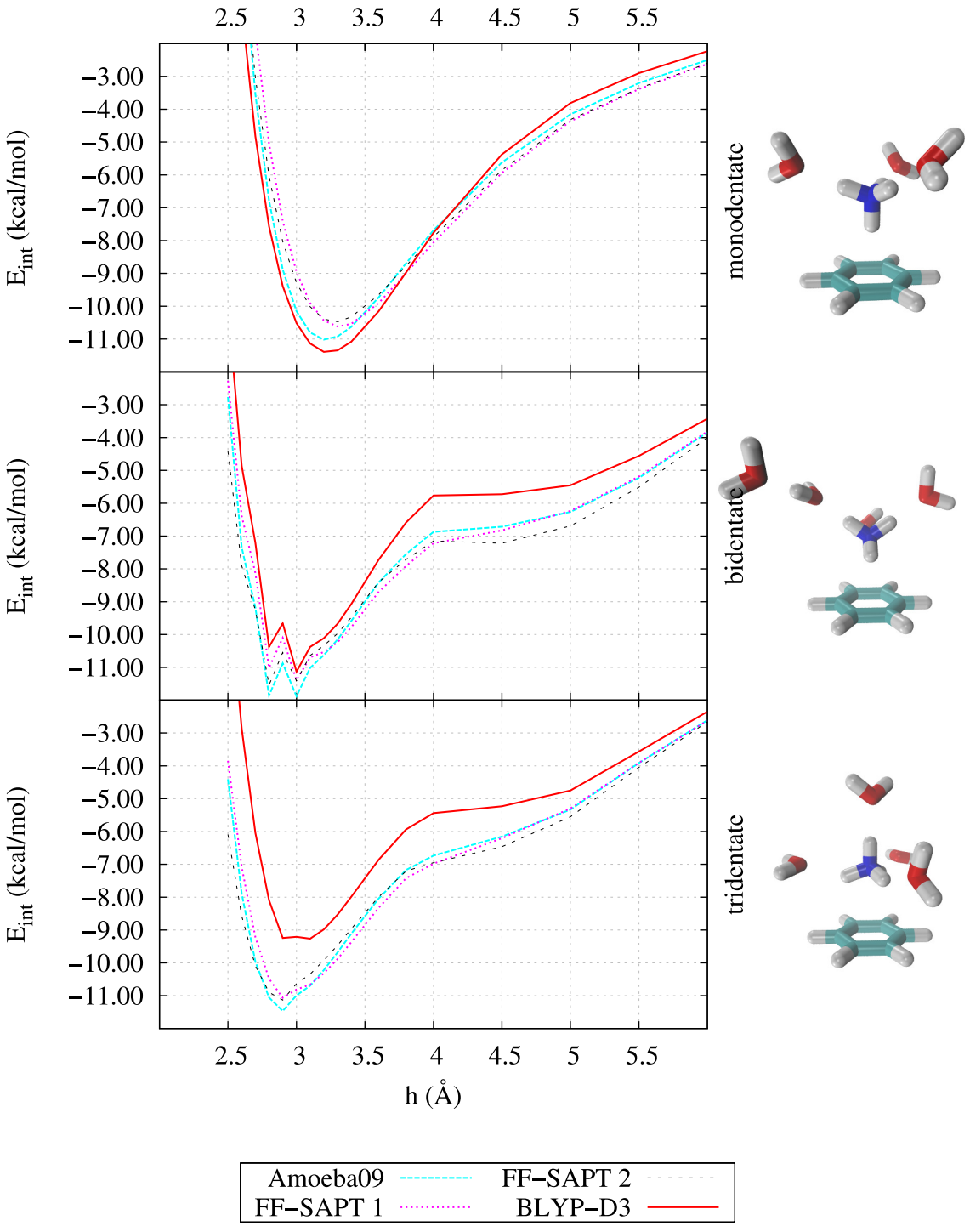

Figure 3.40.: Corrected AMOEBA09, FF-SAPT 1, FF-SAPT 2 and DFT interaction energies (kcal/mol) of the $H_2O...NH_4^+...C_6H_6$ cluster using the correction procedure shown in Tab. 3.4.

Part II.

Computational Investigation of Covalent Irreversible Vinyl Sulfone-based Protease Inhibitors

4. Introduction and Motivation

Proteases are peptide-bond-cleaving enzymes which are found in nearly all organisms throughout nature. Some proteases are essential for the survival of pathogenic organisms. In Fig. 4.1 (right cycle) the life cycle of such a protease is shown schematically. A protease reacts with a naturally occurring substrate which fits, according to the key-lock principle, exactly into the active site of the enzyme. After the reaction the products are removed from the active site and the protease again is prepared for the next substrate. To prevent this reaction an artificial ligand has to be created which has a higher affinity to the protease active site than the naturally occurring substrate. If this ligand binds irreversible to the protease (Fig. 4.1 left cycle) the original bond cleaving process can not take place anymore.

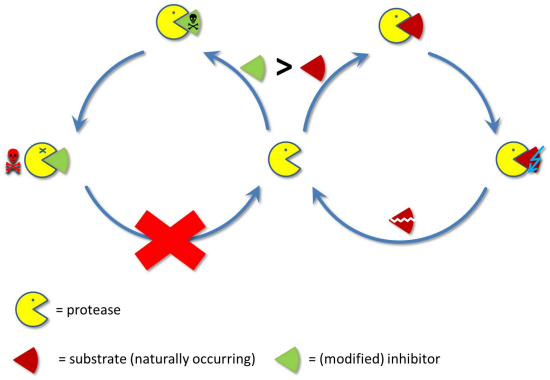

Figure 4.1.: Scheme of covalent-irreversible inhibition mechanism.

As mentioned above, to block an enzyme E the inhibitor I has to fit perfectly in the active site of the enzyme.[147] In Fig. 4.2 (bottom) the inhibitor of interest is shown. It fits perfectly into the active site of the enzyme as shown on top of Fig.

4.2 where it is stabilized only due to polar (hydrogen bonds, ionic interactions) and non-polar (vdW interactions) non-covalent interactions.

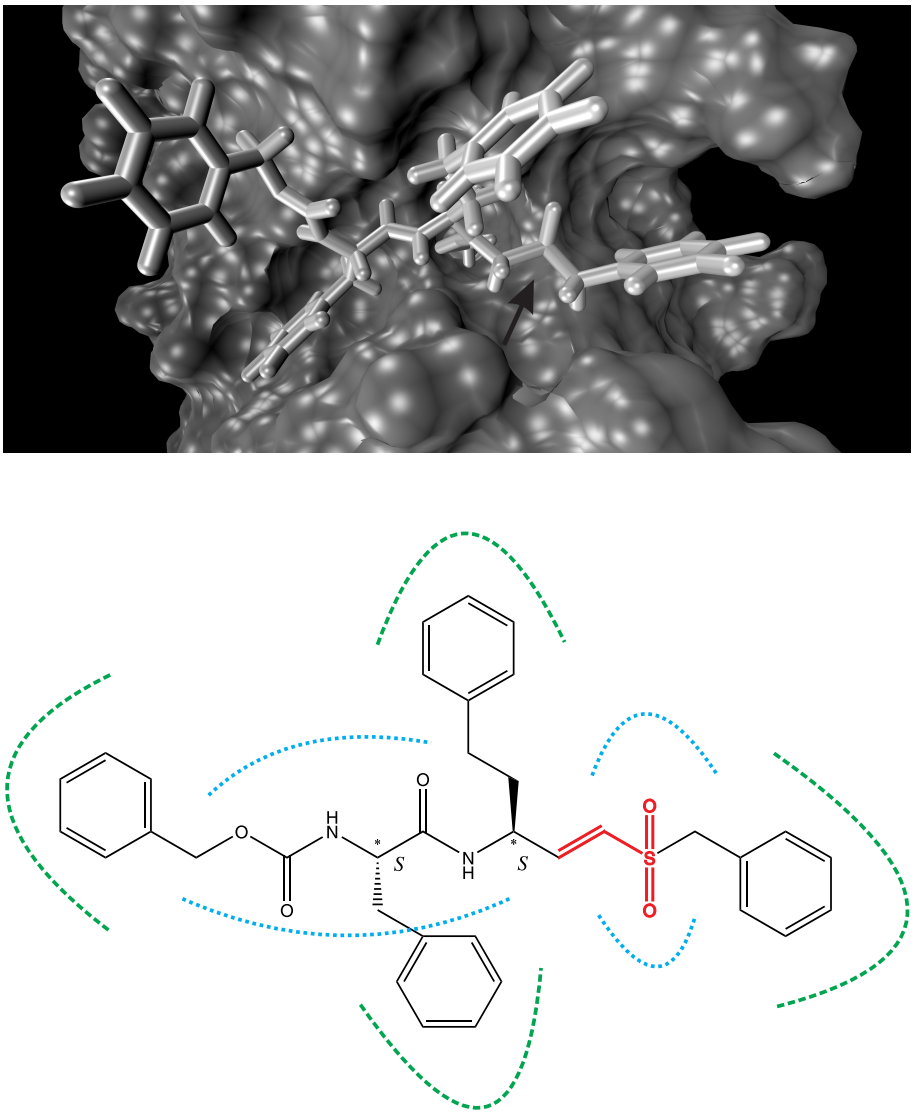

Figure 4.2.: Top: Enzyme-inhibitor complex of cruzain (surface representation) and vinyl sulfone (VS) inhibitor VS2[148]. The arrow points towards the VS SO_2 moiety. Bottom: Chemical structure of the VS2 inhibitor with a rough draft of non-polar (green interrupted line) and polar (blue dotted line) non-covalent interactions. The vinyl sulfone warhead is marked bold red.

To understand the mechanism of this kind of reaction the energy profile has to be

taken into account as shown in Fig. 4.3. The mentioned enzyme-inhibitor complex $E \cdots I$ can be found in the middle of Fig. 4.3. The reactants of the inhibition reaction are the solvated inhibitor and the solvated enzyme (E + I). The formation of the enzyme-inhibitor complex assumes the desolvation of the inhibitor and the removing of the water molecules located in the active site of the enzyme to achieve the needed space for the inhibitor. The energy gain of the newly created complex compared to the reactants is expressed in the free energy ΔG_b^0. Since this complex is stabilized by weak non-covalent interactions the complex can as easily cleaved as it is formed and thus the enzyme is only blocked reversible for a certain amount of time. The residence time depends on the thermodynamic properties (ΔG_b^0) of the reaction.The formation of a chemical bond (ΔG_R^0) is a possible way to increase the total interaction energy ($\Delta G_b^0 + \Delta G_R^0$) and consequently the residence time of the inhibitor inside the enzyme.[149] In the end, the inhibitor is covalently bound to the enzyme $E - I$ (red dotted line in Fig. 4.3).

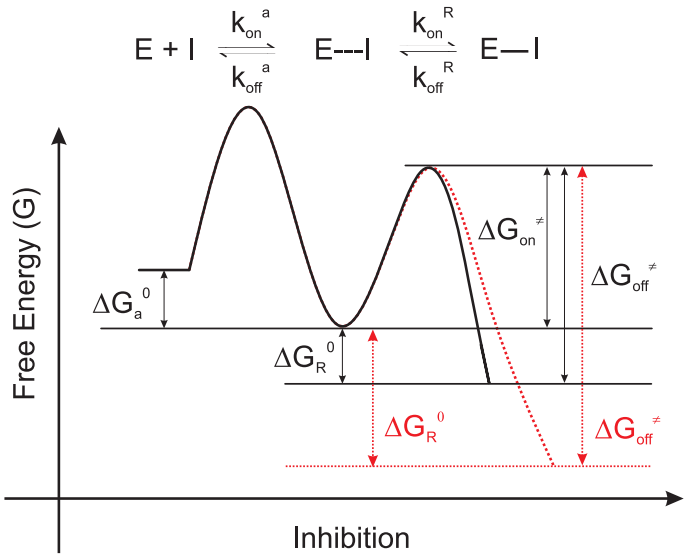

Figure 4.3.: Schematic energy diagram of the covalent inhibition reaction. The reversible reaction path is drawn solid in black and the irreversible reaction path is drawn dotted in red.

Irreversible covalent drugs (dotted red line in Fig. 4.3) are very successful and well

known. Famous representatives of covalent inhibitors are Penicillin and Aspirin.[150] The high reactivity of such inhibitors did not exclude unspecific reactions with various amino acids of proteins and DNA. Such side effects can accidentally stop the biosynthesis of human needed enzymes or can cause allergic reactions as known from Penicillin. Since the pharmaceutical industry is afraid of such off-target reactivity, covalent drugs are rarely considered in new drug discovery projects.[150] The residence time of reversible covalent drugs (solid black line in Fig. 4.3) is limited since the for- and backward reaction path of the inhibition reaction are energetically nearly identical. This entails that undesired side reactions do not take place since the thermodynamics of such reactions are not preferred. Drawback of reversible drugs are that the interaction with the target molecule is also short and the inhibition is temporary restricted. To combine the advantages of irreversible (long residence time) and reversible (minor side effects) inhibitors the forming of an reversible-covalent chemical bond is obvious.[151]

In medicinal chemistry vinyl sulfone-based (VS) inhibitors serve as building blocks for inhibitors of cysteine proteases.[152,153] The latter represents promising drug targets for many diseases, like osteoporosis[154], arthritis[155], cancer[156], or Alzheimer's disease[157], and in several parasitic infections, such as malaria[158], African trypanosomiasis ("sleeping sickness")[159], and Chagas' disease[160,161]. One of the most promising vinyl sulfone-based inhibitors is K11777 (N-methylpiperazine-Phe-homoPhe-vinylsufone-phenyl).[162] In several studies the efficacy of K777[163] (or K11777[153] - two identifier for one inhibitor) were tested in cell culture screen, Chagas' disease infected beagle dogs and mice without significant toxicity and is currently in late-stage preclinical trials for Chagas' disease.[164,165]

Peptidyl vinyl sulfones are stable, unreactive toward nucleophiles and need the catalytic machinery of the cysteine proteases for activation.[166]

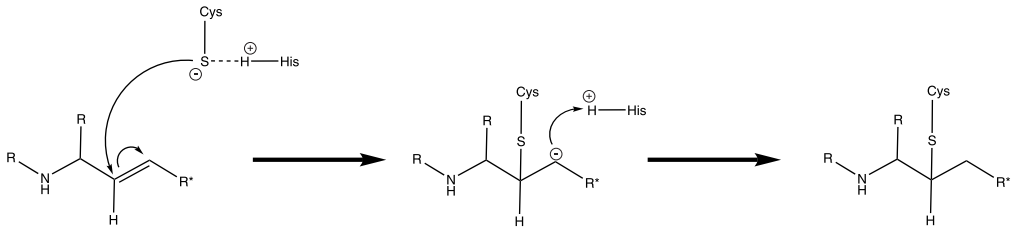

Figure 4.4.: Mechanism of inhibition of cysteine proteases by vinyl sulfones ($R^{\star} = SO_2R$) and α,β-unsaturated ester derivatives ($R^{\star} = CO_2R$).[166]

The mechanism of the inhibition of cysteine proteases by vinyl sulfones is deduced from the inhibition reaction of vinylogous amino acid esters, which proceeds via the Michael addition. The active site cysteine residue attacks the β-carbon, followed by a protonation of the α-carbon.[167] Palmer suggest in 1995 that the Michael addition is promoted by a hydrogen bond between the protonated His159 and one vinyl sulfone oxygen atom. The formed bond polarized the vinyl sulfone moiety and causes a positive charge at the β-carbon atom which support the nucleophilic attack of the Cys25.[168] In 2002 Powers found a further hydogen bond between the other vinyl sulfone oxygen atom and a glutamine residue of the active site.[166]

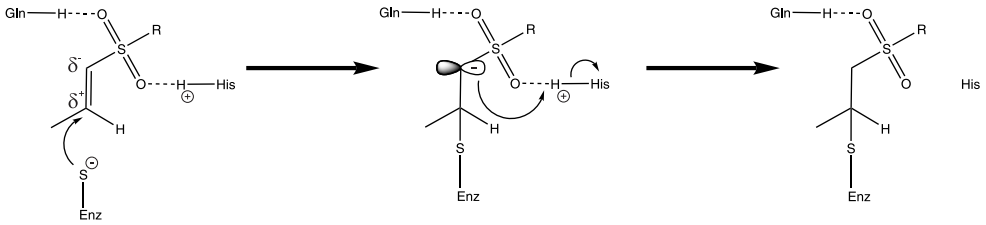

Figure 4.5.: Polarized double bond moiety of the vinyl sulfone.[168]

4.1. Aim of this Work

Since in the most publications concerning inhibition reaction the structural knowledge of the enzyme inhibitor complex is limited to crystal structures in which the inhibition reaction already occurred, they can not provide a picture for the non-covalent structure. Information concerning the non-bonded enzyme inhibitor com-

plexes are mostly provided by docking studies which are inaccurate due to the accuracy of the used methods. The inhibition reaction of cysteine proteases is a two-step process where in the first step a reversible enzyme-inhibitor complex is formed. The second step is initiated by the nucleophilic attack of the negatively charged Cys thiolate at one of the VS carbon atoms.

The formation and break of a chemical bond can accurately be described using quantum mechanical methods. This means if one wants to get insights into the enzyme-inhibitor complex, the formed bond from the inhibition reaction has to be broken. Due to the size of the enzyme-inhibitor complex, the method of choice is QM/MM where the part of the enzyme which is involved in the bond forming process is treated quantum mechanically (red marked in Fig. 6.4).[169] The rest of the enzyme as well as the surrounding water shell is treated by molecular mechanical methods.

Starting from a X-ray crystal structure (1f2a.pdb[148]) QM, QM/MM and QM/MM MD computations should be performed to investigate the mechanistic details of the inhibition reaction. Furthermore, the inhibitor should be modified by the substitution of the hydrogen atom located at the β-carbon with a chlorine atom. This modification of the inhibitor enables further reaction path ways which should be examined more closely.

5. Computational Methods

The systems were built from the X-ray crystal structure of cruzain complexed with the inhibitor VS2* (PDB ID: 1F2A[148]) as shown in Fig. 4.2. For the pure QM studies the inhibitor was extracted from the X-ray structure and modified manually. All QM computations were done using the Turbomole 6.5[132] program.

The sander module of AMBER[95,170] together with ff99SB parameters[96] was used for all MD simulations. Using the leap module of AMBERTOOLS 1.4 the protein was embedded in a TIP3P water shell with a radius of 45 Å in combination with spherical boundary conditions to retain the water molecules inside the shell.[171] The neutralization of the system was done using sodium ions. After the minimization of the created system for 500 steps the solvent shell was equilibrated by gradually increasing temperature with a solute restrained until the temperature reached 310 K, followed by a gradually reducing of the restrain applied to the solute. The productive MD was performed for 10 ns using a time step of 1 fs after the equilibration dynamics of 1 ns. For temperature control the Langevin thermostat was used. During structure optimization the protein structure and outer water layer were kept fixed for radii greater than 10 Å. The same condition employed for the force field MD simulations mentioned above are used for QM/MM and QM/MM MD simulations. The QM part of the QM/MM MD calculations was calculated using the PM3[172,173] method. The QM region is sketched in Fig. 6.4 (red part). It contains the vinyl sulfone part of the VS2 inhibitor and the Cys25 and His159 residues (cruzain numbering). The protein residues forming the hydrogen bonds to the inhibitor are not

*3-[N-[benzyloxycarbonyl]-phenylalaninyl-amino]- 5-phenyl-pentane-1-sulfonylmethylbenzene

included in the QM part, since their electrostatic interactions with the active site should to be well represented by the electrostatic embedding scheme.[174] In assigning the QM region for amino acids, the link atom approach using hydrogen atoms was utilized. Again, the AMBER ff99SB parameter set was used for the MM region and the neutralization of the system was done using sodium ions. For the umbrella sampling the same conditions as used for the QM/MM MD simulations are applied. The α- and β-carbon atoms of the VS inhibitor are direct involved in the reaction (Fig. 6.1). The reaction coordinates are the bond length between (1) the sulfur atom of Cys25 residue and the VS β-carbon atom, (2) the VS α-carbon atom and the transferred hydrogen atom, and (3) the His162 δ-nitrogen atom and the transferred hydrogen atom. The used pair of reaction coordinates is mentioned in the discussed results respectively. Each step contain a 10 ps equilibration and a subsequent 10 ps productive run for data collection. The potential of mean force (PMF) profiles were obtained with weighted histogram analysis (WHAM)[175–177] using the code by Grossfield[178].

For the QM/MM calculations the same conditions as used for the QM/MM MD calculations are applied in combination with the ChemShell 3.3 program[179]. The QM/MM boundary was described using an electrostatic embedding scheme and the link atom approach.[180?,181] The QM part was calculated using semiempirical (PM3) and DFT (BLYP/TZVP, B3-LYP/TZVP) methods.

6. Results

In order to investigate the mode of action of the vinyl sulfone inhibitor, shown in top of Fig. 6.1, the following procedure was performed: As a first step the VS2 inhibitor was used to perform QM, QM/MM, and QM/MM MD calculations of the inhibition reaction. The archived results are used as reference values for the obtained reaction profiles using the modified inhibitors. To save computational time, the QM calculations were used to screen a large amount of possible substitution patterns at the vinyl sulfone moiety. Then, only the most promising candidates are used for further calculations using the QM/MM and QM/MM MD methods. On the upper right side of Fig. 6.1 the possible substitution positions located at the α- and β-carbon atoms are shown. The substitution of the hydrogen atoms connected to this positions should influence the nature of the inhibitor and of the respective reaction mechanism.

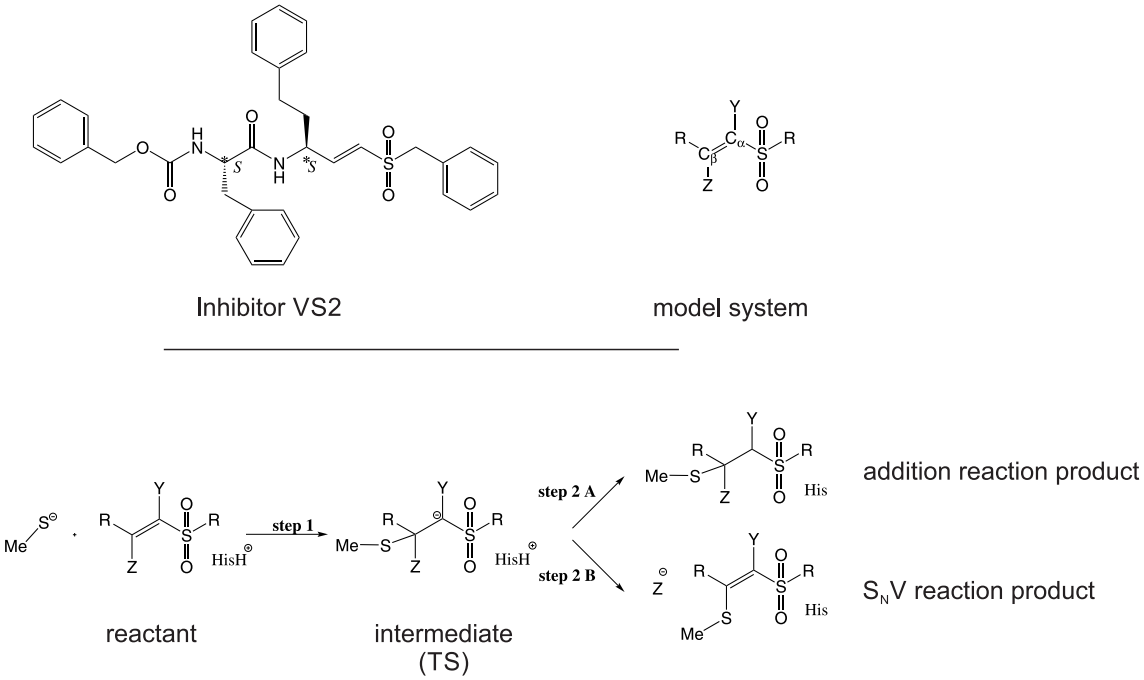

Figure 6.1.: Structure of the inhibitor considered in this part of the work. Left: the complete inhibitor. Right: Model system of the mentioned inhibitor used for the QM calculations.

6.1. QM Results

To calculate the thermodynamic properties of the reaction shown in Fig. 6.1 the energy difference between the products and reactants has to be computed. To get also information about the kinetics of the reaction the energy difference between the transition state and the reactants is used. Here the optimized structure resulting from the attack of the MeS^- moiety to the inhibitor act as transition state geometry. This method is only a rough assumption since it assumes a two step mechanism. Since the protonation state of the enzyme active site is assumed to be zwitterionic, the residues $MeS^-/HisH^+$ are included in the calculation. The possible intermolecular interactions between the residues and the inhibitor are not taken into account to get comparable results since such interactions can have a drastically impact on the obtained results. The influence of substituents located at the

Y (C_α-atom) and Z position (C_β-atom) were investigated in this way. Beside the hydrogen atom as reference substituent, the (pseudo)halogens F, Cl, Br, and CN are chosen since the influence of the mesomeric and inductive effects can be investigated in this way. While the inductive effect decreases (F>Cl>Br>CN) with smaller electro-negativity, the mesomeric (+M) effect also decreases (F>Cl>Br) and turns into a negative mesomeric effect (-M). Crucial for the course of the reaction is the combination of mesomeric and inductive effects.

The influence of the substituents in C_α position is shown on the left side of Tab. 6.1. The formation energy of the intermediate (TS) is endothermic for Y=H (5.7 kcal/mol) and becomes most exothermic for Y=CN (-18.6 kcal/mol). As already mentioned, the CN group has a -M/-I effect and is able to stabilize a negative charge very well. In case of the halogenes, the +M effect is dominating since considering only the -I effect the energy should become more exothermic in the order Br>Cl>F. However, this is not the case due to the +M effect destabilizing the negative charge. Compared with the original inhibitor, the first step of the addition reaction is favored for all calculated possibilities. The second step of the addition reaction is the protonation of the negative charge at C_α position. Now, the stability of the charged intermediate determines the exothermicity of the reaction. These opposing trends in reaction energy results in an interesting total energy of the addition reaction. Within the accuracy of the used methods the reactions with Y=H and F give similar results (-30.5 and -31.0 kcal/mol), while the other halogens give slightly less exothermic results (Cl: -28.9, Br: -28.7, CN: -26.3 kcal/mol).

When the halogen atom is located at Z position, two possible reaction mechanisms are possible: an addition and a substitution reaction. For Z=F, Cl and Br the computations obtains no TS structures and the substitution reaction takes place without an energy barrier. For Z=CN the MeS moiety is separated from the TS structure instead of the CN group. However, the total energies of the substitution reaction increase in the order CN<F<Cl<Br which represents the order of the strength of

the corresponding acid going from the weakest (HCN) to the strongest (HBr). The total reaction energies of the addition reaction did not differ much from the reference value -30.5 kcal/mol. The halogen atom located at Z position has no significant influence on the addition reaction.

	Z=H, Y=Hal			Z=Hal, Y=H Add			Subst
Hal	R → TS	TS → P	R → P	R → TS	TS → P	R → P	R → P
H	5.7	-36.2	-30.5	5.7	-36.2	-30.5	–
F	3.3	-34.3	-31.0	–	–	-32.8	-20.2
Cl	0.3	-29.2	-28.9	–	–	-31.9	-47.7
Br	-0.5	-28.2	-28.7	–	–	-32.2	-53.5
CN	-18.6	-7.7	-26.3	–	–	-28.9	-8.1

Table 6.1.: Calculated reaction energies for the reactions shown in Fig. 6.1 (bottom) in kcal/mol. Left part: modification of the inhibitor at C_α-atom and right part: modification of the inhibitor at C_β-atom results in two possible reaction mechanisms. B-LYP/TZVP//B3-LYP/TZVP (COSMO $\epsilon = 78.39$).

Using semiempirical methods the computed geometries of reactants and products agrees with the DFT results. The corresponding reaction energies differ significantly from the DFT energies but show the same trends (Tab. 6.2). The semiempirical methods could be used to compute the molecular geometries very efficiently. This benefit will be used in the following QM/MM and QM/MM MD calculations.

Hal	Z=H, Y=Hal				Z=Hal, Y=H Add				Z=Hal, Y=H Subst			
	DFT	PM3	PM6	PM6-D3	DFT	PM3	PM6	PM6-D3	DFT	PM3	PM6	PM6-D3
H	-30.5	-20.6	-12.8	-15.3	-30.5	-20.6	-12.8	-15.3	–	–	–	–
F	-31.0	-16.7	-13.3	-14.1	-32.8	-11.9	-15.8	-16.0	-20.2	10.0	-4.8	-5.0
Cl	-28.9	-16.4	-8.1	-9.9	-31.9	-17.1	-12.0	-10.7	-47.7	-35.0	-33.2	-33.3
Br	-28.7	-18.6	-6.8	-6.8	-32.2	-21.7	-11.7	-11.5	-53.5	-51.6	-36.4	-36.6
CN	-26.3	-14.0	-10.8	-10.9	-28.9	-15.0	-17.1	-16.5	-8.1	9.7	31.6	31.4

Table 6.2.: Comparison of the thermodynamics using DFT (B-LYP/TZVP//B3-LYP/TZVP) and semiempirical methods (PM3, PM6, PM6-D3) in combination with COSMO ($\epsilon = 78.39$) in kcal/mol.

6.2. QM/MM Results

Figure 6.3 shows schematically the enzymatic surrounding of the covalently bound VS2 inhibitor in cruzain (product structure) obtained after the preparation procedure as described in the previous chapter. This structure corresponds to the experimental derived X-ray structure and shows no significant structural differences. A minor movement of the protein side chains and the phenyl moieties of the inhibitor are mentionable but do not influence the interactions between inhibitor and protein. These differences arise from a higher flexibility caused by the physiology environment of the protein compared to the rigid crystal environment. Figure 6.4 shows the corresponding reactant structure obtained from QM/MM computations. The shown structure represents the minimum energy geometry of the corresponding potential energy surface (PES) obtained by a full optimization without constraints. The calculated PES of the addition reaction is depicted in Fig. 6.5, while Table 7.27 gives some selected geometrical parameters.

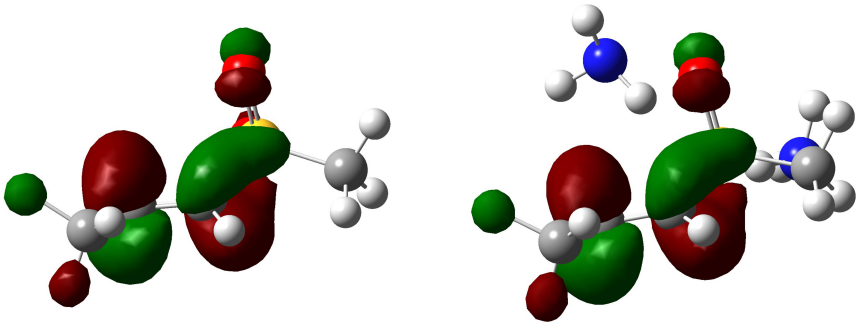

Figure 6.2.: LUMO orbitals of VS inhibitor model without (left) and with (right) hydrogen bonds to the vinyl sulfone oxygen atoms.

Let us first concentrate on the differences between the hydrogen network before and after the reaction. In the non-covalent complex the hydrogen network has to stabilize the zwitterionic form of the Cys25-S^-/His162-H^+ ion pair in the active site. The often discussed hydrogen bond between the His162 and one vinyl sulfone oxygen atom and the resulting polarization of the double bond (see literature[168])

could not be substantiated. The computation shows two hydrogen bonds between one vinyl sulfone oxygen atom and Trp184 (1.78 Å) and Gln19 (1.86 Å). The purpose of these bonds is either the fixation of the inhibitor in the right position for the attack of the nucleophilic sulfur or to polarize the double bond is proven by a QM model calculation (the position of heavy atoms are obtained from pdb structure; optimization of added hydrogen atoms using D3-BLYP/TZVP/COSMO(78.39); orbitals B3-LYP/TZVP). As shown in Fig. 6.2, the hydrogen bonds did not influence the LUMO orbital of the vinyl sulfone moiety. The only function of the sulfone group is to keep the double bond in the right position for the inhibition reaction.

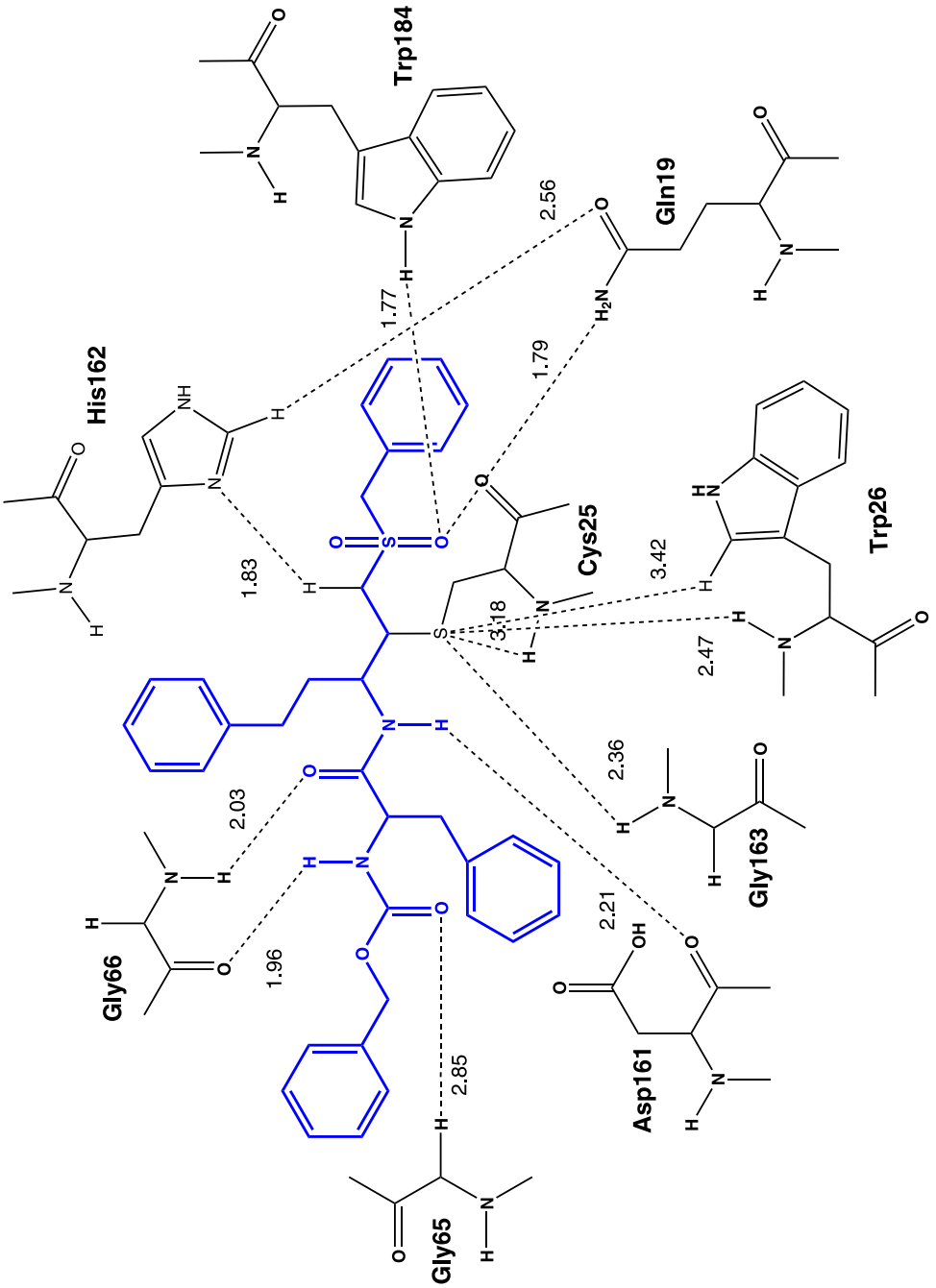

Figure 6.3.: Geometric details of the covalent bonded inhibitor in the active site of cruzain. This structure corresponds to the X-ray structure and was prepared and optimized using the QM/MM method as described in chapter 5. The arrangement of the cruzain residues corresponds not the exact position in the protein to get a clearer insight in the interactions between inhibitor and protein.

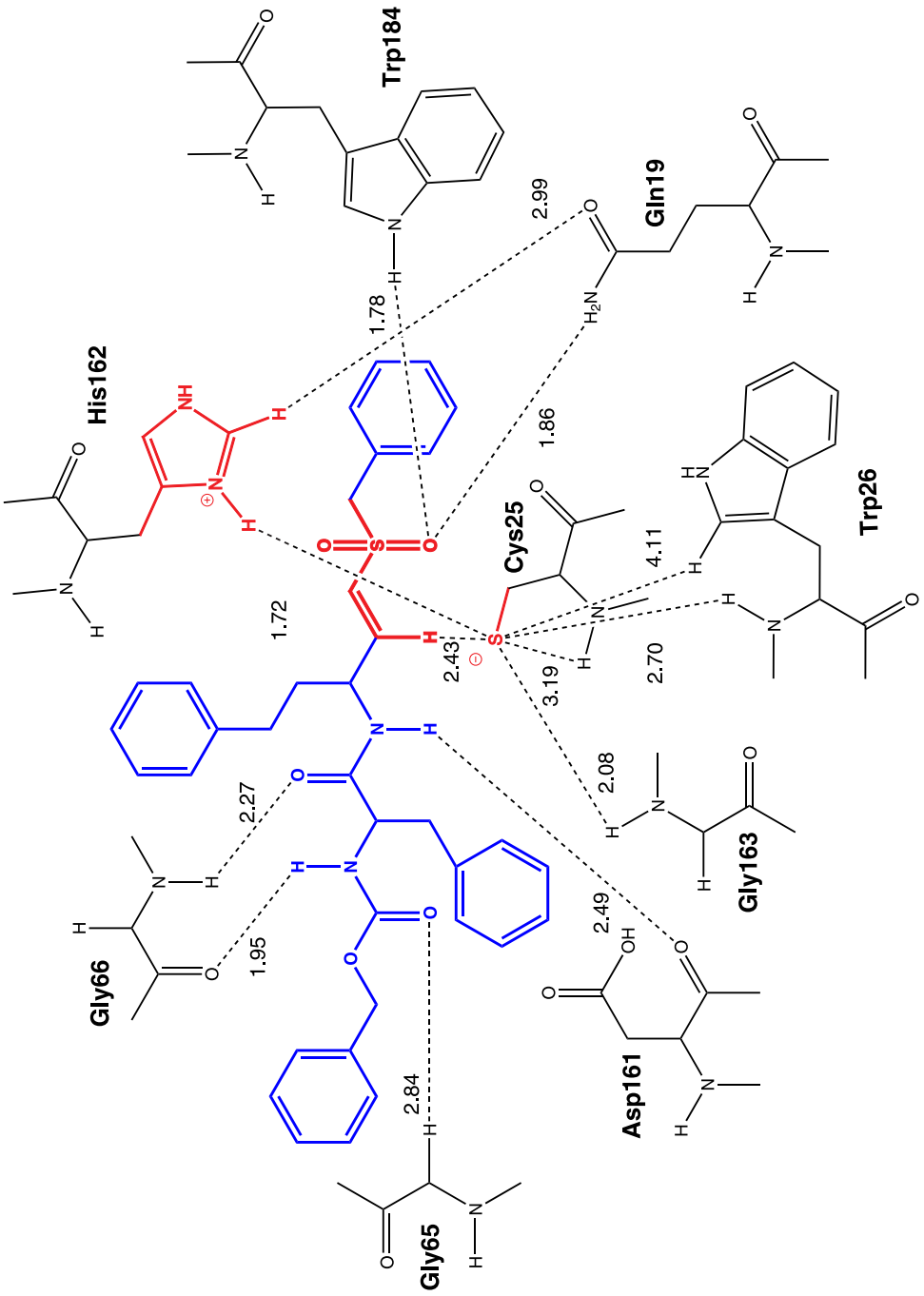

Figure 6.4.: Geometric details of the non-covalent bonded inhibitor in the active site of cruzain. The structure was calculated using the QM/MM method. The arrangement of the cruzain residues corresponds not the exact position in the protein to get a clearer insight in the interactions between inhibitor and protein.

The differences in the hydrogen bond network between the covalent bound product (Fig. 6.3) and non-covalent bound reactant complexes (Fig. 6.4) is given in Tab. 7.27. The nomenclature of the interactions is simplified so that for example the bond Gly66(N) describes the interaction between the glycine hydrogen (located at the glycine backbone nitrogen atom) with the peptide oxygen atom of the inhibitor as can be seen in Fig. 6.3, respectively. Going from the reactants to the products the bond length of Gly66(N) (Δ=-0.24 Å), Gln19 (Δ=-0.07 Å) and Asp161 (Δ=-0.28 Å) decreases, while the bond length of Gly66(O), Gly65 and Trp186 did not change (within the accuracy of the used method) during the reaction. The reaction energy (ΔE=-19 kcal/mol) is in agreement with the experimental values.[148] One reason for the exothermicity of the reaction could be the formation of a neutral resting state out of the zwitterionic form. The calculated inhibition reaction shows one reaction barrier (Fig. 6.5) for the attack of the sulfur atom. The protonation of the resulting negative charged inhibitor takes place without a reaction barrier. As a result, the inhibition reaction has a two-step-one-barrier mechanism.

On the one side a small change of the position of the inhibitor is caused by the used method since in QM/MM only a minimization is performed. On the other side, one may conclude that the inhibitor fits perfectly into the enzymatic environment so that the reaction can take place without any distortion forming other parts of the molecule.

To increase the efficiency of the inhibition reaction, the inhibitor was modified by replacing the hydrogen atom at the vinyl sulfone double bond β-carbon atom by a chlorine atom. This substitution enables the possibility of a normal addition reaction like the original inhibitor on the one side and a vinylogous nucleophile substitution (S_NV) on the other side.

As a first step, we compare the non-covalent bounded reactants before having a closer look on the reaction progress. Some selected geometrical parameters are given in Tab. 7.29. The inhibitor side chain interaction with the enzyme prefers the

substituted (X=Cl) inhibitor, since the two hydrogen bonds to Gly66(N) (2.66 Å) and Asp161 (2.20 Å) are shorter than in the original inhibitor, while the bond to Gly66(N) is slightly weaker but with 2.50 Å still existing. The H bonds to the vinyl sulfone oxygen atoms are stronger compared to the original inhibitor. A comparison shows a 0.18 Å (Trp184) respectively 0.83 Å (Gln19) shorter bond length in the original enzyme inhibitor complex compared with the modified one. The hydrogen bonds which are present in both (X=H, Cl) inhibitors did not differ significantly from each other except for the interaction with Trp26 which is 0.30 Å shorter in the original inhibitor. The interaction of interest is the one of Cys25 thiolate with the hydrogen bond at the β-carbon atom where the attack takes place. In case of the original inhibitor we found a hydrogen-bond of 2.43 Å, where the hydrogen sits more or less between the nucleophile and electrophilic partners of the reaction. During the inhibition reaction this hydrogen must be pushed away to give the Cys25 enough space for the reaction. In the complex containing the modified inhibitor this hydrogen bond is not present. Due to the repulsion between the chlorine atom and negatively charged sulfur, the chlorine atom is not in the vicinity of the reaction path of the nucleophilic attack. Based on this geometrical data, one may conclude that the reaction barrier for the modified inhibitor (X=Cl) should be less high since the attacked double bond is already in the right position for the reaction. Comparing Fig. 6.5 with Fig. 6.6, the reaction barriers did not differ from each other. A reason could be that the original inhibitor compensates the unfavorable position of the double bond with a stronger hydrogen network allocated over the whole inhibitor.

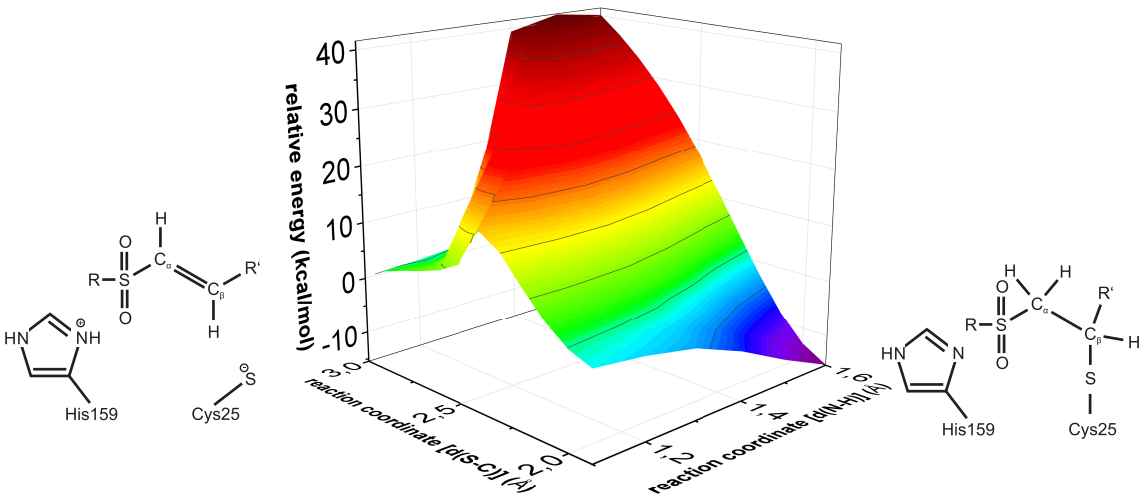

Figure 6.5.: Potential energy surface of the inhibition reaction with the original inhibitor. QM: PM3 MM: Amber (TS = +16.7 kcal/mol; Rx = -19.0 kcal/mol) The interactions of the inhibitor with the enzymatic surrounding is sketched for the reactant in Fig. 6.4 and for the product in Fig. 6.3.

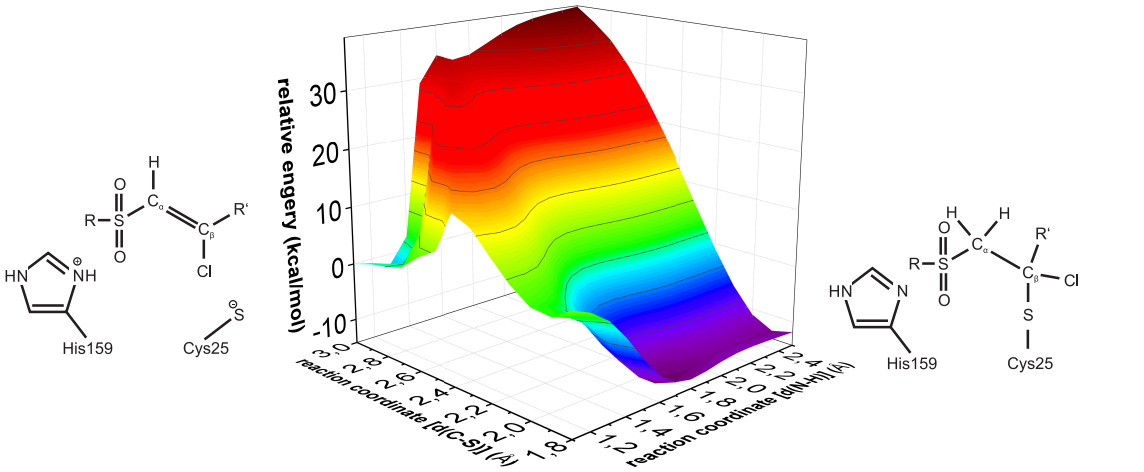

Figure 6.6.: Potential energy surface of the addition reaction with the modified inhibitor. QM: PM3 MM: Amber (TS = +16.1 kcal/mol; Rx = -9.9 kcal/mol). The interactions of the inhibitor with the enzymatic surrounding is sketched for the reactant in Fig. 7.3 and for the product in Fig. 7.4.

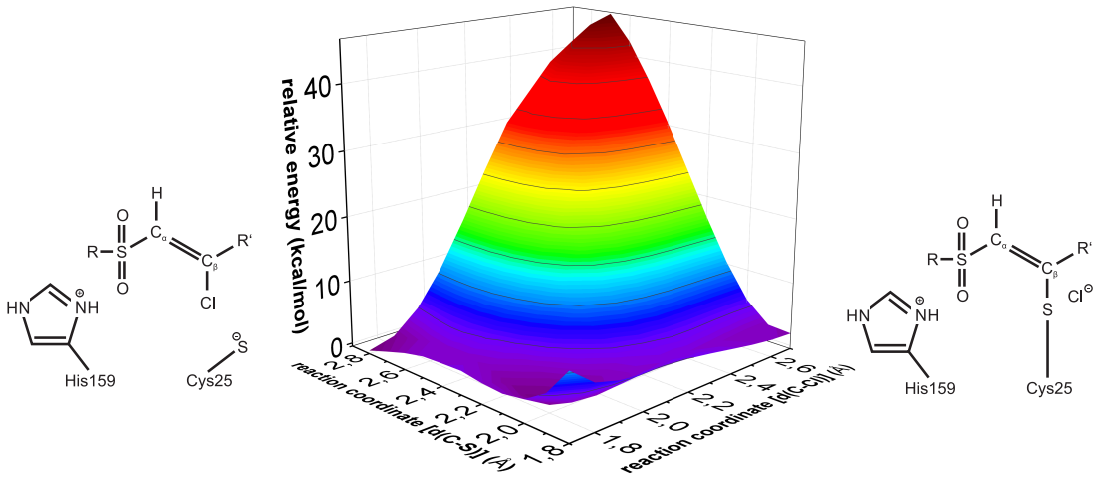

Figure 6.7.: Potential energy surface of the S_NV reaction with the modifed inhibitor. QM: PM3 MM: Amber (TS1 = +2.8 kcal/mol; ZP = +0.6 kcal/mol; TS2 = +3.1 kcal/mol; Rx = +9.4 kcal/mol). The interactions of the inhibitor with the enzymatic surrounding is sketched for the reactant in Fig. 7.3 and for the product in Fig. 7.5.

To describe the inhibition reaction containing the modified inhibitor, the following calculation scheme was performed: Starting point for the calculation is a frame from the MD simulation with the modified inhibitor like it was done with the original one before. Since the starting point is the product of the addition reaction, we increase the distances between the Cys25 sulfur - VS β-carbon and His162 hydrogen - VS α-carbon and end up at the non-bonded enzyme inhibitor complex (reactant of the inhibition reaction) (Fig. 6.6). Changing at this point the reaction coordinates into the bonds between Cys25 sulfur - VS β-carbon and VS chlorine - VS α-carbon, one can calculate the S_NV reaction from the reactants to the products (Fig. 6.7). The PES shape of the addition reaction with the modified inhibitor looks similar to the one with the original inhibitor. The reaction energy (ΔE=-9.9 kcal/mol) is 9 kcal/mol less exotherm compared to the original inhibitor. The reason may be the magnitude of the chlorine atom compared to the hydrogen atom. Since in the product complex the position of the chlorine atom is nearly fixed and the resulting steric interaction leads to a less favored reaction energy.

The activation energy does not shows significant differences (one reason may be that the PM3 method did not well enough describe the transition state of the investigated reaction). The shape of the S_NV PES (Fig. 6.7) shows no barrier for the thiolate attack of the Cys25 and the overall reaction energy is endotherm (ΔE=+9.4 kcal/mol). This result is somewhat unexpected, since the first step of the reaction (thiolate attack) is present in both, the addition and the S_NV reaction, and so the shape of the PES's should look similar for this first step.

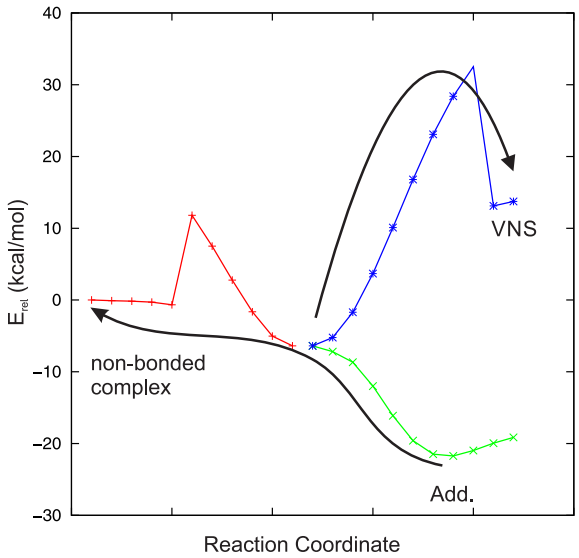

Figure 6.8.: Two dimensional PES of calculated (QM/MM) inhibition reaction with the modified inhibitor. The red line show the energy curve of the Cys25 attack towards the β-carbon of the VS creating the enzyme-inhibitor complex (crossing point of the red, blue and green line). In the following the addition reaction (green) or S_NV reaction paths (blue) are possible. The black arrows show the order of calculation.

To have a closer look to that problem the two reaction steps were calculated separately. In Fig. 6.8 the procedure of the following investigation is shown. Again, starting from the addition product, the proton is shifted stepwise to the His162 moiety. In the next step the Cys25-VS bond or the chlorine-VS bond could be decreased to either calculate the reaction path to the reactants or the path to the S_NV products. This could be done since we know from the previous PES (Fig. 6.6

and 6.7) that the Cys25 sulfur - carbon distance is 1.9 Å when the system has to decide whether the addition reaction or the S_NV reaction will take place. During the calculation all three bonds involved in the reaction were kept fixed.

The addition reaction (shown in Fig. 6.8) is in accordance with the reaction shown in Fig. 6.6. The origin of the strong increase of energy (red line) at the beginning of the reaction lies in a motion of the His162 residue. At the beginning of the reaction the proton of His162 points towards the Cys25 thiolate. During the reaction the His162 ring rotates so that the proton now points towards the VS α-carbon atom and cannot further stabilize the Cys25 thiolate. This rotation is not caused due to the fixation of bonds, since only the His162-hydrogen bond is fixed. The process of the S_NV reaction in Fig. 6.8 looks different than the one in Fig. 6.7. Again, the first step of the reaction is the attack of the Cys25 thiolate towards the VS β-carbon. After that the system could decide either to take the way of the addition or either the way of the S_NV reaction. Independently of the way of the reaction the His162 ring rotates during the first step, so that the proton points towards the VS α-carbon. If now the distance of the chlorine - VS β-carbon increases, the energy of the reaction path increases too. The energy jump at the end of the S_NV reaction again is caused by a rotation of the His162 moiety. At this stage of the reaction the His162 rotates backward with the proton pointing to the Cys25 sulfur atom. During the attack of the thiolate in the first step of the reaction the VS α-carbon character goes from sp^2 to sp^3 since the electrons from the previous double bond form an electron pair at this atom. In case of the addition reaction the negative charge at the sp3 center is stabilized due to the addition of the His162 proton. In case of the S_NV reaction, the chlorine atom is removed and the electron pair is shifted into the double bond. The electronic character of carbon atoms goes from sp^3 to sp^2, and the attraction between the negatively charged sp^3 carbon and the $His162H^+$ is lost.

Now a question comes up: why is the S_NV reaction so endothermic? Several possible answers exists. (i) The used Method (PM3) is unable to describe this reaction. (ii)

The environment (protein, water shell) is optimized for the addition product. (iii) The chlorine can't leave the active site, so the reaction is not complete.

To (i): To compare PM3 with DFT method, the structures from Fig. 6.8 were used as an input for constrained optimization with BLYP/TZVP. The resulting PES is given in the upper part of Fig. 6.10. From previous results it is obvious that in DFT calculations the zwitterionic state is not stable. This may be the reason why the reaction energy of both possibilities is so exothermic. The obtained structures from the DFT calculations do not differ from the PM3 structures, which confirmed the use of this method.

(ii) A closer look to the environment of the reaction shows that due to the order of the QM/MM calculations, the environment is optimized to the addition product state of the enzyme inhibitor complex. During the QM/MM calculation only a minimization and no relaxation of the system is performed. That means that in both, the non-bonded complex and the S_NV reaction products, the enzymatic environment corresponds to the addition product. To solve this problem a QM/MM MD calculation could be performed. That means at every point of the QM/MM PES a MD simulation is performed to relax the enzymatic environment accordingly to the current state of the reaction in the QM part. The QM/MM MD results will be discussed later.

A further point (iii) is that the chlorine ion did not leave the active site within the QM/MM calculations. In Fig. 6.9 the three stationary points of the PES (non-bonded complex, addition product, S_NV product) are shown. The chlorine (pink ball) is located in the active site between the inhibitor (ball and stick / wire frame) and the enzyme (surface representation). To get a hint of the proportion of the chlorine, the vdW representation is used. The pictures show a small channel which the ion has to pass before it could be solvated from the surrounding water molecules. From the QM/MM calculations it is not clear if that solvation is possible. Also for that point the QM/MM MD calculation should give an appropriate answer.

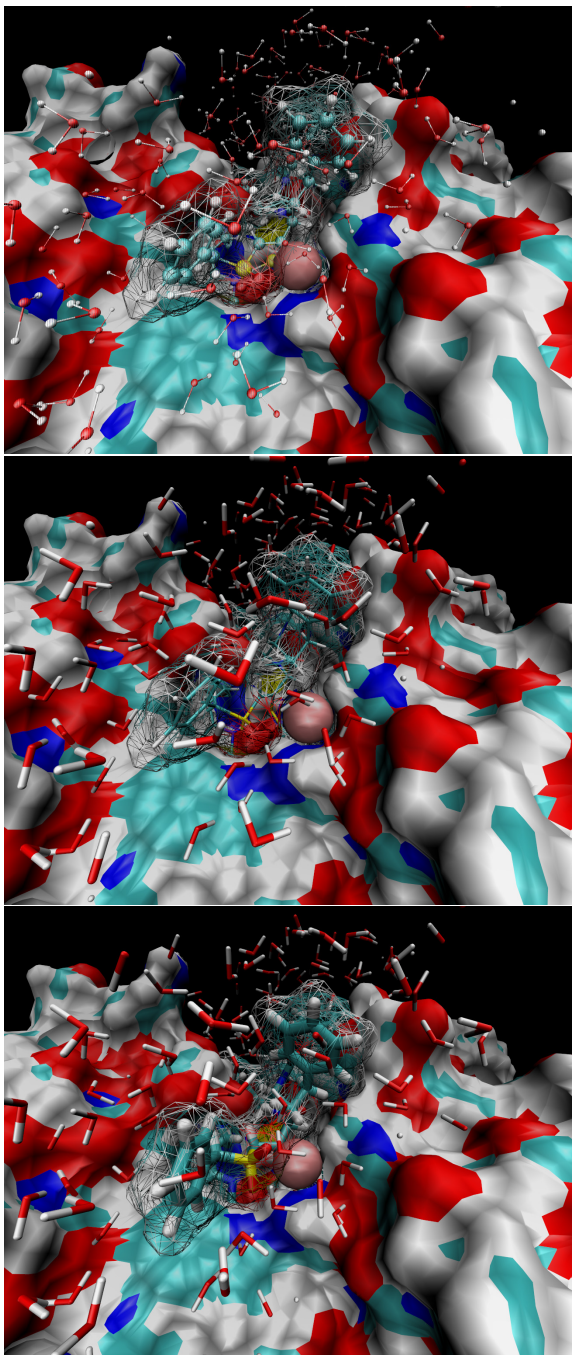

Figure 6.9.: Active site of cruzain (surface representation) with modified inhibitor (wired frame representation) and separate highlighted chlorine atom (pink vdW representation) top: non-bonded complex; middle: product of S_NV reaction; bottom: product of addition reaction. (QM/MM results, optimized without constraints)

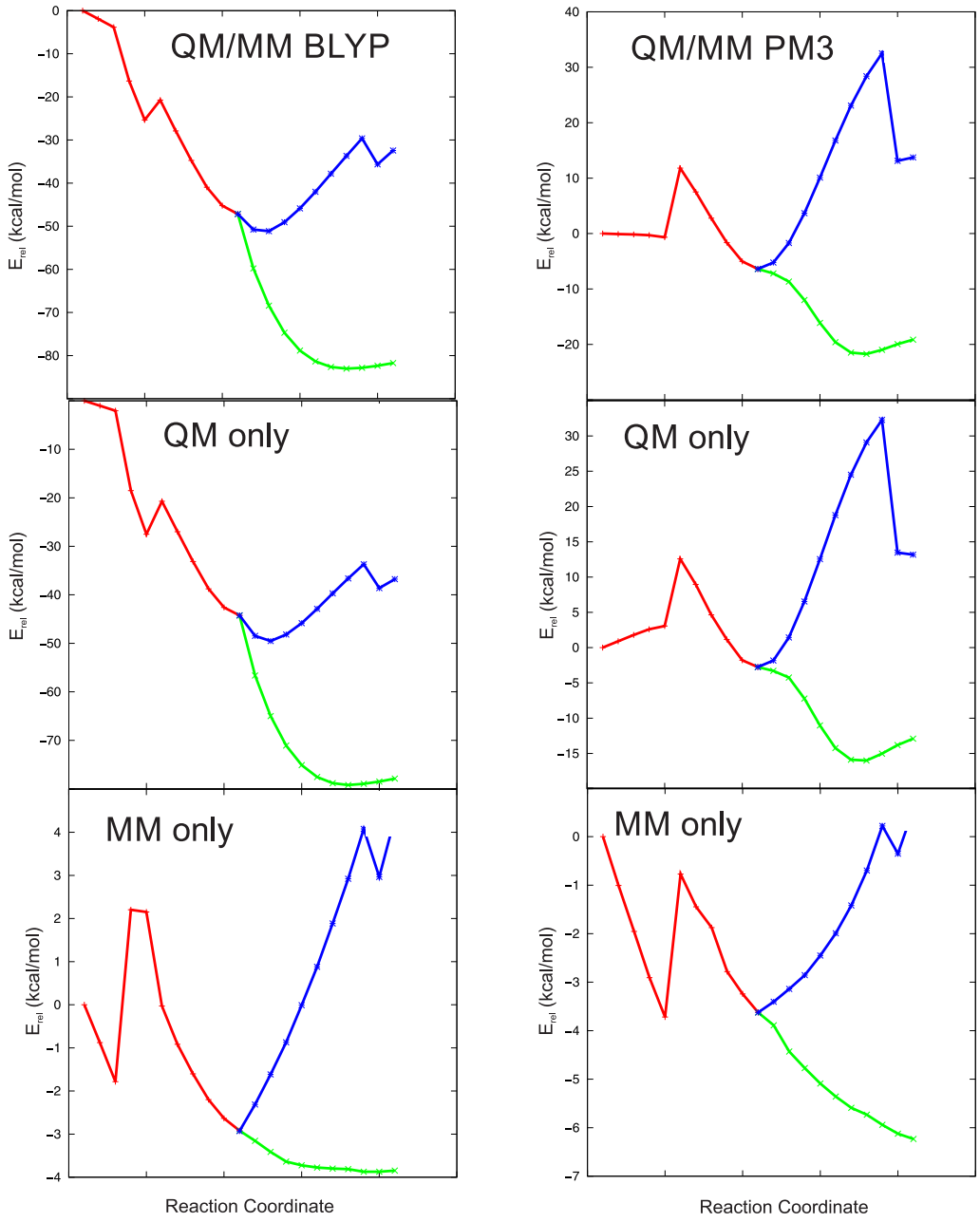

Figure 6.10.: QM/MM energies (right:PM3; left:BLYP/TZVP) total energies (top) are divided in QM (middle) and MM (bottom) parts. Beginning of the left side the red line represents energy curve of the attack of the Cys25 toward the β-carbon of the VS creating the enzyme-inhibitor complex (crossing point of the red, blue and green line). In the following the addition (green) or S_NV (blue) reaction paths are possible.

6.3. QM/MM MD Results

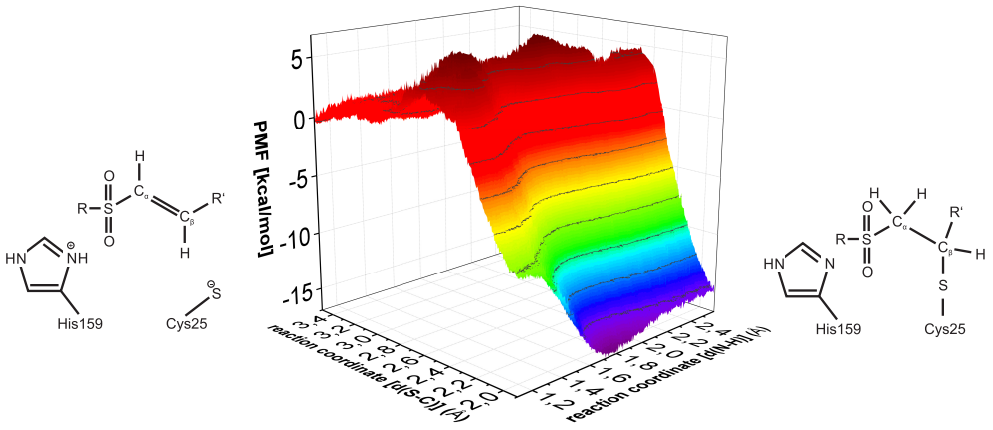

Figure 6.11.: Potential of mean force (PMF) energy surface of the inhibition reaction with the original inhibitor. QM: PM3, MM: Amber. The interactions of the inhibitor with the enzymatic surrounding is sketched for the reactant in Fig. 7.1 and for the product in Fig. 7.2.

The computed QM/MM and QM/MM MD reaction paths of the inhibition reaction including the original inhibitor agree very well as can be seen comparing the potential of mean force (PMF) in Fig. 6.11 with the PES shown in Fig. 6.5. The reaction energies obtained from the QM/MM (-19 kcal/mol) and QM/MM MD (-15 kcal/mol) methods are comparable. The major effect of the QM/MM MD method is an increasing of the energy of the transition state geometry.

The chronology of the QM/MM MD calculation steps of the modified inhibitor is exemplify shown in Fig. 6.12. Starting from the addition product (green graph in Fig. 6.12), the hydrogen located at the VS α-carbon is moved to the His162 moiety. In the second step (a) the carbon - sulfur bond between the Cys25 and VS β-carbon is broken to end up in the non-bonded complex of the reactants, and (b) the bond length between VS β-carbon and the chlorine atom is increased to end up in the S_NV reaction product. During the MD simulation, which is performed at each point of the energy surface, the enzymatic environment and the surrounding water shell is adapted to the situation in the active site. This did not influence the

addition product since this is the initial point of the calculation which is already in a balanced state. The influence of the MD simulation could be observed comparing the QM/MM and QM/MM MD relative energies of the non-bonded complex (reactants), the product of the S_NV reaction, and the energy of the representative reaction courses.

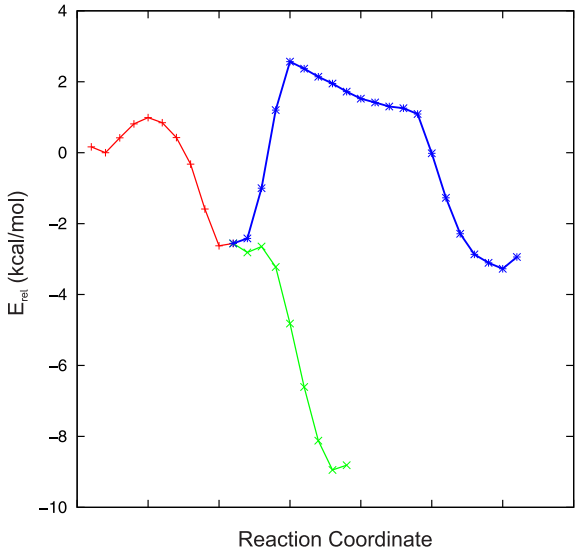

Figure 6.12.: Two dimensional PMF of calculated (QM/MM MD) inhibition reaction with the modified inhibitor. The red line show the energy curve of the Cys25 attack towards the β-carbon of the VS creating the enzyme-inhibitor complex (crossing point of the red, blue and green line). In the following the addition reaction (green) or S_NV reaction paths (blue) are possible. The bond length of the three reactions coordinates were kept fix for all calculations.

The reaction energy obtained from the QM/MM MD method (-9 kcal/mol) for the addition reaction including the modified inhibitor corresponds to the QM/MM energy. The main difference between the two methods are the computed activation barriers of +1 kcal/mol (QM/MM MD) and +16 kcal/mol (QM/MM). The rate determining step for the addition reaction is still the thiolate attack of the Cys25. For the S_NV reaction the activation barrier is +15 kcal/mol (QM/MM MD) and +3 kcal/mol (QM/MM) respectively. The complete S_NV reaction is endotherm

with +10 kcal/mol. To compare the QM/MM MD structures with the geometries obtained from the QM/MM calculations, a QM/MM optimization of the QM/MM MD reactants and products were done.

First, we do have a look on the changes between the reactants obtained from the QM/MM and QM/MM MD calculations. The zwitterionic state is stable and the position of the VS double bond is the same independently from which method is used. A difference is found in the arrangement of the SO_2-CH_2-Ph unit of the inhibitor. In the QM/MM calculation the orientation of this group did not change significantly. The QM/MM MD calculations shows an approximately 90° rotation around the α-carbon - SO_2 bond (Fig. 6.15). The new position of this part of the inhibitor results in more possibilities to interact with the protein (namely with the Trp184 residue): (a) two hydrogen bonds between Trp184 hydrogen and the SO_2 oxygen atoms (2.05 Å, 2.56 Å) and (b) a $\pi - \pi$ interaction between the VS-Ph and the Trp184 (3.46 Å). The stabilization of the reactants in the QM/MM MD calculation explains the decreased exothermicity of the reaction compared with the QM/MM results.

During the reaction from the non-bonded complex to the product, the SO_2-CH_2-Ph unit of the inhibitor has to rotate back in his former position, so that the VS β-carbon can form a covalent bond to the Cys25 thiolate atom. After that bond forming reaction, the inhibitor has two possible options for its reaction paths (addition and S_NV). In the case of the addition mechanism the VS α-carbon atom is protonated. The position of the inhibitor after the addition reaction did not differ from the position after the S_NV reaction. The point of interest at the S_NV reaction is the movement of the substituted chlorine ion. After a MD sampling like it was done for the free energy reaction path the chlorine is caged by several hydrogen bonds: VSαCH(1.74 Å),Trp184 (2.33 Å), Gln19 (2.23 Å), His162 (1.70 Å, 3.46 Å), Cys25 (2.93 Å, 2.37 Å), Wat 1362 (3.33 Å). In this arrangement the chlorine ion is 3.75 Å away from the β-carbon atom where it could trigger the backward reaction.

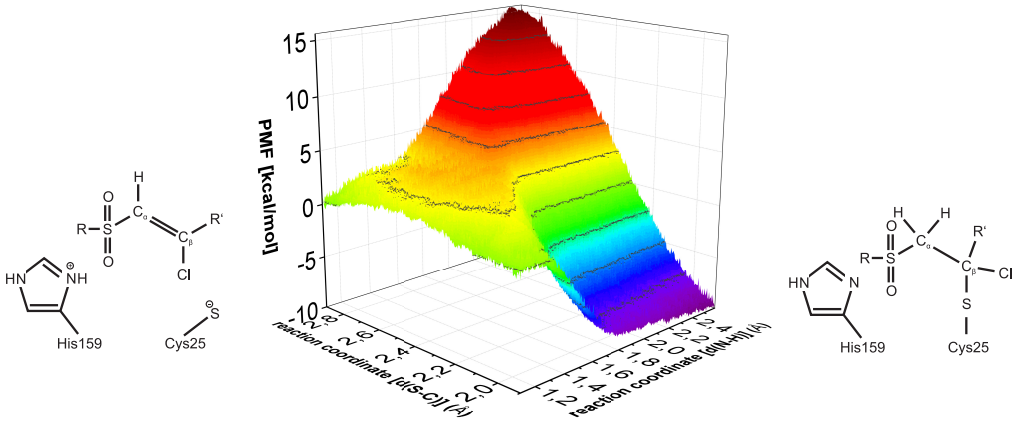

Figure 6.13.: Potential mean force energy surface of the addition reaction with the modified inhibitor. QM: PM3 MM: Amber. The interactions of the inhibitor with the enzymatic surrounding is sketched for the reactant in Fig. 7.6 and for the product in Fig. 7.7.

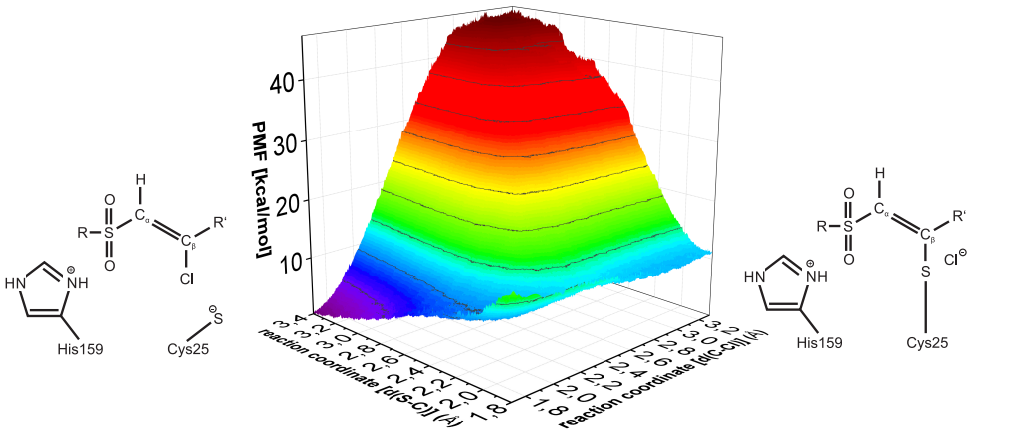

Figure 6.14.: Potential mean force energy surface of the S_NV reaction with the modified inhibitor. QM: PM3 MM: Amber. The interactions of the inhibitor with the enzymatic surrounding is sketched for the reactant in Fig. 7.6 and for the product in Fig. 7.8.

The computed energies and geometries derived by the used methods are in good agreement. The inhibition reaction of cruzain and the original inhibitor is an irreversible addition reaction. The substitution of a hydrogen atom with a chlorine atom leads to a less exothermic - and thus reversible - addition reaction caused by a larger sterically interaction of the chlorin atom and the modified non-bonded

interactions in the active site of the enzyme. The substitution reaction, which can be obtained via a S_NV mechanism, is energetically not the favored reaction path. But, if the chlorine leave the active site this reaction becomes irreversible. Finally, the longer the inhibitor stays in the active site the higher is the probability that the irreversible S_NV reaction will take place.

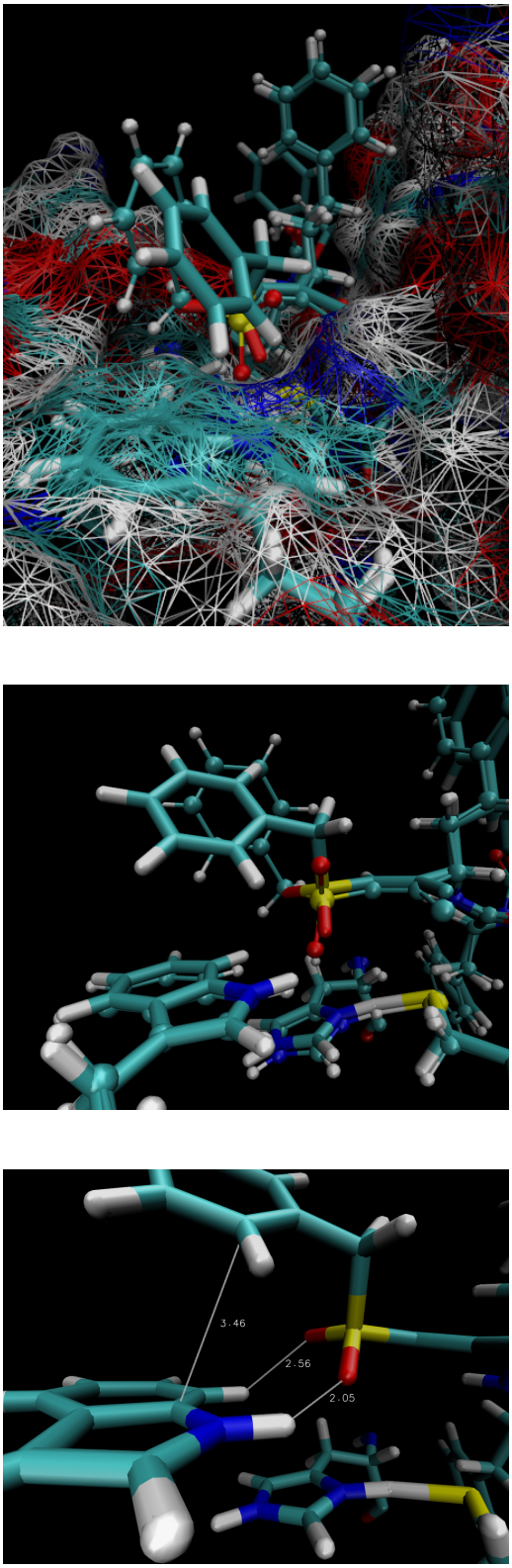

Figure 6.15.: Different orientations of the VS inhibitor obtained from QM/MM (ball and stick) and QM/MM MD (thick stick) calculations. Top: superposition of both states including the enzymatic environment and the Trp184. Middle: superposition of VS inhibitor, His162, Cys25 and Trp184. Bottom: distances of new interactions found in the QM/MM MD results.

Part III.

Summary

Summary

Part 1 of this work describes the development of accurate physically grounded force fields for intermolecular Cation-π interactions based on SAPT energy decomposition analysis.

The presented results demonstrate the benefits of the used DFT-SAPT method to describe non-bonding interactions. First of all, this method is able to reproduce the high level CCSD(T) energy values but using much less computational time. Second it provides the possibility to separate the total intermolecular interaction energy into several physically meaningful contributions. The relative contributions of the dimers investigated can be seen in Fig. 6.16. In Tab. 6.3 the percentage contribution of the attractive energy parts to the stabilization energy is shown. The polarization energy is important for the $NH_4^+...C_6H_6$ interaction, whereas it becomes less crucial considering other dimers. The dispersion energy contribution is large in the case of the $C_6H_6...H_2O$ dimers, whereas it is relatively less important for the $NH_4^+...C_6H_6$ interaction. The electrostatic energy contributes a large amount of stabilizing energy in all considered dimer interactions.

The performance of the new force fields developed starting from the AMOEBA09 force field is checked using the DFT-SAPT results as a reference. It can be seen that the FF-SAPT 1 force field is able to describe the $C_6H_6...NH4^+$ interaction accurately since it can capture the right physics of the intermolecular interaction. Further development of this force field, namely the FF-SAPT 2 force field, can reproduce the interaction between water molecules and between the benzene or ammonium ion and water. Finally it has been shown that the new force fields are

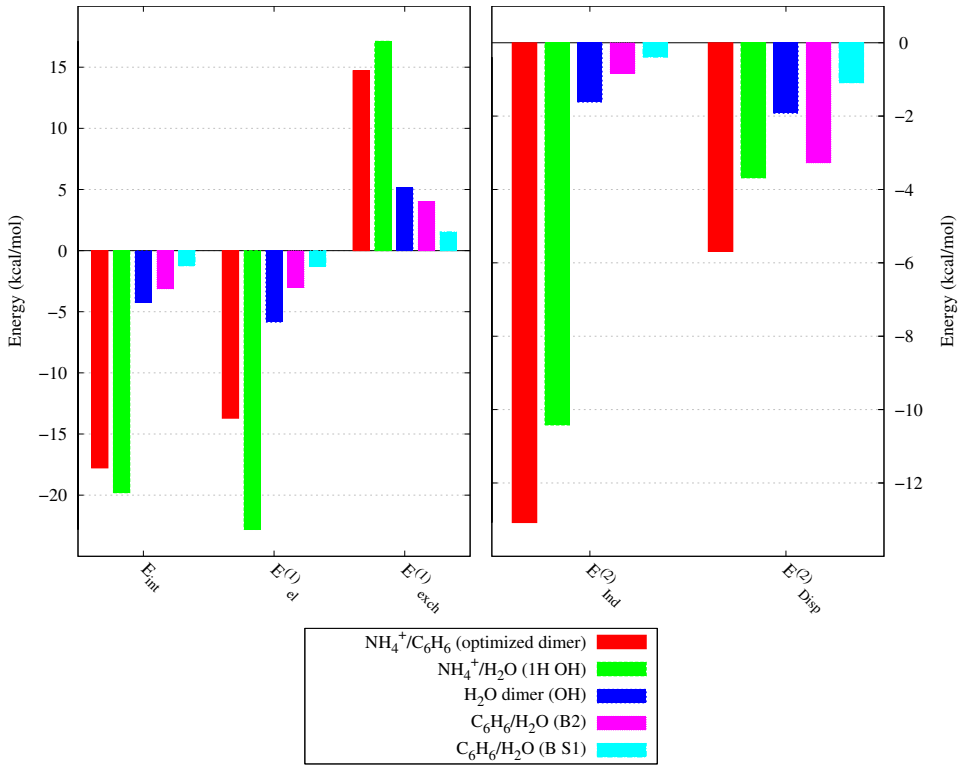

Figure 6.16.: Energy decomposition analysis (DFT-SAPT) of all interaction types presented in this work.

able to reproduce the right energies of the $H_2O...NH_4^+...C_6H_6$ clusters. That means that the force field is able describe the interactions fairly accurate both in the gas phase and in a liquid environment.

The main goal was to calculate the reference intermolecular interaction energies using force field methods by reproduce the physically right behavior of the energy components, namely the electrostatic, exchange, dispersion, and induction energies. The results show that, in principle, the FF-SAPT 2 force field has the ability to reproduce these contributions accurately. It has to be pointed out that the discussed results are derived from mixed molecular dimers and the force field parameters were fitted using homo dimers. This approach enables the effective preparation of parameters for the computation of a broad range of application. The resulting interaction energy does not always corresponds to the reference energies. Due to the

	electrostatic	dispersion	polarization
NH_4^+/C_6H_6 [a]	42	18	40
NH_4^+/H_2O [b]	62	10	28
H_2O dimer [c]	62	20	17
C_6H_6/H_2O H-π [d]	43	46	11
C_6H_6/H_2O side-on [e]	46	39	14

Table 6.3.: Percentage contributions of the electrostatic, dispersion and polarization energy to the total stabilization energy at the representative equilibrium distance. The used geometries of the dimers are:[a]optimized dimer,[b]1H OH, [c]OH, [d]B2, and [e]B S1.

lack of error cancellation the quality of the energy components must be improved. Especially the Pauli repulsion part (exchange energy) should more closely reproduce the reference values. This can be achieved by including some additional parameters. By implementing more advanced models to treat polarization, the agreement with the accurate reference data can be improved as well. This will be important for the interactions between charged species and neutral molecules.

Part 2 gains insight in computational investigation of covalent irreversible Vinyl Sulfone-based protease inhibitors.

The results discussed in this part give an insight in the interactions between the vinyl sulfone-based VS2 inhibitor and the enzyme cruzain. Based on the experimentally investigated covalently bounded inhibitor enzyme complex, the direction of the natural reaction course was reversed and the geometry of the non-covalently bounded complex was computed. This computational results enable the determining of a structure which is not accessible with experimental methods. Based on the exact knowledge of reactants and products, the nature of the inhibitor can be modified to tune the mode of action, kinetics and thermodynamics of the inhibition reaction towards the favored properties.

Furthermore, the results show that it is not trivial to conclude from pure QM results to QM/MM or QM/MM MD results. While the QM results indicated an energeti-

cally highly preferred substitution reaction, the QM/MM and QM/MM MD results show that this irreversible reaction is disadvantaged since the concurrent reversible addition reaction is more exothermic. However, the equilibrium reaction will be shifted towards the irreversible S_NV reaction when the substituted chloride ion leave the active site. These results underline the important influence of the environmental enzymatic surrounding.

Zusammenfassung

In Teil 1 dieser Arbeit wird die Entwicklung eines akkuraten physikalisch fundierten Kraftfeldes für die exakte Beschreibung zwischenmolekularer Cation-π Wechselwirkungen basierend auf Analysen der SAPT Energieaufspaltungen beschrieben. Die Ergebnisse zeigen die Vorteile der benutzten DFT-SAPT Methode zur Beschreibung von nicht-kovalent gebundenen Wechselwirkungen. Diese Methode ist zum einen in der Lage höchst akkurate CCSD(T) Ergebnisse zu reproduzieren wobei ein sehr viel geringerer computertechnicher Aufwand benötigt wird. Zum anderen ermöglicht es diese Methode die gesamte Wechselwirkungsenergie in einzelne physikalisch sinnvolle Komponenten zu separieren. In Abb. 6.17 sind die Energiekomponenten der untersuchten Dimere graphisch dargestellt. In Tab. 6.4 sind die Anteile der attraktiven Energiebeiträge zur Gesamtstabilisierungsenergie prozentual aufgelistet. Die Polarisationsenergie repräsentiert einen entscheidenden Anteil an der $NH_4^+...C_6H_6$ Wechselwirkung, wobei diese für die weiteren hier gezeigten Dimere keine entscheidende Rolle spielt. Die Dispersionsenergie hingegen liefert einen großen Beitrag zur $C_6H_6...H_2O$ Wechselwirkung, ist aber für die $NH_4^+...C_6H_6$ Wechselwirkung relativ unbedeutend. Die Elektrostatische Energie liefert in allen untersuchten Dimeren einen entscheidenden Anteil zur Stabilisierungsenergie.

Die Leistungsfähigkeit der auf Basis des AMOEBA09 Kraftfeldes neu entwickelten Kraftfelder wurde mit Hilfe der DFT-SAPT Ergebnisse überprüft. Es wurde gezeigt, dass das FF-SAPT 1 Kraftfeld in der Lage ist die $C_6H_6...NH4^+$ Wechselwirkung sehr gut zu beschreiben. Die Weiterentwicklung dieses Kraftfeldes ist das FF-SAPT 2 Kraftfeld. Dieses Kraftfeld kann zusätzlich die Wechselwirkungsenergien

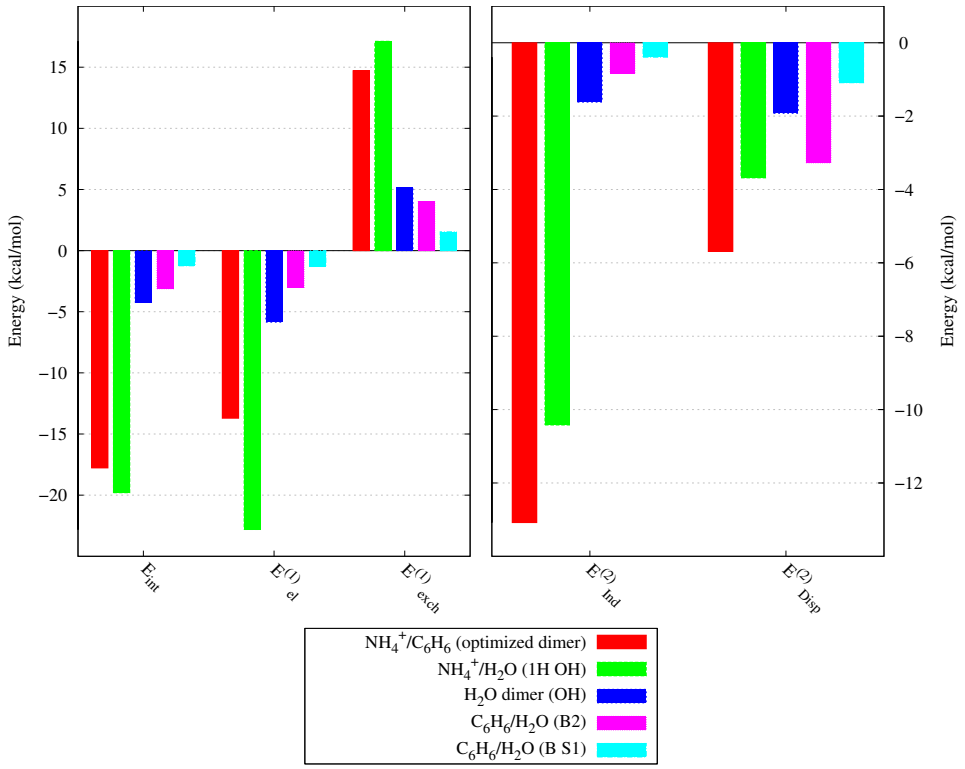

Abbildung 6.17.: Energiekomponenten erhalten aus Separierungsanalyse der DFT-SAPT Rechnungen aller Wechselwirkungsarten welche in dieser Arbeit verwendet wurden.

zwischen Wassermolekülen sowie zwischen den Dimeren Benzol/Wasser und Ammonium/Wasser reproduzieren. Letztlich konnte gezeigt werden, dass die neuen Kraftfelder auch die Wechselwirkungen von Clustern, wie z.B. $H_2O...NH_4^+...C_6H_6$, richtig beschreiben können. Die neu entwickelten Kraftfelder liefern eine gute Beschreibung der Wechselwirkungen sowohl in der Gasphase als auch in der kondensierter Phase liefern. Das Kernziel der Arbeit war die Berechnung von zwischenmolekularen Wechselwirkungen mit Hilfe von Kraftfeldmethoden in welchen die Energiekomponenten (Elektrostatische-, Austausch-, Dispersions- und Induktionsenergie) physikalisch richtig wiedergegeben werden sollen. Die erhaltenen Ergebnisse zeigen, dass das FF-SAPT 2 Kraftfeld die genannten Beiträge am genausten reproduzieren kann. Die Kraftfeldparameter wurden mit Hilfe von homomolekularen Dimeren optimiert

	electrostatic	dispersion	polarization
NH_4^+/C_6H_6 [a]	42	18	40
NH_4^+/H_2O [b]	62	10	28
H_2O dimer [c]	62	20	17
C_6H_6/H_2O H-π [d]	43	46	11
C_6H_6/H_2O side-on [e]	46	39	14

Tabelle 6.4.: Prozentuale Anteile von elektrostatischer, dispersions und polarisations Energie zur Gesamtstabilisierungsenergie berechnet am Gleichgewichtsabstand der Dimere. Die gezeigten Dimere sind:[a] optimiertes Dimer,[b]1H OH, [c]OH, [d]B2, und [e]B S1.

und anschließend an gemischt molekularen Dimeren getestet. Dieser Ansatz ermöglicht eine sehr effektive Generierung von Parametern zur Berechnung eines breiten Anwendungsspektrums. Die erhaltenen Wechselwirkungsenergien stimmen nicht immer zufriedenstellend mit den Referenzenergien überein. Durch das Ausbleiben von Fehlerkompensation muss die Qualität der Energiekomponenten weiter verbessert werden. Insbesondere die Pauli Abstoßung (Austausch Energie) muss dabei besser reproduziert werden. Dies könnte durch das Einführen weiterer Parameter erreicht werden. Weiterhin können erweiterte Polarisationsmodelle implementiert werden um die Leistungsfähigkeit des Kraftfeldes zu erhöhen, da diese Komponente einen wichtigen Beitrag zur der Wechselwirkungsenergie zwischen geladenen und neutralen Molekülen leistet.

Der zweite Teil der Arbeit beschäftigt sich mit der computerbasierten Untersuchung von kovalent-irreversiblen Vinylsulfon-basierter Protease Inhibitoren. Die gezeigten Ergebnisse geben einen Einblick in die Wechselwirkung zwischen Vinylsulfon-basierten Inhibitoren und dem Enzym Cruzain. Ausgehend von dem experimentell bestimmten, kovalent gebundenen Inhibitor-Enzym Komplex wurde die Struktur des nicht-kovalent gebundenen Komplexes berechnet. Diese computerbasierten Ergebnisse ermöglichen die Untersuchungen von Strukturen welche experimentell nicht zugänglich sind. Basierend auf der genauen Kenntnis von Edukt und Pro-

dukt Geometrien kann der Inhibitor modifiziert werden um den Reaktionsverlauf, Reaktionsgeschwindigkeit und Reaktionsenergie der Inhibierungsreaktion gezielt zu beeinflussen. Die Ergebnisse zeigen, dass es nicht möglich ist direkt von QM Ergebnissen auf QM/MM oder QM/MM MD Ergebnisse zu schließen. Die Resultate der QM Rechnungen deuten auf eine energetisch bevorzugte Substitutionsreaktion (S_NV) hin. Die QM/MM und QM/MM MD Ergebnisse hingegen zeigen, dass diese Reaktion energetisch benachteiligt ist und somit die konkurrierende Additionsreaktion bevorzugt wird. Erst durch das Austreten des substituieren Chlorid Ions aus dem aktiven Zentrum des Enzyms wird das Gleichgewicht der Inhibierungsreaktion auf die Seite der somit irreversiblen S_NV Reaktion verschoben. Diese Ergebnisse belegen den immensen Einfluss der enzymatischen Umgebung auf den Verlauf solcher Reaktion.

Teil IV.

Appendix

7. Appendix and Literature

7.1. Appendix Part 1

7.1.1. SAPT Results

TMA +	E_{int}	$E_{pol}^{(1)}$	$E_{exch}^{(1)}$	$E_{Ind}^{(2)}$	$E_{Disp}^{(2)}$
Phe	-6.33	-4.05	2.34	-1.87	-2.76
Tyr	-7.37	-4.80	2.95	-2.42	-3.10
Trp	-9.30	-6.26	3.31	-2.91	-3.44

Table 7.1.: DFT-SAPT/avtz energies of factor Xa interaction with (±)-1 in the S4 pocket.

	x	y	z
C	-0.636674	1.217326	-0.658041
C	-0.685571	0.012318	-1.365230
C	-0.638258	-1.204968	-0.679234
C	-0.546616	-1.218180	0.715367
C	-0.501389	-0.012269	1.424594
C	-0.545061	1.205962	0.736603
H	-0.791241	0.021828	-2.442801
H	-0.702434	-2.137280	-1.225422
H	-0.538447	-2.159744	1.249330
H	-0.461203	-0.021763	2.506477
H	-0.535660	2.138011	1.286993
H	-0.699569	2.159148	-1.187808
N	2.283808	-0.000124	-0.111035
H	2.851508	-0.835141	0.025622
H	2.851827	0.834368	0.027490
H	1.881339	0.001006	-1.050626
H	1.478645	-0.000694	0.543629

Table 7.2.: Coordinates of C_6H_6/NH_4^+ dimer minimum structure.

structure	CCSD(T)	$E_{int/CBS}^{SAPT}$	E_{int}^{SAPT}	$E_{el}^{(1)}$	$E_{exch}^{(1)}$	$E_{ind}^{(2)}$	$E_{ind-ex}^{(2)}$	$E_{disp}^{(2)}$	$E_{disp-ex}^{(2)}$
optimized	-18.89	-17.99	-17.77	-13.71	14.71	-14.85	5.28	-6.58	0.89
monodentate	-17.52	-17.81	-17.61	-11.31	10.52	-13.48	4.08	-5.78	0.70
bidentate	-17.79	-18.13	-17.91	-12.67	12.67	-14.73	5.25	-6.47	0.84
tridentate	-16.19	-16.47	-16.27	-12.01	10.99	-13.32	4.84	-5.98	0.78

Table 7.3.: CCSD(T)/avtz and DFT-SAPT/avtz Energy decomposition results of the optimized and 3 ideal structures in kcal/mol.

h	monodentate		bidendate		tridendate	
	SAPT	CCSD(T)	SAPT	CCSD(T)	SAPT	CCSD(T)
2.5	-8.52	-6.80	-11.88	-10.37	-9.70	-8.45
2.6	-12.49	-11.32	-14.99	-14.02	-12.92	-12.13
2.7	-15.09	-14.34	-16.80	-16.22	-14.87	-14.40
2.8	-16.64	-16.19	-17.69	-17.38	-15.89	-15.66
2.9	-17.41	-17.17	**-17.91**	**-17.79**	**-16.27**	**-16.19**
3.0	**-17.61**	**-17.52**	-17.69	-17.69	-16.19	-16.21
3.1	-17.40	-17.41	-17.16	-17.23	-15.80	-15.89
3.2	-16.91	-16.97	-16.45	-16.56	-15.22	-15.35
3.4	-15.46	-15.56	-14.75	-14.88	-13.76	-13.90
3.5	-14.62	-14.72	-13.85	-13.98	-12.97	-13.10
3.8	-12.06	-12.14	-11.31	-11.40	-10.69	-10.77
4.0	-10.51	-10.57	-9.84	-9.90	-9.34	-9.39
5.0	-5.36	-5.34	-5.07	-5.05	-4.90	-4.88

Table 7.4.: KatPi h-shift CCSD(T)/avtz (CP) vs. DFT-SAPT/avtz kcal/mol.

monodentate											
h	E_{int}	$E^{(1)}_{pol}$	$E^{(1)}_{exch}$	$E^{(2)}_{ind}$	$E^{(2)}_{ind-exch}$	$E^{(2)}_{disp}$	$E^{(2)}_{disp-exch}$	δ_{HF}	E_{Ind}	E_{Disp}	$E_{Disp}(cbs)$
2.5	-8.52	-19.65	43.28	-31.53	16.01	-14.02	2.56	-5.15	-20.67	-11.46	-11.47
2.6	-12.50	-17.22	32.92	-26.17	12.27	-11.76	2.01	-4.55	-18.45	-9.75	-10.18
2.7	-15.10	-15.28	24.92	-21.90	9.37	-9.85	1.56	-3.92	-16.45	-8.29	-8.29
2.8	-16.65	-13.69	18.77	-18.48	7.12	-8.25	1.21	-3.33	-14.69	-7.04	-7.32
2.9	-17.42	-12.40	14.08	-15.72	5.40	-6.91	0.93	-2.80	-13.12	-5.98	-6.21
3.0	-17.61	-11.32	10.52	-13.48	4.08	-5.78	0.71	-2.34	-11.74	-5.07	-5.27
3.1	-17.41	-10.40	7.83	-11.65	3.08	-4.85	0.54	-1.95	-10.52	-4.31	-4.46
3.2	-16.92	-9.62	5.81	-10.14	2.32	-4.07	0.41	-1.63	-9.45	-3.66	-3.78
3.3	-16.25	-8.94	4.30	-8.88	1.74	-3.41	0.30	-1.36	-8.50	-3.11	-3.21
3.4	-15.47	-8.34	3.17	-7.82	1.31	-2.87	0.23	-1.14	-7.65	-2.64	-2.72
3.5	-14.62	-7.80	2.33	-6.92	0.98	-2.42	0.17	-0.96	-6.90	-2.25	-2.25
3.6	-13.76	-7.32	1.71	-6.16	0.73	-2.04	0.13	-0.81	-6.24	-1.91	-1.97
3.8	-12.06	-6.47	0.91	-4.93	0.41	-1.47	0.07	-0.58	-5.10	-1.40	-1.44
4.0	-10.51	-5.76	0.48	-4.01	0.22	-1.06	0.04	-0.42	-4.21	-1.02	-1.06
4.5	-7.44	-4.38	0.10	-2.51	0.05	-0.50	0.01	-0.20	-2.66	-0.49	-0.50
5.0	-5.37	-3.39	0.02	-1.66	0.01	-0.26	0.00	-0.09	-1.74	-0.26	-0.25
5.5	-3.98	-2.66	0.00	-1.14	0.00	-0.14	0.00	-0.05	-1.19	-0.14	-0.14
bidentate											
h	E_{int}	$E^{(1)}_{pol}$	$E^{(1)}_{exch}$	$E^{(2)}_{ind}$	$E^{(2)}_{ind-exch}$	$E^{(2)}_{disp}$	$E^{(2)}_{disp-exch}$	δ_{HF}	E_{Ind}	E_{Disp}	$E_{Disp}(cbs)$
2.5	-11.88	-21.40	42.04	-31.03	16.23	-13.69	2.49	-6.52	-21.32	-11.20	-11.19
2.6	-14.99	-18.46	31.31	-25.37	12.29	-11.34	1.92	-5.34	-18.42	-9.42	-9.83
2.7	-16.81	-16.11	23.23	-20.96	9.28	-9.40	1.47	-4.33	-16.01	-7.93	-7.93
2.8	-17.69	-14.21	17.18	-17.49	6.99	-7.80	1.12	-3.49	-13.99	-6.68	-6.95
2.9	-17.92	-12.68	12.68	-14.74	5.25	-6.47	0.85	-2.81	-12.30	-5.62	-5.84
3.0	-17.69	-11.42	9.33	-12.54	3.94	-5.38	0.64	-2.26	-10.86	-4.74	-4.91
3.1	-17.17	-10.37	6.85	-10.76	2.95	-4.48	0.48	-1.83	-9.64	-4.00	-4.14
3.2	-16.45	-9.49	5.02	-9.31	2.20	-3.74	0.36	-1.49	-8.60	-3.38	-3.49
3.3	-15.63	-8.74	3.67	-8.12	1.65	-3.12	0.26	-1.22	-7.69	-2.86	-2.95
3.4	-14.75	-8.09	2.68	-7.13	1.23	-2.62	0.20	-1.00	-6.90	-2.42	-2.49
3.5	-13.86	-7.53	1.95	-6.31	0.91	-2.20	0.14	-0.83	-6.23	-2.06	-2.06
3.6	-12.98	-7.03	1.42	-5.60	0.68	-1.85	0.11	-0.69	-5.61	-1.74	-1.80
3.8	-11.32	-6.18	0.75	-4.49	0.37	-1.33	0.06	-0.49	-4.61	-1.27	-1.30
4.0	-9.84	-5.48	0.39	-3.67	0.20	-0.96	0.03	-0.35	-3.82	-0.93	-0.95
4.5	-6.98	-4.16	0.08	-2.32	0.04	-0.46	0.01	-0.17	-2.45	-0.45	-0.46
5.0	-5.08	-3.23	0.01	-1.56	0.01	-0.24	0.00	-0.08	-1.63	-0.24	-0.23
5.5	-3.79	-2.55	0.00	-1.08	0.00	-0.13	0.00	-0.04	-1.12	-0.13	-0.13
tridentate											
h	E_{int}	$E^{(1)}_{pol}$	$E^{(1)}_{exch}$	$E^{(2)}_{ind}$	$E^{(2)}_{ind-exch}$	$E^{(2)}_{disp}$	$E^{(2)}_{disp-exch}$	δ_{HF}	E_{Ind}	E_{Disp}	$E_{Disp}(cbs)$
2.5	-9.70	-20.35	37.16	-27.60	15.10	-12.76	2.36	-3.61	-16.11	-10.40	-10.40
2.6	-12.93	-17.51	27.52	-22.65	11.41	-10.55	1.81	-2.96	-14.20	-8.74	-9.11
2.7	-14.87	-15.26	20.32	-18.79	8.59	-8.72	1.38	-2.40	-12.60	-7.34	-7.34
2.8	-15.90	-13.46	14.96	-15.74	6.46	-7.22	1.04	-1.94	-11.22	-6.18	-6.42
2.9	-16.27	-12.01	10.99	-13.32	4.85	-5.98	0.78	-1.57	-10.04	-5.20	-5.40
3.0	-16.19	-10.83	8.06	-11.39	3.63	-4.97	0.58	-1.27	-9.03	-4.39	-4.54
3.1	-15.81	-9.86	5.90	-9.81	2.71	-4.14	0.44	-1.05	-8.15	-3.70	-3.83
3.2	-15.23	-9.03	4.31	-8.53	2.03	-3.45	0.32	-0.87	-7.37	-3.13	-3.23
3.3	-14.53	-8.33	3.14	-7.47	1.51	-2.88	0.24	-0.73	-6.69	-2.64	-2.73
3.4	-13.76	-7.73	2.28	-6.59	1.12	-2.42	0.18	-0.61	-6.08	-2.24	-2.31
3.5	-12.98	-7.20	1.66	-5.84	0.83	-2.03	0.13	-0.52	-5.53	-1.90	-1.90
3.6	-12.19	-6.73	1.20	-5.21	0.62	-1.72	0.10	-0.45	-5.04	-1.62	-1.67
3.8	-10.69	-5.93	0.63	-4.21	0.34	-1.23	0.05	-0.34	-4.21	-1.18	-1.21
4.0	-9.34	-5.27	0.33	-3.45	0.18	-0.90	0.03	-0.26	-3.53	-0.87	-0.89
4.5	-6.70	-4.02	0.06	-2.22	0.04	-0.43	0.01	-0.13	-2.31	-0.42	-0.43
5.0	-4.90	-3.13	0.01	-1.50	0.01	-0.22	0.00	-0.07	-1.56	-0.22	-0.23
5.5	-3.69	-2.48	0.00	-1.05	0.00	-0.12	0.00	-0.04	-1.09	-0.12	-0.13

Table 7.5.: DFT-SAPT/avtz $C_6H_6...NH_4^+$ h-shift of mono-, bi-, and tridentate conformations. Distance (h) in Å and energies in kcal/mol. The E_{Disp}(cbs) value was obtained by the DT extrapolation. A graphical representation of these energies can be found in Fig. 3.8.

h	X	θ	E_{int}	$E^{(1)}_{pol}$	$E^{(1)}_{exch}$	$E^{(2)}_{ind}$	$E^{(2)}_{ind-exch}$	$E^{(2)}_{disp}$	$E^{(2)}_{disp-exch}$	δ_{HF}	E_{Ind}	E_{Disp}
2.5	0.0	0	-8.52	-19.65	43.28	-31.53	16.01	-14.02	2.56	-5.15	-20.67	-11.46
2.5	0.5	0	-6.89	-21.45	51.01	-37.61	19.83	-14.58	2.66	-6.76	-24.54	-11.92
2.5	1.0	0	-3.57	-22.53	63.04	-48.82	26.53	-15.18	2.72	-9.32	-31.61	-12.46
2.5	1.5	0	-1.98	-18.90	60.58	-50.32	27.62	-14.03	2.45	-9.38	-32.08	-11.58
2.5	2.0	0	-4.01	-14.32	43.99	-38.55	20.72	-11.02	1.91	-6.75	-24.58	-9.11
2.5	2.5	0	-5.99	-8.85	25.82	-24.87	12.09	-7.52	1.23	-3.88	-16.66	-6.29
2.5	3.0	0	-6.31	-3.87	12.39	-15.00	5.90	-4.57	0.64	-1.80	-10.90	-3.93
2.5	3.5	0	-5.72	-1.18	4.79	-8.83	2.41	-2.51	0.27	-0.69	-7.11	-2.24
2.5	4.0	0	-4.55	-0.07	1.54	-5.37	0.84	-1.29	0.10	-0.28	-4.81	-1.19
3.0	0.0	0	-17.61	-11.32	10.52	-13.48	4.08	-5.78	0.71	-2.34	-11.74	-5.07
3.0	0.5	0	-17.41	-11.61	12.01	-14.74	4.96	-5.88	0.76	-2.89	-12.67	-5.12
3.0	1.0	0	-16.58	-11.59	14.24	-16.89	6.49	-5.90	0.81	-3.74	-14.14	-5.09
3.0	1.5	0	-14.95	-10.14	13.65	-16.97	6.76	-5.39	0.75	-3.62	-13.83	-4.64
3.0	2.0	0	-12.83	-7.71	10.12	-14.27	5.31	-4.32	0.58	-2.55	-11.51	-3.74
3.0	2.5	0	-10.49	-5.09	6.06	-10.59	3.28	-3.07	0.36	-1.43	-8.74	-2.71
3.0	3.0	0	-8.10	-2.86	3.02	-7.41	1.67	-1.99	0.19	-0.72	-6.46	-1.80
3.0	3.5	0	-5.96	-1.37	1.26	-5.10	0.73	-1.19	0.08	-0.36	-4.73	-1.11
3.0	4.0	0	-4.22	-0.53	0.44	-3.55	0.27	-0.68	0.03	-0.20	-3.48	-0.65
3.5	0.0	0	-14.62	-7.80	2.33	-6.92	0.98	-2.42	0.17	-0.96	-6.90	-2.25
3.5	0.5	0	-14.50	-7.75	2.60	-7.19	1.17	-2.43	0.18	-1.10	-7.12	-2.25
3.5	1.0	0	-13.96	-7.40	3.03	-7.62	1.51	-2.38	0.20	-1.30	-7.41	-2.18
3.5	1.5	0	-12.74	-6.52	2.93	-7.52	1.61	-2.16	0.19	-1.27	-7.18	-1.97
3.5	2.0	0	-10.90	-5.19	2.25	-6.68	1.32	-1.77	0.15	-0.97	-6.33	-1.62
3.5	2.5	0	-8.79	-3.74	1.39	-5.45	0.86	-1.32	0.09	-0.63	-5.22	-1.23
3.5	3.0	0	-6.74	-2.46	0.72	-4.23	0.46	-0.91	0.05	-0.38	-4.15	-0.86
3.5	3.5	0	-4.96	-1.47	0.32	-3.22	0.21	-0.59	0.02	-0.23	-3.24	-0.57
3.5	4.0	0	-3.55	-0.81	0.12	-2.45	0.09	-0.37	0.01	-0.14	-2.50	-0.36
4.0	0.0	0	-10.51	-5.76	0.48	-4.01	0.22	-1.06	0.04	-0.42	-4.21	-1.02
4.0	0.5	0	-10.40	-5.66	0.53	-4.06	0.26	-1.06	0.04	-0.46	-4.26	-1.02
4.0	1.0	0	-9.98	-5.33	0.62	-4.12	0.34	-1.02	0.04	-0.51	-4.29	-0.98
4.0	1.5	0	-9.16	-4.72	0.61	-4.02	0.37	-0.93	0.04	-0.51	-4.16	-0.89
4.0	2.0	0	-7.95	-3.89	0.49	-3.68	0.32	-0.78	0.03	-0.43	-3.79	-0.75
4.0	2.5	0	-6.56	-3.00	0.32	-3.19	0.22	-0.61	0.02	-0.32	-3.29	-0.59
4.0	3.0	0	-5.16	-2.16	0.17	-2.65	0.12	-0.45	0.01	-0.21	-2.74	-0.44
4.0	3.5	0	-3.92	-1.46	0.08	-2.16	0.06	-0.31	0.01	-0.14	-2.24	-0.30
4.0	4.0	0	-2.91	-0.93	0.03	-1.73	0.03	-0.21	0.00	-0.09	-1.79	-0.21

h	X	θ	E_{int}	$E^{(1)}_{pol}$	$E^{(1)}_{exch}$	$E^{(2)}_{ind}$	$E^{(2)}_{ind-exch}$	$E^{(2)}_{disp}$	$E^{(2)}_{disp-exch}$	δ_{HF}	E_{Ind}	E_{Disp}
2.5	0.0	30	-8.53	-19.66	43.27	-31.53	16.01	-14.02	2.56	-5.15	-20.67	-11.46
2.5	0.5	30	-6.90	-21.47	51.00	-37.58	19.81	-14.58	2.67	-6.75	-24.52	-11.91
2.5	1.0	30	-4.01	-23.34	62.63	-47.89	26.03	-15.11	2.73	-9.06	-30.92	-12.38
2.5	1.5	30	-3.35	-20.79	58.00	-46.76	25.77	-13.68	2.48	-8.38	-29.37	-11.20
2.5	2.0	30	-5.61	-14.60	37.93	-33.51	18.13	-10.25	1.86	-5.16	-20.54	-8.39
2.5	2.5	30	-7.91	-8.19	18.66	-20.15	9.53	-6.56	1.08	-2.30	-12.92	-5.48
2.5	3.0	30	-8.12	-3.79	7.45	-11.69	4.04	-3.75	0.49	-0.86	-8.51	-3.26
2.5	3.5	30	-6.74	-1.46	2.53	-7.08	1.46	-2.01	0.18	-0.35	-5.97	-1.83
2.5	4.0	30	-4.91	-0.36	0.75	-4.58	0.47	-1.05	0.06	-0.20	-4.31	-0.99
3.0	0.0	30	-17.61	-11.32	10.52	-13.48	4.08	-5.79	0.71	-2.34	-11.74	-5.08
3.0	0.5	30	-17.41	-11.61	12.01	-14.74	4.96	-5.88	0.76	-2.89	-12.67	-5.12
3.0	1.0	30	-16.60	-11.65	14.19	-16.82	6.45	-5.89	0.81	-3.71	-14.08	-5.08
3.0	1.5	30	-15.01	-10.29	13.34	-16.61	6.58	-5.32	0.75	-3.46	-13.49	-4.57
3.0	2.0	30	-12.87	-7.75	9.32	-13.56	4.96	-4.16	0.56	-2.25	-10.85	-3.60
3.0	2.5	30	-10.54	-5.03	5.01	-9.73	2.86	-2.86	0.33	-1.12	-7.99	-2.53
3.0	3.0	30	-8.19	-2.90	2.18	-6.67	1.33	-1.78	0.15	-0.51	-5.85	-1.63
3.0	3.5	30	-6.03	-1.50	0.80	-4.60	0.53	-1.04	0.06	-0.27	-4.34	-0.98
3.0	4.0	30	-4.24	-0.68	0.26	-3.27	0.18	-0.60	0.02	-0.16	-3.25	-0.58
3.5	0.0	30	-14.62	-7.80	2.33	-6.92	0.98	-2.42	0.17	-0.96	-6.90	-2.25
3.5	0.5	30	-14.50	-7.75	2.60	-7.19	1.17	-2.43	0.18	-1.10	-7.12	-2.25
3.5	1.0	30	-13.96	-7.41	3.02	-7.61	1.51	-2.37	0.20	-1.30	-7.40	-2.17
3.5	1.5	30	-12.73	-6.53	2.90	-7.47	1.59	-2.15	0.19	-1.25	-7.13	-1.96
3.5	2.0	30	-10.87	-5.20	2.15	-6.56	1.27	-1.74	0.14	-0.93	-6.22	-1.60
3.5	2.5	30	-8.74	-3.75	1.25	-5.28	0.80	-1.27	0.09	-0.57	-5.05	-1.18
3.5	3.0	30	-6.69	-2.49	0.59	-4.05	0.41	-0.86	0.04	-0.33	-3.97	-0.82
3.5	3.5	30	-4.93	-1.53	0.24	-3.08	0.17	-0.55	0.02	-0.20	-3.11	-0.53
3.5	4.0	30	-3.53	-0.88	0.08	-2.34	0.07	-0.34	0.01	-0.12	-2.39	-0.33
4.0	0.0	30	-10.51	-5.76	0.48	-4.01	0.22	-1.06	0.04	-0.42	-4.21	-1.02
4.0	0.5	30	-10.40	-5.66	0.53	-4.06	0.26	-1.06	0.04	-0.46	-4.26	-1.02
4.0	1.0	30	-9.98	-5.33	0.62	-4.12	0.34	-1.02	0.04	-0.51	-4.29	-0.98
4.0	1.5	30	-9.15	-4.72	0.60	-4.01	0.37	-0.93	0.04	-0.51	-4.15	-0.89
4.0	2.0	30	-7.94	-3.90	0.47	-3.66	0.31	-0.78	0.03	-0.42	-3.77	-0.75
4.0	2.5	30	-6.53	-3.00	0.30	-3.15	0.21	-0.60	0.02	-0.30	-3.24	-0.58
4.0	3.0	30	-5.13	-2.17	0.15	-2.60	0.11	-0.43	0.01	-0.20	-2.69	-0.42
4.0	3.5	30	-3.90	-1.48	0.07	-2.11	0.05	-0.30	0.01	-0.13	-2.19	-0.29
4.0	4.0	30	-2.90	-0.96	0.03	-1.69	0.02	-0.20	0.00	-0.09	-1.76	-0.20

Table 7.6.: DFT-SAPT/avtz $C_6H_6...NH_4^+$ X-shift of monodentate conformation. Distance (h and X) in Å, θ in ° and energies in kcal/mol. A graphical representation of these energies can be found in Figs. 3.10 and 3.11.

h	X	θ	E_{int}	$E^{(1)}_{pol}$	$E^{(1)}_{exch}$	$E^{(2)}_{ind}$	$E^{(2)}_{ind-exch}$	$E^{(2)}_{disp}$	$E^{(2)}_{disp-exch}$	δ_{HF}	E_{Ind}	E_{Disp}
2.5	0.0	0	-11.88	-21.40	42.04	-31.03	16.23	-13.69	2.49	-6.52	-21.32	-11.20
2.5	0.5	0	-10.08	-20.91	41.60	-32.06	17.65	-13.42	2.49	-5.42	-19.83	-10.93
2.5	1.0	0	-6.63	-19.92	40.42	-33.60	20.01	-12.64	2.44	-3.34	-16.93	-10.20
2.5	1.5	0	-4.77	-18.06	37.78	-33.10	20.08	-11.31	2.23	-2.38	-15.40	-9.08
2.5	2.0	0	-6.21	-14.44	31.29	-29.19	16.64	-9.36	1.78	-2.93	-15.48	-7.58
2.5	2.5	0	-8.70	-9.80	21.43	-22.51	11.16	-6.96	1.19	-3.21	-14.56	-5.77
2.5	3.0	0	-9.43	-5.81	12.17	-15.50	6.13	-4.64	0.67	-2.45	-11.82	-3.97
2.5	3.5	0	-8.23	-2.87	5.85	-10.10	2.85	-2.82	0.33	-1.47	-8.72	-2.49
2.5	4.0	0	-6.17	-0.93	2.36	-6.51	1.14	-1.59	0.13	-0.78	-6.15	-1.46
3.0	0.0	0	-17.69	-11.42	9.33	-12.54	3.94	-5.38	0.64	-2.26	-10.86	-4.74
3.0	0.5	0	-16.82	-11.07	9.23	-12.66	4.25	-5.26	0.64	-1.95	-10.36	-4.62
3.0	1.0	0	-14.88	-10.19	8.93	-12.81	4.79	-4.92	0.64	-1.33	-9.35	-4.28
3.0	1.5	0	-13.11	-8.99	8.28	-12.53	4.88	-4.37	0.59	-0.98	-8.63	-3.78
3.0	2.0	0	-11.98	-7.42	6.90	-11.46	4.16	-3.64	0.48	-1.00	-8.30	-3.16
3.0	2.5	0	-10.91	-5.57	4.86	-9.60	2.92	-2.79	0.33	-1.05	-7.73	-2.46
3.0	3.0	0	-9.32	-3.75	2.86	-7.45	1.69	-1.96	0.19	-0.89	-6.65	-1.77
3.0	3.5	0	-7.28	-2.23	1.43	-5.50	0.83	-1.27	0.09	-0.63	-5.30	-1.18
3.0	4.0	0	-5.25	-1.10	0.61	-3.98	0.35	-0.78	0.04	-0.39	-4.02	-0.74
3.5	0.0	0	-13.86	-7.53	1.95	-6.31	0.91	-2.20	0.14	-0.83	-6.23	-2.06
3.5	0.5	0	-13.45	-7.32	1.94	-6.30	0.98	-2.15	0.15	-0.74	-6.06	-2.00
3.5	1.0	0	-12.43	-6.76	1.89	-6.25	1.10	-2.01	0.15	-0.54	-5.69	-1.86
3.5	1.5	0	-11.22	-5.97	1.76	-6.07	1.14	-1.79	0.14	-0.42	-5.35	-1.65
3.5	2.0	0	-10.00	-5.02	1.48	-5.66	1.00	-1.51	0.11	-0.41	-5.07	-1.40
3.5	2.5	0	-8.69	-3.96	1.08	-4.99	0.73	-1.19	0.08	-0.43	-4.69	-1.11
3.5	3.0	0	-7.19	-2.90	0.66	-4.17	0.45	-0.88	0.05	-0.39	-4.11	-0.83
3.5	3.5	0	-5.60	-1.95	0.34	-3.34	0.23	-0.61	0.02	-0.31	-3.42	-0.59
3.5	4.0	0	-4.13	-1.17	0.15	-2.61	0.10	-0.40	0.01	-0.21	-2.72	-0.39
4.0	0.0	0	-9.84	-5.48	0.39	-3.67	0.20	-0.96	0.03	-0.35	-3.82	-0.93
4.0	0.5	0	-9.63	-5.35	0.39	-3.65	0.22	-0.94	0.03	-0.33	-3.76	-0.91
4.0	1.0	0	-9.08	-4.99	0.38	-3.59	0.24	-0.88	0.03	-0.27	-3.62	-0.85
4.0	1.5	0	-8.31	-4.46	0.36	-3.48	0.26	-0.79	0.03	-0.24	-3.46	-0.76
4.0	2.0	0	-7.42	-3.81	0.31	-3.27	0.23	-0.68	0.03	-0.23	-3.27	-0.65
4.0	2.5	0	-6.41	-3.10	0.23	-2.96	0.18	-0.55	0.02	-0.22	-3.00	-0.53
4.0	3.0	0	-5.33	-2.39	0.15	-2.59	0.11	-0.43	0.01	-0.20	-2.68	-0.42
4.0	3.5	0	-4.23	-1.73	0.08	-2.18	0.06	-0.31	0.01	-0.16	-2.28	-0.30
4.0	4.0	0	-3.23	-1.16	0.04	-1.79	0.03	-0.22	0.00	-0.12	-1.88	-0.22

h	X	θ	E_{int}	$E^{(1)}_{pol}$	$E^{(1)}_{exch}$	$E^{(2)}_{ind}$	$E^{(2)}_{ind-exch}$	$E^{(2)}_{disp}$	$E^{(2)}_{disp-exch}$	δ_{HF}	E_{Ind}	E_{Disp}
2.5	0.0	30	-11.94	-21.51	42.00	-30.97	16.21	-13.67	2.49	-6.49	-21.25	-11.18
2.5	0.5	30	-10.17	-21.12	41.41	-31.78	17.53	-13.38	2.49	-5.31	-19.56	-10.89
2.5	1.0	30	-6.71	-19.96	39.63	-32.87	19.63	-12.49	2.43	-3.08	-16.32	-10.06
2.5	1.5	30	-5.39	-17.75	36.03	-31.91	19.32	-11.04	2.18	-2.21	-14.80	-8.86
2.5	2.0	30	-7.64	-14.09	28.85	-27.60	15.46	-8.98	1.68	-2.95	-15.09	-7.30
2.5	2.5	30	-10.46	-9.56	18.64	-20.66	9.75	-6.51	1.07	-3.19	-14.10	-5.44
2.5	3.0	30	-10.82	-5.53	9.46	-13.72	4.86	-4.17	0.56	-2.27	-11.13	-3.61
2.5	3.5	30	-8.94	-2.69	3.87	-8.69	1.98	-2.42	0.24	-1.23	-7.94	-2.18
2.5	4.0	30	-6.37	-0.98	1.32	-5.56	0.69	-1.32	0.08	-0.60	-5.47	-1.24
3.0	0.0	30	-17.69	-11.42	9.32	-12.53	3.94	-5.38	0.64	-2.26	-10.85	-4.74
3.0	0.5	30	-16.82	-11.09	9.20	-12.63	4.24	-5.25	0.64	-1.94	-10.33	-4.61
3.0	1.0	30	-14.87	-10.20	8.83	-12.70	4.75	-4.88	0.64	-1.30	-9.25	-4.24
3.0	1.5	30	-13.15	-8.97	8.06	-12.34	4.78	-4.31	0.58	-0.94	-8.50	-3.73
3.0	2.0	30	-12.13	-7.40	6.56	-11.20	4.00	-3.56	0.46	-0.99	-8.19	-3.10
3.0	2.5	30	-11.13	-5.57	4.46	-9.29	2.70	-2.70	0.30	-1.05	-7.64	-2.40
3.0	3.0	30	-9.49	-3.76	2.45	-7.10	1.48	-1.85	0.17	-0.87	-6.49	-1.68
3.0	3.5	30	-7.34	-2.25	1.10	-5.17	0.67	-1.18	0.07	-0.58	-5.08	-1.11
3.0	4.0	30	-5.22	-1.16	0.42	-3.71	0.26	-0.71	0.03	-0.35	-3.80	-0.68
3.5	0.0	30	-13.86	-7.53	1.95	-6.30	0.91	-2.20	0.14	-0.83	-6.22	-2.06
3.5	0.5	30	-13.44	-7.32	1.93	-6.30	0.98	-2.15	0.15	-0.73	-6.05	-2.00
3.5	1.0	30	-12.42	-6.77	1.88	-6.24	1.10	-2.00	0.15	-0.54	-5.68	-1.85
3.5	1.5	30	-11.21	-5.98	1.73	-6.04	1.12	-1.78	0.14	-0.41	-5.33	-1.64
3.5	2.0	30	-10.01	-5.03	1.44	-5.60	0.98	-1.49	0.11	-0.41	-5.03	-1.38
3.5	2.5	30	-8.70	-3.98	1.02	-4.92	0.70	-1.17	0.08	-0.43	-4.65	-1.09
3.5	3.0	30	-7.19	-2.92	0.60	-4.09	0.41	-0.85	0.04	-0.39	-4.07	-0.81
3.5	3.5	30	-5.59	-1.97	0.29	-3.25	0.20	-0.59	0.02	-0.30	-3.35	-0.57
3.5	4.0	30	-4.10	-1.21	0.12	-2.53	0.09	-0.38	0.01	-0.20	-2.64	-0.37
4.0	0.0	30	-9.84	-5.48	0.39	-3.67	0.20	-0.96	0.03	-0.35	-3.82	-0.93
4.0	0.5	30	-9.63	-5.35	0.39	-3.65	0.22	-0.94	0.03	-0.33	-3.76	-0.91
4.0	1.0	30	-9.08	-4.99	0.38	-3.59	0.24	-0.88	0.03	-0.27	-3.62	-0.85
4.0	1.5	30	-8.31	-4.46	0.36	-3.47	0.25	-0.79	0.03	-0.23	-3.45	-0.76
4.0	2.0	30	-7.41	-3.82	0.31	-3.26	0.23	-0.67	0.02	-0.22	-3.25	-0.65
4.0	2.5	30	-6.41	-3.11	0.23	-2.95	0.17	-0.55	0.02	-0.22	-3.00	-0.53
4.0	3.0	30	-5.32	-2.40	0.14	-2.56	0.11	-0.42	0.01	-0.20	-2.65	-0.41
4.0	3.5	30	-4.22	-1.74	0.07	-2.15	0.06	-0.31	0.01	-0.16	-2.25	-0.30
4.0	4.0	30	-3.21	-1.18	0.03	-1.77	0.03	-0.22	0.00	-0.11	-1.85	-0.22

Table 7.7.: DFT-SAPT/avtz $C_6H_6...NH_4^+$ X-shift of bidentate conformation. Distance (h and X) in Å, θ in ° and energies kcal/mol. A graphical representation of this energies can be found in Figs. 3.10 and 3.11.

h	X	θ	E_{int}	$E^{(1)}_{pol}$	$E^{(1)}_{exch}$	$E^{(2)}_{ind}$	$E^{(2)}_{ind-exch}$	$E^{(2)}_{disp}$	$E^{(2)}_{disp-exch}$	δ_{HF}	E_{Ind}	E_{Disp}
2.5	0.0	0	-9.70	-20.35	37.16	-27.60	15.10	-12.76	2.36	-3.61	-16.11	-10.40
2.5	0.5	0	-9.20	-20.37	37.42	-29.20	16.73	-12.63	2.39	-3.54	-16.01	-10.24
2.5	1.0	0	-8.08	-19.82	37.30	-31.98	19.53	-12.10	2.37	-3.39	-15.84	-9.73
2.5	1.5	0	-7.36	-17.52	33.72	-31.39	19.36	-10.76	2.14	-2.91	-14.94	-8.62
2.5	2.0	0	-7.90	-13.31	25.31	-25.89	15.07	-8.56	1.63	-2.14	-12.96	-6.93
2.5	2.5	0	-8.56	-8.57	15.46	-18.46	9.32	-6.03	1.02	-1.32	-10.46	-5.01
2.5	3.0	0	-8.15	-4.70	7.93	-12.17	4.76	-3.82	0.54	-0.69	-8.10	-3.28
2.5	3.5	0	-6.78	-2.10	3.49	-7.88	2.08	-2.24	0.24	-0.37	-6.17	-2.00
2.5	4.0	0	-5.07	-0.61	1.31	-5.19	0.79	-1.24	0.09	-0.23	-4.63	-1.15
3.0	0.0	0	-16.19	-10.83	8.06	-11.39	3.63	-4.97	0.58	-1.27	-9.03	-4.39
3.0	0.5	0	-15.76	-10.62	8.08	-11.66	3.97	-4.89	0.59	-1.24	-8.93	-4.30
3.0	1.0	0	-14.67	-9.95	7.98	-12.11	4.59	-4.63	0.59	-1.15	-8.67	-4.04
3.0	1.5	0	-13.27	-8.72	7.23	-11.86	4.63	-4.11	0.54	-0.99	-8.22	-3.57
3.0	2.0	0	-11.76	-6.96	5.60	-10.48	3.77	-3.34	0.42	-0.76	-7.47	-2.92
3.0	2.5	0	-10.07	-4.99	3.59	-8.41	2.48	-2.47	0.27	-0.53	-6.46	-2.20
3.0	3.0	0	-8.17	-3.21	1.94	-6.35	1.35	-1.67	0.15	-0.36	-5.36	-1.52
3.0	3.5	0	-6.23	-1.83	0.90	-4.68	0.62	-1.06	0.07	-0.25	-4.31	-0.99
3.0	4.0	0	-4.49	-0.87	0.36	-3.43	0.25	-0.64	0.03	-0.18	-3.36	-0.61
3.5	0.0	0	-12.98	-7.20	1.66	-5.84	0.83	-2.03	0.13	-0.52	-5.53	-1.90
3.5	0.5	0	-12.70	-7.03	1.67	-5.88	0.90	-2.00	0.13	-0.50	-5.48	-1.87
3.5	1.0	0	-11.96	-6.54	1.65	-5.91	1.04	-1.88	0.13	-0.46	-5.33	-1.75
3.5	1.5	0	-10.89	-5.76	1.51	-5.74	1.06	-1.68	0.12	-0.40	-5.08	-1.56
3.5	2.0	0	-9.57	-4.76	1.21	-5.27	0.90	-1.40	0.10	-0.35	-4.72	-1.30
3.5	2.5	0	-8.08	-3.66	0.81	-4.55	0.63	-1.08	0.07	-0.29	-4.21	-1.01
3.5	3.0	0	-6.50	-2.61	0.46	-3.75	0.36	-0.78	0.04	-0.23	-3.62	-0.74
3.5	3.5	0	-4.99	-1.71	0.23	-3.00	0.18	-0.53	0.02	-0.18	-3.00	-0.51
3.5	4.0	0	-3.68	-1.02	0.10	-2.36	0.08	-0.35	0.01	-0.13	-2.41	-0.34
4.0	0.0	0	-9.34	-5.27	0.33	-3.45	0.18	-0.90	0.03	-0.26	-3.53	-0.87
4.0	0.5	0	-9.18	-5.15	0.33	-3.45	0.20	-0.88	0.03	-0.25	-3.50	-0.85
4.0	1.0	0	-8.71	-4.82	0.33	-3.41	0.23	-0.83	0.03	-0.24	-3.42	-0.80
4.0	1.5	0	-8.00	-4.30	0.31	-3.31	0.23	-0.74	0.03	-0.22	-3.30	-0.71
4.0	2.0	0	-7.09	-3.64	0.25	-3.09	0.21	-0.63	0.02	-0.20	-3.08	-0.61
4.0	2.5	0	-6.04	-2.92	0.18	-2.78	0.15	-0.51	0.01	-0.18	-2.81	-0.50
4.0	3.0	0	-4.95	-2.21	0.11	-2.41	0.09	-0.39	0.01	-0.15	-2.47	-0.38
4.0	3.5	0	-3.89	-1.58	0.06	-2.03	0.05	-0.28	0.00	-0.12	-2.10	-0.28
4.0	4.0	0	-2.96	-1.05	0.03	-1.68	0.02	-0.20	0.00	-0.08	-1.74	-0.20

h	X	θ	E_{int}	$E^{(1)}_{pol}$	$E^{(1)}_{exch}$	$E^{(2)}_{ind}$	$E^{(2)}_{ind-exch}$	$E^{(2)}_{disp}$	$E^{(2)}_{disp-exch}$	δ_{HF}	E_{Ind}	E_{Disp}
2.5	0.0	30	-9.73	-20.43	37.12	-27.54	15.09	-12.75	2.36	-3.58	-16.03	-10.39
2.5	0.5	30	-9.18	-20.39	37.33	-29.10	16.68	-12.60	2.38	-3.48	-15.90	-10.22
2.5	1.0	30	-8.17	-19.86	36.88	-31.63	19.34	-12.00	2.36	-3.26	-15.55	-9.64
2.5	1.5	30	-7.76	-17.45	32.98	-30.90	19.01	-10.63	2.10	-2.87	-14.76	-8.53
2.5	2.0	30	-8.46	-13.06	24.61	-25.42	14.55	-8.44	1.58	-2.29	-13.16	-6.86
2.5	2.5	30	-9.35	-8.28	14.77	-17.97	8.64	-5.91	0.97	-1.57	-10.90	-4.94
2.5	3.0	30	-9.01	-4.43	7.14	-11.69	4.11	-3.69	0.48	-0.92	-8.50	-3.21
2.5	3.5	30	-7.37	-1.91	2.83	-7.49	1.62	-2.11	0.20	-0.51	-6.38	-1.91
2.5	4.0	30	-5.32	-0.53	0.94	-4.91	0.55	-1.15	0.07	-0.29	-4.65	-1.08
3.0	0.0	30	-16.19	-10.84	8.05	-11.38	3.63	-4.97	0.58	-1.27	-9.02	-4.39
3.0	0.5	30	-15.75	-10.62	8.07	-11.64	3.97	-4.88	0.59	-1.23	-8.90	-4.29
3.0	1.0	30	-14.67	-9.96	7.93	-12.06	4.57	-4.61	0.59	-1.13	-8.62	-4.02
3.0	1.5	30	-13.30	-8.72	7.14	-11.78	4.58	-4.08	0.54	-0.98	-8.18	-3.54
3.0	2.0	30	-11.83	-6.95	5.50	-10.40	3.69	-3.32	0.41	-0.77	-7.48	-2.91
3.0	2.5	30	-10.20	-4.97	3.49	-8.34	2.37	-2.44	0.26	-0.57	-6.54	-2.18
3.0	3.0	30	-8.32	-3.19	1.81	-6.27	1.24	-1.64	0.14	-0.40	-5.43	-1.50
3.0	3.5	30	-6.32	-1.80	0.78	-4.59	0.54	-1.03	0.06	-0.28	-4.33	-0.97
3.0	4.0	30	-4.51	-0.87	0.29	-3.35	0.20	-0.62	0.02	-0.19	-3.34	-0.60
3.5	0.0	30	-12.97	-7.20	1.66	-5.84	0.83	-2.03	0.13	-0.52	-5.53	-1.90
3.5	0.5	30	-12.70	-7.03	1.66	-5.87	0.90	-1.99	0.13	-0.50	-5.47	-1.86
3.5	1.0	30	-11.96	-6.54	1.64	-5.90	1.03	-1.88	0.13	-0.46	-5.33	-1.75
3.5	1.5	30	-10.89	-5.77	1.50	-5.73	1.05	-1.67	0.12	-0.40	-5.08	-1.55
3.5	2.0	30	-9.58	-4.77	1.19	-5.26	0.89	-1.39	0.10	-0.35	-4.72	-1.29
3.5	2.5	30	-8.10	-3.66	0.80	-4.54	0.61	-1.07	0.06	-0.29	-4.22	-1.01
3.5	3.0	30	-6.52	-2.61	0.44	-3.73	0.34	-0.77	0.04	-0.24	-3.63	-0.73
3.5	3.5	30	-5.00	-1.71	0.21	-2.98	0.16	-0.52	0.02	-0.18	-3.00	-0.50
3.5	4.0	30	-3.67	-1.02	0.08	-2.33	0.07	-0.34	0.01	-0.13	-2.39	-0.33
4.0	0.0	30	-9.34	-5.27	0.33	-3.45	0.18	-0.90	0.03	-0.26	-3.53	-0.87
4.0	0.5	30	-9.18	-5.16	0.33	-3.45	0.20	-0.88	0.03	-0.25	-3.50	-0.85
4.0	1.0	30	-8.71	-4.82	0.33	-3.41	0.23	-0.83	0.03	-0.24	-3.42	-0.80
4.0	1.5	30	-8.00	-4.30	0.31	-3.30	0.23	-0.74	0.03	-0.22	-3.29	-0.71
4.0	2.0	30	-7.09	-3.64	0.25	-3.09	0.21	-0.63	0.02	-0.20	-3.08	-0.61
4.0	2.5	30	-6.04	-2.92	0.18	-2.77	0.15	-0.51	0.01	-0.18	-2.80	-0.50
4.0	3.0	30	-4.95	-2.22	0.10	-2.40	0.09	-0.38	0.01	-0.15	-2.46	-0.37
4.0	3.5	30	-3.89	-1.58	0.05	-2.02	0.05	-0.28	0.00	-0.12	-2.09	-0.28
4.0	4.0	30	-2.95	-1.06	0.02	-1.66	0.02	-0.20	0.00	-0.08	-1.72	-0.20

Table 7.8.: DFT-SAPT/avtz $C_6H_6...NH_4^+$ X-shift of tridentate conformation. Distance (h and X) in Å, θ in ° and energies in kcal/mol. A graphical representation of these energies can be found in Figs. 3.10 and 3.11.

O-H												
R	E_{int}	$E^{(1)}_{pol}$	$E^{(1)}_{exch}$	$E^{(2)}_{ind}$	$E^{(2)}_{i.-exch}$	$E^{(2)}_{disp}$	$E^{(2)}_{d.-exch}$	δ_{HF}	E_{Ind}	E_{Disp}	$E^{(2)}_{Disp}(tz)$	$E^{(2)}_{Disp}(cbs)$
2.6	-1.94	-13.15	21.64	-9.95	6.65	-5.81	1.36	-2.68	-5.98	-4.45	-4.28	-4.57
2.7	-3.23	-10.55	15.17	-6.73	4.34	-4.62	1.02	-1.87	-4.26	-3.60	-3.46	-3.70
2.8	-3.92	-8.56	10.60	-4.59	2.83	-3.67	0.76	-1.29	-3.05	-2.91	-2.80	-2.99
2.9	-4.21	-7.03	7.40	-3.16	1.84	-2.93	0.57	-0.89	-2.21	-2.36	-2.28	-2.42
3.0	-4.24	-5.85	5.15	-2.20	1.19	-2.34	0.42	-0.61	-1.62	-1.92	-1.86	-1.96
3.1	-4.12	-4.93	3.58	-1.55	0.77	-1.88	0.31	-0.42	-1.20	-1.57	-1.51	-1.61
3.2	-3.90	-4.21	2.48	-1.11	0.50	-1.51	0.23	-0.28	-0.89	-1.28	-1.24	-1.31
3.3	-3.63	-3.63	1.72	-0.80	0.33	-1.22	0.17	-0.19	-0.66	-1.05	-1.02	-1.07
3.4	-3.35	-3.16	1.19	-0.59	0.21	-0.99	0.12	-0.13	-0.51	-0.87	-0.84	-0.89
3.5	-3.07	-2.78	0.82	-0.44	0.14	-0.80	0.09	-0.09	-0.39	-0.71	-0.69	-0.72
3.6	-2.80	-2.47	0.57	-0.33	0.09	-0.65	0.06	-0.06	-0.30	-0.59	-0.57	-0.60
3.7	-2.55	-2.20	0.39	-0.26	0.06	-0.54	0.05	-0.04	-0.24	-0.49	-0.48	-0.50
3.8	-2.31	-1.98	0.27	-0.20	0.04	-0.44	0.03	-0.03	-0.19	-0.41	-0.40	-0.42
3.9	-2.10	-1.79	0.19	-0.16	0.03	-0.36	0.02	-0.02	-0.15	-0.34	-0.33	-0.35
4.0	-1.91	-1.63	0.13	-0.13	0.02	-0.30	0.02	-0.01	-0.12	-0.28	-0.27	-0.29

O-O												
R	E_{int}	$E^{(1)}_{pol}$	$E^{(1)}_{exch}$	$E^{(2)}_{ind}$	$E^{(2)}_{i.-exch}$	$E^{(2)}_{disp}$	$E^{(2)}_{d.-exch}$	δ_{HF}	E_{Ind}	E_{Disp}	$E^{(2)}_{Disp}(tz)$	$E^{(2)}_{Disp}(cbs)$
2.6	5.65	2.25	6.13	-2.10	1.66	-2.56	0.57	-0.30	-0.74	-1.99	-1.87	-2.08
2.7	4.56	2.51	4.26	-1.45	1.07	-2.05	0.42	-0.20	-0.58	-1.63	-1.53	-1.70
2.8	3.77	2.61	2.96	-1.02	0.69	-1.64	0.31	-0.13	-0.46	-1.33	-1.26	-1.38
2.9	3.19	2.60	2.06	-0.73	0.44	-1.32	0.22	-0.08	-0.37	-1.10	-1.03	-1.15
3.0	2.76	2.53	1.43	-0.53	0.28	-1.06	0.16	-0.05	-0.30	-0.90	-0.86	-0.93
3.1	2.43	2.43	0.99	-0.40	0.18	-0.86	0.12	-0.03	-0.25	-0.74	-0.71	-0.76
3.2	2.17	2.30	0.69	-0.30	0.12	-0.70	0.08	-0.02	-0.20	-0.62	-0.59	-0.64
3.3	1.96	2.17	0.47	-0.24	0.08	-0.57	0.06	-0.01	-0.17	-0.51	-0.49	-0.52
3.4	1.80	2.04	0.33	-0.19	0.05	-0.47	0.04	-0.01	-0.15	-0.43	-0.41	-0.44
3.5	1.66	1.91	0.23	-0.15	0.03	-0.39	0.03	-0.00	-0.12	-0.36	-0.34	-0.37
3.6	1.54	1.78	0.16	-0.12	0.02	-0.32	0.02	-0.00	-0.10	-0.30	-0.29	-0.31
3.7	1.43	1.66	0.11	-0.10	0.01	-0.27	0.02	0.00	-0.09	-0.25	-0.24	-0.26
3.8	1.34	1.55	0.07	-0.08	0.01	-0.23	0.01	0.00	-0.07	-0.22	-0.20	-0.23
3.9	1.26	1.45	0.05	-0.07	0.01	-0.19	0.01	0.00	-0.06	-0.18	-0.17	-0.19
4.0	1.18	1.35	0.04	-0.06	0.00	-0.16	0.01	0.00	-0.06	-0.15	-0.14	-0.16

H-H												
R	E_{int}	$E^{(1)}_{pol}$	$E^{(1)}_{exch}$	$E^{(2)}_{ind}$	$E^{(2)}_{i.-exch}$	$E^{(2)}_{disp}$	$E^{(2)}_{d.-exch}$	δ_{HF}	E_{Ind}	E_{Disp}	$E^{(2)}_{Disp}(tz)$	$E^{(2)}_{Disp}(cbs)$
2.6	81.42	50.81	74.47	-51.71	26.80	-12.87	2.08	-8.18	-33.09	-10.79	-10.50	-11.00
2.7	55.09	33.27	53.50	-35.32	18.74	-10.30	1.70	-6.51	-23.09	-8.60	-8.38	-8.76
2.8	38.21	23.04	38.15	-24.13	12.90	-8.23	1.36	-4.87	-16.10	-6.87	-6.71	-6.99
2.9	27.07	16.79	27.03	-16.52	8.77	-6.57	1.06	-3.50	-11.25	-5.51	-5.38	-5.60
3.0	19.54	12.79	19.06	-11.34	5.90	-5.24	0.82	-2.45	-7.89	-4.42	-4.33	-4.49
3.1	14.36	10.10	13.37	-7.81	3.94	-4.19	0.63	-1.69	-5.56	-3.56	-3.48	-3.62
3.2	10.75	8.20	9.35	-5.41	2.62	-3.35	0.48	-1.14	-3.93	-2.87	-2.80	-2.92
3.3	8.20	6.80	6.52	-3.76	1.73	-2.68	0.36	-0.77	-2.80	-2.32	-2.26	-2.36
3.4	6.37	5.73	4.53	-2.64	1.14	-2.15	0.27	-0.51	-2.01	-1.88	-1.84	-1.91
3.5	5.05	4.89	3.14	-1.86	0.75	-1.73	0.20	-0.34	-1.45	-1.53	-1.49	-1.56
3.6	4.08	4.21	2.17	-1.33	0.49	-1.39	0.15	-0.22	-1.06	-1.24	-1.21	-1.26
3.7	3.35	3.65	1.50	-0.95	0.32	-1.12	0.11	-0.15	-0.78	-1.01	-0.99	-1.02
3.8	2.80	3.19	1.03	-0.69	0.21	-0.91	0.08	-0.10	-0.58	-0.83	-0.82	-0.84
3.9	2.38	2.80	0.70	-0.51	0.14	-0.74	0.06	-0.06	-0.43	-0.68	-0.67	-0.69
4.0	2.05	2.46	0.48	-0.38	0.09	-0.60	0.04	-0.04	-0.33	-0.56	-0.55	-0.57

Table 7.9.: DFT-SAPT/avqz energy decomposition results obtained from the $H_2O...H_2O$ interaction. The distance (R) in Å and energies in kcal/mol. A graphical representation of these energies can be found in Fig. 3.16.

B1

R	E_{int}	$E^{(1)}_{pol}$	$E^{(1)}_{exch}$	$E^{(2)}_{ind}$	$E^{(2)}_{ind-exch}$	$E^{(2)}_{disp}$	$E^{(2)}_{disp-exch}$	δ_{HF}	E_{Ind}	E_{Disp}
2.7	2.85	-8.07	22.90	-9.63	7.38	-10.46	2.27	-1.54	-3.79	-8.19
2.8	0.66	-6.54	17.27	-7.11	5.31	-8.80	1.79	-1.26	-3.06	-7.01
2.9	-0.86	-5.36	12.96	-5.25	3.80	-7.40	1.41	-1.01	-2.46	-5.99
3.0	-1.86	-4.44	9.69	-3.89	2.71	-6.23	1.10	-0.80	-1.98	-5.13
3.1	-2.49	-3.73	7.21	-2.89	1.92	-5.24	0.85	-0.62	-1.59	-4.39
3.2	-2.85	-3.17	5.35	-2.16	1.36	-4.41	0.66	-0.48	-1.28	-3.75
3.3	-3.01	-2.73	3.96	-1.62	0.96	-3.72	0.51	-0.37	-1.03	-3.21
3.4	-3.04	-2.39	2.92	-1.23	0.68	-3.13	0.39	-0.28	-0.83	-2.74
3.5	-2.98	-2.11	2.15	-0.94	0.48	-2.65	0.30	-0.21	-0.67	-2.35
3.6	-2.87	-1.88	1.57	-0.73	0.34	-2.24	0.23	-0.16	-0.55	-2.01
3.7	-2.71	-1.69	1.15	-0.56	0.24	-1.90	0.17	-0.12	-0.44	-1.73
3.8	-2.54	-1.53	0.84	-0.44	0.17	-1.61	0.13	-0.09	-0.36	-1.48
3.9	-2.36	-1.40	0.61	-0.35	0.12	-1.37	0.10	-0.07	-0.30	-1.27
4.0	-2.19	-1.28	0.44	-0.28	0.08	-1.17	0.08	-0.05	-0.25	-1.09

B2

R	E_{int}	$E^{(1)}_{pol}$	$E^{(1)}_{exch}$	$E^{(2)}_{ind}$	$E^{(2)}_{ind-exch}$	$E^{(2)}_{disp}$	$E^{(2)}_{disp-exch}$	δ_{HF}	E_{Ind}	E_{Disp}
2.7	2.00	-10.32	24.45	-10.26	8.30	-11.08	2.53	-1.63	-3.59	-8.55
2.8	-0.05	-8.19	18.22	-7.43	5.92	-9.26	1.98	-1.28	-2.79	-7.28
2.9	-1.41	-6.56	13.53	-5.39	4.20	-7.75	1.54	-0.99	-2.18	-6.21
3.0	-2.27	-5.30	10.02	-3.92	2.97	-6.48	1.20	-0.76	-1.71	-5.28
3.1	-2.78	-4.34	7.40	-2.86	2.10	-5.43	0.93	-0.58	-1.34	-4.50
3.2	-3.03	-3.59	5.46	-2.10	1.48	-4.55	0.71	-0.43	-1.05	-3.84
3.3	-3.12	-3.02	4.01	-1.55	1.04	-3.82	0.55	-0.33	-0.84	-3.27
3.4	-3.08	-2.56	2.94	-1.15	0.73	-3.21	0.42	-0.24	-0.66	-2.79
3.5	-2.98	-2.21	2.15	-0.86	0.51	-2.71	0.32	-0.18	-0.53	-2.39
3.6	-2.83	-1.93	1.57	-0.65	0.36	-2.29	0.24	-0.14	-0.43	-2.05
3.7	-2.65	-1.70	1.15	-0.50	0.25	-1.93	0.19	-0.10	-0.35	-1.74
3.8	-2.47	-1.51	0.83	-0.39	0.18	-1.64	0.14	-0.08	-0.29	-1.50
3.9	-2.28	-1.36	0.61	-0.30	0.12	-1.40	0.11	-0.06	-0.24	-1.29
4.0	-2.10	-1.23	0.44	-0.24	0.09	-1.19	0.08	-0.04	-0.19	-1.11

BO

R	E_{int}	$E^{(1)}_{pol}$	$E^{(1)}_{exch}$	$E^{(2)}_{ind}$	$E^{(2)}_{ind-exch}$	$E^{(2)}_{disp}$	$E^{(2)}_{disp-exch}$	δ_{HF}	E_{Ind}	E_{Disp}
2.7	2.84	-1.16	9.81	-3.43	2.92	-6.09	1.22	-0.42	-0.93	-4.87
2.8	1.98	-0.34	7.25	-2.50	2.04	-5.10	0.95	-0.31	-0.77	-4.15
2.9	1.38	0.24	5.34	-1.83	1.42	-4.28	0.73	-0.23	-0.64	-3.55
3.0	0.99	0.63	3.93	-1.36	0.99	-3.59	0.56	-0.17	-0.54	-3.03
3.1	0.73	0.90	2.88	-1.02	0.68	-3.02	0.43	-0.12	-0.46	-2.59
3.2	0.56	1.06	2.11	-0.77	0.47	-2.55	0.33	-0.08	-0.38	-2.22
3.3	0.47	1.16	1.54	-0.60	0.33	-2.15	0.25	-0.06	-0.33	-1.90
3.4	0.41	1.20	1.12	-0.47	0.23	-1.82	0.19	-0.04	-0.28	-1.63
3.5	0.39	1.21	0.81	-0.37	0.16	-1.55	0.14	-0.02	-0.23	-1.41
3.6	0.38	1.20	0.59	-0.30	0.11	-1.32	0.11	-0.02	-0.21	-1.21
3.7	0.38	1.17	0.43	-0.24	0.08	-1.12	0.08	-0.01	-0.17	-1.04
3.8	0.39	1.13	0.31	-0.20	0.05	-0.96	0.06	-0.00	-0.15	-0.90
3.9	0.39	1.08	0.22	-0.17	0.04	-0.82	0.05	-0.00	-0.13	-0.77
4.0	0.40	1.03	0.16	-0.14	0.03	-0.71	0.03	-0.00	-0.11	-0.68

Table 7.10.: DFT-SAPT/avtz energy decomposition results obtained from the $H_2O...C_6H_6$ interaction. The distance (R) in Å and energies in kcal/mol.

B S1										
R	E_{int}	$E^{(1)}_{pol}$	$E^{(1)}_{exch}$	$E^{(2)}_{ind}$	$E^{(2)}_{ind-exch}$	$E^{(2)}_{disp}$	$E^{(2)}_{disp-exch}$	δ_{HF}	E_{Ind}	E_{Disp}
4.4	0.92	-5.61	12.02	-4.31	3.31	-4.20	0.91	-1.21	-2.21	-3.29
4.5	-0.01	-4.26	8.56	-2.96	2.20	-3.41	0.69	-0.84	-1.60	-2.72
4.6	-0.60	-3.27	6.09	-2.06	1.46	-2.77	0.52	-0.58	-1.18	-2.25
4.7	-0.96	-2.54	4.33	-1.44	0.97	-2.26	0.39	-0.40	-0.87	-1.87
4.8	-1.15	-2.00	3.07	-1.03	0.64	-1.85	0.30	-0.28	-0.67	-1.55
4.9	-1.23	-1.60	2.18	-0.74	0.42	-1.52	0.22	-0.19	-0.51	-1.30
5.0	-1.25	-1.30	1.54	-0.55	0.28	-1.26	0.16	-0.13	-0.40	-1.10
5.1	-1.21	-1.07	1.09	-0.41	0.19	-1.04	0.12	-0.09	-0.31	-0.92
5.2	-1.15	-0.90	0.77	-0.31	0.12	-0.86	0.09	-0.06	-0.25	-0.77
5.3	-1.08	-0.77	0.54	-0.24	0.08	-0.72	0.07	-0.04	-0.20	-0.65
5.4	-1.00	-0.66	0.38	-0.19	0.05	-0.60	0.05	-0.03	-0.17	-0.55
5.5	-0.91	-0.58	0.27	-0.15	0.04	-0.51	0.04	-0.02	-0.13	-0.47
5.6	-0.83	-0.51	0.19	-0.12	0.02	-0.43	0.03	-0.01	-0.11	-0.40
5.7	-0.76	-0.45	0.13	-0.10	0.02	-0.36	0.02	-0.01	-0.09	-0.34
5.8	-0.69	-0.40	0.09	-0.08	0.01	-0.31	0.01	-0.01	-0.08	-0.30
5.9	-0.63	-0.37	0.07	-0.07	0.01	-0.27	0.01	-0.00	-0.06	-0.26
6.0	-0.57	-0.33	0.05	-0.06	0.00	-0.23	0.01	-0.00	-0.06	-0.22
B S2										
R	E_{int}	$E^{(1)}_{pol}$	$E^{(1)}_{exch}$	$E^{(2)}_{ind}$	$E^{(2)}_{ind-exch}$	$E^{(2)}_{disp}$	$E^{(2)}_{disp-exch}$	δ_{HF}	E_{Ind}	E_{Disp}
4.0	1.76	-3.83	11.00	-3.33	2.75	-5.20	1.01	-0.64	-1.22	-4.19
4.1	0.63	-2.90	8.00	-2.38	1.89	-4.28	0.78	-0.47	-0.96	-3.50
4.2	-0.12	-2.22	5.81	-1.71	1.29	-3.54	0.59	-0.35	-0.77	-2.95
4.3	-0.61	-1.72	4.20	-1.24	0.88	-2.93	0.45	-0.25	-0.61	-2.48
4.4	-0.90	-1.36	3.03	-0.91	0.60	-2.43	0.34	-0.18	-0.49	-2.09
4.5	-1.06	-1.09	2.18	-0.67	0.40	-2.02	0.25	-0.13	-0.40	-1.77
4.6	-1.13	-0.89	1.57	-0.51	0.27	-1.68	0.19	-0.09	-0.33	-1.49
4.7	-1.15	-0.74	1.13	-0.39	0.19	-1.40	0.14	-0.06	-0.26	-1.26
4.8	-1.12	-0.63	0.81	-0.30	0.13	-1.18	0.11	-0.05	-0.22	-1.07
4.9	-1.07	-0.55	0.58	-0.24	0.08	-0.99	0.08	-0.03	-0.19	-0.91
5.0	-1.01	-0.48	0.41	-0.19	0.06	-0.83	0.06	-0.02	-0.15	-0.77
5.1	-0.94	-0.43	0.29	-0.16	0.04	-0.71	0.04	-0.02	-0.14	-0.67
5.2	-0.86	-0.39	0.21	-0.13	0.03	-0.60	0.03	-0.01	-0.11	-0.57
5.3	-0.80	-0.35	0.15	-0.11	0.02	-0.51	0.02	-0.01	-0.10	-0.49
5.4	-0.73	-0.32	0.10	-0.09	0.01	-0.44	0.02	-0.01	-0.09	-0.42
5.5	-0.67	-0.30	0.07	-0.08	0.01	-0.38	0.01	-0.00	-0.07	-0.37

Table 7.11.: DFT-SAPT/avtz energy decomposition results obtained from the $H_2O...C_6H_6$ interaction. The distance (R) in Å and energies in kcal/mol.

1H-HH										
R	E_{int}	$E^{(1)}_{pol}$	$E^{(1)}_{exch}$	$E^{(2)}_{ind}$	$E^{(2)}_{ind-exch}$	$E^{(2)}_{disp}$	$E^{(2)}_{disp-exch}$	δ_{HF}	E_{Ind}	E_{Disp}
2.2	89.81	-8.57	166.61	-99.84	55.24	-23.68	5.00	-4.95	-49.55	-18.68
2.3	68.28	-1.98	122.60	-72.54	42.13	-18.94	4.08	-7.07	-37.48	-14.86
2.4	52.12	2.96	89.58	-53.07	31.61	-15.11	3.25	-7.09	-28.55	-11.86
2.5	40.05	6.47	65.04	-39.13	23.39	-12.04	2.53	-6.20	-21.94	-9.51
2.6	31.10	8.83	46.96	-29.11	17.11	-9.59	1.94	-5.04	-17.04	-7.65
2.7	24.50	10.32	33.74	-21.88	12.41	-7.63	1.46	-3.92	-13.39	-6.17
2.8	19.67	11.17	24.13	-16.62	8.93	-6.07	1.09	-2.97	-10.66	-4.98
2.9	16.15	11.57	17.19	-12.78	6.39	-4.83	0.81	-2.21	-8.60	-4.02
3.0	13.59	11.65	12.20	-9.94	4.55	-3.85	0.59	-1.62	-7.01	-3.26
3.1	11.72	11.52	8.64	-7.84	3.23	-3.08	0.43	-1.19	-5.80	-2.65
3.2	10.36	11.25	6.09	-6.25	2.29	-2.46	0.31	-0.87	-4.83	-2.15
3.3	9.36	10.89	4.29	-5.05	1.62	-1.97	0.23	-0.64	-4.07	-1.74
3.4	8.60	10.49	3.01	-4.14	1.14	-1.59	0.16	-0.47	-3.47	-1.43
3.5	8.03	10.05	2.11	-3.42	0.80	-1.28	0.12	-0.35	-2.97	-1.16
3.6	7.57	9.61	1.47	-2.87	0.56	-1.03	0.08	-0.26	-2.57	-0.95
3.7	7.20	9.18	1.03	-2.42	0.39	-0.84	0.06	-0.20	-2.23	-0.78
3.8	6.89	8.76	0.71	-2.07	0.28	-0.69	0.04	-0.15	-1.94	-0.65
3.9	6.62	8.36	0.50	-1.78	0.19	-0.56	0.03	-0.12	-1.71	-0.53
4.0	6.38	7.98	0.34	-1.55	0.13	-0.46	0.02	-0.09	-1.51	-0.44
1H-OH										
R	E_{int}	$E^{(1)}_{pol}$	$E^{(1)}_{exch}$	$E^{(2)}_{ind}$	$E^{(2)}_{ind-exch}$	$E^{(2)}_{disp}$	$E^{(2)}_{disp-exch}$	δ_{HF}	E_{Ind}	E_{Disp}
2.2	-2.03	-48.30	100.16	-62.17	33.13	-14.96	2.96	-12.85	-41.89	-12.00
2.3	-10.27	-40.99	70.97	-43.24	22.94	-11.75	2.38	-10.59	-30.89	-9.37
2.4	-15.25	-34.88	50.03	-30.61	15.78	-9.22	1.86	-8.21	-23.04	-7.36
2.5	-18.06	-29.94	35.12	-22.08	10.81	-7.24	1.43	-6.15	-17.42	-5.81
2.6	-19.42	-25.98	24.56	-16.24	7.39	-5.69	1.07	-4.52	-13.37	-4.62
2.7	-19.80	-22.81	17.12	-12.19	5.05	-4.48	0.80	-3.29	-10.43	-3.68
2.8	-19.55	-20.25	11.89	-9.32	3.46	-3.53	0.59	-2.38	-8.24	-2.94
2.9	-18.91	-18.18	8.24	-7.26	2.37	-2.80	0.43	-1.72	-6.61	-2.37
3.0	-18.05	-16.47	5.70	-5.76	1.63	-2.22	0.31	-1.25	-5.38	-1.91
3.1	-17.07	-15.04	3.94	-4.64	1.12	-1.77	0.22	-0.91	-4.43	-1.55
3.2	-16.05	-13.82	2.71	-3.79	0.77	-1.41	0.16	-0.67	-3.69	-1.25
3.3	-15.04	-12.79	1.86	-3.14	0.53	-1.13	0.11	-0.49	-3.10	-1.02
3.4	-14.07	-11.88	1.28	-2.63	0.37	-0.91	0.08	-0.37	-2.63	-0.83
3.5	-13.15	-11.09	0.88	-2.23	0.25	-0.74	0.06	-0.28	-2.26	-0.68
3.6	-12.30	-10.39	0.60	-1.91	0.18	-0.60	0.04	-0.21	-1.94	-0.56
3.7	-11.51	-9.77	0.41	-1.65	0.12	-0.49	0.03	-0.16	-1.69	-0.46
3.8	-10.78	-9.20	0.28	-1.44	0.08	-0.40	0.02	-0.13	-1.49	-0.38
3.9	-10.12	-8.69	0.19	-1.26	0.06	-0.33	0.01	-0.10	-1.30	-0.32
4.0	-9.51	-8.23	0.13	-1.11	0.04	-0.27	0.01	-0.08	-1.15	-0.26

Table 7.12.: DFT-SAPT/avqz energy decomposition results obtained from the $H_2O...NH_4^+$ interaction. The distance (R) in Å and energies in kcal/mol.

3H-HH										
R	E_{int}	$E^{(1)}_{pol}$	$E^{(1)}_{exch}$	$E^{(2)}_{ind}$	$E^{(2)}_{ind-exch}$	$E^{(2)}_{disp}$	$E^{(2)}_{disp-exch}$	δ_{HF}	E_{Ind}	E_{Disp}
2.2	54.64	1.29	75.88	-43.65	33.66	-15.07	3.80	-1.26	-11.25	-11.27
2.3	41.71	5.38	54.27	-31.89	24.47	-11.94	2.88	-1.44	-8.86	-9.06
2.4	32.31	8.05	38.67	-23.48	17.62	-9.46	2.16	-1.25	-7.11	-7.30
2.5	25.47	9.72	27.47	-17.46	12.60	-7.50	1.61	-0.96	-5.82	-5.89
2.6	20.49	10.68	19.45	-13.15	8.96	-5.95	1.18	-0.69	-4.88	-4.77
2.7	16.86	11.14	13.73	-10.03	6.34	-4.73	0.87	-0.47	-4.16	-3.86
2.8	14.21	11.27	9.67	-7.78	4.48	-3.76	0.63	-0.31	-3.61	-3.13
2.9	12.26	11.19	6.79	-6.13	3.15	-3.00	0.46	-0.20	-3.18	-2.54
3.0	10.83	10.96	4.76	-4.91	2.22	-2.40	0.33	-0.13	-2.82	-2.07
3.1	9.75	10.64	3.33	-4.00	1.56	-1.93	0.23	-0.08	-2.52	-1.70
3.2	8.94	10.27	2.33	-3.31	1.09	-1.55	0.17	-0.06	-2.28	-1.38
3.3	8.31	9.87	1.62	-2.78	0.76	-1.25	0.12	-0.04	-2.06	-1.13
3.4	7.81	9.47	1.13	-2.36	0.53	-1.01	0.08	-0.04	-1.87	-0.93
3.5	7.40	9.07	0.79	-2.03	0.37	-0.83	0.06	-0.03	-1.69	-0.77
3.6	7.06	8.68	0.55	-1.76	0.26	-0.68	0.04	-0.03	-1.53	-0.64
3.7	6.76	8.30	0.38	-1.55	0.18	-0.56	0.03	-0.03	-1.40	-0.53
3.8	6.50	7.94	0.26	-1.37	0.13	-0.46	0.02	-0.02	-1.26	-0.44
3.9	6.27	7.60	0.18	-1.22	0.09	-0.38	0.01	-0.02	-1.15	-0.37
4.0	6.05	7.28	0.13	-1.09	0.06	-0.32	0.01	-0.02	-1.05	-0.31
3H-OH										
R	E_{int}	$E^{(1)}_{pol}$	$E^{(1)}_{exch}$	$E^{(2)}_{ind}$	$E^{(2)}_{ind-exch}$	$E^{(2)}_{disp}$	$E^{(2)}_{disp-exch}$	δ_{HF}	E_{Ind}	E_{Disp}
2.2	-6.32	-28.25	34.77	-19.78	14.10	-8.18	1.95	-0.93	-6.61	-6.23
2.3	-10.38	-24.16	24.33	-14.53	9.76	-6.44	1.45	-0.80	-5.57	-4.99
2.4	-12.88	-21.10	16.99	-10.87	6.74	-5.07	1.06	-0.63	-4.76	-4.01
2.5	-14.27	-18.75	11.83	-8.30	4.65	-4.01	0.77	-0.48	-4.13	-3.24
2.6	-14.92	-16.91	8.22	-6.47	3.21	-3.18	0.56	-0.36	-3.62	-2.62
2.7	-15.05	-15.44	5.70	-5.14	2.21	-2.52	0.40	-0.27	-3.20	-2.12
2.8	-14.85	-14.23	3.95	-4.16	1.53	-2.01	0.29	-0.21	-2.84	-1.72
2.9	-14.43	-13.21	2.73	-3.43	1.05	-1.61	0.20	-0.16	-2.54	-1.41
3.0	-13.89	-12.34	1.88	-2.87	0.73	-1.29	0.14	-0.13	-2.27	-1.15
3.1	-13.28	-11.59	1.29	-2.44	0.50	-1.04	0.10	-0.11	-2.05	-0.94
3.2	-12.64	-10.91	0.89	-2.10	0.35	-0.84	0.07	-0.09	-1.84	-0.77
3.3	-12.00	-10.31	0.61	-1.82	0.24	-0.69	0.05	-0.08	-1.66	-0.64
3.4	-11.37	-9.77	0.42	-1.60	0.17	-0.56	0.03	-0.07	-1.50	-0.53
3.5	-10.77	-9.27	0.29	-1.41	0.12	-0.46	0.02	-0.06	-1.35	-0.44
3.6	-10.20	-8.81	0.20	-1.25	0.08	-0.38	0.02	-0.05	-1.22	-0.36
3.7	-9.67	-8.39	0.13	-1.12	0.06	-0.32	0.01	-0.04	-1.10	-0.31
3.8	-9.17	-8.00	0.09	-1.01	0.04	-0.26	0.01	-0.04	-1.01	-0.25
3.9	-8.70	-7.63	0.06	-0.91	0.03	-0.22	0.01	-0.03	-0.91	-0.21
4.0	-8.26	-7.29	0.04	-0.82	0.02	-0.19	0.00	-0.03	-0.83	-0.19

Table 7.13.: DFT-SAPT/avqz energy decomposition results obtained from the $H_2O...NH_4^+$ interaction. The distance (R) in Å and energies in kcal/mol.

1H-HH														
	Amoeba09				FF-SAPT1				FF-SAPT2					
R	E_{int}	E_{vdw}	E_{Ind}	E_{el}	E_{int}	E_{vdw}	E_{Ind}	E_{el}	E_{int}	E_{vdw}	E_{Ind}	E_{el}	E_{Disp}	E_{exch}
2.2	144.59	140.20	-12.71	17.10	240.42	241.49	-16.09	-37.41	142.93	144.34	-16.09	-37.75	-17.12	161.46
2.3	95.76	91.01	-11.85	16.60	157.83	156.25	-14.54	-29.14	103.09	101.80	-14.54	-29.43	-13.86	115.66
2.4	64.57	59.33	-10.92	16.16	106.51	102.98	-12.95	-22.96	74.85	71.57	-12.95	-23.20	-11.18	82.75
2.5	44.49	38.72	-9.96	15.73	73.88	68.86	-11.41	-18.29	54.95	50.13	-11.41	-18.48	-9.01	59.13
2.6	31.47	25.18	-8.98	15.26	52.71	46.54	-9.95	-14.69	40.98	34.95	-9.95	-14.83	-7.25	42.20
2.7	22.97	16.24	-8.01	14.74	38.72	31.67	-8.61	-11.88	31.19	24.25	-8.61	-11.99	-5.83	30.08
2.8	17.41	10.32	-7.08	14.17	29.31	21.63	-7.40	-9.66	24.32	16.72	-7.40	-9.74	-4.69	21.41
2.9	13.77	6.40	-6.20	13.57	22.89	14.76	-6.32	-7.88	19.50	11.44	-6.32	-7.95	-3.78	15.23
3.0	11.40	3.84	-5.40	12.96	18.42	10.04	-5.39	-6.47	16.10	7.76	-5.39	-6.52	-3.05	10.82
3.1	9.85	2.19	-4.69	12.34	15.26	6.76	-4.60	-5.35	13.67	5.20	-4.60	-5.38	-2.47	7.68
3.2	8.84	1.15	-4.06	11.75	13.00	4.49	-3.93	-4.45	11.91	3.44	-3.93	-4.47	-2.01	5.44
3.3	8.17	0.52	-3.51	11.17	11.34	2.92	-3.38	-3.74	10.62	2.22	-3.38	-3.75	-1.64	3.86
3.4	7.71	0.15	-3.05	10.61	10.11	1.85	-2.91	-3.15	9.64	1.39	-2.91	-3.17	-1.34	2.73
3.5	7.37	-0.06	-2.65	10.09	9.17	1.12	-2.53	-2.70	8.88	0.83	-2.53	-2.71	-1.10	1.93
3.6	7.11	-0.17	-2.31	9.59	8.46	0.63	-2.20	-2.31	8.28	0.46	-2.20	-2.32	-0.91	1.37
3.7	6.88	-0.22	-2.03	9.12	7.89	0.31	-1.93	-2.00	7.79	0.21	-1.93	-2.01	-0.75	0.97
3.8	6.67	-0.23	-1.78	8.68	7.43	0.10	-1.70	-1.75	7.38	0.06	-1.70	-1.75	-0.63	0.68
3.9	6.47	-0.22	-1.58	8.27	7.05	-0.02	-1.50	-1.53	7.03	-0.04	-1.50	-1.53	-0.53	0.48
4.0	6.28	-0.20	-1.40	7.88	6.72	-0.09	-1.34	-1.36	6.72	-0.10	-1.34	-1.36	-0.44	0.34

Table 7.14.: DFT-SAPT/avqz energy decomposition results obtained from the $H_2O...NH_4^+$ interaction. The distance (R) in Å and energies in kcal/mol.

7.1.2. Force Field Results

monodentate									
	Amoeba09				FF-SAPT 1				
h	E_{Int}	E_{vdW}	E_{Pol}	E_{El}	E_{Int}	E_{vdW}	E_{Pol}	E_{El}	E_{Extra}
2.5	-0.97	24.09	-18.25	-6.81	0.95	37.85	-18.56	-6.81	-11.54
2.6	-7.28	16.72	-16.44	-7.56	-4.90	27.87	-16.65	-7.56	-8.56
2.7	-11.62	11.29	-14.85	-8.05	-9.13	20.26	-14.93	-8.05	-6.40
2.8	-14.42	7.33	-13.44	-8.32	-12.00	14.49	-13.40	-8.32	-4.77
2.9	-16.08	4.51	-12.17	-8.42	-13.81	10.16	-12.03	-8.42	-3.52
3.0	-16.87	2.52	-11.01	-8.39	-14.82	6.95	-10.82	-8.39	-2.56
3.1	-17.05	1.17	-9.96	-8.26	-15.27	4.58	-9.73	-8.26	-1.86
3.2	-16.80	0.27	-9.01	-8.06	-15.34	2.87	-8.78	-8.06	-1.38
3.4	-15.55	-0.64	-7.38	-7.53	-14.66	0.80	-7.17	-7.53	-0.76
3.5	-14.74	-0.82	-6.69	-7.23	-14.06	0.23	-6.50	-7.23	-0.55
3.8	-12.22	-0.89	-5.03	-6.30	-11.91	-0.52	-4.90	-6.30	-0.19
4.0	-10.67	-0.77	-4.20	-5.71	-10.53	-0.61	-4.10	-5.71	-0.11
5.0	-5.57	-0.25	-1.89	-3.43	-5.57	-0.27	-1.87	-3.43	-0.00
6.0	-3.21	-0.08	-0.98	-2.15	-3.21	-0.09	-0.98	-2.15	0.00
bidentate									
	Amoeba09				FF-SAPT 1				
h	E_{Int}	E_{vdW}	E_{Pol}	E_{El}	E_{Int}	E_{vdW}	E_{Pol}	E_{El}	E_{Extra}
2.5	-12.88	18.86	-17.62	-14.12	-11.21	31.67	-17.64	-14.12	-11.12
2.6	-16.76	12.27	-15.87	-13.16	-14.48	22.49	-15.60	-13.16	-8.20
2.7	-18.91	7.64	-14.25	-12.29	-16.54	15.69	-13.83	-12.29	-6.11
2.8	-19.83	4.44	-12.77	-11.50	-17.65	10.70	-12.30	-11.50	-4.54
2.9	-19.94	2.27	-11.43	-10.78	-18.03	7.07	-10.99	-10.78	-3.34
3.0	-19.50	0.85	-10.24	-10.11	-17.89	4.48	-9.84	-10.11	-2.42
3.1	-18.74	-0.05	-9.19	-9.50	-17.46	2.64	-8.84	-9.50	-1.76
3.2	-17.79	-0.60	-8.26	-8.93	-16.82	1.38	-7.97	-8.93	-1.30
3.4	-15.69	-1.05	-6.73	-7.91	-15.20	-0.04	-6.53	-7.91	-0.72
3.5	-14.64	-1.09	-6.10	-7.45	-14.29	-0.39	-5.94	-7.45	-0.52
3.8	-11.82	-0.95	-4.61	-6.26	-11.69	-0.74	-4.52	-6.26	-0.17
4.0	-10.25	-0.78	-3.87	-5.59	-10.21	-0.71	-3.81	-5.59	-0.11
5.0	-5.35	-0.24	-1.80	-3.31	-5.36	-0.27	-1.78	-3.31	-0.00
6.0	-3.12	-0.08	-0.95	-2.09	-3.12	-0.09	-0.95	-2.09	0.00
tridentate									
	Amoeba09				FF-SAPT 1				
h	E_{Int}	E_{vdW}	E_{Pol}	E_{El}	E_{Int}	E_{vdW}	E_{Pol}	E_{El}	E_{Extra}
2.5	-15.92	14.38	-16.60	-13.70	-14.17	26.24	-15.96	-13.70	-10.75
2.6	-18.61	8.99	-14.83	-12.77	-16.66	18.26	-14.20	-12.77	-7.95
2.7	-19.90	5.27	-13.24	-11.93	-18.10	12.42	-12.67	-11.93	-5.92
2.8	-20.24	2.75	-11.83	-11.16	-18.71	8.19	-11.34	-11.16	-4.40
2.9	-19.95	1.10	-10.59	-10.45	-18.71	5.17	-10.18	-10.45	-3.24
3.0	-19.26	0.05	-9.50	-9.81	-18.28	3.05	-9.17	-9.81	-2.35
3.1	-18.35	-0.59	-8.55	-9.21	-17.61	1.59	-8.28	-9.21	-1.71
3.2	-17.32	-0.95	-7.71	-8.66	-16.80	0.61	-7.49	-8.66	-1.26
3.4	-15.18	-1.18	-6.33	-7.67	-14.97	-0.42	-6.18	-7.67	-0.70
3.5	-14.16	-1.17	-5.76	-7.23	-14.02	-0.65	-5.63	-7.23	-0.51
3.8	-11.42	-0.95	-4.39	-6.08	-11.39	-0.81	-4.32	-6.08	-0.18
4.0	-9.92	-0.78	-3.70	-5.44	-9.93	-0.74	-3.65	-5.44	-0.10
5.0	-5.23	-0.24	-1.75	-3.24	-5.24	-0.26	-1.74	-3.24	-0.00
6.0	-3.06	-0.08	-0.93	-2.05	-3.07	-0.09	-0.93	-2.05	0.00

Table 7.15.: Amoeba09 and FF-SAPT 1 $C_6H_6...NH_4^+$ h-shift of mono-, bi-, and tridentate conformations. Distance (h) in Å and energies in kcal/mol. A graphical representation of these energies can be found in Figs. 3.12-3.14.

monodentate							
	FF-SAPT 2						
h	E_{Int}	E_{vdW}	E_{Pol}	E_{El}	E_{Extra}	E_{Disp}	E_{Exch}
2.5	-2.19	34.71	-18.56	-6.81	-11.54	-12.25	46.97
2.6	-7.33	25.44	-16.65	-7.56	-8.56	-10.33	35.77
2.7	-10.97	18.41	-14.93	-8.05	-6.40	-8.72	27.13
2.8	-13.36	13.13	-13.40	-8.32	-4.77	-7.36	20.49
2.9	-14.77	9.20	-12.03	-8.42	-3.52	-6.22	15.42
3.0	-15.47	6.30	-10.82	-8.39	-2.56	-5.27	11.57
3.1	-15.68	4.18	-9.73	-8.26	-1.86	-4.47	8.65
3.2	-15.56	2.65	-8.78	-8.06	-1.38	-3.80	6.45
3.4	-14.68	0.79	-7.17	-7.53	-0.76	-2.77	3.56
3.5	-14.03	0.26	-6.50	-7.23	-0.55	-2.38	2.63
3.8	-11.86	-0.47	-4.90	-6.30	-0.19	-1.52	1.05
4.0	-10.50	-0.58	-4.10	-5.71	-0.11	-1.15	0.57
5.0	-5.60	-0.30	-1.87	-3.43	-0.00	-0.32	0.02
6.0	-3.23	-0.11	-0.98	-2.15	0.00	-0.11	0.00
bidentate							
	FF-SAPT 2						
h	E_{Int}	E_{vdW}	E_{Pol}	E_{El}	E_{Extra}	E_{Disp}	E_{Exch}
2.5	-14.14	28.75	-17.64	-14.12	-11.12	-11.33	40.07
2.6	-16.74	20.23	-15.60	-13.16	-8.20	-9.47	29.70
2.7	-18.22	14.02	-13.83	-12.29	-6.11	-7.94	21.96
2.8	-18.82	9.53	-12.30	-11.50	-4.54	-6.67	16.20
2.9	-18.80	6.30	-10.99	-10.78	-3.34	-5.63	11.93
3.0	-18.36	4.01	-9.84	-10.11	-2.42	-4.76	8.77
3.1	-17.70	2.40	-8.84	-9.50	-1.76	-4.04	6.44
3.2	-16.92	1.28	-7.97	-8.93	-1.30	-3.44	4.72
3.4	-15.15	0.01	-6.53	-7.91	-0.72	-2.51	2.52
3.5	-14.22	-0.32	-5.94	-7.45	-0.52	-2.16	1.84
3.8	-11.63	-0.68	-4.52	-6.26	-0.17	-1.39	0.71
4.0	-10.19	-0.68	-3.81	-5.59	-0.11	-1.06	0.38
5.0	-5.39	-0.29	-1.78	-3.31	-0.00	-0.31	0.01
6.0	-3.14	-0.11	-0.95	-2.09	0.00	-0.11	0.00
tridentate							
	FF-SAPT 2						
h	E_{Int}	E_{vdW}	E_{Pol}	E_{El}	E_{Extra}	E_{Disp}	E_{Exch}
2.5	-16.84	23.57	-15.96	-13.70	-10.75	-10.49	34.06
2.6	-18.55	16.36	-14.20	-12.77	-7.95	-8.79	25.15
2.7	-19.36	11.15	-12.67	-11.93	-5.92	-7.38	18.53
2.8	-19.49	7.41	-11.34	-11.16	-4.40	-6.22	13.63
2.9	-19.12	4.75	-10.18	-10.45	-3.24	-5.26	10.01
3.0	-18.44	2.88	-9.17	-9.81	-2.35	-4.46	7.34
3.1	-17.62	1.58	-8.28	-9.21	-1.71	-3.79	5.37
3.2	-16.72	0.69	-7.49	-8.66	-1.26	-3.24	3.93
3.4	-14.84	-0.29	-6.18	-7.67	-0.70	-2.38	2.09
3.5	-13.90	-0.53	-5.63	-7.23	-0.51	-2.05	1.52
3.8	-11.32	-0.75	-4.32	-6.08	-0.18	-1.33	0.58
4.0	-9.90	-0.71	-3.65	-5.44	-0.10	-1.01	0.31
5.0	-5.27	-0.29	-1.74	-3.24	-0.00	-0.30	0.01
6.0	-3.09	-0.11	-0.93	-2.05	0.00	-0.11	0.00

Table 7.16.: FF-SAPT 2 $C_6H_6...NH_4^+$ h-shift of mono-, bi-, and tridentate conformations. Distance (h) in Å and energies in kcal/mol. A graphical representation of these energies can be found in Figs. 3.12-3.14.

O-H									
	Amoeba09				FF-SAPT 1				
R	E_{Int}	E_{vdW}	E_{Pol}	E_{El}	E_{Int}	E_{vdW}	E_{Pol}	E_{El}	E_{Extra}
2.6	-1.28	9.77	-2.51	-8.54	0.70	15.28	-2.37	-7.84	-4.37
2.7	-3.20	6.23	-2.10	-7.32	-1.47	10.30	-2.01	-6.74	-3.02
2.8	-4.12	3.91	-1.70	-6.32	-2.65	6.93	-1.65	-5.84	-2.09
2.9	-4.46	2.39	-1.35	-5.50	-3.23	4.62	-1.31	-5.10	-1.44
3.0	-4.47	1.40	-1.05	-4.82	-3.46	3.05	-1.03	-4.48	-1.00
3.1	-4.29	0.77	-0.82	-4.24	-3.48	1.97	-0.80	-3.95	-0.69
3.2	-4.02	0.37	-0.63	-3.75	-3.38	1.23	-0.62	-3.51	-0.48
3.3	-3.71	0.13	-0.50	-3.34	-3.21	0.74	-0.49	-3.13	-0.33
3.4	-3.38	-0.01	-0.39	-2.98	-3.01	0.41	-0.39	-2.80	-0.23
3.5	-3.07	-0.08	-0.31	-2.68	-2.79	0.19	-0.31	-2.52	-0.15
3.6	-2.78	-0.12	-0.25	-2.41	-2.57	0.06	-0.25	-2.28	-0.10
3.7	-2.52	-0.13	-0.20	-2.18	-2.36	-0.02	-0.20	-2.06	-0.07
3.8	-2.28	-0.13	-0.17	-1.98	-2.15	-0.07	-0.16	-1.88	-0.05
3.9	-2.06	-0.13	-0.14	-1.80	-1.96	-0.09	-0.14	-1.71	-0.03
4.0	-1.87	-0.11	-0.11	-1.64	-1.79	-0.10	-0.11	-1.56	-0.02

O-O									
	Amoeba09				FF-SAPT 1				
R	E_{Int}	E_{vdW}	E_{Pol}	E_{El}	E_{Int}	E_{vdW}	E_{Pol}	E_{El}	E_{Extra}
2.3	11.01	5.53	-0.78	6.27	0.45	3.71	-0.82	7.12	-9.56
2.4	8.45	3.48	-0.64	5.60	1.14	2.24	-0.67	6.30	-6.74
2.5	6.63	2.12	-0.52	5.03	1.60	1.28	-0.54	5.60	-4.74
2.6	5.33	1.22	-0.42	4.53	1.89	0.67	-0.44	5.00	-3.34
2.7	4.39	0.65	-0.35	4.10	2.07	0.29	-0.36	4.48	-2.34
2.8	3.71	0.29	-0.29	3.71	2.15	0.06	-0.30	4.04	-1.64
2.9	3.21	0.07	-0.24	3.38	2.18	-0.07	-0.25	3.65	-1.15
3.0	2.83	-0.05	-0.20	3.08	2.16	-0.14	-0.21	3.31	-0.81
3.1	2.53	-0.12	-0.17	2.82	2.11	-0.17	-0.17	3.01	-0.56
3.2	2.29	-0.15	-0.14	2.58	2.03	-0.18	-0.14	2.75	-0.39
3.3	2.10	-0.16	-0.12	2.37	1.95	-0.17	-0.12	2.51	-0.27
3.4	1.93	-0.15	-0.10	2.19	1.85	-0.16	-0.10	2.31	-0.19
3.5	1.79	-0.14	-0.09	2.02	1.76	-0.15	-0.09	2.12	-0.13
3.6	1.66	-0.13	-0.07	1.87	1.66	-0.13	-0.08	1.95	-0.09
3.7	1.55	-0.12	-0.06	1.73	1.56	-0.12	-0.07	1.81	-0.06
3.8	1.44	-0.11	-0.06	1.61	1.47	-0.10	-0.06	1.67	-0.04
3.9	1.35	-0.09	-0.05	1.49	1.39	-0.09	-0.05	1.55	-0.02
4.0	1.27	-0.08	-0.04	1.39	1.30	-0.08	-0.04	1.44	-0.01

H-H									
	Amoeba09				FF-SAPT 1				
R	E_{Int}	E_{vdW}	E_{Pol}	E_{El}	E_{Int}	E_{vdW}	E_{Pol}	E_{El}	E_{Extra}
3.1	22.50	9.01	-1.17	14.66	45.25	35.51	-1.32	11.89	-0.83
3.2	15.60	5.36	-1.20	11.43	30.89	23.34	-1.19	9.31	-0.57
3.3	11.08	3.14	-1.17	9.11	21.56	15.54	-1.06	7.46	-0.39
3.4	8.08	1.78	-1.08	7.39	15.35	10.45	-0.94	6.10	-0.26
3.5	6.06	0.95	-0.96	6.08	11.14	7.07	-0.81	5.06	-0.18
3.6	4.69	0.45	-0.83	5.06	8.24	4.80	-0.69	4.26	-0.12
3.7	3.74	0.16	-0.69	4.26	6.21	3.25	-0.58	3.62	-0.08
3.8	3.07	0.00	-0.56	3.62	4.77	2.19	-0.47	3.10	-0.05
3.9	2.58	-0.08	-0.44	3.11	3.73	1.46	-0.38	2.69	-0.03
4.0	2.21	-0.12	-0.35	2.68	2.96	0.95	-0.30	2.34	-0.02

Table 7.17.: Amoeba09 and FF-SAPT 1 $H_2O...H_2O$ interaction. Distance (R) in Å and energies in kcal/mol. A graphical representation of these energies can be found in Figs. 3.17-3.19.

O-H							
	FF-SAPT 2						
R	E_{Int}	E_{vdW}	E_{Pol}	E_{El}	E_{Extra}	E_{Disp}	E_{Exch}
2.6	2.83	20.79	-5.62	-7.84	-4.50	-4.18	24.96
2.7	0.45	14.21	-3.89	-6.74	-3.13	-3.41	17.62
2.8	-1.10	9.66	-2.74	-5.84	-2.18	-2.78	12.44
2.9	-2.08	6.50	-1.97	-5.10	-1.52	-2.28	8.78
3.0	-2.65	4.33	-1.44	-4.48	-1.06	-1.87	6.20
3.1	-2.94	2.83	-1.08	-3.95	-0.74	-1.54	4.38
3.2	-3.03	1.82	-0.82	-3.51	-0.51	-1.28	3.09
3.3	-3.00	1.12	-0.64	-3.13	-0.36	-1.06	2.18
3.4	-2.89	0.66	-0.50	-2.80	-0.25	-0.88	1.54
3.5	-2.74	0.35	-0.40	-2.52	-0.17	-0.74	1.09
3.6	-2.56	0.15	-0.32	-2.28	-0.12	-0.62	0.77
3.7	-2.38	0.02	-0.26	-2.06	-0.08	-0.52	0.54
3.8	-2.20	-0.06	-0.21	-1.88	-0.05	-0.44	0.38
3.9	-2.02	-0.10	-0.17	-1.71	-0.03	-0.37	0.27
4.0	-1.86	-0.13	-0.14	-1.56	-0.02	-0.32	0.19
O-O							
	FF-SAPT 2						
R	E_{Int}	E_{vdW}	E_{Pol}	E_{El}	E_{Extra}	E_{Disp}	E_{Exch}
2.3	10.20	14.45	-1.01	7.12	-10.36	-3.58	18.02
2.4	7.72	9.57	-0.81	6.30	-7.34	-2.95	12.51
2.5	6.01	6.25	-0.65	5.60	-5.19	-2.44	8.69
2.6	4.82	4.02	-0.53	5.00	-3.66	-2.02	6.03
2.7	3.98	2.51	-0.43	4.48	-2.58	-1.68	4.19
2.8	3.37	1.51	-0.36	4.04	-1.82	-1.40	2.91
2.9	2.92	0.85	-0.30	3.65	-1.28	-1.17	2.02
3.0	2.59	0.42	-0.25	3.31	-0.90	-0.98	1.40
3.1	2.32	0.15	-0.21	3.01	-0.63	-0.82	0.97
3.2	2.11	-0.02	-0.17	2.75	-0.44	-0.69	0.68
3.3	1.94	-0.12	-0.15	2.51	-0.31	-0.59	0.47
3.4	1.80	-0.17	-0.12	2.31	-0.21	-0.50	0.33
3.5	1.67	-0.20	-0.10	2.12	-0.15	-0.43	0.23
3.6	1.56	-0.21	-0.09	1.95	-0.10	-0.36	0.16
3.7	1.46	-0.20	-0.08	1.81	-0.07	-0.31	0.11
3.8	1.37	-0.19	-0.07	1.67	-0.04	-0.27	0.08
3.9	1.29	-0.18	-0.06	1.55	-0.03	-0.23	0.05
4.0	1.21	-0.16	-0.05	1.44	-0.02	-0.20	0.04
H-H							
	FF-SAPT 2						
R	E_{Int}	E_{vdW}	E_{Pol}	E_{El}	E_{Extra}	E_{Disp}	E_{Exch}
3.1	20.22	11.97	-2.79	11.89	-0.85	-3.36	15.33
3.2	14.51	8.25	-2.46	9.31	-0.59	-2.72	10.97
3.3	10.61	5.64	-2.09	7.46	-0.40	-2.20	7.85
3.4	7.94	3.82	-1.71	6.10	-0.28	-1.79	5.62
3.5	6.08	2.56	-1.35	5.06	-0.19	-1.46	4.02
3.6	4.76	1.68	-1.05	4.26	-0.13	-1.20	2.88
3.7	3.80	1.08	-0.81	3.62	-0.09	-0.98	2.06
3.8	3.08	0.66	-0.63	3.10	-0.06	-0.81	1.47
3.9	2.54	0.38	-0.49	2.69	-0.04	-0.67	1.06
4.0	2.13	0.20	-0.39	2.34	-0.02	-0.56	0.76

Table 7.18.: FF-SAPT 2 $C_6H_6...NH_4^+$ h-shift of mono-, bi-, and tridentate conformations. Distance (h) in Å and energies in kcal/mol. A graphical representation of these energies can be found in Figs. 3.17-3.19.

B1									
	Amoeba09				FF-SAPT 1				
R	E_{Int}	E_{vdW}	E_{Pol}	E_{El}	E_{Int}	E_{vdW}	E_{Pol}	E_{El}	E_{Extra}
2.7	10.93	10.46	-1.57	2.04	17.75	24.34	-1.51	1.26	-6.33
2.8	6.59	6.84	-1.35	1.11	12.47	17.98	-1.29	0.52	-4.73
2.9	3.47	4.25	-1.19	0.40	8.45	13.12	-1.13	-0.04	-3.49
3.0	1.26	2.43	-1.06	-0.11	5.45	9.43	-1.00	-0.45	-2.52
3.1	-0.24	1.19	-0.94	-0.49	3.18	6.64	-0.90	-0.74	-1.83
3.2	-1.23	0.36	-0.84	-0.75	1.46	4.56	-0.80	-0.94	-1.36
3.3	-1.85	-0.17	-0.75	-0.93	0.21	3.02	-0.72	-1.07	-1.03
3.4	-2.20	-0.48	-0.67	-1.05	-0.64	1.90	-0.64	-1.15	-0.77
3.5	-2.37	-0.66	-0.59	-1.11	-1.20	1.10	-0.57	-1.18	-0.55
3.6	-2.41	-0.74	-0.53	-1.15	-1.54	0.54	-0.51	-1.19	-0.38
3.7	-2.38	-0.76	-0.47	-1.15	-1.73	0.16	-0.45	-1.18	-0.25
3.8	-2.29	-0.74	-0.42	-1.13	-1.83	-0.10	-0.40	-1.15	-0.18
3.9	-2.17	-0.70	-0.37	-1.11	-1.87	-0.26	-0.36	-1.12	-0.14
4.0	-2.05	-0.64	-0.33	-1.07	-1.86	-0.35	-0.32	-1.07	-0.11

B2									
	Amoeba09				FF-SAPT 1				
R	E_{Int}	E_{vdW}	E_{Pol}	E_{El}	E_{Int}	E_{vdW}	E_{Pol}	E_{El}	E_{Extra}
2.7	3.02	7.57	-1.27	-3.29	10.54	20.66	-1.30	-2.69	-6.13
2.8	0.35	4.46	-1.13	-2.98	6.42	14.69	-1.15	-2.54	-4.57
2.9	-1.35	2.35	-0.99	-2.71	3.49	10.25	-1.02	-2.39	-3.35
3.0	-2.38	0.97	-0.87	-2.48	1.43	6.99	-0.90	-2.24	-2.42
3.1	-2.95	0.08	-0.76	-2.27	-0.03	4.61	-0.79	-2.10	-1.75
3.2	-3.21	-0.45	-0.67	-2.09	-1.05	2.91	-0.69	-1.97	-1.29
3.3	-3.26	-0.75	-0.59	-1.92	-1.74	1.70	-0.61	-1.84	-0.99
3.4	-3.19	-0.90	-0.52	-1.78	-2.13	0.87	-0.54	-1.72	-0.74
3.5	-3.05	-0.95	-0.46	-1.64	-2.32	0.30	-0.47	-1.61	-0.53
3.6	-2.87	-0.94	-0.40	-1.52	-2.36	-0.07	-0.42	-1.51	-0.36
3.7	-2.67	-0.89	-0.36	-1.42	-2.33	-0.30	-0.38	-1.41	-0.24
3.8	-2.46	-0.83	-0.32	-1.32	-2.26	-0.44	-0.34	-1.32	-0.17
3.9	-2.27	-0.76	-0.29	-1.23	-2.18	-0.51	-0.30	-1.24	-0.13
4.0	-2.08	-0.68	-0.26	-1.14	-2.07	-0.53	-0.27	-1.16	-0.10

BO									
	Amoeba09				FF-SAPT 1				
R	E_{Int}	E_{vdW}	E_{Pol}	E_{El}	E_{Int}	E_{vdW}	E_{Pol}	E_{El}	E_{Extra}
2.7	2.84	0.81	-0.21	2.24	-0.80	2.83	-0.23	2.19	-5.58
2.8	2.06	0.04	-0.16	2.18	-0.63	1.59	-0.18	2.14	-4.18
2.9	1.55	-0.43	-0.12	2.10	-0.41	0.74	-0.14	2.07	-3.08
3.0	1.22	-0.71	-0.09	2.02	-0.16	0.17	-0.10	1.99	-2.22
3.1	1.02	-0.84	-0.06	1.92	0.03	-0.19	-0.07	1.90	-1.61
3.2	0.89	-0.89	-0.04	1.83	0.16	-0.41	-0.05	1.81	-1.20
3.3	0.82	-0.89	-0.02	1.73	0.24	-0.53	-0.03	1.72	-0.92
3.4	0.77	-0.85	-0.01	1.63	0.34	-0.59	-0.01	1.63	-0.68
3.5	0.75	-0.79	0.00	1.54	0.43	-0.61	-0.00	1.53	-0.49
3.6	0.73	-0.73	0.01	1.45	0.52	-0.60	0.01	1.44	-0.34
3.7	0.72	-0.66	0.02	1.36	0.59	-0.57	0.02	1.36	-0.22
3.8	0.71	-0.59	0.02	1.28	0.61	-0.53	0.02	1.28	-0.16
3.9	0.70	-0.53	0.03	1.20	0.62	-0.49	0.03	1.20	-0.12
4.0	0.69	-0.47	0.03	1.13	0.61	-0.44	0.03	1.13	-0.10

Table 7.19.: Amoeba09, FF-SAPT 1, FF-SAPT 2 $C_6H_6...H_2O$ interaction. Distance (R) in Å and energies in kcal/mol. A graphical representation of these energies can be found in Figs. 3.34-3.36.

B1							
	FF-SAPT 2						
R	E_{Int}	E_{vdW}	E_{Pol}	E_{El}	E_{Extra}	E_{Disp}	E_{Exch}
2.7	12.38	19.03	-1.47	1.26	-6.45	-9.17	28.20
2.8	8.18	13.76	-1.28	0.52	-4.82	-7.79	21.55
2.9	5.05	9.80	-1.14	-0.04	-3.57	-6.62	16.42
3.0	2.78	6.83	-1.03	-0.45	-2.58	-5.64	12.47
3.1	1.10	4.64	-0.93	-0.74	-1.87	-4.81	9.44
3.2	-0.14	3.03	-0.84	-0.94	-1.40	-4.10	7.13
3.3	-1.01	1.87	-0.75	-1.07	-1.06	-3.51	5.38
3.4	-1.57	1.03	-0.67	-1.15	-0.79	-3.01	4.04
3.5	-1.91	0.45	-0.60	-1.18	-0.57	-2.59	3.03
3.6	-2.08	0.05	-0.54	-1.19	-0.40	-2.23	2.27
3.7	-2.14	-0.22	-0.48	-1.18	-0.26	-1.92	1.70
3.8	-2.16	-0.39	-0.42	-1.15	-0.18	-1.66	1.27
3.9	-2.14	-0.50	-0.38	-1.12	-0.14	-1.44	0.95
4.0	-2.08	-0.55	-0.34	-1.07	-0.12	-1.25	0.70
B2							
	FF-SAPT 2						
R	E_{Int}	E_{vdW}	E_{Pol}	E_{El}	E_{Extra}	E_{Disp}	E_{Exch}
2.7	5.62	15.91	-1.31	-2.69	-6.29	-8.88	24.79
2.8	2.67	11.06	-1.16	-2.54	-4.70	-7.51	18.57
2.9	0.66	7.52	-1.02	-2.39	-3.45	-6.37	13.89
3.0	-0.67	4.96	-0.90	-2.24	-2.50	-5.41	10.37
3.1	-1.58	3.12	-0.79	-2.10	-1.82	-4.60	7.73
3.2	-2.18	1.82	-0.69	-1.97	-1.34	-3.93	5.75
3.3	-2.56	0.91	-0.61	-1.84	-1.03	-3.36	4.27
3.4	-2.73	0.29	-0.53	-1.72	-0.76	-2.88	3.17
3.5	-2.77	-0.13	-0.47	-1.61	-0.55	-2.48	2.35
3.6	-2.70	-0.40	-0.42	-1.51	-0.38	-2.14	1.74
3.7	-2.59	-0.56	-0.37	-1.41	-0.25	-1.85	1.29
3.8	-2.48	-0.65	-0.33	-1.32	-0.18	-1.60	0.95
3.9	-2.36	-0.69	-0.30	-1.24	-0.14	-1.39	0.70
4.0	-2.23	-0.70	-0.27	-1.16	-0.11	-1.22	0.52
BO							
	FF-SAPT 2						
R	E_{Int}	E_{vdW}	E_{Pol}	E_{El}	E_{Extra}	E_{Disp}	E_{Exch}
2.7	5.62	5.96	-0.24	2.19	-5.86	-5.53	11.49
2.8	2.67	3.80	-0.18	2.14	-4.40	-4.73	8.53
2.9	0.66	2.26	-0.14	2.07	-3.25	-4.05	6.31
3.0	-0.67	1.19	-0.10	1.99	-2.35	-3.48	4.66
3.1	-1.58	0.45	-0.07	1.90	-1.71	-2.99	3.44
3.2	-2.18	-0.04	-0.05	1.81	-1.27	-2.58	2.53
3.3	-2.56	-0.36	-0.03	1.72	-0.97	-2.23	1.86
3.4	-2.73	-0.56	-0.02	1.63	-0.72	-1.93	1.37
3.5	-2.77	-0.67	-0.01	1.53	-0.52	-1.67	1.00
3.6	-2.70	-0.72	0.00	1.44	-0.36	-1.46	0.73
3.7	-2.59	-0.73	0.01	1.36	-0.24	-1.27	0.54
3.8	-2.48	-0.72	0.02	1.28	-0.17	-1.11	0.39
3.9	-2.36	-0.69	0.02	1.20	-0.13	-0.97	0.29
4.0	-2.23	-0.65	0.03	1.13	-0.11	-0.86	0.21

Table 7.20.: FF-SAPT 2 $C_6H_6...H_2O$ h-shift of mono-, bi-, and tridentate conformations. Distance (h) in Å and energies in kcal/mol. A graphical representation of these energies can be found in Figs. 3.34-3.36.

B S1									
	Amoeba09				FF-SAPT 1				
R	E_{Int}	E_{vdW}	E_{Pol}	E_{El}	E_{Int}	E_{vdW}	E_{Pol}	E_{El}	E_{Extra}
4.4	2.30	4.91	-1.47	-1.13	-2.89	3.83	-1.49	-1.01	-4.22
4.5	0.78	2.99	-1.20	-1.01	-2.71	2.34	-1.24	-0.90	-2.92
4.6	-0.15	1.74	-0.98	-0.90	-2.49	1.36	-1.01	-0.82	-2.02
4.7	-0.69	0.92	-0.80	-0.81	-2.25	0.72	-0.83	-0.74	-1.40
4.8	-0.98	0.41	-0.66	-0.73	-2.01	0.31	-0.67	-0.67	-0.97
4.9	-1.11	0.09	-0.54	-0.67	-1.78	0.05	-0.55	-0.61	-0.67
5.0	-1.14	-0.09	-0.45	-0.61	-1.57	-0.09	-0.46	-0.56	-0.46
5.1	-1.11	-0.18	-0.38	-0.55	-1.39	-0.18	-0.38	-0.51	-0.32
5.2	-1.05	-0.23	-0.32	-0.51	-1.22	-0.21	-0.32	-0.47	-0.22
5.3	-0.98	-0.24	-0.27	-0.46	-1.08	-0.23	-0.27	-0.43	-0.14
5.4	-0.90	-0.24	-0.23	-0.43	-0.95	-0.22	-0.23	-0.40	-0.10
5.5	-0.82	-0.23	-0.20	-0.39	-0.84	-0.21	-0.20	-0.37	-0.06
5.6	-0.74	-0.21	-0.17	-0.36	-0.75	-0.20	-0.17	-0.34	-0.04
5.7	-0.67	-0.19	-0.15	-0.34	-0.67	-0.18	-0.15	-0.32	-0.02
5.8	-0.61	-0.17	-0.13	-0.31	-0.60	-0.16	-0.13	-0.29	-0.01
5.9	-0.55	-0.15	-0.12	-0.29	-0.54	-0.14	-0.12	-0.27	-0.01
6.0	-0.50	-0.13	-0.10	-0.27	-0.49	-0.13	-0.10	-0.25	-0.01

B S2									
	Amoeba09				FF-SAPT 1				
R	E_{Int}	E_{vdW}	E_{Pol}	E_{El}	E_{Int}	E_{vdW}	E_{Pol}	E_{El}	E_{Extra}
4.0	1.48	4.08	-0.98	-1.62	-2.82	4.62	-0.89	-1.43	-5.12
4.1	0.14	2.40	-0.82	-1.45	-2.85	2.89	-0.74	-1.29	-3.71
4.2	-0.70	1.29	-0.69	-1.29	-2.76	1.70	-0.63	-1.16	-2.67
4.3	-1.19	0.56	-0.59	-1.16	-2.60	0.90	-0.53	-1.05	-1.92
4.4	-1.44	0.10	-0.50	-1.05	-2.40	0.38	-0.46	-0.95	-1.38
4.5	-1.54	-0.17	-0.43	-0.95	-2.18	0.05	-0.39	-0.86	-0.98
4.6	-1.55	-0.32	-0.37	-0.86	-1.96	-0.15	-0.34	-0.79	-0.69
4.7	-1.49	-0.39	-0.32	-0.78	-1.76	-0.26	-0.29	-0.72	-0.49
4.8	-1.40	-0.42	-0.28	-0.71	-1.57	-0.31	-0.26	-0.66	-0.34
4.9	-1.30	-0.41	-0.24	-0.65	-1.40	-0.33	-0.23	-0.60	-0.24
5.0	-1.20	-0.39	-0.21	-0.59	-1.25	-0.33	-0.20	-0.55	-0.17
5.1	-1.09	-0.36	-0.19	-0.54	-1.11	-0.32	-0.18	-0.51	-0.11
5.2	-0.99	-0.33	-0.16	-0.50	-1.00	-0.29	-0.16	-0.47	-0.08
5.3	-0.90	-0.29	-0.15	-0.46	-0.89	-0.27	-0.14	-0.43	-0.06
5.4	-0.82	-0.26	-0.13	-0.42	-0.81	-0.24	-0.12	-0.40	-0.04
5.5	-0.74	-0.23	-0.12	-0.39	-0.73	-0.22	-0.11	-0.37	-0.03

Table 7.21.: Amoeba09, FF-SAPT 1, FF-SAPT 2 $C_6H_6...H_2O$ interaction. Distance (R) in Å and energies in kcal/mol. A graphical representation of these energies can be found in Figs. 3.37-3.38.

B S1							
	FF-SAPT 2						
R	E_{Int}	E_{vdW}	E_{Pol}	E_{El}	E_{Extra}	E_{Disp}	E_{Exch}
4.4	1.82	8.74	-1.53	-1.01	-4.39	-3.32	12.07
4.5	0.55	5.76	-1.26	-0.90	-3.05	-2.74	8.50
4.6	-0.24	3.72	-1.03	-0.82	-2.12	-2.27	5.99
4.7	-0.72	2.33	-0.84	-0.74	-1.47	-1.88	4.22
4.8	-0.98	1.40	-0.68	-0.67	-1.02	-1.57	2.97
4.9	-1.11	0.77	-0.56	-0.61	-0.71	-1.32	2.09
5.0	-1.15	0.36	-0.46	-0.56	-0.49	-1.11	1.47
5.1	-1.14	0.10	-0.39	-0.51	-0.34	-0.94	1.04
5.2	-1.09	-0.07	-0.32	-0.47	-0.23	-0.80	0.73
5.3	-1.03	-0.17	-0.27	-0.43	-0.16	-0.68	0.52
5.4	-0.96	-0.22	-0.23	-0.40	-0.10	-0.59	0.36
5.5	-0.89	-0.25	-0.20	-0.37	-0.07	-0.50	0.26
5.6	-0.81	-0.26	-0.17	-0.34	-0.04	-0.44	0.18
5.7	-0.74	-0.25	-0.15	-0.32	-0.03	-0.38	0.13
5.8	-0.68	-0.24	-0.13	-0.29	-0.02	-0.33	0.09
5.9	-0.62	-0.23	-0.12	-0.27	-0.01	-0.29	0.06
6.0	-0.57	-0.21	-0.10	-0.25	-0.01	-0.25	0.04
B S2							
	FF-SAPT 2						
R	E_{Int}	E_{vdW}	E_{Pol}	E_{El}	E_{Extra}	E_{Disp}	E_{Exch}
4.0	0.94	8.65	-0.92	-1.43	-5.37	-4.54	13.20
4.1	-0.09	5.85	-0.77	-1.29	-3.89	-3.81	9.66
4.2	-0.76	3.85	-0.64	-1.16	-2.81	-3.20	7.06
4.3	-1.18	2.45	-0.55	-1.05	-2.03	-2.70	5.14
4.4	-1.41	1.46	-0.47	-0.95	-1.45	-2.28	3.74
4.5	-1.51	0.79	-0.40	-0.86	-1.03	-1.93	2.72
4.6	-1.53	0.33	-0.34	-0.79	-0.73	-1.64	1.97
4.7	-1.51	0.03	-0.30	-0.72	-0.52	-1.40	1.43
4.8	-1.45	-0.16	-0.26	-0.66	-0.36	-1.19	1.03
4.9	-1.37	-0.28	-0.23	-0.60	-0.26	-1.02	0.74
5.0	-1.28	-0.34	-0.20	-0.55	-0.18	-0.88	0.54
5.1	-1.18	-0.37	-0.18	-0.51	-0.12	-0.76	0.39
5.2	-1.09	-0.38	-0.16	-0.47	-0.09	-0.66	0.28
5.3	-1.00	-0.37	-0.14	-0.43	-0.06	-0.57	0.20
5.4	-0.92	-0.35	-0.12	-0.40	-0.04	-0.50	0.14
5.5	-0.84	-0.33	-0.11	-0.37	-0.03	-0.43	0.10

Table 7.22.: FF-SAPT 2 $C_6H_6...H_2O$ h-shift of mono-, bi-, and tridentate conformations. Distance (h) in Å and energies in kcal/mol. A graphical representation of these energies can be found in Figs. 3.37-3.38.

1H-HH									
	Amoeba09				FF-SAPT 1				
R	E_{Int}	E_{vdW}	E_{Pol}	E_{El}	E_{Int}	E_{vdW}	E_{Pol}	E_{El}	E_{Extra}
2.2	144.59	140.20	-12.71	17.10	270.43	273.83	-18.41	36.34	-21.32
2.3	95.76	91.01	-11.85	16.60	181.63	182.00	-16.48	30.72	-14.60
2.4	64.57	59.33	-10.92	16.16	123.82	121.90	-14.56	26.49	-10.01
2.5	44.49	38.72	-9.96	15.73	85.96	82.25	-12.71	23.30	-6.88
2.6	31.47	25.18	-8.98	15.26	60.95	55.83	-11.00	20.86	-4.74
2.7	22.97	16.24	-8.01	14.74	44.27	38.05	-9.44	18.93	-3.27
2.8	17.41	10.32	-7.08	14.17	33.02	25.99	-8.05	17.34	-2.26
2.9	13.77	6.40	-6.20	13.57	25.35	17.74	-6.84	16.01	-1.56
3.0	11.40	3.84	-5.40	12.96	20.06	12.08	-5.80	14.86	-1.08
3.1	9.85	2.19	-4.69	12.34	16.35	8.17	-4.92	13.85	-0.75
3.2	8.84	1.15	-4.06	11.75	13.71	5.47	-4.19	12.95	-0.52
3.3	8.17	0.52	-3.51	11.17	11.81	3.60	-3.58	12.14	-0.36
3.4	7.71	0.15	-3.05	10.61	10.41	2.32	-3.08	11.41	-0.24
3.5	7.37	-0.06	-2.65	10.09	9.37	1.45	-2.67	10.75	-0.17
3.6	7.11	-0.17	-2.31	9.59	8.57	0.86	-2.32	10.15	-0.11
3.7	6.88	-0.22	-2.03	9.12	7.95	0.47	-2.03	9.59	-0.07
3.8	6.67	-0.23	-1.78	8.68	7.46	0.21	-1.78	9.08	-0.05
3.9	6.47	-0.22	-1.58	8.27	7.06	0.05	-1.57	8.61	-0.03
4.0	6.28	-0.20	-1.40	7.88	6.72	-0.04	-1.39	8.17	-0.02
1H-OH									
	Amoeba09				FF-SAPT 1				
R	E_{Int}	E_{vdW}	E_{Pol}	E_{El}	E_{Int}	E_{vdW}	E_{Pol}	E_{El}	E_{Extra}
2.2	14.80	60.61	-11.72	-34.10	-19.63	51.25	-15.64	-35.22	-20.03
2.3	-2.64	38.49	-11.12	-30.00	-25.15	33.24	-13.79	-30.85	-13.75
2.4	-12.32	24.71	-10.34	-26.69	-26.75	21.72	-11.69	-27.33	-9.45
2.5	-17.38	15.94	-9.36	-23.96	-26.36	14.22	-9.62	-24.45	-6.51
2.6	-19.65	10.26	-8.23	-21.68	-25.06	9.27	-7.79	-22.05	-4.49
2.7	-20.26	6.54	-7.06	-19.74	-23.43	5.99	-6.28	-20.03	-3.10
2.8	-19.94	4.09	-5.95	-18.08	-21.74	3.80	-5.09	-18.30	-2.15
2.9	-19.11	2.49	-4.96	-16.64	-20.12	2.34	-4.16	-16.81	-1.49
3.0	-18.05	1.44	-4.12	-15.38	-18.61	1.38	-3.45	-15.51	-1.03
3.1	-16.92	0.78	-3.43	-14.26	-17.21	0.76	-2.89	-14.37	-0.71
3.2	-15.79	0.36	-2.87	-13.28	-15.94	0.36	-2.44	-13.36	-0.49
3.3	-14.71	0.11	-2.42	-12.40	-14.78	0.12	-2.09	-12.46	-0.34
3.4	-13.71	-0.04	-2.06	-11.61	-13.72	-0.03	-1.80	-11.66	-0.23
3.5	-12.78	-0.12	-1.77	-10.90	-12.77	-0.10	-1.57	-10.94	-0.16
3.6	-11.94	-0.15	-1.53	-10.26	-11.90	-0.14	-1.37	-10.28	-0.11
3.7	-11.17	-0.16	-1.33	-9.67	-11.12	-0.16	-1.21	-9.69	-0.07
3.8	-10.47	-0.16	-1.17	-9.14	-10.42	-0.16	-1.07	-9.15	-0.05
3.9	-9.83	-0.15	-1.03	-8.65	-9.78	-0.15	-0.95	-8.65	-0.03
4.0	-9.25	-0.14	-0.92	-8.20	-9.20	-0.14	-0.85	-8.20	-0.02

Table 7.23.: Amoeba09 and FF-SAPT 1 $NH_4^+...H_2O$ interaction. Distance (R) in Å and energies in kcal/mol. A graphical representation of these energies can be found in Figs. 3.27 and 3.29.

1H-HH							
	FF-SAPT 2						
R	E_{Int}	E_{vdW}	E_{Pol}	E_{El}	E_{Extra}	E_{Disp}	E_{Exch}
2.2	142.93	144.34	-16.09	36.34	-21.66	-17.12	161.46
2.3	103.09	101.80	-14.54	30.72	-14.89	-13.86	115.66
2.4	74.85	71.57	-12.95	26.49	-10.25	-11.18	82.75
2.5	54.95	50.13	-11.41	23.30	-7.07	-9.01	59.13
2.6	40.98	34.95	-9.95	20.86	-4.88	-7.25	42.20
2.7	31.19	24.25	-8.61	18.93	-3.38	-5.83	30.08
2.8	24.32	16.72	-7.40	17.34	-2.34	-4.69	21.41
2.9	19.50	11.44	-6.32	16.01	-1.63	-3.78	15.23
3.0	16.10	7.76	-5.39	14.86	-1.13	-3.05	10.82
3.1	13.67	5.20	-4.60	13.85	-0.78	-2.47	7.68
3.2	11.91	3.44	-3.93	12.95	-0.54	-2.01	5.44
3.3	10.62	2.22	-3.38	12.14	-0.37	-1.64	3.86
3.4	9.64	1.39	-2.91	11.41	-0.26	-1.34	2.73
3.5	8.88	0.83	-2.53	10.75	-0.18	-1.10	1.93
3.6	8.28	0.46	-2.20	10.15	-0.12	-0.91	1.37
3.7	7.79	0.21	-1.93	9.59	-0.08	-0.75	0.97
3.8	7.38	0.06	-1.70	9.08	-0.05	-0.63	0.68
3.9	7.03	-0.04	-1.50	8.61	-0.03	-0.53	0.48
4.0	6.72	-0.10	-1.34	8.17	-0.02	-0.44	0.34

1H-OH							
	FF-SAPT 2						
R	E_{Int}	E_{vdW}	E_{Pol}	E_{El}	E_{Extra}	E_{Disp}	E_{Exch}
2.2	24.42	99.18	-18.85	-35.22	-20.69	-10.46	109.64
2.3	5.85	67.51	-16.56	-30.85	-14.25	-8.34	75.85
2.4	-5.31	45.81	-13.97	-27.33	-9.83	-6.66	52.47
2.5	-11.69	30.98	-11.43	-24.45	-6.79	-5.33	36.30
2.6	-15.10	20.85	-9.20	-22.05	-4.69	-4.27	25.11
2.7	-16.72	13.95	-7.38	-20.03	-3.25	-3.43	17.38
2.8	-17.25	9.26	-5.95	-18.30	-2.26	-2.76	12.02
2.9	-17.14	6.08	-4.84	-16.81	-1.57	-2.24	8.32
3.0	-16.65	3.94	-3.99	-15.51	-1.09	-1.82	5.75
3.1	-15.96	2.50	-3.33	-14.37	-0.75	-1.48	3.98
3.2	-15.15	1.54	-2.81	-13.36	-0.52	-1.21	2.75
3.3	-14.31	0.91	-2.40	-12.46	-0.36	-1.00	1.91
3.4	-13.48	0.49	-2.06	-11.66	-0.25	-0.83	1.32
3.5	-12.67	0.23	-1.79	-10.94	-0.17	-0.69	0.91
3.6	-11.90	0.06	-1.56	-10.28	-0.12	-0.57	0.63
3.7	-11.18	-0.04	-1.37	-9.69	-0.08	-0.48	0.44
3.8	-10.51	-0.10	-1.21	-9.15	-0.05	-0.40	0.30
3.9	-9.89	-0.13	-1.07	-8.65	-0.03	-0.34	0.21
4.0	-9.32	-0.15	-0.96	-8.20	-0.02	-0.29	0.14

Table 7.24.: FF-SAPT 2 $NH_4^+...H_2O$ interaction. Distance (R) in Å and energies in kcal/mol. A graphical representation of these energies can be found in Figs. 3.27 and 3.29.

3H-HH									
	Amoeba09				FF-SAPT 1				
R	E_{Int}	E_{vdW}	E_{Pol}	E_{El}	E_{Int}	E_{vdW}	E_{Pol}	E_{El}	E_{Extra}
2.2	53.69	44.84	-10.82	19.67	83.96	89.34	-10.87	20.54	-15.05
2.3	39.12	30.02	-9.30	18.40	60.96	61.54	-9.15	19.20	-10.63
2.4	29.16	19.89	-7.97	17.24	45.20	42.49	-7.77	17.97	-7.49
2.5	22.33	12.97	-6.83	16.18	34.23	29.30	-6.66	16.85	-5.27
2.6	17.63	8.29	-5.87	15.22	26.48	20.10	-5.75	15.82	-3.69
2.7	14.40	5.15	-5.08	14.33	20.97	13.67	-4.99	14.88	-2.59
2.8	12.18	3.08	-4.41	13.52	17.02	9.18	-4.36	14.01	-1.82
2.9	10.65	1.74	-3.85	12.77	14.18	6.05	-3.82	13.22	-1.28
3.0	9.58	0.88	-3.38	12.07	12.12	3.89	-3.36	12.48	-0.90
3.1	8.81	0.36	-2.98	11.43	10.63	2.42	-2.96	11.80	-0.63
3.2	8.25	0.05	-2.64	10.84	9.54	1.43	-2.62	11.17	-0.44
3.3	7.82	-0.13	-2.34	10.29	8.73	0.77	-2.33	10.59	-0.30
3.4	7.48	-0.22	-2.08	9.78	8.12	0.35	-2.07	10.05	-0.21
3.5	7.19	-0.26	-1.86	9.30	7.65	0.09	-1.85	9.55	-0.14
3.6	6.93	-0.27	-1.66	8.86	7.27	-0.07	-1.65	9.08	-0.09
3.7	6.70	-0.26	-1.49	8.45	6.95	-0.15	-1.48	8.65	-0.06
3.8	6.48	-0.24	-1.34	8.06	6.67	-0.20	-1.33	8.24	-0.04
3.9	6.27	-0.22	-1.21	7.70	6.42	-0.21	-1.20	7.86	-0.03
4.0	6.07	-0.19	-1.09	7.36	6.19	-0.21	-1.09	7.50	-0.02
3H-OH									
	Amoeba09				FF-SAPT 1				
R	E_{Int}	E_{vdW}	E_{Pol}	E_{El}	E_{Int}	E_{vdW}	E_{Pol}	E_{El}	E_{Extra}
2.2	-11.17	16.81	-7.45	-20.53	-27.23	13.84	-6.54	-20.60	-13.92
2.3	-14.25	11.17	-6.23	-19.19	-25.64	9.00	-5.53	-19.25	-9.86
2.4	-15.93	7.28	-5.25	-17.96	-23.99	5.70	-4.70	-18.01	-6.97
2.5	-16.67	4.62	-4.45	-16.84	-22.34	3.48	-4.03	-16.88	-4.91
2.6	-16.78	2.83	-3.80	-15.81	-20.75	2.01	-3.47	-15.84	-3.45
2.7	-16.49	1.65	-3.27	-14.86	-19.25	1.07	-3.01	-14.89	-2.43
2.8	-15.94	0.88	-2.83	-13.99	-17.86	0.48	-2.62	-14.01	-1.71
2.9	-15.26	0.40	-2.47	-13.19	-16.58	0.12	-2.30	-13.20	-1.20
3.0	-14.51	0.10	-2.16	-12.45	-15.41	-0.08	-2.02	-12.46	-0.84
3.1	-13.74	-0.07	-1.90	-11.77	-14.35	-0.19	-1.79	-11.77	-0.59
3.2	-12.98	-0.16	-1.68	-11.14	-13.38	-0.24	-1.59	-11.14	-0.41
3.3	-12.25	-0.20	-1.49	-10.55	-12.51	-0.26	-1.42	-10.55	-0.28
3.4	-11.56	-0.22	-1.33	-10.01	-11.72	-0.26	-1.27	-10.01	-0.20
3.5	-10.91	-0.22	-1.19	-9.51	-11.01	-0.24	-1.13	-9.50	-0.13
3.6	-10.31	-0.20	-1.07	-9.04	-10.36	-0.22	-1.02	-9.03	-0.09
3.7	-9.75	-0.19	-0.96	-8.60	-9.77	-0.20	-0.92	-8.59	-0.06
3.8	-9.23	-0.17	-0.86	-8.20	-9.23	-0.18	-0.83	-8.19	-0.04
3.9	-8.75	-0.15	-0.78	-7.82	-8.74	-0.15	-0.76	-7.81	-0.03
4.0	-8.31	-0.13	-0.71	-7.47	-8.29	-0.14	-0.69	-7.45	-0.02

Table 7.25.: Amoeba09 and FF-SAPT 1 $NH_4^+...H_2O$ interaction. Distance (R) in Å and energies in kcal/mol. A graphical representation of these energies can be found in Figs. 3.28 and 3.30.

3H-HH							
	FF-SAPT 2						
R	E_{Int}	E_{vdW}	E_{Pol}	E_{El}	E_{Extra}	E_{Disp}	E_{Exch}
2.2	52.17	57.30	-10.34	20.54	-15.33	-10.69	67.99
2.3	39.45	39.82	-8.71	19.20	-10.86	-8.61	48.43
2.4	30.42	27.52	-7.40	17.97	-7.67	-6.95	34.46
2.5	23.98	18.88	-6.34	16.85	-5.41	-5.61	24.50
2.6	19.39	12.85	-5.48	15.82	-3.80	-4.55	17.40
2.7	16.09	8.65	-4.77	14.88	-2.67	-3.69	12.35
2.8	13.71	5.74	-4.17	14.01	-1.88	-3.01	8.75
2.9	11.98	3.74	-3.65	13.22	-1.32	-2.46	6.20
3.0	10.70	2.37	-3.22	12.48	-0.93	-2.02	4.39
3.1	9.75	1.44	-2.84	11.80	-0.65	-1.67	3.11
3.2	9.02	0.82	-2.52	11.17	-0.46	-1.38	2.20
3.3	8.45	0.41	-2.24	10.59	-0.32	-1.14	1.56
3.4	7.99	0.15	-1.99	10.05	-0.22	-0.95	1.10
3.5	7.60	-0.02	-1.78	9.55	-0.15	-0.80	0.78
3.6	7.26	-0.12	-1.59	9.08	-0.10	-0.67	0.55
3.7	6.97	-0.18	-1.43	8.65	-0.07	-0.57	0.39
3.8	6.70	-0.21	-1.29	8.24	-0.05	-0.48	0.27
3.9	6.45	-0.22	-1.16	7.86	-0.03	-0.41	0.19
4.0	6.22	-0.21	-1.05	7.50	-0.02	-0.35	0.14

3H-OH							
	FF-SAPT 2						
R	E_{Int}	E_{vdW}	E_{Pol}	E_{El}	E_{Extra}	E_{Disp}	E_{Exch}
2.2	-13.72	28.90	-7.57	-20.60	-14.46	-6.02	34.93
2.3	-16.48	19.41	-6.38	-19.25	-10.26	-4.89	24.29
2.4	-17.78	12.92	-5.41	-18.01	-7.27	-3.98	16.89
2.5	-18.14	8.50	-4.62	-16.88	-5.13	-3.24	11.74
2.6	-17.93	5.50	-3.97	-15.84	-3.62	-2.65	8.16
2.7	-17.39	3.49	-3.44	-14.89	-2.55	-2.18	5.67
2.8	-16.66	2.14	-2.99	-14.01	-1.80	-1.80	3.93
2.9	-15.84	1.24	-2.62	-13.20	-1.27	-1.49	2.73
3.0	-14.99	0.66	-2.30	-12.46	-0.89	-1.23	1.89
3.1	-14.14	0.29	-2.03	-11.77	-0.63	-1.03	1.31
3.2	-13.32	0.05	-1.80	-11.14	-0.44	-0.86	0.91
3.3	-12.54	-0.09	-1.60	-10.55	-0.30	-0.72	0.63
3.4	-11.81	-0.17	-1.43	-10.01	-0.21	-0.61	0.44
3.5	-11.13	-0.21	-1.28	-9.50	-0.14	-0.52	0.30
3.6	-10.50	-0.23	-1.15	-9.03	-0.10	-0.44	0.21
3.7	-9.92	-0.23	-1.03	-8.59	-0.07	-0.37	0.15
3.8	-9.38	-0.22	-0.93	-8.19	-0.04	-0.32	0.10
3.9	-8.89	-0.21	-0.85	-7.81	-0.03	-0.28	0.07
4.0	-8.43	-0.19	-0.77	-7.45	-0.02	-0.24	0.05

Table 7.26.: FF-SAPT 2 $NH_4^+...H_2O$ interaction. Distance (R) in Å and energies in kcal/mol. A graphical representation of these energies can be found in Figs. 3.28 and 3.30.

7.2. Appendix Part 2

Residue	non-bonded complex	bonded complex	Δ bond length
H-bonds to inhibitor side chain			
Gly66(O)	1.95	1.96	–
Gly66(N)	2.27	2.03	-0.24
Gly65	2.84	2.85	–
Asp161	2.49	2.21	-0.28
H-bonds to Cys25 S^-			
Gly163	2.08	2.36	+0.28
Trp26	2.70	2.47	-0.23
Cys25	3.19	3.18	–
His162	1.72	(1.83)	–
VS216	2.43	–	–
H-bonds to vinyl sulfone oxygen			
Trp184	1.78	1.77	–
Gln19	1.86	1.79	-0.07

Table 7.27.: Table 1: Comparison of the H bond network within the active site of the non-bonded and bonded inhibitor resulting from QM/MM calculations. The major changes of the bond length are shown. All distances are given in Angstrom (Å). Comparison of the H bond network within the active site of the non-bonded and bonded inhibitor. The major changes of the bond length are shown in the last column. All distances are given in Angstrom (Å).

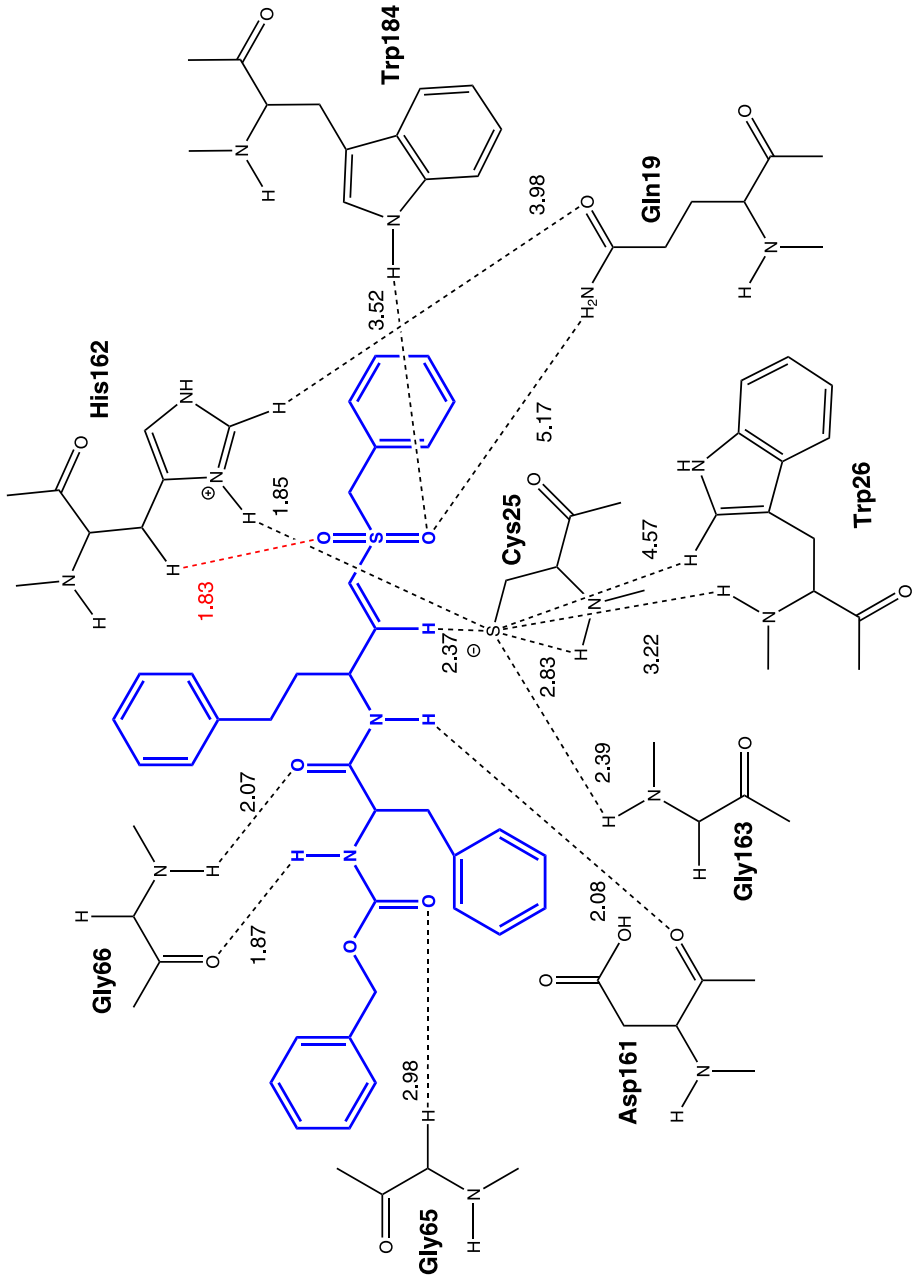

Figure 7.1.: Geometric details of the non-covalent bonded inhibitor in the active site of cruzain. The structure was calculated using the QM/MM MD method. The arrangement of the cruzain residues corresponds not the exact position in the protein to get a clearer insight in the interactions between inhibitor and protein.

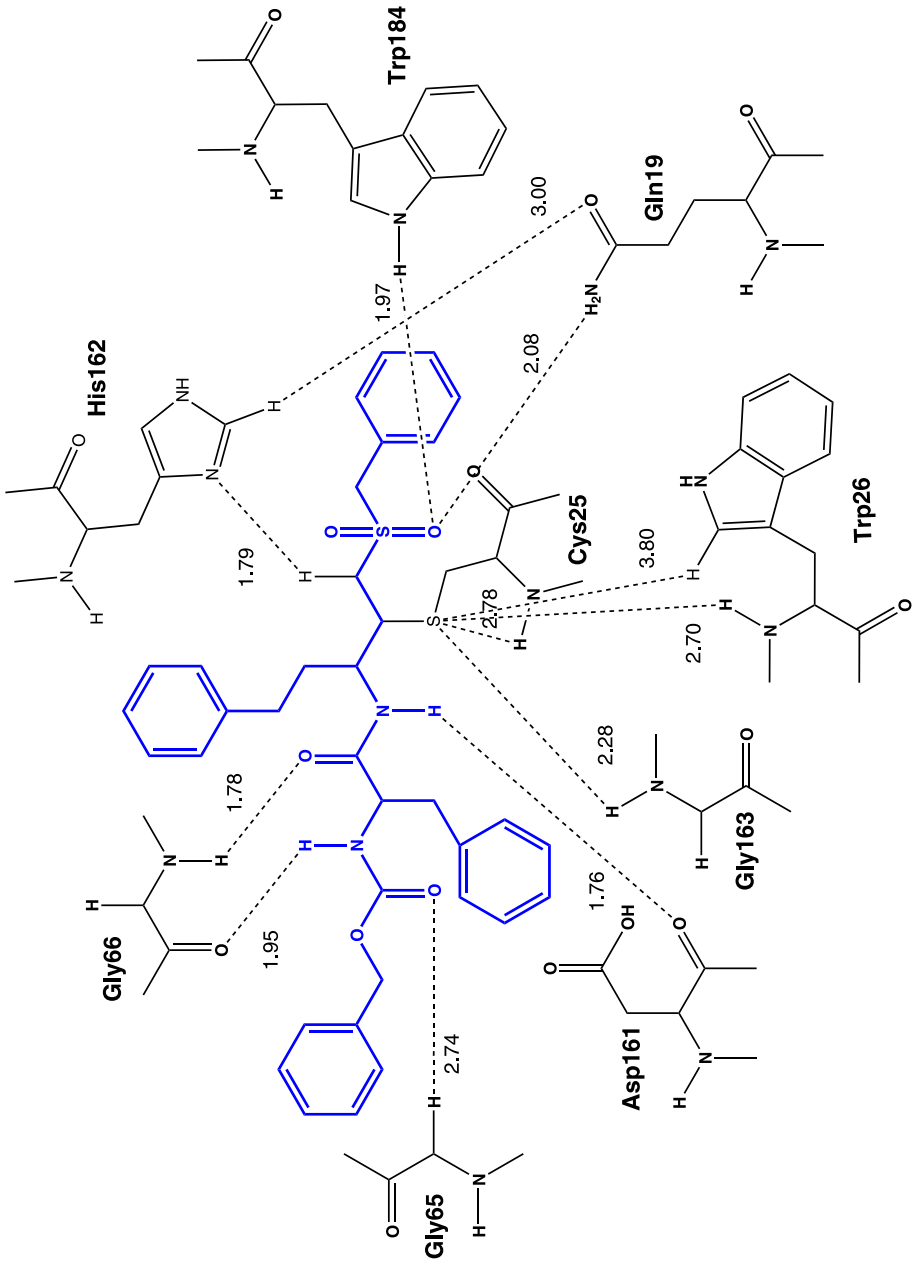

Figure 7.2.: Geometric details of the covalent bonded inhibitor in the active site of cruzain. The structure was calculated using the QM/MM MD method. The arrangement of the cruzain residues corresponds not the exact position in the protein to get a clearer insight in the interactions between inhibitor and protein.

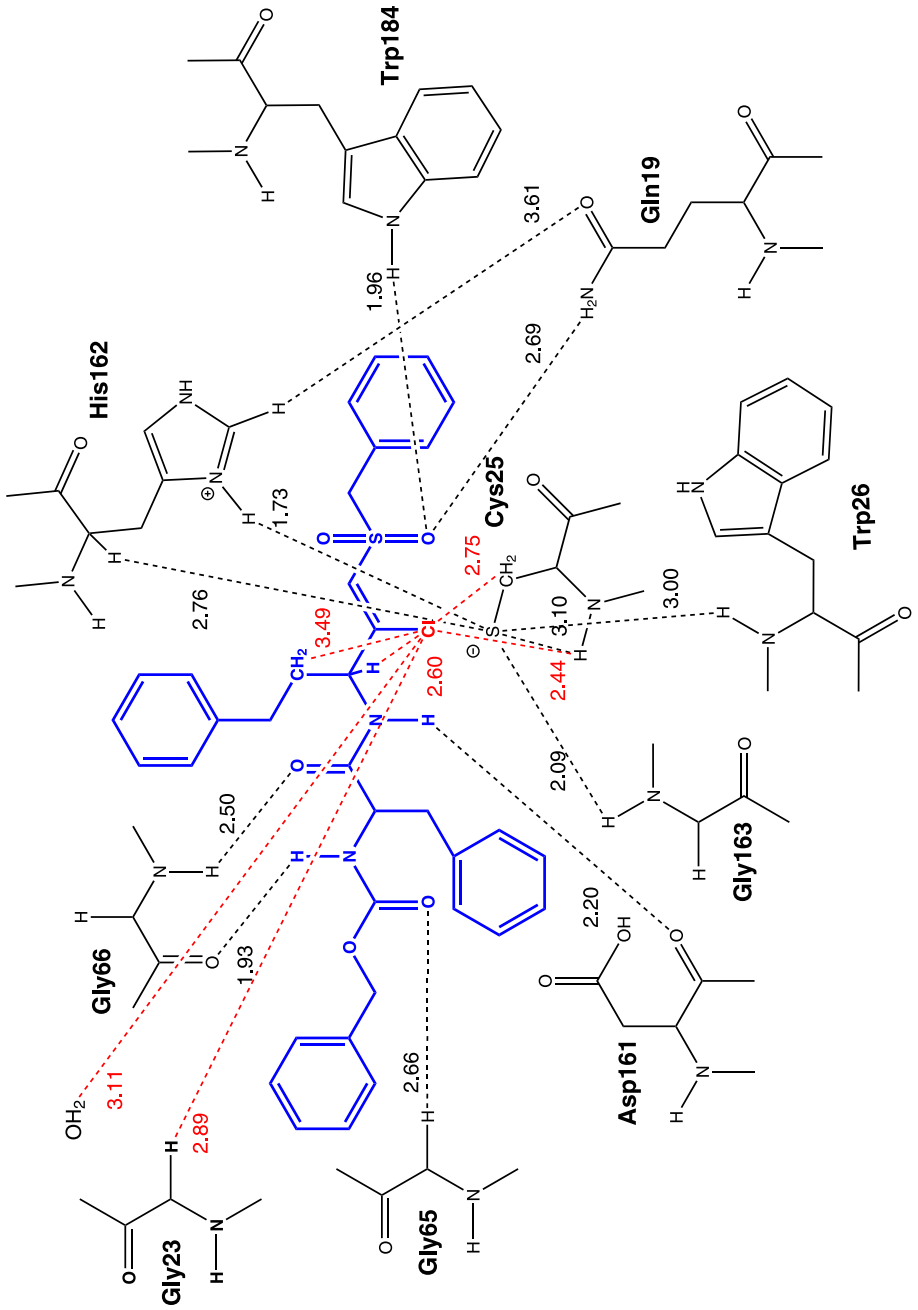

Figure 7.3.: Geometric details of the non-covalent bonded modified inhibitor in the active site of cruzain. The structure was calculated using the QM/MM method. The arrangement of the cruzain residues corresponds not the exact position in the protein to get a clearer insight in the interactions between inhibitor and protein.

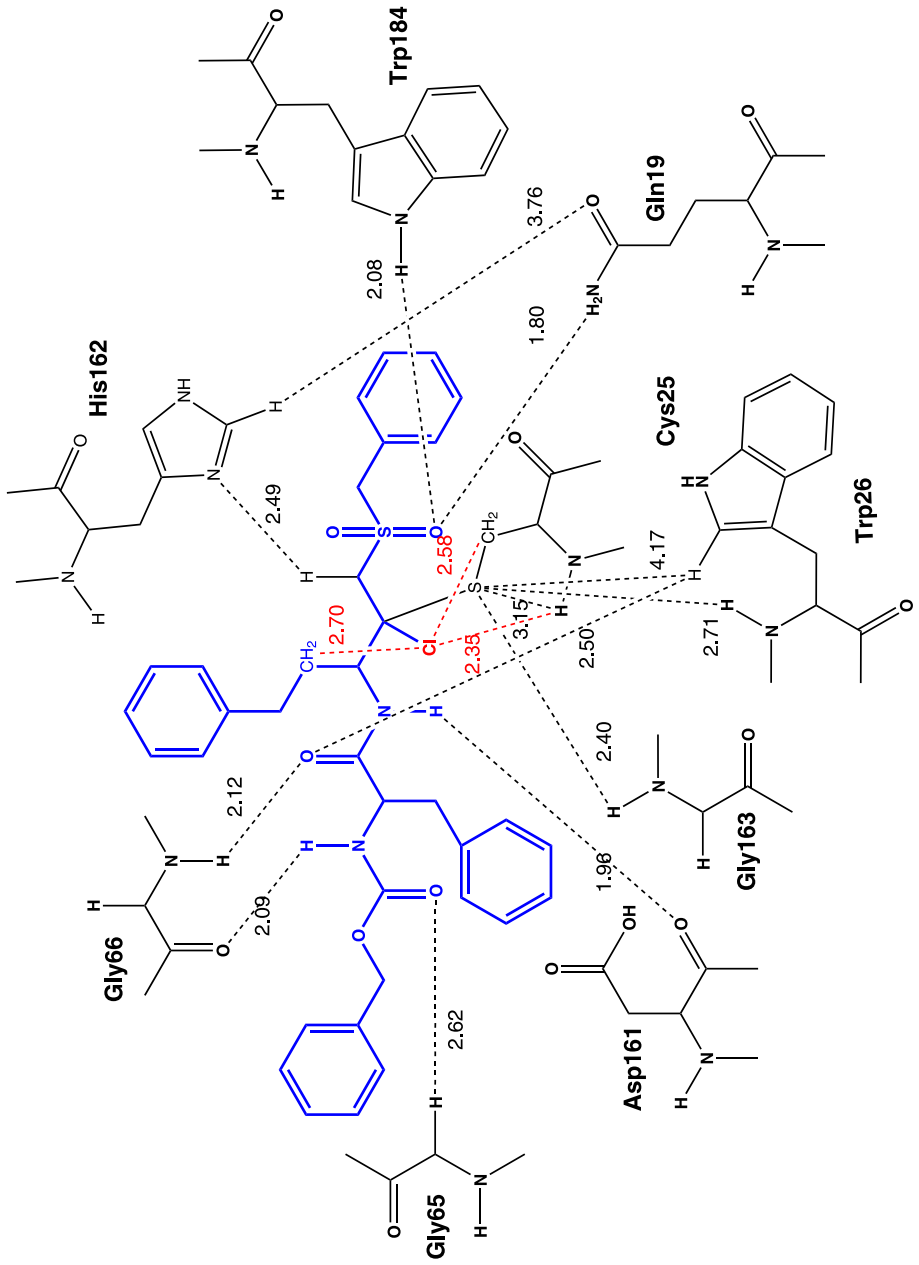

Figure 7.4.: Geometric details of the covalent bonded modified inhibitor after addition reaction mechanism in the active site of cruzain. The structure was calculated using the QM/MM method. The arrangement of the cruzain residues corresponds not the exact position in the protein to get a clearer insight in the interactions between inhibitor and protein.

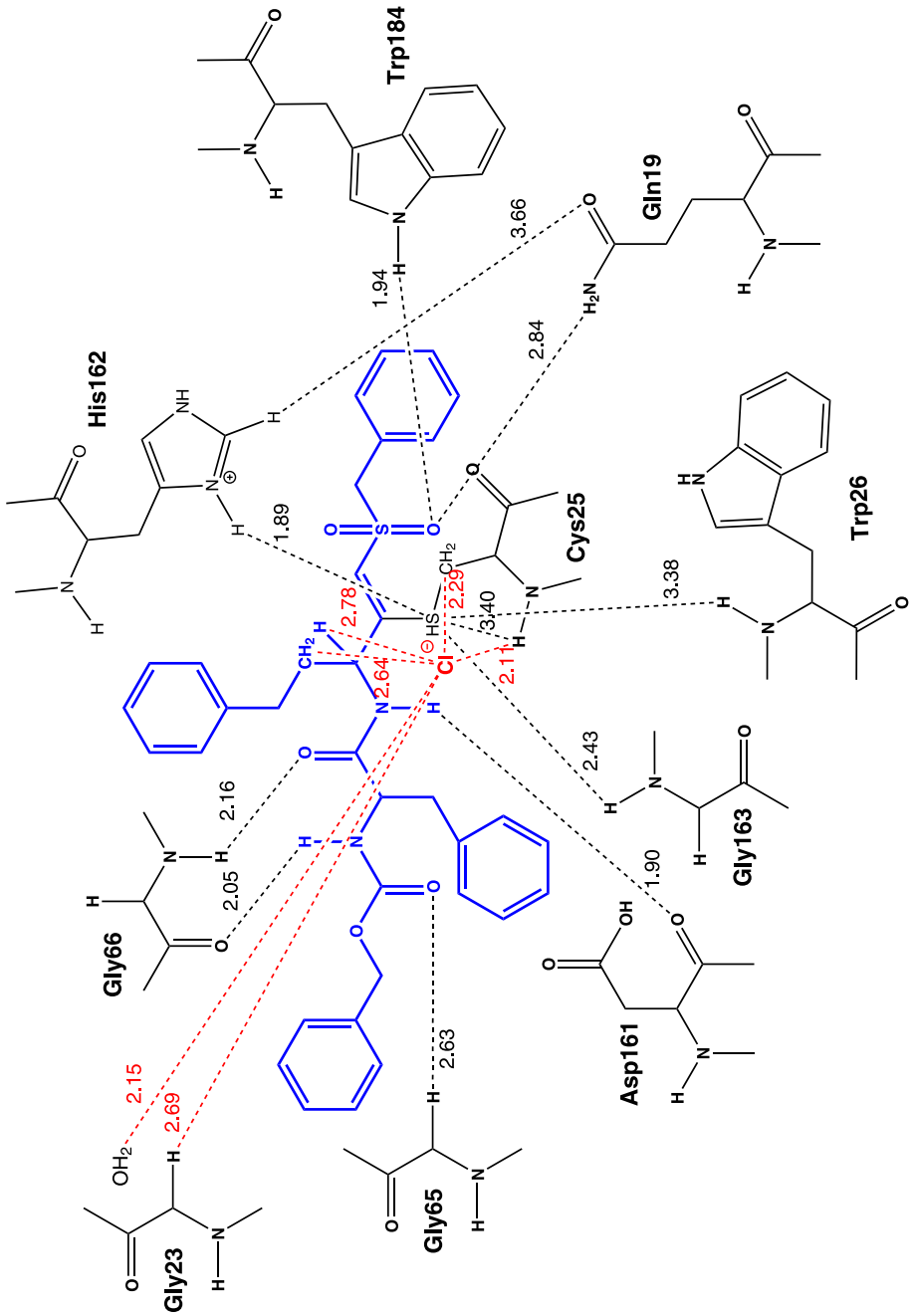

Figure 7.5.: Geometric details of the covalent bonded modified inhibitor after VNS reaction mechanism in the active site of cruzain. The structure was calculated using the QM/MM method. The arrangement of the cruzain residues corresponds not the exact position in the protein to get a clearer insight in the interactions between inhibitor and protein.

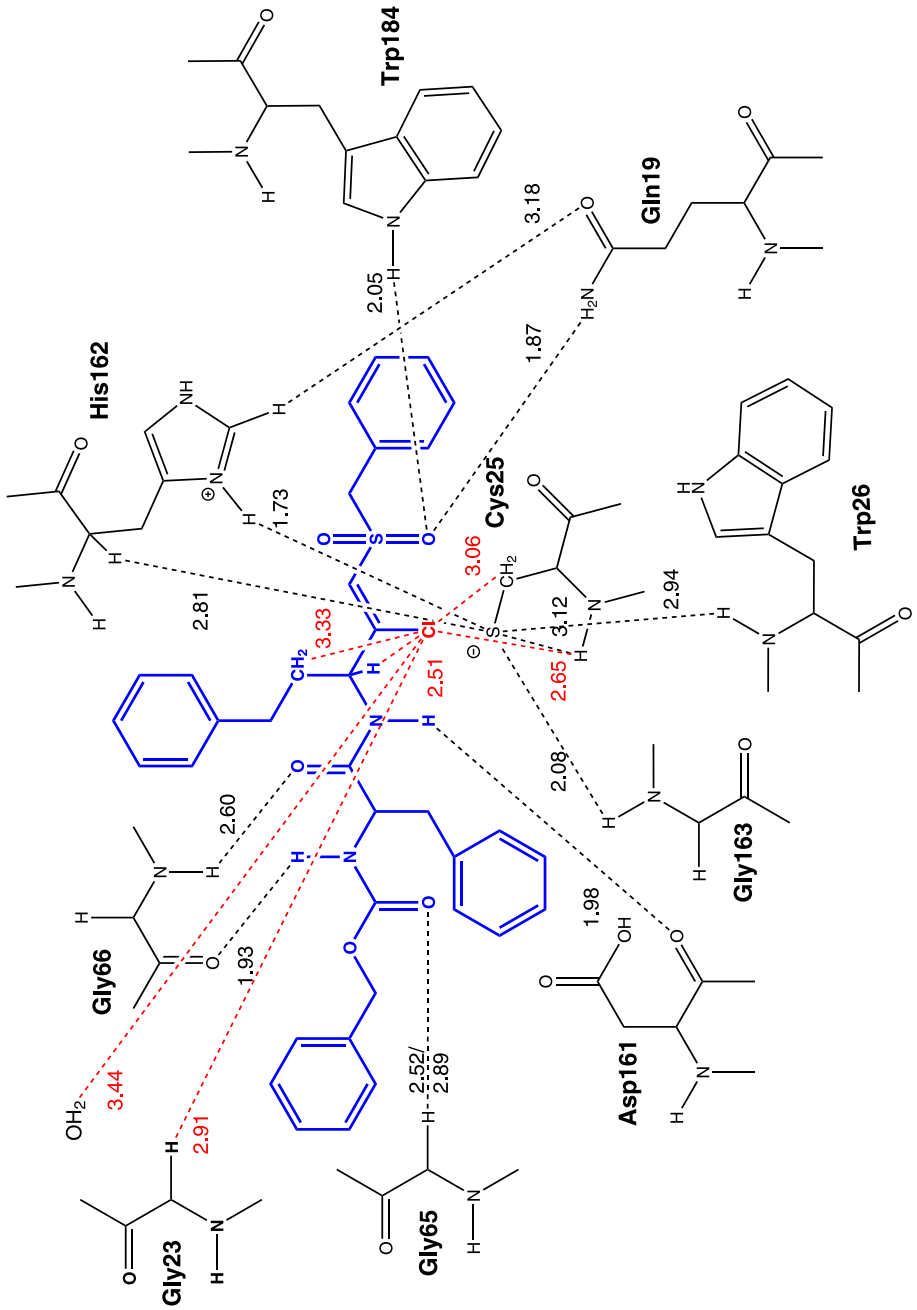

Figure 7.6.: Geometric details of the non-covalent bonded modified inhibitor in the active site of cruzain. The structure was calculated using the QM/MM MD method. The arrangement of the cruzain residues corresponds not the exact position in the protein to get a clearer insight in the interactions between inhibitor and protein.

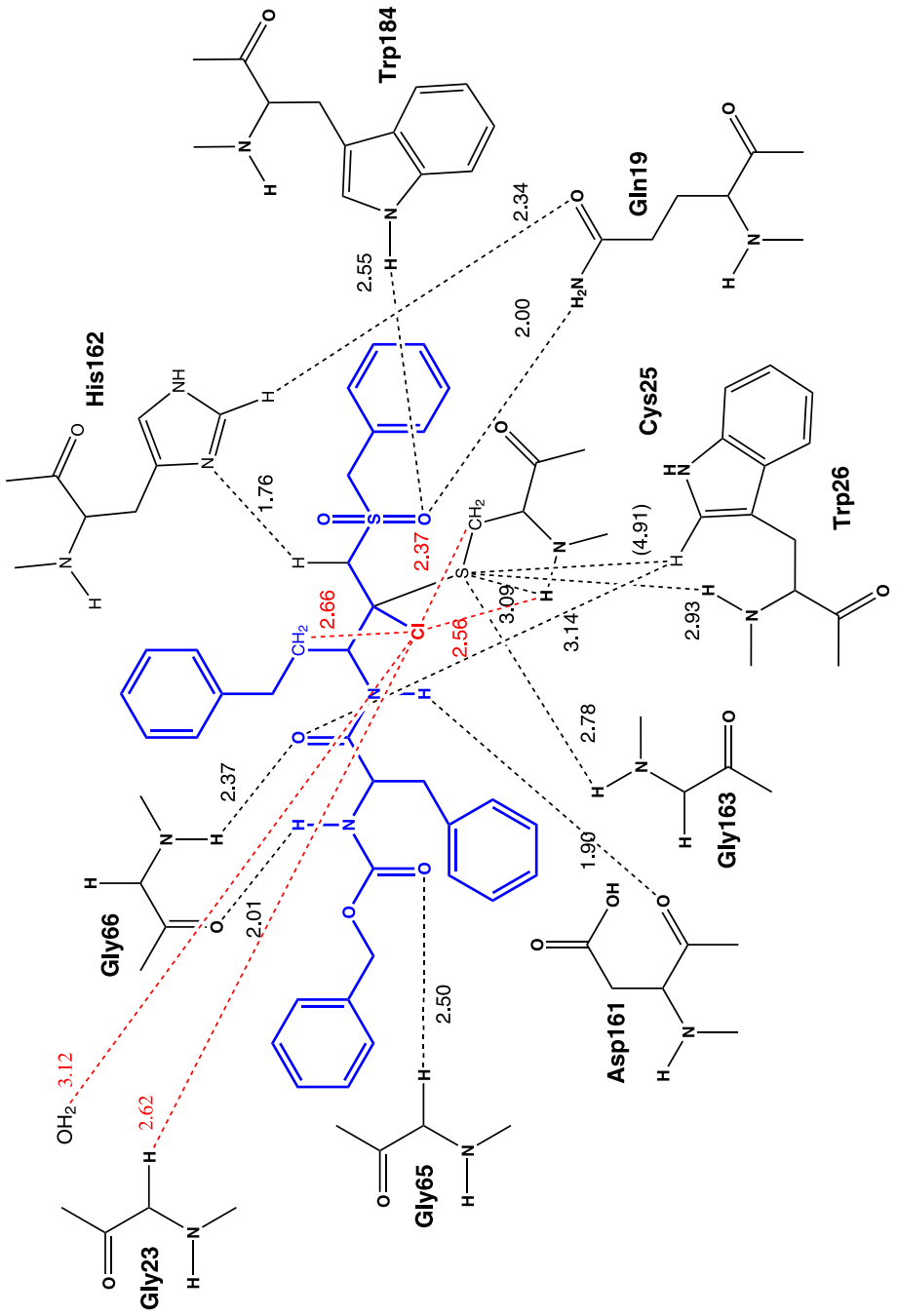

Figure 7.7.: Geometric details of the covalent bonded modified inhibitor after addition reaction mechanism in the active site of cruzain. The structure was calculated using the QM/MM MD method. The arrangement of the cruzain residues corresponds not the exact position in the protein to get a clearer insight in the interactions between inhibitor and protein.

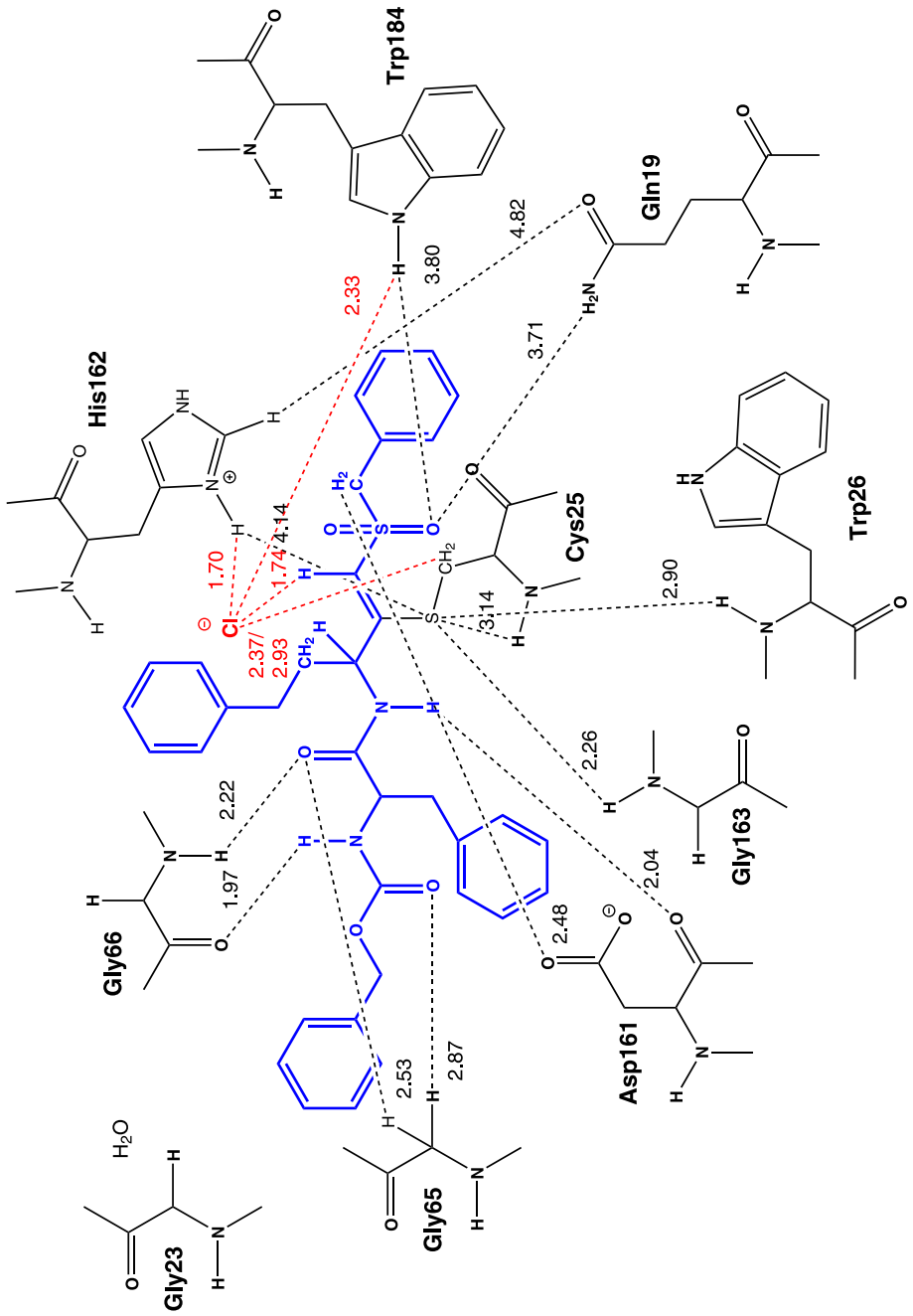

Figure 7.8.: Geometric details of the covalent bonded modified inhibitor after VNS reaction mechanism in the active site of cruzain. The structure was calculated using the QM/MM MD method. The arrangement of the cruzain residues corresponds not the exact position in the protein to get a clearer insight in the interactions between inhibitor and protein.

Residue	Non-bonded complex	bonded complex (Add)	Δ bond length	bonded complex (VNS)	Δ bond length
H-bonds to inhibitor side chain					
Gly66(O)	1.93	2.09	+0.16	2.05	+0.12
Gly66(N)	2.50	2.12	-0.38	2.16	-0.34
Gly65	2.66	2.62	-0.04	2.63	-0.03
Asp161	2.20	1.96	-0.24	1.90	-0.30
H-bonds to Cys25 S^-					
Gly163	2.09	2.40	+0.31	2.43	+0.34
Trp26	3.00	2.71	-0.29	3.38	+0.38
Cys25	3.10	3.15	-0.05	3.40	+0.30
His162	1.73	(2.49)		1.89	+0.16
VS216	– !	–		–	
H-bonds to vinyl sulfone oxygen					
Trp184	1.96	2.08	+0.12	1.94	-0.02
Gln19	2.69	1.80	-0.89	2.84	+0.15
H-bonds to Cl					
Cys25(BB)	2.44	2.35	-0.11	2.11	-0.33
Cys25(SC)	2.75	2.58	-0.17	2.29	-0.46
VS216(CH2)	3.49	2.70	-0.79	2.64	-0.85
VS216(CH)	2.60	2.68	+0.08	2.78	+0.18
Gly23	2.89	2.79	-0.10	2.69	-0.20
H2O	3.11	4.36	+1.25	2.15	-0.96

Table 7.28.: Table 2: Comparison of the H bond network within the active site of the non-bonded and bonded inhibitor resulting from QM/MM calculations. The major changes of the bond length are shown. All distances are given in Angstrom (Å).

Residue	Non-bonded complex (X=H)	Non-bonded complex (X=Cl)	Δ bond length
H-bonds to inhibitor side chain			
Gly66(O)	1.95	1.93	-0.02
Gly66(N)	2.27	2.50	+0.23
Gly65	2.84	2.66	-0.18
Asp161	2.49	2.20	-0.29
H-bonds to Cys25 S^-			
Gly163	2.08	2.09	+0.01
Trp26	2.70	3.00	+0.30
Cys25	3.19	3.10	-0.09
His162	1.72	1.73	+0.01
VS216	2.43	– !	
H-bonds to vinyl sulfone oxygen			
Trp184	1.78	1.96	+0.18
Gln19	1.86	2.69	+0.83
H-bonds to Cl			
Cys25(BB)	– !	2.44	
Cys25(SC)	– !	2.75	
VS216(CH2)	– !	3.49	
VS216(CH)	– !	2.60	
Gly23	– !	2.89	
H2O	– !	3.11	
Reaction coordinates			
Cys25(S-Cβ)	3.24	3.44	
His162(H-Cα)	4.02	3.38	

Table 7.29.: Table 3: Comparison of the H bond network within the active site of the non-bonded inhibitors X=H, Cl. The major changes of the bond length are shown in the last column. All distances are given in Angstrom (Å).

Residue	Non-bonded complex	bonded complex (Add)	Δ bond length	bonded complex (VNS)	Δ bond length
H-bonds to inhibitor side chain					
Gly66(O)	1.93	2.09	+0.16	2.05	+0.12
Gly66(N)	2.50	2.12	+0.38	2.16	-0.34
Gly65	2.66	2.62	-0.04	2.63	-0.03
Asp161	2.20	1.96	-0.24	1.90	-0.30
H-bonds to Cys25 S^-					
Gly163	2.09	2.40	+0.31	2.43	+0.34
Trp26	3.00	2.71	-0.29	3.38	+0.38
Cys25	3.10	3.15	+0.05	3.40	+0.30
His162	1.73	(2.49)		1.89	+0.16
VS216	– !	–		–	
H-bonds to vinyl sulfone oxygen					
Trp184	1.96	2.08	+0.12	1.94	-0.02
Gln19	2.69	1.80	-0.89	2.84	+0.15
H-bonds to Cl					
Cys25(BB)	2.44	2.35	-0.09	2.11	-0.33
Cys25(SC)	2.75	2.58	-0.17	2.29	-0.46
VS216(CH2)	3.49	2.70	-0.79	2.64	-0.85
VS216(CH)	2.60	?		2.78	+0.18
Gly23	2.89	–		2.69	-0.20
H2O	3.11	–		2.15	-0.96

Table 7.30.: Table 4: Comparison of the H bond network within the active site of the non-bonded and bonded modified inhibitor resulting from QM/MM calculations. The major changes of the bond length are shown. All distances are given in Angstrom (Å).

Residue	Non-b. complex	bonded complex (Add)	Δ bond length	bonded complex (VNS)	Δ bond length
H-bonds to inhibitor side chain					
Gly66(O)	1.93	2.01	+0.08	1.97	+0.04
Gly66(N)	2.60	2.37	-0.23	2.22	-0.38
Gly65	2.52/2.89	2.50	-0.02	2.87 (2.53)	+0.01/-0.02
Asp161	1.98	1.90	-0.08	2.04 (2.48)	+0.06
H-bonds to Cys25 S^-					
Gly163	2.08	2.78	+0.70	2.26	+0.18
Trp26	2.94	2.93	-0.01	2.90	-0.04
Cys25	3.12	3.09	-0.03	3.14	+0.02
His162	1.73	(1.76)	–	4.14	+2,41
VS216	–	–		–	
H-bonds to vinyl sulfone oxygen					
Trp184	2.05	2.55	+0.50	3.80	1.75
Gln19	1.87	2.00	+0.13	3.71	+1.84
H-bonds to Cl					
Cys25(BB)	2.65	2.56	-0.09	–	–
Cys25(SC)	3.06	2.37	-0.69	2.37 / 2.93	-0.69
VS216(CH2)	3.33	2.66	-0.67	1.70 His162	–
VS216(CH)	2.51	–?		2.33 Trp184	–
Gly23	2.91	2.62	-0.29	1.74 VSαCH	–
H2O	3.44	3.12	-0.32	–	–

Table 7.31.: Table 5: Comparison of the H bond network within the active site of the non-bonded and bonded modified inhibitor resulting from QM/MM MD calculations. The major changes of the bond length are shown. All distances are given in Angstrom (Å).

Bibliography

[1] Hobza, P.; Zahradnik, R.; Muller-Dethlefs, K. *Collection of Czechoslovak Chemical Communications*, **2006**, *71*(4), 443–531.

[2] Muller-Dethlefs, K.; Hobza, P. *Chemical Reviews*, **2000**, *100*(1), 143–167.

[3] Stone, A. *The theory of intermolecular forces*. Oxford University Press, 2013.

[4] Tsuzuki, S.; Yoshida, M.; Uchimaru, T.; Mikami, M. *Journal of Physical Chemistry A*, **2001**, *105*(4), 769–773.

[5] Marshall, M. S.; Steele, R. P.; Thanthiriwatte, K. S.; Sherrill, C. D. *Journal of Physical Chemistry A*, **2009**, *113*(48), 13628–13632.

[6] Kumpf, R. A.; Dougherty, D. A. *Science*, **1993**, *261*(5129), 1708–1710.

[7] Sherrill, C. D. *Accounts of Chemical Research*, **2012**, *46*(4), 1020–1028.

[8] Mahadevi, A. S.; Sastry, G. N. *Chemical Reviews*, **2013**, *113*(3), 2100–2138.

[9] Xiu, X.; Puskar, N. L.; Shanata, J. A. P.; Lester, H. A.; Dougherty, D. A. *Nature*, **2009**, *458*(7237), 534–U10.

[10] Lester, H. A.; Xiao, C.; Srinivasan, R.; Son, C. D.; Miwa, J.; Pantoja, R.; Banghart, M. R.; Dougherty, D. A.; Goate, A. M.; Wang, J. C. *Aaps Journal*, **2009**, *11*(1), 167–177.

[11] Dougherty, D. A. *Science*, **1996**, *271*(5246), 163–168.

[12] Dougherty, D. A. *Journal of Nutrition*, **2007**, *137*(6), 1504–1508.

[13] Ma, J. C.; Dougherty, D. A. *Chemical Reviews*, **1997**, *97*(5), 1303–1324.

[14] Cheng, J.; Luo, X.; Yan, X.; Li, Z.; Tang, Y.; Jiang, H.; Zhu, W. *Science in China Series B-Chemistry*, **2008**, *51*(8), 709–717.

[15] Zacharias, N.; Dougherty, D. A. *Trends in Pharmacological Sciences*, **2002**, *23*(6), 281–287.

[16] Gallivan, J. P.; Dougherty, D. A. *Proceedings of the National Academy of Sciences of the United States of America*, **1999**, *96*(17), 9459–9464.

[17] Haynes, W. M.; Lide, D. R.; Press, C. *CRC handbook of chemistry and physics a ready-reference book of chemical and physical data*. CRC Press, Boca Raton, Fla. [u.a.], 91. edition, 2010.

[18] Scharer, K.; Morgenthaler, M.; Paulini, R.; Obst-Sander, U.; Banner, D. W.; Schlatter, D.; Benz, J.; Stihle, M.; Diederich, F. *Angewandte Chemie-International Edition*, **2005**, *44*(28), 4400–4404.

[19] Salonen, L. M.; Bucher, C.; Banner, D. W.; Haap, W.; Mary, J. L.; Benz, J.; Kuster, O.; Seiler, P.; Schweizer, W. B.; Diederich, F. *Angewandte Chemie-International Edition*, **2009**, *48*(4), 811–814.

[20] Salonen, L. M.; Holland, M. C.; Kaib, P. S. J.; Haap, W.; Benz, J.; Mary, J.-L.; Kuster, O.; Schweizer, W. B.; Banner, D. W.; Diederich, F. *Chemistry-a European Journal*, **2012**, *18*(1), 213–222.

[21] Salonen, L. M.; Ellermann, M.; Diederich, F. *Angewandte Chemie-International Edition*, **2011**, *50*(21), 4808–4842.

[22] Boys, S. F.; Bernardi, F. *Molecular Physics*, **1970**, *19*(4), 553–566.

[23] Boys, S. F.; Bernardi, F. *Molecular Physics*, **2002**, *100*(1), 65–73.

[24] Burns, L. A.; Marshall, M. S.; Sherrill, C. D. *Journal of Chemical Theory and Computation*, **2014**, *10*(1), 49–57.

[25] Riley, K. E.; Pitonak, M.; Jurecka, P.; Hobza, P. *Chemical Reviews*, **2010**, *110*(9), 5023–5063.

[26] Grimme, S.; Antony, J.; Ehrlich, S.; Krieg, H. *Journal of Chemical Physics*, **2010**, *132*(15), 154104.

[27] Grimme, S.; Ehrlich, S.; Goerigk, L. *Journal of Computational Chemistry*, **2011**, *32*(7), 1456–1465.

[28] Goerigk, L.; Grimme, S. *Physical Chemistry Chemical Physics*, **2011**, *13*(14), 6670–6688.

[29] Riley, K. E.; Pitonak, M.; Cerny, J.; Hobza, P. *Journal of Chemical Theory and Computation*, **2010**, *6*(1), 66–80.

[30] Hobza, P.; Sponer, J. *Chemical Reviews*, **1999**, *99*(11), 3247–3276.

[31] Pitonak, M.; Hesselmann, A. *Journal of Chemical Theory and Computation*, **2010**, *6*(1), 168–178.

[32] Grimme, S.; Steinmetz, M.; Korth, M. *Journal of Organic Chemistry*, **2007**, *72*(6), 2118–2126.

[33] Schwabe, T.; Grimme, S. *Physical Chemistry Chemical Physics*, **2007**, *9*(26), 3397–3406.

[34] Grimme, S. *Angew Chem Int Ed Engl*, **2006**, *45*(27), 4460–4464.

[35] Bryantsev, V. S.; Diallo, M. S.; van Duin, A. C. T.; Goddard, I. William A. *Journal of Chemical Theory and Computation*, **2009**, *5*(4), 1016–1026.

[36] Jurecka, P.; Sponer, J.; Cerny, J.; Hobza, P. *Physical Chemistry Chemical Physics*, **2006**, *8*(17), 1985–1993.

[37] Cerny, J.; Hobza, P. *Physical Chemistry Chemical Physics*, **2007**, *9*(39), 5291–5303.

[38] Rezac, J.; Riley, K. E.; Hobza, P. *Journal of Chemical Theory and Computation*, **2011**, *7*(8), 2427–2438.

[39] Rezac, J.; Riley, K. E.; Hobza, P. *Journal of Chemical Theory and Computation*, **2014**, *10*(3), 1359–1360.

[40] Reha, D.; Valdes, H.; Vondrasek, J.; Hobza, P.; Abu-Riziq, A.; Crews, B.; de Vries, M. S. *Chemistry-a European Journal*, **2005**, *11*(23), 6803–6817.

[41] Gruzman, D.; Karton, A.; Martin, J. M. L. *Journal of Physical Chemistry A*, **2009**, *113*(43), 11974–11983.

[42] Goerigk, L.; Grimme, S. *Journal of Chemical Theory and Computation*, **2010**, *6*(1), 107–126.

[43] Csonka, G. I.; French, A. D.; Johnson, G. P.; Stortz, C. A. *Journal of Chemical Theory and Computation*, **2009**, *5*(4), 679–692.

[44] Wilke, J. J.; Lind, M. C.; Schaefer, I. Henry F.; Csaszar, A. G.; Allen, W. D. *Journal of Chemical Theory and Computation*, **2009**, *5*(6), 1511–1523.

[45] Simova, L.; Rezac, J.; Hobza, P. *Journal of Chemical Theory and Computation*, **2013**, *9*(8), 3420–3428.

[46] Hesselmann, A.; Gorling, A. *Chemical Physics Letters*, **2008**, *455*(1-3), 110–119.

[47] Jeziorski, B.; Moszynski, R.; Szalewicz, K. *Chemical Reviews*, **1994**, *94*(7), 1887–1930.

[48] Misquitta, A. J.; Podeszwa, R.; Jeziorski, B.; Szalewicz, K. *Journal of Chemical Physics*, **2005**, *123*(21), 214103.

[49] Jansen, G.; Hesselmann, A. *Journal of Physical Chemistry A*, **2001**, *105*(49), 11156–11157.

[50] Hesselmann, A.; Jansen, G. *Chemical Physics Letters*, **2002**, *357*(5-6), 464–470.

[51] Hesselmann, A.; Jansen, G. *Chemical Physics Letters*, **2002**, *362*(3-4), 319–325.

[52] Hesselmann, A.; Jansen, G. *Chemical Physics Letters*, **2003**, *367*(5-6), 778–784.

[53] Werner, H.-J.; Knowles, P. J.; Knizia, G.; Manby, F. R.; Schütz, M.; Celani, P.; Korona, T.; Lindh, R.; Mitrushenkov, A.; Rauhut, G.; Shamasundar, K. R.; Adler, T. B.; Amos, R. D.; Bernhardsson, A.; Berning, A.; Cooper, D. L.; Deegan, M. J. O.; Dobbyn, A. J.; Eckert, F.; Goll, E.; Hampel, C.; Hesselmann, A.; Hetzer, G.; Hrenar, T.; Jansen, G.; Köppl, C.; Liu, Y.; Lloyd, A. W.; Mata, R. A.; May, A. J.; McNicholas, S. J.; Meyer, W.; Mura, M. E.; Nicklass, A.; O'Neill, D. P.; Palmieri, P.; Peng, D.; Pflüger, K.; Pitzer, R.; Reiher, M.; Shiozaki, T.; Stoll, H.; Stone, A. J.; Tarroni, R.; Thorsteinsson, T.; Wang, M. Molpro, version 2010.1, a package of ab initio programs, 2010. see http://www.molpro.net.

[54] Moszynski, R.; Jeziorski, B.; Szalewicz, K. *Chemical Physics*, **1992**, *166*(3), 329–339.

[55] Cwiok, T.; Jeziorski, B.; Kolos, W.; Moszynski, R.; Szalewicz, K. *Theochem-Journal of Molecular Structure*, **1994**, *113*, 135–151.

[56] Misquitta, A. J.; Szalewicz, K. *Chemical Physics Letters*, **2002**, *357*(3-4), 301–306.

[57] Mas, E. M.; Bukowski, R.; Szalewicz, K. *Journal of Chemical Physics*, **2003**, *118*(10), 4386–4403.

[58] Mas, E. M.; Bukowski, R.; Szalewicz, K. *Journal of Chemical Physics*, **2003**, *118*(10), 4404–4413.

[59] Jeziorski, B.; Szalewicz, K. *Encyclopedia of Computational Chemistry*, **1998**, *Intermolecular Interactions by Pertubation Theory*, 1376 – 1398.

[60] Bukowski, R.; Szalewicz, K.; Groenenboom, G.; van der Avoird, A. *Journal of Chemical Physics*, **2006**, *125*(4), 044301.

[61] Patkowski, K.; Szalewicz, K.; Jeziorski, B. *Journal of Chemical Physics*, **2006**, *125*(15), 154107.

[62] Podeszwa, R.; Bukowski, R.; Szalewicz, K. *Journal of Physical Chemistry A*, **2006**, *110*(34), 10345–10354.

[63] Jeziorska, M.; Cencek, W.; Patkowski, K.; Jeziorski, B.; Szalewicz, K. *International Journal of Quantum Chemistry*, **2008**, *108*(12), 2053–2075.

[64] Patkowski, K.; Podeszwa, R.; Szalewicz, K. *Journal of Physical Chemistry A*, **2007**, *111*(49), 12822–12838.

[65] Misquitta, A. J.; Szalewicz, K. *Journal of Chemical Physics*, **2005**, *122*(21), 214109.

[66] Podeszwa, R.; Szalewicz, K. *Chemical Physics Letters*, **2005**, *412*(4-6), 488–493.

[67] Hesselmann, A.; Jansen, G. *Physical Chemistry Chemical Physics*, **2003**, *5*(22), 5010–5014.

[68] Sedlak, R.; Jurecka, P.; Hobza, P. *Journal of Chemical Physics*, **2007**, *127*(7), 075104.

[69] Hesselmann, A. *Journal of Chemical Physics*, **2008**, *128*(14), 144112.

[70] Patkowski, K.; Jeziorski, B.; Szalewicz, K. *Journal of Chemical Physics*, **2004**, *120*(15), 6849–6862.

[71] Patkowski, K.; Szalewicz, K. *Journal of Chemical Physics*, **2007**, *127*(16), 164103.

[72] Podeszwa, R.; Szalewicz, K. *Journal of Chemical Physics*, **2007**, *126*(19), 194101.

[73] Zuchowski, P. S.; Podeszwa, R.; Moszynski, R.; Jeziorski, B.; Szalewicz, K. *Journal of Chemical Physics*, **2008**, *129*(8), 084101.

[74] Patkowski, K.; Szalewicz, K.; Jeziorski, B. *Theoretical Chemistry Accounts*, **2010**, *127*(3), 211–221.

[75] Morgado, C. A.; Jurecka, P.; Svozil, D.; Hobza, P.; Sponer, J. *Journal of Chemical Theory and Computation*, **2009**, *5*(6), 1524–1544.

[76] Morgado, C. A.; Jurecka, P.; Svozil, D.; Hobza, P.; Sponer, J. *Physical Chemistry Chemical Physics*, **2010**, *12*(14), 3522–3534.

[77] Hobza, P.; Sedlak, R.; Fanfrlik, J.; Hnyk, D.; Lepsik, M. *Journal of Physical Chemistry A*, **2010**, *114*(42), 11304–11311.

[78] Szalewicz, K.; Patkowski, K.; Jeziorski, B. *Intermolecular Forces and Clusters Ii*, **2005**, *116*, 43–117.

[79] Hesselmann, A.; Jansen, G.; Schutz, M. *Journal of the American Chemical Society*, **2006**, *128*(36), 11730–11731.

[80] Fiethen, A.; Jansen, G.; Hesselmann, A.; Schutz, M. *Journal of the American Chemical Society*, **2008**, *130*(6), 1802–1803.

[81] Grimme, S. *J Comput Chem*, **2004**, *25*(12), 1463–1473.

[82] Hujo, W.; Grimme, S. *Physical Chemistry Chemical Physics*, **2011**, *13*(31), 13942–13950.

[83] Goerigk, L.; Kruse, H.; Grimme, S. *Chemphyschem*, **2011**, *12*(17), 3421–3433.

[84] Vydrov, O. A.; Van Voorhis, T. *Journal of Chemical Theory and Computation*, **2012**, *8*(6), 1929–1934.

[85] Rezac, J.; Fanfrlik, J.; Salahub, D.; Hobza, P. *Journal of Chemical Theory and Computation*, **2009**, *5*(7), 1749–1760.

[86] Korth, M.; Pitonak, M.; Rezac, J.; Hobza, P. *Journal of Chemical Theory and Computation*, **2010**, *6*(1), 344–352.

[87] Antila, H. S.; Salonen, E. *Methods in molecular biology (Clifton, N.J.)*, **2013**, *924*, 215–41.

[88] Allinger, N. L. *Journal of the American Chemical Society*, **1977**, *99*(25), 8127–8134.

[89] Lii, J. H.; Gallion, S.; Bender, C.; Wikstrom, H.; Allinger, N. L.; Flurchick, K. M.; Teeter, M. M. *Journal of Computational Chemistry*, **1989**, *10*(4), 503–513.

[90] Allinger, N. L.; Yuh, Y. H.; Lii, J. H. *Journal of the American Chemical Society*, **1989**, *111*(23), 8551–8566.

[91] Lii, J. H.; Allinger, N. L. *Journal of the American Chemical Society*, **1989**, *111*(23), 8566–8575.

[92] Lii, J. H.; Allinger, N. L. *Journal of the American Chemical Society*, **1989**, *111*(23), 8576–8582.

[93] Lii, J. H.; Allinger, N. L. *Journal of Computational Chemistry*, **1991**, *12*(2), 186–199.

[94] Cornell, W. D.; Cieplak, P.; Bayly, C. I.; Gould, I. R.; Merz, K. M.; Ferguson, D. M.; Spellmeyer, D. C.; Fox, T.; Caldwell, J. W.; Kollman, P. A. *Journal of the American Chemical Society*, **1995**, *117*(19), 5179–5197.

[95] Wang, J. M.; Wolf, R. M.; Caldwell, J. W.; Kollman, P. A.; Case, D. A. *Journal of Computational Chemistry*, **2004**, *25*(9), 1157–1174.

[96] Hornak, V.; Abel, R.; Okur, A.; Strockbine, B.; Roitberg, A.; Simmerling, C. *Proteins-Structure Function and Bioinformatics*, **2006**, *65*(3), 712–725.

[97] Damm, W.; Halgren, T. A.; Murphy, R. B.; Smondyrev, A. M.; Friesner, R. A.; Jorgensen, W. L. *Abstracts of Papers of the American Chemical Society*, **2002**, *224*, U471–U471.

[98] Jorgensen, W. L.; Tirado-Rives, J. *Abstracts of Papers of the American Chemical Society*, **1998**, *216*, U696–U696.

[99] Kaminski, G. A.; Friesner, R. A.; Tirado-Rives, J.; Jorgensen, W. L. *Journal of Physical Chemistry B*, **2001**, *105*(28), 6474–6487.

[100] McDonald, N. A.; Jorgensen, W. L. *Journal of Physical Chemistry B*, **1998**, *102*(41), 8049–8059.

[101] Halgren, T. A. *Journal of the American Chemical Society*, **1992**, *114*(20), 7827–7843.

[102] Halgren, T. A. *Journal of Computational Chemistry*, **1996**, *17*(5-6), 490–519.

[103] Halgren, T. A. *Journal of Computational Chemistry*, **1996**, *17*(5-6), 520–552.

[104] Halgren, T. A. *Journal of Computational Chemistry*, **1996**, *17*(5-6), 553–586.

[105] Halgren, T. A. *Journal of Computational Chemistry*, **1996**, *17*(5-6), 616–641.

[106] Halgren, T. A.; Nachbar, R. B. *Journal of Computational Chemistry*, **1996**, *17*(5-6), 587–615.

[107] Kolar, M.; Berka, K.; Jurecka, P.; Hobza, P. *Chemphyschem*, **2010**, *11*(11), 2399–2408.

[108] Tafipolsky, M.; Engels, B. *Journal of Chemical Theory and Computation*, **2011**, *7*(6), 1791–1803.

[109] Ponder, J. W.; Wu, C.; Ren, P.; Pande, V. S.; Chodera, J. D.; Schnieders, M. J.; Haque, I.; Mobley, D. L.; Lambrecht, D. S.; DiStasio, J. Robert A.; Head-Gordon, M.; Clark, G. N. I.; Johnson, M. E.; Head-Gordon, T. *Journal of Physical Chemistry B*, **2010**, *114*(8), 2549–2564.

[110] Alonso, J. L.; Antolinez, S.; Blanco, S.; Lesarri, A.; Lopez, J. C.; Caminati, W. *Journal of the American Chemical Society*, **2004**, *126*(10), 3244–3249.

[111] Blanco, S.; Lopez, J. C.; Lesarri, A.; Caminati, W.; Alonso, J. L. *Molecular Physics*, **2005**, *103*(11-12), 1473–1479.

[112] Caminati, W.; Lopez, J. C.; Alonso, J. L.; Grabow, J. U. *Angewandte Chemie-International Edition*, **2005**, *44*(25), 3840–3844.

[113] Cole, G. C.; Legon, A. C. *Journal of Chemical Physics*, **2004**, *121*(21), 10467–10473.

[114] Grant, E. R.; White, M. G. *Nature*, **1991**, *354*(6350), 249–250.

[115] Zhu, L. C.; Johnson, P. *Journal of Chemical Physics*, **1991**, *94*(8), 5769–5771.

[116] Haines, S. R.; Geppert, W. D.; Chapman, D. M.; Watkins, M. J.; Dessent, C. E. H.; Cockett, M. C. R.; Muller-Dethlefs, K. *Journal of Chemical Physics*, **1998**, *109*(21), 9244–9251.

[117] Chapman, D. M.; Muller-Dethlefs, K.; Peel, J. B. *Journal of Chemical Physics*, **1999**, *111*(5), 1955–1963.

[118] Dessent, C. E. H.; Haines, S. R.; Muller-Dethlefs, K. *Chemical Physics Letters*, **1999**, *315*(1-2), 103–108.

[119] Haines, S. R.; Dessent, C. E. H.; Muller-Dethlefs, K. *Journal of Chemical Physics*, **1999**, *111*(5), 1947–1954.

[120] Hobza, P.; Muller-Dethlefs, K.; Hirst, J.; Lim, C.; Jordan, K. D.; Thiel, W. *Non-covalent interactions Theory and Experiment*. RSC Theoretical and computational chemistry series. Royal Society of Chemistry, Cambridge, 2009.

[121] Szalewicz, K. *Wiley Interdisciplinary Reviews-Computational Molecular Science*, **2012**, *2*(2), 254–272.

[122] Cwiok, T.; Jeziorski, B.; Kolos, W.; Moszynski, R.; Szalewicz, K. *Journal of Chemical Physics*, **1992**, *97*(10), 7555–7559.

[123] Jeziorski, B.; Szalewicz, K.; Chalasinski, G. *International Journal of Quantum Chemistry*, **1978**, *14*(3), 271–287.

[124] Gruning, M.; Gritsenko, O. V.; van Gisbergen, S. J. A.; Baerends, E. J. *Journal of Chemical Physics*, **2001**, *114*(2), 652–660.

[125] Hesselmann, A.; Jansen, G.; Schutz, M. *Journal of Chemical Physics*, **2005**, *122*(1), 014103.

[126] Spackman, M. A. *Chemical Physics Letters*, **2006**, *418*(1-3), 158–162.

[127] Su, Z.; Coppens, P. *Journal of Applied Crystallography*, **1990**, *23*, 71–73.

[128] Tafipolsky, M.; Schmid, R. *Journal of Physical Chemistry B*, **2009**, *113*(5), 1341–1352.

[129] Charbonneau, P. *Astrophysical Journal Supplement Series*, **1995**, *101*(2), 309–334.

[130] Ansorg, K.; Tafipolsky, M.; Engels, B. *Journal of Physical Chemistry B*, **2013**, *117*(35), 10093–10102.

[131] Tafipolski, M. *Chemical Reviews*, **2014**, *1*(1), 1–2.

[132] TURBOMOLE V6.5 2013, a development of University of Karlsruhe and Forschungszentrum Karlsruhe GmbH, 1989-2007, TURBOMOLE GmbH, since 2007; available from `http://www.turbomole.com`.

[133] Jeziorska, M.; Jankowski, P.; Szalewicz, K.; Jeziorski, B. *Journal of Chemical Physics*, **2000**, *113*(8), 2957–2968.

[134] Torheyden, M.; Jansen, G. *Molecular Physics*, **2006**, *104*(13-14), 2101–2138.

[135] Bukowski, R.; Szalewicz, K.; Groenenboom, G. C.; van der Avoird, A. *Journal of Chemical Physics*, **2008**, *128*(9), 094313.

[136] Frisch, M. J.; Trucks, G. W.; Schlegel, H. B.; Scuseria, G. E.; Robb, M. A.; Cheeseman, J. R.; Scalmani, G.; Barone, V.; Mennucci, B.; Petersson, G. A.; Nakatsuji, H.; Caricato, M.; Li, X.; Hratchian, H. P.; Izmaylov, A. F.; Bloino, J.; Zheng, G.; Sonnenberg, J. L.; Hada, M.; Ehara, M.; Toyota, K.; Fukuda, R.; Hasegawa, J.; Ishida, M.; Nakajima, T.; Honda, Y.; Kitao, O.; Nakai, H.; Vreven, T.; Montgomery Jr., J. A.; Peralta, J. E.; Ogliaro, F.; Bearpark, M. J.; Heyd, J.; Brothers, E. N.; Kudin, K. N.; Staroverov, V. N.; Kobayashi, R.; Normand, J.; Raghavachari, K.; Rendell, A. P.; Burant, J. C.; Iyengar, S. S.; Tomasi, J.; Cossi, M.; Rega, N.; Millam, N. J.; Klene, M.; Knox, J. E.; Cross, J. B.; Bakken, V.; Adamo, C.; Jaramillo, J.; Gomperts, R.; Stratmann, R. E.; Yazyev, O.; Austin, A. J.; Cammi, R.; Pomelli, C.; Ochterski, J. W.; Martin, R. L.; Morokuma, K.; Zakrzewski, V. G.; Voth, G. A.; Salvador, P.; Dannenberg, J. J.; Dapprich, S.; Daniels, A. D.; Farkas, O.; Foresman, J. B.; Ortiz, J. V.; Cioslowski, J.; Fox, D. J. Gaussian 09, 2009.

[137] Lias, S. "ionization energy evaluation" in nist chemistry webbook, nist standard reference database number 69, eds. p.j. linstrom and w.g. mallard, national institute of standards and technology, gaithersburg md, 20899, http://webbook.nist.gov, (retrieved september 11, 2014), 2014.

[138] van Leeuwen, R.; Baerends, E. J. *Physical Review A*, **1994**, *49*, 2421–2431.

[139] Della Sala, F.; Gorling, A. *Journal of Chemical Physics*, **2001**, *115*(13), 5718–5732.

[140] Hesselmann, A.; Manby, F. R. *Journal of Chemical Physics*, **2005**, *123*(16), 164116.

[141] Perdew, J. P.; Burke, K.; Ernzerhof, M. *Physical Review Letters*, **1996**, *77*(18), 3865–3868.

[142] Adamo, C.; Barone, V. *Journal of Chemical Physics*, **1999**, *110*(13), 6158–6170.

[143] Kutzelnigg, W.; Morgan, J. D. *Journal of Chemical Physics*, **1992**, *96*(6), 4484–4508.

[144] Huh, S. B.; Lee, J. S. *Journal of Chemical Physics*, **2003**, *118*(7), 3035–3042.

[145] Halkier, A.; Helgaker, T.; Jorgensen, P.; Klopper, W.; Koch, H.; Olsen, J.; Wilson, A. K. *Chemical Physics Letters*, **1998**, *286*(3-4), 243–252.

[146] Reinhardt, P.; Piquemal, J. P. *International Journal of Quantum Chemistry*, **2009**, *109*(14), 3259–3267.

[147] Kuntz, I. D.; Chen, K.; Sharp, K. A.; Kollman, P. A. *Proceedings of the National Academy of Sciences of the United States of America*, **1999**, *96*(18), 9997–10002.

[148] Brinen, L. S.; Hansell, E.; Cheng, J. M.; Roush, W. R.; McKerrow, J. H.; Fletterick, R. J. *Structure with Folding and Design*, **2000**, *8*(8), 831–840.

[149] Smith, A. J. T.; Zhang, X.; Leach, A. G.; Houk, K. N. *Journal of Medicinal Chemistry*, **2009**, *52*(2), 225–233.

[150] Singh, J.; Petter, R. C.; Baillie, T. A.; Whitty, A. *Nature Reviews Drug Discovery*, **2011**, *10*(4), 307–317.

[151] Schneider, T. H.; Rieger, M.; Ansorg, K.; Sobolev, A. N.; Schirmeister, T.; Engels, B.; Grabowsky, S. *New Journal of Chemistry*, **2015**, *39*(7), 5841–5853.

[152] Otto, H. H.; Schirmeister, T. *Chemical Reviews*, **1997**, *97*(1), 133–171.

[153] Kerr, I. D.; Lee, J. H.; Farady, C. J.; Marion, R.; Rickert, M.; Sajid, M.; Pandey, K. C.; Caffrey, C. R.; Legac, J.; Hansell, E.; McKerrow, J. H.; Craik, C. S.; Rosenthal, P. J.; Brinen, L. S. *Journal of Biological Chemistry*, **2009**, *284*(38), 25697–25703.

[154] Kim, T. S.; Tasker, A. S. *Current Topics in Medicinal Chemistry*, **2006**, *6*(4), 355–360.

[155] Roberts, R. *Drug News and Perspectives*, **2005**, *18*(10), 605–614.

[156] Obermajer, N.; Doljak, B.; Kos, J. *Expert Opinion on Biological Therapy*, **2006**, *6*(12), 1295–1309.

[157] Hook, V. Y. H. *Biodrugs*, **2006**, *20*(2), 105–119.

[158] Rosenthal, P. J.; McKerrow, J. H.; Aikawa, M.; Nagasawa, H.; Leech, J. H. *Journal of Clinical Investigation*, **1988**, *82*(5), 1560–1566.

[159] Caffrey, C. R.; Scory, S.; Steverding, D. *Current Drug Targets*, **2000**, *1*(2), 155–162.

[160] Jose Cazzulo, J.; Stoka, V.; Turk, V. *Current pharmaceutical design*, **2001**, *7*(12), 1143–56.

[161] Clayton, J. *Nature*, **2010**, *465*(7301), S12–S15.

[162] Yang, P.-Y.; Wang, M.; He, C. Y.; Yao, S. Q. *Chemical Communications*, **2012**, *48*(6), 835–837.

[163] Bryant, C.; Kerr, I. D.; Debnath, M.; Ang, K. K. H.; Ratnam, J.; Ferreira, R. S.; Jaishankar, P.; Zhao, D.; Arkin, M. R.; McKerrow, J. H.; Brinen, L. S.; Renslo, A. R. *Bioorganic and Medicinal Chemistry Letters*, **2009**, *19*(21), 6218–6221.

[164] Engel, J. C.; Doyle, P. S.; Hsieh, I.; McKerrow, J. H. *Journal of Experimental Medicine*, **1998**, *188*(4), 725–734.

[165] Barr, S. C.; Warner, K. L.; Kornreic, B. G.; Piscitelli, J.; Wolfe, A.; Benet, L.; McKerrow, J. H. *Antimicrobial Agents and Chemotherapy*, **2005**, *49*(12), 5160–5161.

[166] Powers, J. C.; Asgian, J. L.; Ekici, O. D.; James, K. E. *Chemical Reviews*, **2002**, *102*(12), 4639–4750.

[167] Hanzlik, R. P.; Thompson, S. A. *Journal of Medicinal Chemistry*, **1984**, *27*(6), 711–712.

[168] Palmer, J. T.; Rasnick, D.; Klaus, J. L.; Bromme, D. *Journal of Medicinal Chemistry*, **1995**, *38*(17), 3193–3196.

[169] Schmidt, T. C.; Paasche, A.; Grebner, C.; Ansorg, K.; Becker, J.; Lee, W.; Engels, B. *Top Curr Chem*, **2012**.

[170] Case, D.; Darden, T.; Cheatham, T.; Simmerling, C.; Wang, J.; Duke, R.; Luo, R.; Walker, R.; Zhang, W.; Merz, K.; Roberts, B.; Hayik, S.; Roitberg, A.; Seabra, G.; Swails, J.; Goetz, A.; Kolossvary, I.; Wong, K.; Paesani, F.; Vanicek, J.; Wolf, R.; Liu, J.; Wu, X.; Brozell, S.; Steinbrecher, T.; Gohlke, H.; Cai, Q.; Ye, X.; Wang, J.; Hsieh, M.-J.; Cui, G.; Roe, D.; Mathews, D.; Seetin, M.; Salomon-Ferrer, R.; Sagui, C.; Babin, V.; Luchko, T.; Gusarov, S.; Kovalenko, A.; Kollman, P. Amber 12, 2012.

[171] Jorgensen, W. L.; Chandrasekhar, J.; Madura, J. D.; Impey, R. W.; Klein, M. L. *Journal of Chemical Physics*, **1983**, *79*(2), 926–935.

[172] Stewart, J. J. P. *Journal of Computational Chemistry*, **1989**, *10*(2), 209–220.

[173] Stewart, J. J. P. *Journal of Computational Chemistry*, **1989**, *10*(2), 221–264.

[174] Mladenovic, M.; Fink, R. F.; Thiel, W.; Schirmeister, T.; Engels, B. *Journal of the American Chemical Society*, **2008**, *130*(27), 8696–8705.

[175] Kumar, S.; Bouzida, D.; Swendsen, R. H.; Kollman, P. A.; Rosenberg, J. M. *Journal of Computational Chemistry*, **1992**, *13*(8), 1011–1021.

[176] Ferrenberg, A. M.; Swendsen, R. H. *Physical Review Letters*, **1988**, *61*(23), 2635–2638.

[177] Souaille, M.; Roux, B. *Computer Physics Communications*, **2001**, *135*(1), 40–57.

[178] Grossfield, A. Wham: the weighted histogram analysis method, version 2.0.4, 2013.

[179] Sherwood, P.; de Vries, A. H.; Guest, M. F.; Schreckenbach, G.; Catlow, C. R. A.; French, S. A.; Sokol, A. A.; Bromley, S. T.; Thiel, W.; Turner, A. J.; Billeter, S.; Terstegen, F.; Thiel, S.; Kendrick, J.; Rogers, S. C.; Casci, J.; Watson, M.; King, F.; Karlsen, E.; Sjovoll, M.; Fahmi, A.; Schafer, A.; Lennartz, C. *Journal of Molecular Structure-Theochem*, **2003**, *632*, 1–28.

[180] Field, M. J.; Bash, P. A.; Karplus, M. *Journal of Computational Chemistry*, **1990**, *11*(6), 700–733.

[181] Sinclair, P. E.; de Vries, A.; Sherwood, P.; Catlow, C. R. A.; van Santen, R. A. *Journal of the Chemical Society-Faraday Transactions*, **1998**, *94*(22), 3401–3408.